Dissertation

submitted to the

Combined Faculties of the Natural Sciences and Mathematics

of the Ruperto-Carola-University of Heidelberg, Germany

for the degree of

Doctor of Natural Sciences

Put forward by

Moritz Ernst Lothar Platscher

Born in Schwäbisch Hall

Date of oral examination: 9 January 2019

Phenomenology of Massive Spin-2 Fields

1st Referee: Prof. Dr. Dr. h.c. Manfred Lindner

2nd Referee: Prof. Dr. Björn Malte Schäfer

Abstract

Phenomenology of massive spin-2 fields. We derive and discuss the implications of massive spin-2 fields as possible extensions of the standard theory of gravity, general relativity, in the spirit of extension of the standard model of particle physics. We give a thorough introduction to the topic of massive gravity from the point of view of bi- or multi-metric extensions of general relativity, focussing on the bimetric case in the phenomenological considerations. Furthermore, known shortcomings and benefits of such models are discussed. From this discussion it is evident that the parameter regime of interest is mostly that of very small spin-2 masses, such that effects on galactic and extra-galactic length scales are expected. On these grounds, we investigate the dynamics of spiral galaxies in the form of rotation curves, from which we derive constraints on the model's parameter space. Moreover, we discuss the modifications of gravitational lensing by galaxy clusters, which strongly constrain these parameters. We also highlight how these modifications could explain tentative anomalies in the observations of such systems. Finally, we make use of the recent detection and conformation of gravitational waves. If more than one spin-2 field is present, they are expected to mix dynamically in close analogy to the oscillation of neutrino flavours. This observation is confirmed quantitatively, and subsequently used to derive new constraints on the allowed masses and mixings of the two tensors. To this end, we employ both the available data as well as a future, hypothetical sample of many such signals and their distribution as a function of the cosmological redshift. We conclude our discussion with another critical contemplation of the current status and provide an outlook onto possible ultraviolet completions.

Zusammenfassung

Phänomenologie massiver Spin-2-Felder. Ziel dieser Arbeit ist es die Auswirkungen massiver Spin-2-Felder als Erweiterungen der Allgemeinen Relativitätstheorie zu erkunden, angelehnt an das Vorgehen in der Teilchenphysik. Das Thema soll im Kontext sogenannter Bi- bzw. Multi-Metrik-Erweiterungen der Allgemeinen Relativitätstheorie eingeführt und detailliert besprochen werden, wobei die phänomenologische Diskussion auf den Fall zweier Tensorfelder beschränkt bleibt. Darüber hinaus wird diese Klasse von Erweiterungen der Allgemeinen Relativitätstheorie kritisch diskutiert, indem bekannte Vor- und Nachteile solcher Modelle gegenübergestellt werden. Aus dieser Diskussion folgt, dass der interessante Massenbereich jener mit besonders kleinen Massen ist, sodass Effekte auf galaktischen und extragalaktischen Längenskalen zu erwarten sind. Aus diesen Erwägungen heraus wird die Dynamik von Spiralgalaxien in Form von Rotationskurven untersucht und daraus folgende Schranken an den Parameterraum hergeleitet. Weiterhin diskutiert wird die veränderte Vorhersage des Gravitationslinseneffekts in Galaxienhaufen, welcher erhebliche Einschränkungen der Parameter mit sich bringt. Jedoch beobachtet man gleichzeitig, dass diese Modifikationen mögliche Anomalien solcher Systeme erklären können. Zuletzt werden die unlängst erstmals gemessenen Gravitationswellensignale herangezogen. In Gegenwart mehrerer Spin-2-Felder erwartet man, dass diese dynamisch mischen, ähnlich den Oszillationen mehrerer Neutrinogenerationen. Diese Beobachtung wird quantitativ bestätigt und im weiteren Verlauf dazu verwendet die erlaubten Massen und Mischungsparameter beider Spin-2-Felder einzuschränken. Zu diesem Zweck werden sowohl die aktuell verfügbaren Daten, sowie eine zukünftige, hypothetische Stichprobe vieler solcher Signale und ihre Verteilung als Funktion der kosmologischen Rotverschiebung herangezogen. Die Diskussion wird mit einer kritischen Betrachtung der Sachlage beendet, insbesondere im Hinblick auf mögliche Hochenergievervollständigungen.

Danksagung

Zunächst möchte ich mich bei meinem Betreuer Prof. Dr. Dr. h.c. Manfred Lindner bedanken, der es mir ermöglicht hat am Max-Planck-Institut für Kernphysik zu promovieren. Deine Offenheit für neue Themen, die vielen anregenden Diskussionen, die wir geführt haben, und nicht zuletzt die Freiheit, die du mir in meinen Forschungsarbeiten eingeräumt hast, haben es mir ermöglicht das Beste aus meiner Zeit in der Arbeitsgruppe zu machen.

Außerdem möchte ich an dieser Stelle meine wissenschaftlichen Kollaborateure erwähnen, welche im Laufe meiner Zeit am Max-Planck-Institut für Kernphysik wichtige Ideen und Diskussionen angestoßen haben. An dieser Stelle möchte ich besonders Prof. Dr. Dr. h.c. Manfred Lindner und Dr. Juri Smirnov hervorheben, die durch die Organisation des Studenten-Seminars zum Thema Gravitationswellen die Grundlage für die hier besprochenen Themen gelegt haben.

Weiterhin danke ich vielmals Prof. Dr. Björn Malte Schäfer, der sich als Zweitgutachter angeboten hat. Ebenso danke ich ganz herzlich den beiden anderen Prüfungskommissionsmitgliedern, Prof. Dr. Matthias Bartelmann und PD Dr. Teresa Marrodán Undagoitia, für Ihre Zeit.

Ebenfalls gebührt Anja Berneiser sowie Britta Schwarz ein Dank. Zwar gehen die vielen administrativen Feinheiten im Alltag oft unter, jedoch könnte niemand ohne euer Zutun hier seiner Arbeit nachgehen. Außerdem Danke ich in diesem Zusammenhang Dr. Werner Rodejohann, welcher die IMPRS-PTFS koordiniert, in deren Rahmen meine Promotion finanziert wurde. Auch Frau Heinzelmann von der HGSFP danke ich für die reibungslose Kommunikation.

Ein weiteres großes Dankeschön richte ich an meine Bürokollegen aus dem "Partybüro": Liebe(r) Carlos, Christian, Christiane, Ingolf, Oli, Tobi, Tom und auch an alle die uns irgendwann verlassen haben (Helena, Kevin, Miguel, Veronica, Yannick). Es war mir eine große Freude meine Zeit am Institut mit euch zu verbringen! Danke, dass ihr meine Launen und Macken mit viel Humor ertragen habt. Mit euch sind auch die langen Arbeitstage wie im Nu verflogen.

Ganz besonders möchte ich Ingolf Bischer, Christian Döring, Kevin Max, Sebastian Ohmer, Erik Parr, Thomas Rink, Juri Smirnov und Susan van der Woude erwähnen. Eure Korrekturen und Vorschläge haben diese Arbeit erst in ein lesbares Manuskript verwandelt. Tausend Dank, dass ihr euch durchgekämpft habt! Ebenfalls danke ich Sarah Mohr, die diese Danksagung und die Zusammenfassung korrekturgelesen hat.

Außerdem geht ein Gruß an Jule Häußermann nach Leipzig für die aufbauende Motivations-Postkarte (¡Venceremos!), an meine "Leidensgenossin" Paula Bukieda nach Dresden für viele aufbauende Worte und an meinen Reisegefährten Shahroze Ansari für die vielen 'Pakiventures'. Auch allen meinen Freunden, die hier nicht namentlich

erwähnt werden, danke ich für ihre Freundschaft und Unterstützung.

Zu guter Letzt möchte ich meiner Familie danken, allen voran meinen Eltern, Andreas und Brigitte. Eure unendliche Liebe und Unterstützung hat es mir erst möglich gemacht, heute hier angekommen zu sein. Traditionsgemäß gebührt auch meiner lieben Oma Erika ein Dank für den unerschöpflichen Kuchen- und Marmeladennachschub.

Im Gedenken an Opa Lode

Contents

List of Figures

List of Tables

List of Abbreviations

ΛCDM standard model of cosmology

ADM Arnowitt, Deser, and Misner

BD Boulware–Deser

BH black hole

C.L. confidence level

CC cosmological constant

CMB cosmic microwave background

DE dark energy

DM dark matter

DOF degree of freedom

dRGT de Rham, Gabadadze, and Tolley

EMT energy momentum tensor

EOM equation of motion

FLRW Friedman-Lemaître-Robertson-Walker

GR general relativity

GW gravitational wave

LHC Large Hadron Collider

LSB low surface brightness

MACS MAssive Cluster Survey

MOND modified Newtonian dynamics

NFW Navarro, Frenk, and White

NS neutron star

QFT quantum field theory

QM quantum mechanics

SM standard model of particle physics

SNR signal-to-noise ratio

SZ Sunyaev–Zel'dovich

TT transverse traceless

vDVZ van Dam, Veltman, and Zakharov

w.r.t. with respect to

WIMP weakly interacting massive particle

Chapter 1

Introduction

Habe nun, ach! Philosophie,
Juristerei und Medizin,
Und leider auch Theologie
Durchaus studiert, mit heißem Bemühn.
Da steh ich nun, ich armer Tor!
Und bin so klug als wie zuvor;
[. . .]
Daß ich erkenne, was die Welt
Im Innersten zusammenhält,

– Faust: Der Tragödie Erster Teil,
J. W. von Goethe

Why did Goethe's Faust not study physics 'To learn the hidden mystic lore, Within the world's innermost core' [9]? In fact, physics was considered a branch of philosophy until the early 19^{th} century. But even so, the modern understanding of the field of the physical sciences arguably dates back to the work of Galileo Galilei, who was born only after the historical figure Johann Georg Faust walked the Earth.[1] Indeed, the scientific advances of humankind since these days are quite remarkable: Starting with the early developments of the classical theories of gravitation and electromagnetism, we have now developed an understanding of matter's *innermost core* and their interactions that defies all attempts to replace it – and from the first observations of planetary motion, indicating that the geocentric system needed to be superseded by a heliocentric system, to the very recent direct measurement of gravitational waves (GWs) that help us to develop a model describing the cosmos that surrounds us. A modern *Doktor Faustus* should not have to make a deal with the devil to get a grasp of the world's innermost functioning, which today we believe to be described by the standard model of cosmology (ΛCDM) and the standard model of particle physics (SM). These frameworks have allowed us to make falsifiable predictions from the smallest, sub-atomic realm of quantum mechanics (QM) up to scales as large as the Universe itself.

[1] Johann Georg Faust: *1480 – †1541 [10]; Galileo Galilei: *1564 – †1642 [11].

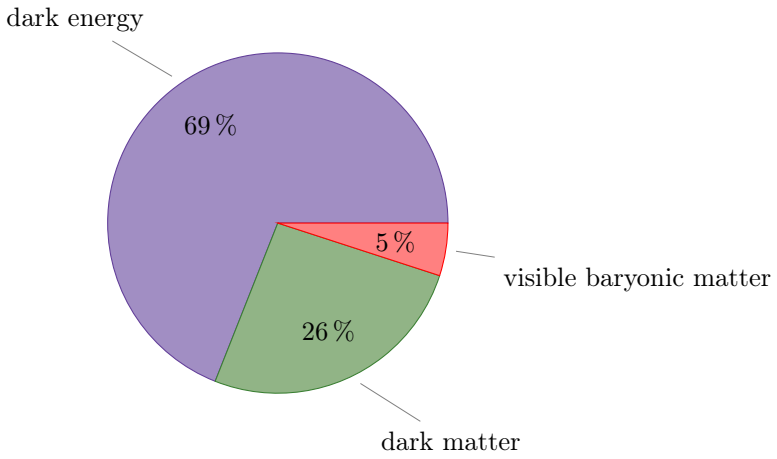

Figure 1.1.: Energy budget of the Universe as measured by the Planck space telescope [12].

Many important developments in theoretical physics have only been conceived in the past century, most notably QM, which describes the structure of matter on the sub-atomic level; and the theories of special and general relativity (GR), which describe the structure of space-time. The unification of the principles of special relativity and QM, which led to the development of quantum field theories (QFTs), marks the beginning of modern particle physics. A further milestone was the formulation of the SM [13–15], whose predictions have been thoroughly tested with many experiments, most notably a decade of scrutinising its predictions at the Large Hadron Collider (LHC). And with the discovery of the last missing piece in the form of the Higgs boson [16, 17], it might seem that we are very close to understanding the *hidden mystic lore* of Nature.

Given that the SM describes Nature at the smallest scales humans can resolve, one may ask if it is also the foundation of Nature at the largest scales, i.e. does it also describe the Universe as we observe it? Unfortunately, the answer is no, as Fig. 1.1 suggests. Observations of the cosmic microwave background (CMB) anisotropies indicate that 95% of the Universe consist of *dark* substances [12, 18], which are needed to explain the late-time acceleration of the Universe's Hubble flow (roughly 69% in the form of so-called dark energy (DE) or a cosmological constant (CC) Λ; evidence for which was first found from supernova observations [19, 20]), and the excess in gravitational attraction observed on galactic and extragalactic scales (approximately 26% non-relativistic, cold dark matter (DM), see e.g. Refs. [21, 22] for early work on the subject). Moreover, the SM does not exhibit enough charge-parity (CP) violation to understand the origin of the asymmetry between matter and anti-matter necessary to explain the remaining 5% visible matter [23], which otherwise would have annihilated into radiation [24]. It seems, therefore, that *Doktor Faustus* would not be any more appeased – even today. However, while many consider this a crisis, it is precisely this disparity that drives the creativity of an agile community of theoreticians to build models beyond the SM attempting to identify the microscopic properties of the dark forms of energy and matter and unravel the matter–anti-matter asymmetry. Simultaneously, many ambitious experimentalists are testing these models' predictions in order to single out a candidate theory. Although theoretically well motivated, many popular extensions of the SM's particle and symmetry content have

escaped experimental confirmation, putting the guiding principles for constructing such models under pressure. While it is premature to jump to conclusions just yet, it is a timely question if we can find new approaches to model building beyond the SM.

In the present work, we employ the methods common to particle physics, studying the implications of adding a light field to the SM particle content. However, we do so with a field of spin 2. This seemingly simple modification will have profound consequences for the predictions of the resulting model, most prominently it will give us an explanation for the observed late-time acceleration in terms of the spin-2 mass, thereby addressing the so-called the CC problem. We consider this the primary motivation to study such theories. A subject of concern in this yet not fully explored class of modifications is the fact that the gauge symmetry, i.e. our guiding principle to constructing forces from a redundant description of Nature, associated with a field of spin 2 is realised non-linearly. This is no new observation given that GR can be formulated as such a gauge theory of non-linear transformations. In contrast, the gauge symmetries associated with fields of spin 1 typically allow a linear realisation. Consequently, we will have to modify the gravitational sector in order for the resulting theory to remain consistent, such that we are led to a hybrid approach: Having introduced a new particle to the spectrum, we are led to a modification of the predictions in the gravitational sector, already at the classical level. The scope of this thesis is to study the implications of these modifications on various length and energy scales, and in a variety of physical systems.

Historically, the quest for a consistent theory of massive spin-2 fields dates back to the late 1930s, when Fierz and Pauli first wrote down a linearised theory for a massive spin-2 field [25, 26]. While consistent at the linear level, coupling the theory to matter immediately challenged the idea, as it appeared that in the limit where the mass goes to zero, the longitudinal mode still couples to matter in a way that is inconsistent with observations. This is the infamous discontinuity found in 1970 by van Dam, Veltman, and Zakharov (vDVZ) [27, 28]. Most importantly, the bending of light, which is correctly described by GR, challenges the massive spin-2 paradigm. Only two years later, in 1972, Vainshtein conjectured that strong-coupling effects restore GR at small distances. However, the theory was still plagued by a tachyonic degree of freedom, also referred to as the Boulware–Deser (BD) ghost, when non-linearly completed [29, 30]. With this, the idea was buried until the turn of the millennium, when a number of models were proposed to address the weakness of gravity compared to the other known forces in Nature, allowing gravity to protrude into a large extra dimension, see Refs. [31–35] for a selection. While not the primary subject of these models, they did renew the interest in realising a consistent four-dimensional description of a massive spin-2 field, because they give rise to precisely such states. It was not until almost another 40 years after the BD ghost was found, that finally a consistent theory of a massive spin-2 field in four dimesnions had been found in 2010, and the absence of the BD ghost was proven rigorously [36–45] in the model of massive gravity proposed by de Rham, Gabadadze, and Tolley (dRGT).

A curiosity of tensor fields is that a mass term can only be constructed by introducing new fields, changing dimensions, or giving up some fundamental construction principle, such as locality [46, 47]. In this sense it is not only natural, but a requirement to consider settings in which more than one tensor field is present, either as a background or a dynamical field itself. This leads to the notion of bimetric theories of gravity, which make

the background tensor a dynamical field, cf. [48, 49], and which are readily extended to the multi-metric case [50].[2] This suggests a study of bimetric theories of gravity, or bigravity for short, in the spirit of contemporary particle physics, where the particle or symmetry content of the SM is extended and modified, and the phenomenological implications are investigated. Due to the non-linear nature of gravity, this question is much more involved for the spin-2 case. For recent review articles on the subject and beyond, see Refs. [52–54], or Refs. [47, 55] for a broader overview.

In this work, we approach the subject in the spirit of particle physics to assess which phenomenological consequences the presence of massive spin-2 fields in Nature might have. Using available data, the model is put to test and the discussion is founded on neutral grounds, allowing the reader to objectively draw their conclusions. While this is much along the lines of surveys of beyond the SM phenomenology, we frequently make use of the fact that the theory will give rise to modified classical gravitation, and we employ this fact to derive self-consistent background solutions and to find constraints on the allowed values of the model parameters. While the phenomenological consequences discussed here are of classical origin, the initial motivation – the study of a massive spin-2 field – was of quantum nature. It should be noted however, that these modifications present no cure to the non-renormalisability of GR [54].

This manuscript is structured as follows. In Chapter 2 we establish the framework that we will be working in. Starting from a general discussion of spin-2 masses, we outline in detail the construction of the action and show how a consistent theory of massive spin-2 fields is obtained. These procedures are straightforwardly generalised to an arbitrary number of such fields, in any space-time dimension. Furthermore, we discuss two solutions to the modified field equations of the resulting gravitational theory and their implications on the CC problem. In Chapter 3 we introduce the phenomenon of GW oscillations, which originates from the modification of the propagation dynamics in this framework. We highlight the analogy to neutrino oscillations that can be drawn and use the recent observation of gravitational waves (GWs) [56–61] to derive constraints. The subsequent Chapter 4 is concerned with astrophysical implications of massive spin-2 fields. We discuss modifications to both, gravitational lensing and galactic dynamics, and use data to constrain the parameter space. We summarise the results and put them into context in Chapter 5 before concluding in Chapter 6. The Appendices contain supplemental material and detailed calculations whenever skipped in the main body of the text.

Units and conventions. We work in natural units with the speed of light and Planck's constant equal to one, $c = 1 = \hbar$, and with the reduced Planck mass $M_{\rm Pl} \equiv (8\pi G_{\rm N})^{-\frac{1}{2}} \simeq 2 \cdot 10^{18}\,\text{GeV}$ constructed from Newton's constant $G_{\rm N}$. Astrophysical masses are expressed in units of the solar mass $M_\odot = 2.0 \cdot 10^{30}\,\text{kg}$ and we use the $(-+++)$ metric convention. Four-dimensional space-time is labelled by Greek letters, $\mu, \nu, \ldots = 0, 1, 2, 3$, where the spatial components will be distinguished by the Latin letters $i, j, \ldots = 1, 2, 3$. Space-time indices other than in four dimension are capitalised, $M, N = 0, \ldots, d-1$, and local Lorentz indices are denoted as $a, b, \ldots$

[2] While the notion of bimetric theories has been used since the 1970s, see e.g. Ref. [51], we will always refer to the framework proposed by Hassan and Rosen [48].

Chapter 2

Theoretical Foundations

In order to appreciate the complications that were overcome in the historical development of massive gravity, and those that still remain, we begin by outlining how theoretically viable models of massive spin-2 fields can be constructed – first at the linear and later also at the non-linear level. In this quest, we derive the action for bigravity from the discretisation of an extra, space-like dimension, which proves to be not only a simple way to understand the structure of the action, but also highlights possible UV completions of the model. Next, we outline the proof that the action is free of any *a priori* inconsistent ghost degrees of freedom (DOF), i.e. that pathological, tachyonic DOF are absent in the theory. Finally, we study two explicit solutions in Sec. 2.3, a spherically symmetric black hole (BH) solution and a cosmological solution. Both solutions are used to address the long-standing CC problem – the observation that the vacuum energy density associated with the observed CC, $\Lambda M_{\rm Pl}^2 = \rho_{\rm vac}^{\rm obs} = (2 \cdot 10^{-3}\,{\rm eV})^4$ is smaller by many orders of magnitude than the known scales of vacuum energy in Nature set, e.g., by the SM particle masses and the electroweak phase transition from which we would expect $\rho_{\rm vac}^{\rm EW} \sim (100\,{\rm GeV})^4$. While the former BH background solution is not apt to resolve this discrepancy entirely, the latter cosmological solution will highlight one of the main motivations to study massive gravity: late-time acceleration induced by the graviton mass. We closely follow Refs. [53–55], to which we also refer the reader for a pedagogical introduction and a broad overview of the topic. Furthermore, we remark that parts of Sec. 2.3.1 are based on work previously published in Ref. [1], while the cosmological solution presented in Sec. 2.3.2 had already been studied in Ref. [2].

2.1 Historical approaches to massive spin-2 fields

GR was developed from a purely geometrical perspective, demanding invariance under general coordinate transformations [62]. Upon linearisation of the field equations, one obtains the equation of motion (EOM) of a massless field of spin $s = 2$. While this remains the textbook approach to GR, one can reverse the logic and obtain Einstein's field equations as the unique, non-linear completion of the theory of a massless spin-2 field invariant under linear coordinate transformations and coupling to matter in accord with the equivalence principle [53, 55, 63]. Thus, one is led to a theory formulated in

terms of a symmetric tensor field. Starting from this reversed logic, it is of – primarily theoretical – interest to see if such a non-linear completion exists for the massive field of spin $s = 2$.

The earliest attempt to giving a mass m to a spin-2 field $h_{\mu\nu}$ in $3 + 1$ space-time dimensions dates back to the year 1939 and is due to M. Fierz and W. Pauli [25, 26]. They found that, at the level of the quadratic action expanded around the Minkowski background $\eta_{\mu\nu} = \mathrm{diag}(-1, 1, 1, 1)$, the unique and consistent combination of terms is

$$S_{\mathrm{FP}} \supset -\frac{m^2}{8} \int \mathrm{d}^4x \, \left[h_{\mu\nu} h^{\mu\nu} - (h^\mu{}_\mu)^2 \right] , \tag{2.1}$$

which leads to the set of equations [54],

$$(\Box - m^2) h_{\mu\nu} = 0 \, , \quad \partial^\mu h_{\mu\nu} = 0 \, , \quad h \equiv h^\mu{}_\mu = 0 \, , \tag{2.2}$$

where $\Box \equiv -\partial_t^2 + \nabla^2$ is the d'Alembertian and $\nabla_i = \partial_i$ the spatial gradient operator. This set of equations can be summarised as follows. The linearised spin-2 field propagating on flat space follows a simple Klein-Gordon equation, and is transverse and traceless. Therefore, it propagates $10 - 4(\mathrm{transverse}) - 1(\mathrm{traceless}) = 5$ DOF. This is precisely what we expect for the massive spin-2 representation of the Lorentz group: $2s + 1 = 5$.

Given that GR is the unique theory of a *massless* spin-2 field invariant under general, non-linear coordinate transformations [63–66], one is immediately led to the question how to generalise the qudratic mass term (2.3) to a non-linear interaction, and whether the resulting theory is also unique. From our experience with scalar ($\mathcal{L}_\phi \supset \frac{m^2}{2}\phi^2$) and vector fields ($\mathcal{L}_A \supset \frac{m^2}{2} A_\mu A^\mu$), one might be led to the conclusion that the mass term of a tensor should read $\mathcal{L}_g \supset \frac{m^2}{2} g_{\mu\nu} g^{\mu\nu}$, where $g_{\mu\nu} = \eta_{\mu\nu} + h_{\mu\nu}$ is the metric. However, this is nothing but a (cosmological) constant which is non-dynamical. Hence, either some of the principles of constructing the theory (four-dimensional flat space-time, Lorentz invariance, locality etc.) have to be abandoned, or additional (tensor) fields must be introduced [46]. Therefore, a local, Lorentz-invariant non-linear extension of the Fierz-Pauli mass in four dimensions must be a function of $g^{\mu\nu} f_{\mu\nu}$, where f is some reference metric.

Let us try to better understand the structure of the mass term (2.1) by allowing for a different relative factor between the two terms,

$$\mathcal{L}'_{\mathrm{FP}} \supset -\frac{m^2}{8} \left[h_{\mu\nu} h^{\mu\nu} - a \, (h^\mu{}_\mu)^2 \right] , \tag{2.3}$$

where we consider the Lagrangian density instead of the action $S = \int \mathrm{d}^4x \, \mathcal{L}$. It should first be noted that under linearised coordinate transformations, the mass terms (2.1, 2.3) are not invariant. It is a well-known fact from the formulation of the SM, that mass terms of gauge bosons apparently break gauge invariance of the action. Nevertheless, the SM is gauge invariant, while simultaneously giving rise to massive gauge bosons by virtue of the Higgs mechanism [67–70]. While a similar mechanism is, unfortunately, not known for gravity, we may invoke the so-called Stückelberg trick (historically first applied to spin-1 fields [71]) by introducing a field that mimics the linearised gauge transformation

$h_{\mu\nu} \to h_{\mu\nu} + \frac{1}{2}(\partial_\mu \xi_\nu + \partial_\nu \xi_\mu)$ [53]:

$$\mathcal{L}'_{\rm FP} \supset -\frac{m^2}{8}\left[\left(h_{\mu\nu} - 2\partial_{(\mu}A_{\nu)}\right)\left(h^{\mu\nu} - 2\partial^{(\mu}A^{\nu)}\right) - a\left(h^{\mu}{}_{\mu} - \partial^{\mu}A_{\mu}\right)^2\right], \tag{2.4}$$

where $\partial_{(\mu}A_{\nu)} \equiv \frac{1}{2}(\partial_\mu A_\nu + \partial_\nu A_\mu)$ signifies the symmetrisation of indices. In order for Eq. (2.4) to be invariant under a gauge transformation, we demand that the transformation of $h_{\mu\nu}$ is compensated by transforming simultaneously $A_\mu \to A_\mu + \frac{1}{2}\xi_\mu$.[1] Furthermore, we can decompose the spin-1 field A_μ into its transverse and longitudinal modes,

$$A_\mu = \frac{1}{m}A^{\perp}_{\mu} + \frac{1}{m^2}\partial_\mu \chi\,. \tag{2.5}$$

With this decomposition we find for the longitudinal field χ, integrating by parts twice,

$$\mathcal{L}'_{\rm FP} \supset \frac{1}{4\,m^2}\left(\partial_\mu\partial_\nu\chi\,\partial^\mu\partial^\nu\chi + \partial_\nu\partial_\mu\chi\,\partial^\mu\partial^\nu\chi - 2a(\partial_\mu\partial^\mu\chi)^2\right) = \frac{1-a}{2\,m^2}(\Box\chi)^2\,. \tag{2.6}$$

Such higher derivative theories are known to give pathological solutions, as they encompass more than the apparent DOF. In the case of Eq. (2.6), this can be seen by rewriting the Lagrangian as was done in Ref. [53]:

$$\mathcal{L}_{\rm ghost} = \frac{1-a}{2\,m^2}\left(\widehat{\chi}\Box\chi - \frac{1}{4}\widehat{\chi}^2\right). \tag{2.7}$$

Now, $\widehat{\chi}$ acts as a Lagrange multiplier enforcing Eq. (2.6). Diagonalising the kinetic term, $\widehat{\chi} = \phi_1 - \phi_2$ and $\chi = \phi_1 + \phi_2$, makes the issue apparent:

$$\mathcal{L}_{\rm ghost} = \frac{1-a}{2\,m^2}\left(\phi_1\Box\phi_1 - \phi_2\Box\phi_2 - \frac{1}{4}(\phi_1 - \phi_2)^2\right). \tag{2.8}$$

There are two DOF, one of which has a *negative* kinetic term, unless $a = 1$ in order to eliminate the pathology. This statement remains true, even if a different field parametrisation is chosen [72]. Therefore, we see that only the Fierz-Pauli mass term eliminates the spurious and pathological DOF.

Even before a non-linear description was found, it was realised by van Dam, Veltman, and Zakharov (vDVZ) that the mass term in Eq. (2.1) is problematic when coupled to matter [27, 28]. We can investigate this by adding a matter coupling of the form

$$S_{\rm matter} = \int \mathrm{d}^4x\, h_{\mu\nu}T^{\mu\nu} \tag{2.9}$$

to Eq. (2.1), where $T^{\mu\nu}$ is an energy momentum tensor (EMT). The linearised EOM

[1] This construction can also be understood in terms of a redefined background, $\eta_{\mu\nu} \to \eta_{\mu\nu} - 2\partial_{(\mu}A_{\nu)}$, which can be generalised non-linearly to $\eta_{\mu\nu} \to \partial_\mu\phi^a\partial_\nu\phi^b\eta_{ab} \equiv f_{\mu\nu}$ [53]. Thus, choosing a background f is equivalent to fixing a gauge in the Stückelberg language.

read[2] [54, 74]

$$\mathcal{E}^{\alpha\beta}_{\mu\nu} h_{\alpha\beta} + \frac{m^2}{2}(h_{\mu\nu} - h\,\eta_{\mu\nu}) = \frac{1}{M_{\rm Pl}} T_{\mu\nu}\,, \tag{2.10}$$

where $h \equiv h^{\mu}{}_{\mu}$, and the so-called Lichnerowicz operator $\mathcal{E}$ follows from the linearisation of the Einstein tensor around the Minkowski background $\eta_{\mu\nu}$.

Assuming the source term on the right-hand side to be conserved, $\partial^{\mu} T_{\mu\nu} = 0$, we can take derivatives of Eq. (2.10) to find $h = -\frac{2}{3}\frac{T}{m^2 M_{\rm Pl}^2}$, which can be used in (2.10) to obtain the generalisation of Eqs. (2.2) [54, 74]:

$$(\Box - m^2) h_{\mu\nu} = -\frac{1}{M_{\rm Pl}}\left(T_{\mu\nu} - \frac{1}{3} T \eta_{\mu\nu}\right) - \frac{1}{3}\frac{\partial_\mu \partial_\nu T}{m^2 M_{\rm Pl}}\,. \tag{2.11}$$

Expanding h in Fourier modes, $h(x) = (2\pi)^{-4} \int \mathrm{d}^4 k\; e^{i k_\mu x^\mu} \widehat{h}(k)$, and analogously for T, one can construct the graviton propagator by the Green's function method, such that

$$\widehat{h}_{\mu\nu} = \widehat{D}^{(m)}_{\mu\nu\rho\sigma} \frac{\widehat{T}^{\rho\sigma}}{M_{\rm Pl}}\,. \tag{2.12}$$

The momentum-space propagator is found to be [74]

$$\widehat{D}^{(m)}_{\mu\nu\rho\sigma} = \frac{1}{k^2 + m^2}\left(\eta_{\rho\mu}\eta_{\sigma\nu} + \eta_{\rho\nu}\eta_{\sigma\mu} - \frac{2}{3}\eta_{\rho\sigma}\eta_{\mu\nu} - \frac{2}{3}\eta_{\rho\sigma}\frac{k_\mu k_\nu}{m^2}\right)\,. \tag{2.13}$$

This should be compared to the zero mass propagator which, up to gauge-dependent terms that are irrelevant for tree-level calculations, reads

$$\widehat{D}^{(0)}_{\mu\nu\rho\sigma} \simeq \frac{1}{k^2}\left(\eta_{\rho\mu}\eta_{\sigma\nu} + \eta_{\rho\nu}\eta_{\sigma\mu} - \eta_{\rho\sigma}\eta_{\mu\nu}\right)\,. \tag{2.14}$$

In order to obtain the classical potential, one computes the amplitude for the exchange of a graviton between two sources, say two resting masses ${T_{1,2}}^{\mu}{}_{\nu} = \mathrm{diag}(M_{1,2}, 0, 0, 0)$ separated by a distance r,

$$\mathcal{A}^{(m)}(x) = \int \mathrm{d}^4 x'\, {T_1}^{\mu\nu}(x) D^{(m)}_{\mu\nu\rho\sigma}(x - x') {T_2}^{\rho\sigma}(x')\,. \tag{2.15}$$

It was found by van Dam, Veltman, and Zakharov in Refs. [27, 28] that in the linearised theory the limit $m \to 0$ is not continuous. This is the so-called vDVZ discontinuity [30, 74]:

$$\lim_{m\to 0} \mathcal{A}^{(m)} = \frac{4}{3}\mathcal{A}^{(0)} = -\frac{4}{3}\frac{G_{\rm N}\, M_1\, M_2}{r}\,. \tag{2.16}$$

This unacceptably large deviation from GR is readily excluded by solar system tests, or, upon rescaling $G_{\rm N}$ by an appropriate factor, by the measured light deflection angle which agrees well with GR [75, 76]. The reason for this discrepancy lies, once again, in the coupling of the scalar χ, which becomes a dynamical field only by mixing with the

[2] Notice that one power of $M_{\rm Pl}$ is absorbed into $h_{\mu\nu}$ in order to give it the canonical mass dimension one. Moreover, one obtains $\mathcal{E}^{\alpha\beta}_{\mu\nu} h_{\alpha\beta} = -\frac{1}{2}\left[\partial_\mu\partial_\nu h + \Box h_{\mu\nu} - \partial_\rho\partial_\mu h^{\rho}{}_{\nu} - \partial_\rho\partial_\nu h^{\rho}{}_{\mu} + \eta_{\mu\nu}(\partial^\rho\partial^\sigma h_{\rho\sigma} - \Box h)\right]$ on a flat background, see e.g. Ref. [73].

tensor field $h_{\mu\nu}$. This is rooted in the fact that the mass term (2.1) gives rise only to higher time-derivatives of χ, which are eliminated by the Fierz-Pauli choice, cf. Eq. (2.6). Indeed, the full Lagrangian (2.4) including a matter coupling (for $a = 1$) is found to be [53]

$$\begin{aligned}\mathcal{L}_{\rm FP} = &-\frac{1}{4}h^{\mu\nu}\mathcal{E}^{\alpha\beta}_{\mu\nu}h_{\alpha\beta} - \frac{m^2}{8}\left[h_{\mu\nu}h^{\mu\nu} - h^2\right] + \frac{1}{2M_{\rm Pl}}h_{\mu\nu}T^{\mu\nu} - \\ &-\frac{1}{8}F^{\mu\nu}F_{\mu\nu} - \frac{m}{2}\left[h^{\mu\nu} - h\,\eta^{\mu\nu}\right]\partial_{(\mu}A_{\nu)} - \\ &-\frac{1}{2}h^{\mu\nu}\left[\partial_\mu\partial_\nu - \eta_{\mu\nu}\Box\right]\chi\,,\end{aligned} \tag{2.17}$$

and we observe that only the mixing with $h_{\mu\nu}$ renders χ dynamical. Redefining $h_{\mu\nu} = \tilde{h}_{\mu\nu} - \chi\,\eta_{\mu\nu}$ allows us to diagonalise the kinetic terms at the price of coupling χ to the trace of the EMT (for clarity we disregard the vector A_μ which does not couple to a conserved EMT at this level) [53]:

$$\begin{aligned}\mathcal{L}_{\rm FP} = &-\frac{1}{4}\tilde{h}^{\mu\nu}\mathcal{E}^{\alpha\beta}_{\mu\nu}\tilde{h}_{\alpha\beta} - \frac{m^2}{8}\left[\tilde{h}_{\mu\nu}\tilde{h}^{\mu\nu} - \tilde{h}^2\right] + \frac{1}{2M_{\rm Pl}}\tilde{h}_{\mu\nu}T^{\mu\nu} - \\ &-\frac{3}{4}(\partial_\mu\chi)(\partial^\mu\chi) + \frac{3}{2}m^2\chi^2 + \frac{3}{2}m^2\chi\,\tilde{h} - \frac{1}{2M_{\rm Pl}}\chi\,T\,,\end{aligned} \tag{2.18}$$

with $T \equiv \eta_{\mu\nu}T^{\mu\nu}$. From this form of the Lagrangian, one can deduce that $\tilde{h}_{\mu\nu}$ will give rise to the transverse traceless (TT) helicity-2 state, A_μ is the helicity-1 mode, and χ is the longitudinal, helicity-0 mode [77]. Clearly, the limit $m \to 0$ does *not* decouple the helicity-0 mode which is the origin of the vDVZ discontinuity found in Eq. (2.16).

This first drawback for a massive spin-2 theory was, however, quickly overcome by the investigations of A. Vainshtein [78], who conjectured, that in the limit $m \to 0$, the longitudinal mode is strongly coupled, precisely to restore a smooth limit to GR. For a detailed and thorough introduction to the Vainshtein mechanism we refer the interested reader to the literature [79–92], see also Ref. [74] for an introduction. To understand the Vainshtein mechanism, it is convenient to employ a decoupling limit [74],

$$M_{\rm Pl} \to \infty, \quad m \to 0\,, \quad \text{keeping} \quad \Lambda_n = \left(M_{\rm Pl}\,m^{n-1}\right)^{\frac{1}{n}} = \text{const}, \quad \frac{T_{\mu\nu}}{M_{\rm Pl}} = \text{const}\,. \tag{2.19}$$

Moreover, one retains in the action only quadratic terms in the helicity-2 mode, but non-linear terms of the helicity-0 mode, which are suppressed by powers of the strong-coupling scale Λ_n. The integer n depends on the structure of the action, most importantly $n = 3$ yields the lowest scale Λ_n for the cases we discuss in this thesis [36]. See also Refs. [53, 93, 94] for further discussions.

While we will see how the Vainshtein mechanism operates in a concrete setting in Sec. 2.3.1, a general discussion is very difficult and beyond the scope of this work. However, the equations governing the dynamics of the perturbations in the decoupling limit on some background generally take the form [74]

$$\overline{\mathcal{E}}^{\alpha\beta}_{\mu\nu}\tilde{h}_{\alpha\beta} = \frac{T_{\mu\nu}}{M_{\rm Pl}}\,, \quad 3\Box\chi + \mathcal{F}^{\rm NL}_\chi = \frac{T}{M_{\rm Pl}}\,, \tag{2.20}$$

with $\overline{\mathcal{E}}$ generalising the Lichnerowicz operator, and where $\mathcal{F}_\chi^{\rm NL}$ is some complicated, non-linear function whose terms are suppressed by powers of Λ_n, e.g. in the cases relevant for us [53],

$$\mathcal{F}_\chi^{\rm NL} \sim \Lambda_3^{-3}\partial_\mu\partial_\nu\chi(\eta^{\mu\nu}\Box - \partial^\mu\partial^\nu)\chi + \Lambda_3^{-6}\dots \tag{2.21}$$

In the limit of small momenta (large distances) the non-linearities will be suppressed by powers of (k/Λ_3), where k is the momentum scale. By virtue of Eqs. (2.20), we observe that $\mathcal{F}_\chi^{\rm NL} \ll \Box\chi$ and $\chi \sim T \sim \tilde{h}$. It is therefore found that, in this limit, the physical metric perturbation will be a composition of helicity-2 and helicity-0 modes [74],

$$h_{\mu\nu} = \tilde{h}_{\mu\nu} - \eta_{\mu\nu}\,\chi - \frac{\partial_\mu\chi\,\partial_\nu\chi}{\Lambda_3^3}\,, \tag{2.22}$$

and the theory is in the regime where the graviton is genuinely massive.

The Vainshtein mechanism will operate once the non-linearities in $\mathcal{F}_\chi^{\rm NL}$ become relevant. To this end, we need to introduce some non-trivial background other than flat space. Suppose that $\chi = \overline{\chi} + \delta\chi$, and $T = \overline{T} + \delta T$, e.g. a point mass $\overline{T} = \delta^{(3)}(\vec{r})M$. Then, terms of the form $\Lambda_3^{-3}\partial^2\overline{\chi}$ will become large, while the perturbations remain small, and we can expand the χ-part of the Lagrangian corresponding to Eq. (2.20) schematically as [55]

$$\mathcal{L} \supset -\frac{3}{4}\left(1 + \frac{(\partial^2\overline{\chi})}{\Lambda_3^3} + \frac{(\partial^2\overline{\chi})^2}{\Lambda_3^6} + \dots\right)(\partial_\mu\delta\chi)(\partial^\mu\delta\chi) - \frac{1}{2M_{\rm Pl}}\delta\chi\,\delta T\,. \tag{2.23}$$

Normalising canonically, we obtain

$$\mathcal{L} \supset -\frac{1}{2}(\partial_\mu\delta\chi)(\partial^\mu\delta\chi) - \frac{1}{3M_{\rm Pl}}\frac{\delta\chi\,\delta T}{\sqrt{1 + \frac{(\partial^2\overline{\chi})}{\Lambda_3^3} + \frac{(\partial^2\overline{\chi})^2}{\Lambda_3^6} + \dots}}\,, \tag{2.24}$$

and the decoupling is manifest: In the limit where $k \to \infty$, the non-linear term becomes dominant and the helicity-0 mode turns out to be subdominant in Eq. (2.22), $\chi \ll T$. Thus, the physical perturbation is purely helicity-2, $h_{\mu\nu} = \tilde{h}_{\mu\nu}$, and GR is restored.

While this resolves the issues posed by the vDVZ discontinuity, it was quickly realised that non-linear generalisations of the Fierz-Pauli action (2.1) are plagued by a ghostly DOF that tends to destabilise the theory. We have already encountered this ghost at the linear level when we allowed for a deviation from the Fierz-Pauli mass, cf. Eq. (2.3).[3] With the work of Boulware and Deser in the 1970s [29, 30] a non-linear extension seemed doomed to failure, because they could argue that the ghost would reenter at each non-linear level; see also Ref. [95] for examples. However, it turns out that a loophole in the argument exists, which allows one to construct a consistent non-linear interaction term that gives rise to Eq. (2.1) when linearised, as we will see in Sec. 2.2.3. One can now appreciate the obstacles one is facing in the construction of a consistent theory of a massive spin-2 field: The scalar mode does not come with a canonical kinetic term, as its purely derivative interactions are pathological and need to be removed. What remains

[3] Another way to see the appearance of this ghost DOF is in the decoupling limit studied above, where the interactions suppressed by a scale Λ_5 turn out to be pathological, see Ref. [93]. Initially, the interactions we derive in Sec. 2.2 were chosen such that in the decoupling limit these terms vanish identically.

is the mixing with the tensor mode, which in turn is the key to the Vainshtein effect. Ensuring that the mixing does not induce new, ghost-like DOF is a difficult task. We now depart from the historical path and construct such a consistent theory which evades all of these inconsistencies and return to this discussion in Sec. 2.2.3.

2.2 From general relativity to massive gravity

In this section we derive the action for bigravity from the discretisation of an extra, space-like dimension, often referred to as dimensional deconstruction [96–105]. We choose this ansatz, because it allows the inclined reader to appreciate the structure of the interactions giving rise to a mass term, and how they could originate from a more fundamental theory. The reader who is not interested in such a derivation can safely skip the following subsection. For a more detailed discussion of the aspects discussed here, we refer to Appendix B.1 and Refs. [73, 106, 107], which also form the basis of this section.

2.2.1 An excursion to extra dimensions

To start with, we recall that GR is a theory of a dynamical rank-2 tensor $g_{\mu\nu}$. It can be formulated through an action principle, via the Einstein-Hilbert action,

$$S = S_{\rm EH} + S_m = \frac{M_{\rm Pl}^2}{2}\int \mathrm{d}^4x\,\sqrt{-\det g}\,R + \int \mathrm{d}^4x\,\sqrt{-\det g}\,\mathcal{L}_m\,, \tag{2.25}$$

where R is the Ricci scalar and $\mathcal{L}_m$ a matter Lagrangian. Varying this action with respect to (w.r.t.) $g_{\mu\nu}$ leads to the Einstein field equations,[4]

$$R_{\mu\nu} - \frac{1}{2}R\,g_{\mu\nu} = \frac{1}{M_{\rm Pl}^2}T_{\mu\nu}\,, \tag{2.26}$$

with the matter EMT $T_{\mu\nu}$ is defined as

$$T_{\mu\nu} = -\frac{2}{\sqrt{-g}}\frac{\delta(\sqrt{-g}\mathcal{L}_m)}{\delta g^{\mu\nu}}\,, \tag{2.27}$$

where $\sqrt{-g}$ is short for $\sqrt{-\det g}$.

In the textbook formulation of GR, see e.g. [73, 107, 110, 111], all geometrical quantities are formulated in terms of coordinates. For example, we write down a metric in a specified

[4] This can be seen as follows:

$$\delta\int \mathrm{d}^4x\,\sqrt{-g}R_{\mu\nu}g^{\mu\nu} = \int \mathrm{d}^4x\,\left[\left(\delta\sqrt{-g}\right)R + \sqrt{-g}(\delta R_{\mu\nu})g^{\mu\nu} + \sqrt{-g}R_{\mu\nu}\delta g^{\mu\nu}\right]$$

Using that $g_{\mu\nu}g^{\mu\nu} = 4$, from which it follows that $\delta g^{\mu\nu} = -g^{\mu\alpha}\delta g_{\alpha\beta}g^{\beta\nu}$, it is straightforward to show that $\delta\sqrt{-g} = -\frac{1}{2}\sqrt{-g}\,g_{\mu\nu}\delta g^{\mu\nu}$ (see also Appendix A.1). The final ingredient is the observation that $g^{\mu\nu}\delta R_{\mu\nu} = \nabla^\alpha\left[\nabla^\beta(\delta g_{\alpha\beta}) - g^{\gamma\delta}\nabla_\alpha(\delta g_{\gamma\delta})\right]$ is a total derivative [73]. Thus, we see that $\delta S_{\rm EH} = \int \mathrm{d}^4x\,\sqrt{-g}\left(R_{\mu\nu} - \frac{1}{2}Rg_{\mu\nu}\right)\delta g^{\mu\nu}$ plus a boundary term, which we will not consider in this thesis. See Refs. [55, 73] for a discussion of this issue and how to resolve it via the so-called Gibbons-Hawking-York boundary term [108, 109].

coordinate system, and compute the Christoffel symbols via

$$\Gamma^{\mu}{}_{\alpha\beta} = \frac{g^{\mu\nu}}{2}\left(\partial_\alpha g_{\nu\beta} + \partial_\beta g_{\alpha\nu} - \partial_\nu g_{\alpha\beta}\right). \tag{2.28}$$

This specific choice of *connection*, the Levi-Cività connection, is compatible with the metric, in the sense that the covariant derivative of the metric vanishes,

$$\nabla_\sigma g_{\mu\nu} = \partial_\sigma g_{\mu\nu} - \Gamma^{\alpha}{}_{\sigma\mu} g_{\alpha\nu} - \Gamma^{\alpha}{}_{\sigma\nu} g_{\mu\alpha} = 0\,. \tag{2.29}$$

In fact, this equation uniquely determines the connection to have the specified form Eq. (2.28). The notion of curvature is subsequently introduced via the parallel transport of a vector around a closed curve, or in differential language as the commutator of two (co-)variant derivatives acting on a covector,

$$[\nabla_\mu, \nabla_\nu]\omega_\rho \equiv R_{\mu\nu\rho}{}^{\sigma}\omega_\sigma \quad \text{or} \quad [\nabla_\mu, \nabla_\nu]v^\rho \equiv R^{\rho}{}_{\sigma\mu\nu}v^\sigma\,. \tag{2.30}$$

Going through the algebra one can see that in terms of the connection,

$$R_{\mu\nu\rho}{}^{\sigma} = \partial_\nu \Gamma^{\sigma}{}_{\mu\rho} - \partial_\mu \Gamma^{\sigma}{}_{\nu\rho} + \Gamma^{\alpha}{}_{\mu\rho}\Gamma^{\sigma}{}_{\alpha\nu} - \Gamma^{\alpha}{}_{\nu\rho}\Gamma^{\sigma}{}_{\alpha\mu}\,. \tag{2.31}$$

Expressed in this manner, we can directly infer that $R_{\mu\nu\rho\sigma} = -R_{\nu\mu\rho\sigma} = -R_{\mu\nu\sigma\rho} = R_{\rho\sigma\mu\nu}$. Moreover, we can finally construct the Ricci tensor $R_{\mu\nu} = R_{\mu\sigma\nu}{}^{\sigma}$ and the Ricci scalar $R = R_{\mu\nu}g^{\mu\nu}$. These are the quantities that describe the curvature of space-time and relate them to matter via Eq. (2.26).

At this point, we stress that while very convenient for practical calculations, the coordinate base method for computing the geometrical quantities has its limitations. A more elegant way to derive the quantities of interest and perform the deconstruction of the extra dimension is the vielbein method, which was first applied to GR by H. Weyl in 1929 (cf. Ref. [112]). As we will see shortly, this approach highlights the formulation of GR as a gauge theory with local Lorentz invariance. Although we will ultimately be interested in a five-dimensional action, let us consider a general number of space-time dimensions. Here and in what follows, we use the convention that Greek letters label the four-dimensional space-time indices, $\mu = 0, 1, 2, 3$, while capital Roman letters stand for the $d > 4$ space time coordinates, $M = 0, \ldots, d-1$. Lower case Roman letters represent the local Minkowski space.

Vielbein method. The generalisation of the coordinate method we seek is one in which the local Lorentz structure of space-time is manifest. To do so, we consider a orthonormal set of basis covectors, or one-forms, $\{\boldsymbol{e}^a\}$, labelled by $a = 0, \ldots, d-1$, such that we can express each covector as a linear combination of the $\boldsymbol{e}^a$. In general, this basis will *not* be a coordinate basis, as can be seen by assuming the contrary. For a coordinate basis in a given coordinate system $\{x^M\}$, we have

$$\boldsymbol{e}^a = \mathrm{d}x^a \quad \Rightarrow \quad e^{a}{}_{M} = \frac{\partial x^a}{\partial x^M} \quad \Rightarrow \quad \partial_N e^{a}{}_{M} = \partial_M e^{a}{}_{N}\,. \tag{2.32}$$

Thus, we find that if the components of $\boldsymbol{e}^a$ in a coordinate system satisfy $\partial_{[M}e^a{}_{N]} \equiv \frac{1}{2}(\partial_M e^a{}_N - \partial_N e^a{}_M) \neq 0$, $\boldsymbol{e}^a \equiv e^a_M(x)\mathrm{d}x^M$ will not be a coordinate basis at a specified point of space-time [107]. Due to the orthonormality, we can define the inverse to the matrix $e^a{}_M(x)$ at every point in space-time, such that

$$e^a{}_M e_b{}^M = \delta^a_b \quad \text{and} \quad e_a{}^N e^a{}_M = \delta^N_M \,, \tag{2.33}$$

and we can express vectors, covectors and more general tensors in terms of the newly chosen basis, e.g. for a vector $V = V^M\partial_M = V^a\boldsymbol{e}_a$ with $\boldsymbol{e}_a = e_a{}^M\partial_M$ and $V^a = V^M e^a{}_M$; and furthermore, we can express $\mathrm{d}x^M = e_a{}^M\boldsymbol{e}^a$.

Most importantly, however, we can express the invariant line element in this basis as

$$\mathrm{d}s^2 = g_{MN}\,\mathrm{d}x^M\mathrm{d}x^N = g_{MN}\,e_a{}^M e_b{}^N \boldsymbol{e}^a\boldsymbol{e}^b \equiv g_{ab}\,\boldsymbol{e}^a\boldsymbol{e}^b \,, \tag{2.34}$$

where we have used that $\boldsymbol{e}^a = e^a{}_M\mathrm{d}x^M$ and $e_a{}^M e^a{}_N = \delta^M_N$. A rather natural choice for the basis is such that the underlying symmetry is manifest, i.e. that the metric coefficients in the vielbein basis are those of the Minkowski metric in d dimensions, $g_{ab} = \eta_{ab} = \mathrm{diag}(-1,+1,\ldots,+1)$, or

$$g_{MN} = e^a{}_M e^b{}_N \eta_{ab} \,. \tag{2.35}$$

A final remark should be made concerning the uniqueness of this basis. By definition, a Lorentz transformation is a transformation that leaves η invariant. Therefore, if $\boldsymbol{e}^a$ satisfies Eq. (2.35), so will $\boldsymbol{e}^{a\prime} = \Lambda^a{}_b\boldsymbol{e}^b$ by virtue of the identity $\Lambda^a{}_b\eta_{ac}\Lambda^c{}_d = \eta_{bd}$. Thus, Lorentz invariance is manifestly implemented as a local redundancy in the description of the the dynamical variables given by the vielbeins $\boldsymbol{e}^a$, i.e. a gauge symmetry.

Let us proceed to write down the desired expressions relating to the curvature. The first step is, of course, to find a connection compatible with the metric. We define the connection one-form [73]

$$\begin{aligned} \Omega^{ab}{}_M &\equiv e^a{}_N\nabla_M e^{b\,N} && \text{(2.36a)} \\ &= \nabla_M \underbrace{(e^a{}_N e^{b\,N})}_{e^a{}_N e^b{}_L g^{NL}} - e^{b\,N}\nabla_M e^a{}_N \\ &= -\Omega^{ba}{}_M \,. && \text{(2.36b)} \end{aligned}$$

Here, the antisymmetry is implied by the definition of the vielbeins (2.35), and employing the compatibility condition $\nabla_L g_{MN} = 0$. Conversely, imposing the antisymmetry of ω, as in Eq. (2.36b), is sufficient to guarantee the compatibility of the covariant derivative and the metric [73].

There is another way to express the connection one-form which implements the requirement that the covariant derivative be torsion-free. We first note that $\nabla_{[M}e^a{}_{N]} = \eta^{ab}e_{b\,[M}\Omega^{ab}{}_{N]}$ and that for a torsion-free connection, this should equal [73]

$$\nabla_{[M}e^a{}_{N]} = e_{b\,[M}\Omega^{ab}{}_{N]} \overset{!}{=} \partial_{[M}e^a{}_{N]} \,. \tag{2.37}$$

In this way, we can express the components as in Ref. [53]:

$$\Omega^{ab}{}_M = \frac{1}{2} e^c{}_M \left(O^{ab}{}_c - O_c{}^{ab} - O^a{}_c{}^b \right), \tag{2.38}$$

where $O^{ab}{}_c \equiv 2e^{aA} e^{bB} \partial_{[A} e_{B]c}$. Reverting to the description in the language of differential forms, we find

$$\boldsymbol{e}^a = e^a{}_M \mathrm{d}x^M \quad \text{and} \quad \boldsymbol{\Omega}^{ab} = \Omega^{ab}{}_M \mathrm{d}x^M \,. \tag{2.39}$$

Using this, we can express Eq. (2.37) more compactly as $\mathrm{d}\boldsymbol{e}^a = \boldsymbol{e}^b \wedge \boldsymbol{\Omega}^a{}_b$.

This allows us to define a covariant derivative of a one-form $\boldsymbol{\xi}$, $D\boldsymbol{\xi} \equiv \mathrm{d}\boldsymbol{\xi} + \boldsymbol{\Omega} \wedge \boldsymbol{\xi}$, which defines the (matrix-valued) two-form Riemann curvature [73],

$$\boldsymbol{R}^{ab} = (D\boldsymbol{\Omega})^{ab} = \mathrm{d}\boldsymbol{\Omega}^{ab} + \boldsymbol{\Omega}^a{}_c \wedge \boldsymbol{\Omega}^{cb} \,. \tag{2.40}$$

Notice the analogy to the field strength tensor of non-Abelian gauge theories.[5] From Eq. (2.40) we can always revert to the coordinate basis formulation via

$$R^M{}_{NLK} = e^M{}_a e^b{}_N R^a{}_{bLK}. \tag{2.41}$$

We are now in a position to write down the d-dimensional action with the conventions of Ref. [113]:

$$\begin{aligned}
S^{(d)}_{\mathrm{EH}} &= \frac{M_d^{d-2}}{4(d-2)!} \int \varepsilon_{a_1 a_2 a_3 \ldots a_d} \boldsymbol{R}^{a_1 a_2} \wedge \overbrace{\boldsymbol{e}^{a_3} \wedge \ldots \wedge \boldsymbol{e}^{a_d}}^{(d-2) \text{ factors}} \\
&= \frac{M_d^{d-2}}{4(d-2)!} \int \varepsilon_{a_1 a_2 a_3 \ldots a_d} R^{KL}{}_{M_1 M_2} e^{a_1}_K e^{a_2}_L e^{a_3}_{M_3} \ldots e^{a_d}_P \, \mathrm{d}x^{M_1} \wedge \ldots \wedge \mathrm{d}x^{M_d} \\
&= \frac{M_d^{d-2}}{4(d-2)!} \int \underbrace{\varepsilon_{KLM_3 \ldots M_d} \varepsilon^{M_1 M_2 \ldots M_d}}_{= 2!(d-2)! (\delta^{M_1}_K \delta^{M_2}_L - \delta^{M_1}_L \delta^{M_2}_K)} \det(e) \, R^{KL}{}_{M_1 M_2} \, \mathrm{d}x^1 \wedge \ldots \wedge \mathrm{d}x^d \\
&\overset{\rightarrow}{=} \frac{M_d^{d-2}}{2} \int \mathrm{d}^d x \, \sqrt{-\det g} \; {}^{(d)}R(g) \,,
\end{aligned} \tag{2.42}$$

with the d-dimensional Ricci scalar ${}^{(d)}R$ and $\det(e) \equiv \varepsilon_{a_1 a_2 \ldots a_d} e^{a_1}{}_1 e^{a_2}{}_2 \cdots e^{a_d}{}_d = \sqrt{-\det g}$.[6] To arrive at the last equality, we used that $R_{KLMN} = -R_{LKMN} = -R_{KLNM} = R_{MNKL}$ and the contraction properties of the d-dimensional totally antisymmetric tensor $\varepsilon_{AB \ldots C}$.

Deconstruction of an extra dimension. Let us now go to $d = 5$ and decompose the action into a 4D action and the remaining fifth dimension, which is then discretised following the procedure presented in Ref. [113]. In doing so we assume that some compactification is applied to the fifth dimension, for definiteness we assume periodic boundary conditions, e.g. $x^4 + L = x^4$. To make the distinction clear, we write $A = 0, \ldots 4$ for a Lorentz index that runs through all five dimensions, and which are associated with

[5] To draw this analogy, notice that the lower case latin letters correspond to the gauge group indices, while the capital letters are the space-time indices.

[6] This last equality holds because by definition $\det g = \det(e^T \, \eta \, e) = (\det e)^2 \, \det \eta = -(\det e)^2$.

tensors named in capital letters, while $a = 0, \dots 3$ is attached to lower case, 4D tensors (the Riemann tensor is an exception to this rule, as it is conventionally written as capital R it will be distinguished by a superscript). Moreover, let us abbreviate $x^4 = y$, and fix a gauge such that, in the metric language, $g_{55} = 1$ and $g_{5\mu} = 0$, or

$$G_{MN}\mathrm{d}x^M\mathrm{d}x^N = \mathrm{d}y^2 + g_{\mu\nu}(x,y)\mathrm{d}x^\mu\mathrm{d}x^\nu \quad \Leftrightarrow \quad \boldsymbol{E}^A = \left(e^a_\mu \mathrm{d}x^\mu, \mathrm{d}y\right)^T . \tag{2.43}$$

Furthermore, we choose six of the remaining Lorentz transformations such that the y-component of the connection one-form reads $\Omega^{ab}{}_5 = \frac{1}{2}(e^{a\mu}\partial_y e^b{}_\mu - e^{b\mu}\partial_y e^a{}_\mu) = 0$. Defining the $d = 4$ Riemann curvature two-form ${}^{(4)}\boldsymbol{R}^{ab} = \mathrm{d}\boldsymbol{\omega}^{ab} + \boldsymbol{\omega}^a{}_c \wedge \boldsymbol{\omega}^{cb}$ constructed from the 4D connection $\boldsymbol{\omega}^{ab}$, and introducing the extrinsic curvature

$$K_{\mu\nu} \equiv \frac{1}{2}\partial_y g_{\mu\nu} = \frac{1}{2}\partial_y(e^a{}_\mu e^b{}_\nu \eta_{ab}) = \frac{1}{2}(e^a{}_\mu \partial_y e^b{}_\nu + e^b{}_\nu \partial_y e^a{}_\mu)\eta_{ab}\,, \tag{2.44}$$

we decompose

$$\boldsymbol{\Omega}^{ab} = \boldsymbol{\omega}^{ab} + \Omega^{ab}{}_5 \mathrm{d}y\,, \tag{2.45a}$$

$$\boldsymbol{\Omega}^{5a} = \boldsymbol{K}^a = K_{\mu\nu}e^{a\nu}\mathrm{d}x^\mu = \frac{1}{2}(e^{b\nu}\partial_y e^a{}_\nu + e^{a\nu}\partial_y e^b{}_\nu)e_{b\mu}\mathrm{d}x^\mu = -\boldsymbol{\Omega}^{a5}\,, \tag{2.45b}$$

$${}^{(5)}\boldsymbol{R}^{ab} = {}^{(4)}\boldsymbol{R}^{ab} - \boldsymbol{K}^a \wedge \boldsymbol{K}^b - \partial_y \boldsymbol{\omega}^{ab} \wedge \mathrm{d}y\,, \tag{2.45c}$$

$${}^{(5)}\boldsymbol{R}^{5a} = \mathrm{d}\boldsymbol{K}^a - \partial_y \boldsymbol{K}^a \wedge \mathrm{d}y + \boldsymbol{\omega}^a{}_b \wedge \boldsymbol{K}^b\,, \tag{2.45d}$$

where in the last line it is understood that $\mathrm{d}\boldsymbol{K}^a = \partial_\mu K^a{}_\nu \mathrm{d}x^\mu \wedge \mathrm{d}x^\nu$ is the exterior derivative in $d = 4$. Assembling the terms and integrating by parts once, one arrives at [113]

$$S^{(5)}_{\mathrm{EH}} = \frac{M_5^3}{4}\int \varepsilon_{abcd}\Big({}^{(4)}\boldsymbol{R}^{ab} \wedge \boldsymbol{e}^c \wedge \boldsymbol{e}^d - \boldsymbol{K}^a \wedge \boldsymbol{K}^b \wedge \boldsymbol{e}^c \wedge \boldsymbol{e}^d + \\ + 2\boldsymbol{K}^a \wedge \partial_y \boldsymbol{e}^b \wedge \boldsymbol{e}^c \wedge \boldsymbol{e}^d\Big) \wedge \mathrm{d}y \tag{2.46a}$$

$$\stackrel{\rightarrow}{=} \frac{M_5^3}{2}\int \mathrm{d}^4x\,\mathrm{d}y\left({}^{(4)}R + (K^\mu{}_\mu)^2 - K^{\mu\nu}K_{\nu\mu}\right). \tag{2.46b}$$

One could have arrived at Eq. (2.46b) without introducing the vielbein formalism; however, it turns out that the discretisation we now carry out yields a viable result only at the vielbein level and *not* at the metric level, since we would have to deal with the square root of the metric. This is an important observation made in Ref. [113], from which we also adopt the discretisation scheme below. Allowing y to take two distinct values, we arrive at a two-site model: $e^a{}_\mu(x,y) \mapsto e^{(i)\,a}{}_\mu(x)$, with $i = 1, 2$. We now discretise the above quantities using an inverse length scale $m \sim L^{-1}$,

$$\partial_y e^a{}_\mu \mapsto m\,(e^{(2)\,a}{}_\mu - e^{(1)\,a}{}_\mu) \quad \text{on site 1,} \quad m\,(e^{(1)\,a}{}_\mu - e^{(2)\,a}{}_\mu) \quad \text{on site 2,} \tag{2.47a}$$

$$\Omega^{ab}{}_5 = 0 \mapsto e^{(1)\,a\mu}\,e^{(2)\,b}{}_\mu = e^{(1)\,b\mu}\,e^{(2)\,a}{}_\mu\,, \tag{2.47b}$$

$$\boldsymbol{K}^a \mapsto m(\boldsymbol{e}^{(2)\,a} - \boldsymbol{e}^{(1)\,a})\,, \tag{2.47c}$$

$$\int \mathrm{d}y\, f(x,y) \mapsto \frac{1}{m}\sum_{j=1}^{2} f_j(x)\,, \tag{2.47d}$$

where Eq. (2.47a) implements the periodicity in y in the discretised formulation. Anticipating the construction of a mass term, we have introduced the length scale as m^{-1}. Dropping the superscript $\boldsymbol{R}^{ab} \equiv {}^{(4)}\boldsymbol{R}^{ab}$, we find ($M_{\mathrm{Pl}}^2 = M_5^3/m$) [113]

$$S_{\mathrm{EH}}^{(5)} \mapsto \frac{M_{\mathrm{Pl}}^2}{4}\int \varepsilon_{abcd}\left[\boldsymbol{R}^{(1)\,ab} + m^2(\boldsymbol{e}^{(2)\,a} - \boldsymbol{e}^{(1)\,a}) \wedge (\boldsymbol{e}^{(2)\,b} - \boldsymbol{e}^{(1)\,b})\right] \wedge \boldsymbol{e}^{(1)\,c} \wedge \boldsymbol{e}^{(1)\,d} + \\ + (1 \leftrightarrow 2)\,. \tag{2.48}$$

Before translating this into a metric-based expression, we highlight that the discretisation procedure above is not unique. For example, in Eq. (2.47a) we could have chosen not to keep the non-derivative terms at a fixed site, i.e. instead of $\boldsymbol{e}^c \mapsto \boldsymbol{e}^{(i)\,c}$ we could replace $\boldsymbol{e}^c \mapsto (1-r)\boldsymbol{e}^{(2)\,c} + r\boldsymbol{e}^{(1)\,c}$ for $0 \leq r \leq 1$. The same could be done for $\boldsymbol{e}^d$ appearing in the interaction term, for a parameter $0 \leq s \leq 1$. Eventually, one finds the most general interaction term of the form

$$\mathcal{M}^{abcd}(\boldsymbol{e},\boldsymbol{f}) \equiv c_0\, \boldsymbol{e}^a \wedge \boldsymbol{e}^b \wedge \boldsymbol{e}^c \wedge \boldsymbol{e}^d + c_1\, \boldsymbol{e}^a \wedge \boldsymbol{e}^b \wedge \boldsymbol{e}^c \wedge \boldsymbol{f}^d + c_2\, \boldsymbol{e}^a \wedge \boldsymbol{e}^b \wedge \boldsymbol{f}^c \wedge \boldsymbol{f}^d \\ + c_3\, \boldsymbol{e}^a \wedge \boldsymbol{f}^b \wedge \boldsymbol{f}^c \wedge \boldsymbol{f}^d + c_4\, \boldsymbol{f}^a \wedge \boldsymbol{f}^b \wedge \boldsymbol{f}^c \wedge \boldsymbol{f}^d\,, \tag{2.49}$$

and the $c_{0,1,2,3,4}$ are combinations of r and s [113]. Had we considered only Eq. (2.48), we would have found the terms proportional to c_0 (which is nothing but a CC on site 1), c_1, and c_2.

For practical calculations, the vielbein formulation is often not very convenient, and hence the next step is to translate it back to a metric formulation. In analogy to the calculation in Eq. (2.42), we wish to translate the action

$$S = \frac{M_{\mathrm{Pl}}^2}{4}\sum_i \int \varepsilon_{abcd}\left[\boldsymbol{R}^{(i)\,ab} \wedge \boldsymbol{e}^{(1)\,c} \wedge \boldsymbol{e}^{(1)\,d} + \mathcal{M}^{abcd}(\boldsymbol{e}^{(i)}, \boldsymbol{e}^{(i+1)})\right] \tag{2.50}$$

into the metric language. While the first summand in square brackets simply yields two copies of the Einstein-Hilbert action, the interaction potential $\mathcal{M}$ requires some care. In Ref. [50] this has been studied for the most general case for N sites in d dimensions. Indeed, it is straightforward to generalise the above discretisation procedure to an arbitrary number of dimensions and sites. The same is true for the generalised interaction terms, which in $d = 4$ dimensions have a structure of the form

$$\varepsilon_{abcd}\, \boldsymbol{e}^{(i_1)\,a} \wedge \boldsymbol{e}^{(i_2)\,b} \wedge \boldsymbol{e}^{(i_3)\,c} \wedge \boldsymbol{e}^{(i_4)\,d} = \varepsilon_{abcd}\, \varepsilon^{\mu_1\mu_2\mu_3\mu_4}\, e^{(i_1)\,a}{}_{\mu_1}\, e^{(i_2)\,b}{}_{\mu_2}\, e^{(i_3)\,c}{}_{\mu_3}\, e^{(i_4)\,d}{}_{\mu_4}\, \mathrm{d}^4x\,,$$

where i_j labels the site and $\mathrm{d}^4x \equiv \mathrm{d}x^1 \wedge \mathrm{d}x^2 \wedge \mathrm{d}x^3 \wedge \mathrm{d}x^4$ is the canonical volume element. A certain number of the i_j will be identical, and therefore we may want to single out one specific site, say i_1, and express it in terms of a determinant. Thus, we factor out exactly $d = 4$ such terms by appropriately multiplying inverse matrices $e^{(i_1)}{}_a{}^{\mu}$ [recall Eq. (2.33)],

to obtain [50]

$$\det(e^{(i_1)})\,\mathrm{d}^4x\,\varepsilon_{abcd}\,\varepsilon^{klmn}\,\delta^a_{\ k}\,\left(e^{(i_1)^{-1}}e^{(i_2)}\right)^b_{\ l}\,\left(e^{(i_1)^{-1}}e^{(i_3)}\right)^c_{\ m}\,\left(e^{(i_1)^{-1}}e^{(i_4)}\right)^d_{\ n}\,. \tag{2.51}$$

For the two-site model we discussed above, the relevant matrix is $\mathbb{X} \equiv e^{(1)^{-1}}e^{(2)}$, and we find[7]

$$\varepsilon_{abcd}\,\boldsymbol{e}^{(1)\,a}\wedge\boldsymbol{e}^{(1)\,b}\wedge\boldsymbol{e}^{(1)\,c}\wedge\boldsymbol{e}^{(2)\,d} = 6\det(e^{(1)})\,\mathrm{d}^4x\,[\mathbb{X}], \tag{2.52a}$$

$$\varepsilon_{abcd}\,\boldsymbol{e}^{(1)\,a}\wedge\boldsymbol{e}^{(1)\,b}\wedge\boldsymbol{e}^{(2)\,c}\wedge\boldsymbol{e}^{(2)\,d} = 2\det(e^{(1)})\,\mathrm{d}^4x\,\left([\mathbb{X}]^2-[\mathbb{X}^2]\right), \tag{2.52b}$$

$$\varepsilon_{abcd}\,\boldsymbol{e}^{(1)\,a}\wedge\boldsymbol{e}^{(2)\,b}\wedge\boldsymbol{e}^{(2)\,c}\wedge\boldsymbol{e}^{(2)\,d} = \det(e^{(1)})\,\mathrm{d}^4x\,\left([\mathbb{X}]^3-3[\mathbb{X}][\mathbb{X}^2]-2[\mathbb{X}^3]\right), \tag{2.52c}$$

where we have made use of the notation $[A] \equiv \mathrm{tr}\,(A)$. In order to relate this expression to the conventional metric formulation of bimetric and massive gravity given below, one needs to impose an additional condition on the vielbeins, which is simply due to the fact that, in general, the defining relation (2.35) cannot be inverted [115]. Let us identify $g^{(1)\mu\nu} = e^{(1)}_{\ a}{}^{\mu}e^{(1)}_{\ b}{}^{\nu}\eta^{ab}$ and $g^{(2)}{}_{\mu\nu} = e^{(2)\,a}{}_{\mu}e^{(2)\,b}{}_{\nu}\eta_{ab}$, such that

$$g^{(1)\mu\lambda}g^{(2)}{}_{\lambda\nu} = \left(e^{(1)}_{\ a}{}^{\mu}e^{(1)}_{\ b}{}^{\lambda}\eta^{ab}\right)\left(e^{(2)\,c}{}_{\lambda}e^{(2)\,d}{}_{\nu}\eta_{cd}\right) \tag{2.53a}$$

$$= \left[\left(e^{(1)^{-1}}\right)^T\eta^{-1}e^{(1)^{-1}}\,e^{(2)^T}\eta\,e^{(2)}\right]^{\mu}_{\ \nu} \tag{2.53b}$$

$$= \left[\eta\,e^{(2)}\left(e^{(1)^{-1}}\right)^T\,\eta^{-1}e^{(1)^{-1}}e^{(2)^T}\right]^{\mu}_{\ \nu}\,, \tag{2.53c}$$

where in the last line we have used that Eqs. (2.52) involve traces that allow cyclic permutations. The sought after condition reads [50],

$$\eta\,e^{(2)}\left(e^{(1)^{-1}}\right)^T = \left[e^{(2)}\left(e^{(1)^{-1}}\right)^T\right]^T\eta = e^{(1)^{-1}}e^{(2)^T}\eta\,, \tag{2.54}$$

and allows us to express

$$g^{(1)\mu\lambda}g^{(2)}{}_{\lambda\nu} = \left[\left(e^{(1)^{-1}}e^{(2)^T}\right)\left(e^{(1)^{-1}}e^{(2)^T}\right)\right]^{\mu}_{\ \nu}\,, \tag{2.55}$$

or more suggestively,

$$\mathbb{X} = e^{(1)^{-1}}e^{(2)} \cong \sqrt{g^{(1)^{-1}}g^{(2)}}\,. \tag{2.56}$$

To see that imposing this condition is dynamically equivalent to the unconstrained theory, consider a decomposition of $e^{(1)} = \exp(\omega)\overline{e}^{(1)}$, where $\overline{e}^{(1)}$ satisfies Eq. (2.54), and $\exp(\omega)$ is a general, parametrised Lorentz transformation:

$$\exp(\omega)^T\eta\exp(\omega) = \eta \Rightarrow \omega\eta = -\omega^T\eta\,. \tag{2.57}$$

[7] We remark, without going into the details, that the ε-structure of these terms ensures the absence of the pathological Λ_5-terms in the decoupling limit [36, 93, 114], and gives rise to interactions of precisely the form (2.21) in this limit [53], where $\mathbb{X}_{\mu\nu} \sim h_{\mu\nu} + \eta_{\mu\nu}\chi$.

Given that the kinetic terms are invariant under independent Lorentz transformations of the vielbeins, we see that ω enters only algebraically through the potential, and has a constant solution $\omega = 0$. This establishes the dynamical equivalence as claimed in Ref. [50]. However, in Ref. [45] it is shown that this equivalence does not generally hold true, which means that there are branches where $\omega = 0$ is not a solution. It is found that the equivalence can be established if the matrix square root in Eq. (2.56) exists and is real. Nonetheless, there exist cases in which the metric formulation does not exist and one must revert to the vielbein method, see also Refs. [116, 117]. For the remainder of this manuscript we assume that the real matrix square-root (2.56) exists and we employ the metric approach, which we discuss in the subsequent section.

2.2.2 The bigravity action in metric form

The considerations of the previous sections lead us to a picture describing two dynamical tensor fields, $g^{(1)} = g$ and $g^{(2)} = \tilde{g}$, as shown schematically in Fig. 2.1. Inspired by the extra-dimensional arguments given above, we couple matter to one of the two metrics only: In the deconstruction of the fifth dimension, we apply the same procedure to the matter sector, decomposing matter fields $\phi(x, y) \mapsto \phi^{(i)}(x)$. We then interpret the tensor that lives on the same site as the matter Lagrangian $\mathcal{L}^{(i)}$ as that sector's physical metric. Remarkably, the two matter sectors will automatically couple only via the gravitational interaction terms. In fact, starting with the action in the metric language and coupling one matter Lagrangian to both metrics reintroduces the BD ghost [118, 119], and must therefore be disregarded for reasons of consistency, analogous to the requirement that a viable QFT contain only anomaly-free interactions, albeit other more symmetric and viable matter couplings have been found in Refs. [120–122], which we will not consider here. With this in mind and disregarding any hidden matter sector for now, the action reads

$$\begin{aligned} S_{\text{bi}} = \frac{M_g^2}{2} \int d^4x \sqrt{-\det g}\; R(g) + \frac{M_{\tilde{g}}^2}{2} \int d^4x \sqrt{-\det \tilde{g}}\; \tilde{R}(\tilde{g}) - \\ - m^2 M_{\text{eff}}^2 \int d^4x \sqrt{-\det g} \sum_{n=0}^{4} \beta_n e_n(\mathbb{X}) + \int d^4x \sqrt{-\det g}\; \mathcal{L}_{\text{matter}}\,. \end{aligned} \tag{2.58}$$

In this expression M_g is the Planck mass of the physical metric g, which measures distances in the matter sector, while $M_{\tilde{g}}$ is the corresponding mass scale of the hidden sector field $\tilde{g}$. Furthermore, we introduce an effective mass $M_{\text{eff}}^{-2} \equiv M_g^{-2} + M_{\tilde{g}}^{-2}$ in order to obtain a more symmetric action; however this has no impact on the physics, see e.g. Ref. [54] which uses a different convention. The kinetic terms of the tensors are given by the corresponding Ricci scalars $R(g)$ and $\tilde{R}(\tilde{g})$. The constants β_n parametrise the potential terms which are given in terms of matrix polynomials of fixed order in $\mathbb{X} \equiv \sqrt{g^{-1}\tilde{g}}$, cf. Eqs. (2.52):

$$\begin{aligned} e_0(\mathbb{X}) = 1 \;\; e_1(\mathbb{X}) = [\mathbb{X}]\,, \;\; e_2(\mathbb{X}) = \frac{1}{2}\left([\mathbb{X}]^2 - \left[\mathbb{X}^2\right]\right), \\ e_3(\mathbb{X}) = \frac{1}{6}\left([\mathbb{X}]^3 - 3\,[\mathbb{X}]\left[\mathbb{X}^2\right] + 2\left[\mathbb{X}^3\right]\right), \\ e_4(\mathbb{X}) = \det \mathbb{X}\,, \end{aligned} \tag{2.59}$$

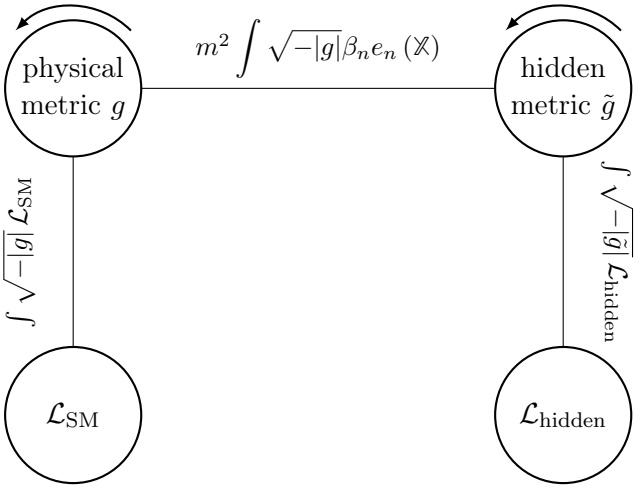

Figure 2.1.: Schematic representation of the action in Eq. (2.58). We have included a hidden matter Lagrangian, which would naturally arise from the discretisation of matter in the deconstructed extra-dimensional theory considered before. We have indicated that the two metrics can only be transformed *simultaneously* due to the interaction term. Only if $m = 0$, the hidden and physical metrics can transform independently. This naively leads us to assume that m is a naturally small parameter, as was confirmed in Ref. [123]. It is interesting that consistency *forbids* us to couple the SM and hidden sectors other than gravitationally [118, 119].

where $[\mathbb{X}] \equiv \mathrm{tr}\,(\mathbb{X})$, $[\mathbb{X}^2] = \mathbb{X}^{\mu}{}_{\nu}\mathbb{X}^{\nu}{}_{\mu}$ etc. For later convenience, we define a mixing angle θ via the relation $\sin^2(\theta) = M^2_{\rm eff}/M^2_g$, $\cos^2(\theta) = M^2_{\rm eff}/M^2_{\tilde{g}}$. Variation of the action yields the equations of motion of the gravitational fields, henceforth referred to as Einstein equations in the light of their GR analogue:

$$R_{\mu\nu} - \frac{1}{2}g_{\mu\nu}R + m^2\sin^2(\theta)\sum_{n=0}^{3}\beta_n V^{(n)}_{\mu\nu} = \frac{1}{M^2_g}T_{\mu\nu}\,, \tag{2.60a}$$

$$\tilde{R}_{\mu\nu} - \frac{1}{2}\tilde{g}_{\mu\nu}\tilde{R} + m^2\cos^2(\theta)\sum_{n=1}^{4}\sqrt{\det(g^{-1}\tilde{g})}\,\beta_n \tilde{V}^{(n)}_{\mu\nu} = 0\,. \tag{2.60b}$$

The interaction terms $V^{(n)}_{\mu\nu}$, $\tilde{V}^{(n)}_{\mu\nu}$ are obtained from the variation of $e_n(\mathbb{X})$, w.r.t. $g, \tilde{g}$. For example, we find $V^{(0)}_{\mu\nu} = g_{\mu\nu}$ (see Appendix A.1 for the remaining $V^{(n)}$). The EMT is obtained from the variation of the matter part of the action via Eq. (2.27). In Appendix A.3 we linearise these interaction terms and find that the above action gives rise to two dynamical fields of spin-2, one massless and one massive.

An interesting observation is that the action is invariant only under a simultaneous transformation of the two sectors, which leaves the trace of the matrix $\mathbb{X}$ invariant, as indicated in Fig. 2.1 by equally oriented arrows. However, if the interactions are turned off, e.g. by setting $m = 0$, the two sectors allow *independent* changes of coordinates (or equivalently space-time diffeomorphisms). Intuitively, one would immediately suspect that the parameter m is therefore *naturally* small, i.e. stable against radiative corrections. It turns out that this naive picture is correct, cf. Ref. [123].

Notice that the field equations (2.60) have two interesting limits. In the limit where the mixing angle $\theta \to 0$, i.e. $M_{\tilde{g}} \ll M_g$, the hidden sector is entirely decoupled from the matter sector and the solution of Eq (2.60a) will coincide with that of GR. Therefore, a smooth limit to GR is feasible without the notorious vDVZ discontinuity. Second, when $M_{\tilde{g}} \gg M_g$, or $\theta \to \pi/2$, one is in the limit of massive gravity, in which only one of the two tensors is a dynamical field. This can be seen from Eq. (2.60b), where all reference to g is lost. From the point of view of the g-Equations, $\tilde{g}$ is therefore merely a fixed background field. This is precisely the point of view taken in the dRGT version of massive gravity, where the kinetic term for $\tilde{g}$ is dropped from the action. Consequently, in the linearised EOM derived in Appendix A.3, the limit $\theta \to 0$ ($\theta \to \pi/2$) manifests the decoupling of the massive (massless) spin-2 field from the matter sector.

A physically well-motivated requirement is that the energy-momentum tensor, $T_{\mu\nu}$ is covariantly conserved, i.e. $\nabla_\mu T^\mu{}_\nu = 0$ as it is true in GR by construction of the Einstein tensor. In order for this to be compatible with the field equations, we demand

$$\nabla_\mu V^{(n)\,\mu}{}_\nu = 0 \qquad \text{and} \qquad \tilde{\nabla}_\mu \tilde{V}^{(n)\,\mu}{}_\nu = 0\,, \tag{2.61}$$

with the covariant derivatives constructed from g or $\tilde{g}$ as indicated. These equations are known as Bianchi constraints. One might be led to the conclusion that these yield an additional set of 8 equations (in four dimensions); however, these equations turn out not to be independent in general. For example, they yield only one independent equation for the cosmological solution we discuss in Sec. 2.3.2. With the machinery developed in this section, we are now in a position to reexamine the discussion of the BD ghost and how its appearance is avoided in Eq. (2.58).

2.2.3 Massive (bi-)gravity is free of the Boulware-Deser ghost

In order to study the consistency of a theory in terms of its propagating DOF, one needs to assure that the dynamics are such that only *healthy* DOF propagate. By healthy, it is understood that the energy of the system must be bounded from below; e.g. by ensuring that the kinetic terms have the correct sign, as otherwise increasing the momentum could lead to arbitrarily low kinetic energy – a state which would not be considered relevant for any physical system. Similarly, we know very well from the study of QFTs that the potential of a scalar needs to be bounded from below, such that arbitrarily low potential energies cannot be achieved by larger and larger field values. All these aspects of 'healthiness' can be studied by considering the Hamiltonian formulation of a given model. Thus, to understand how the BD ghost is avoided by the interactions considered above, we have to study the action in the Hamiltonian language, as was done in Refs. [29, 30]. There, Boulware and Deser argue that non-linear completions of the Fierz-Pauli action (2.1) will encompass six, instead of the expected five DOF of a massive spin-2 field (see Appendix A.3). And moreover, that this state inevitably destabilises the dynamics of the system by spoiling the boundedness from below of the Hamiltonian. The crucial observation made by de Rham, Gabadadze, and Tolley in 2010 [36, 37], was that there is a way around this no-go theorem hidden in the structure of the interaction terms (2.52, 2.59). In order to show the absence of the BD ghost, we reformulate the action (2.58) in the Hamiltonian language and count the DOF that it propagates.

Hamiltonians in classical mechanics. In the Hamiltonian formulation of a theory, all variables are accompanied by their conjugate momenta, e.g. for a classical Lagrangian describing the motion of a particle in one dimension, $L(x, \dot{x})$, we find that the Hamiltonian is a function of x and π, parametrised by a time variable t. Here, the conjugate momentum to the variable x is [124]

$$\pi = \frac{\partial L}{\partial \dot{x}} \quad \Rightarrow \quad H = \pi\, \dot{x}(\pi) - L(x, \dot{x}(\pi))\,, \tag{2.62}$$

and the the Euler-Lagrange equations become the first order Hamilton EOM,

$$\dot{x} = \frac{\partial H}{\partial \pi}\,, \quad \dot{\pi} = -\frac{\partial H}{\partial x}\,, \tag{2.63}$$

which can be obtained by variation of the action,

$$S = \int \mathrm{d}t\, L(x, \dot{x}(\pi)) = \int \mathrm{d}t\, \left[\pi\, \dot{x}(\pi) - H(x, \pi)\right], \tag{2.64}$$

and which describe one DOF, or two phase space variables.

In contrast, GR is not described in a manner where the number of DOF can directly be read off from the action, i.e. the Einstein-Hilbert action is not in canonical form [124], which is intimately related to the general covariance of GR. In analogy to this, let us parametrise the coordinate x of the above particle with an arbitrary parameter τ such that $x(\tau) = x(t(\tau))$. Now $t(\tau)$ appears as a new, independent variable and we see that, since neither H nor L depend explicitly on time, we can write Eq. (2.64) as [125]

$$S = \int \mathrm{d}\tau \left[\pi_x\, x' + \pi_t\, t'\right], \tag{2.65}$$

where we now have $x' = \frac{\mathrm{d}x}{\mathrm{d}\tau}$ and $t' = \frac{\mathrm{d}t}{\mathrm{d}\tau}$. Furthermore, it is necessary to enforce that $\pi_t + H(x, \pi) = 0$, which can generally be implemented by means of a Lagrange multiplier:

$$S = \int \mathrm{d}\tau \left[x'\pi_x + t'\pi_t + N(\tau) R(x, \pi_x, \pi_t)\right], \tag{2.66}$$

such that $R(x, \pi_x, \pi_t)$ has a simple first order zero at $\pi_t = -H(x, \pi)$. The analogy to GR is now manifest in the sense that (2.66) is invariant under general transformations $\tau \to \tilde{\tau}(\tau)$:

$$S = \int \mathrm{d}\tilde{\tau} \left[x'\pi_x + t'\pi_t + \tilde{N}(\tilde{\tau}) R(x, \pi_x, \pi_t)\right], \tag{2.67}$$

with $\tilde{N}(\tilde{\tau}) = \frac{\mathrm{d}\tau}{\mathrm{d}\tilde{\tau}} N(\tau)$, and primes now denote derivatives w.r.t. $\tilde{\tau}$. To summarise, we can obtain from an action with only canonical DOF, and which is not covariant, one which is covariant; however, at the prize of introducing spurious DOF. For the gravitational actions considered here, the logic must now be reversed.

Hamiltonians in GR and beyond. The actions we will consider below are all in the non-canonical form (2.66), and the task is to put them into the form (2.64) in order to read off the number of physical, propagating DOF. This will then be used to circumvent

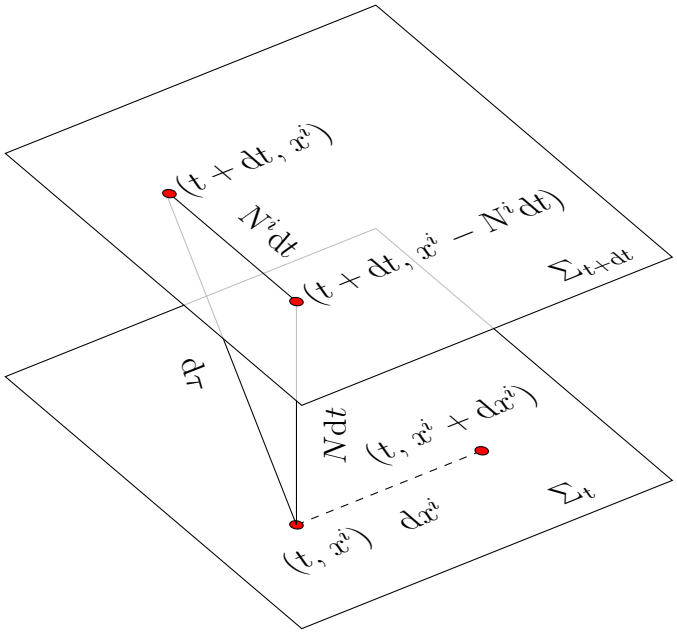

Figure 2.2.: Sketch illustrating the interpretation of the lapse and shift functions. The coordinate time evolution of a point (t, x^i) is decomposed into a *lapse* in coordinate time, perpendicular to the hypersurface Σ_t by a distance $N\mathrm{d}t$, and a *shift* in the plane of constant t by $\Delta x^i = N^i \mathrm{d}t$. This represents the 'time flow' of a point with constant spatial coordinate x^i [73]. The total line element reads $\mathrm{d}s^2 = -N^2 \mathrm{d}t^2 + \gamma_{ij}(\mathrm{d}x^i + N^i \mathrm{d}t)(\mathrm{d}x^j + N^j \mathrm{d}t)$.

the no-go theorem of Refs. [29, 30]. The programme that remains to be completed in this section is first, to find the Hamiltonian form of the GR action, extend it to the generalised action (2.58), and finally revert to the canonical form equivalent to Eq. (2.64). If the remaining DOF are equal to the expected number, the argument given by Boulware and Deser is circumvented. Therefore, we expect to find five DOF for the case of massive gravity where one has one field of spin-2, constituting $(2s + 1) = 5$ DOF, and seven DOF for the bimetric case where a massive and a massless spin-2 mode propagate; cf. Appendix A.3. In principle, one should then verify that the Hamiltonian is bounded from below, but, as it turns out, other instabilities may persist due to the peculiarities associated with the dynamics of the helicity-0 mode. We will return to this discussion in Sec. 2.3.2.

Following Ref. [73], we apply the same procedure to gravity. We first note that the action $S = \int \mathrm{d}^4x\, \mathcal{L}$ splits into a GR and a non-derivative interaction contribution, cf. Eq. (2.58),

$$\mathcal{L}_{\mathrm{bi}} = \mathcal{L}_{\mathrm{EH}} + \mathcal{L}_{\mathrm{int}}\,, \tag{2.68}$$

such that we may consider them separately. Let us first focus on the Einstein-Hilbert part. In the standard procedure due to Arnowitt, Deser, and Misner (ADM), the metric is decomposed into spatial slices as follows [125]:

$$g_{00} = -N^2 + N_i N_j \gamma^{ij},\ g_{0i} = g_{i0} = N_i \text{ and } g_{ij} = \gamma_{ij}\,, \tag{2.69}$$

whose inverse reads

$$g^{00} = -1/N^2,\ g_{0i} = g^{i0} = N^i/N^2 \text{ and } g^{ij} = \gamma^{ij} - \frac{N^i N^j}{N^2}\,, \tag{2.70}$$

with $N^i = \gamma^{ij} N_j$ and γ^{ij} denoting the inverse of γ_{ij}. N is often referred to as the lapse, while the N^i are conventionally called shift functions. We give a geometric interpretation of these variables in Fig. 2.2. A rather tedious, but straightforward calculation allows us to express the Einstein-Hilbert action in terms of these new fields and their conjugate momenta, most prominently $\pi^{ij} \equiv \frac{\partial \mathcal{L}_{\text{EH}}}{\partial \gamma_{ij}}$ [53, 54, 125],

$$S_{\text{EH}} = -\int \mathrm{d}^4x \left[\gamma_{ij}\partial_t \pi^{ij} - NR^0 - N_i R^i + 2\partial_i \left(\pi^{ij} N_j - \frac{\pi^j{}_j}{2} N^i + \sqrt{\det\gamma}\nabla^i_\gamma N\right)\right], \tag{2.71}$$

where the last term is a total derivative. The symbol ∇_γ is the covariant derivative w.r.t. the spatial metric only, and

$$R^0 = \sqrt{\det\gamma}\left[R_\gamma + \frac{1}{\det\gamma}\left(\frac{\pi^j{}_j}{2} - \pi^{ij}\pi_{ij}\right)\right], \quad R^i = 2\partial_j \pi^{ij}\,, \tag{2.72}$$

with the 3D Ricci scalar R_γ built from γ_{ij}. From here, we could proceed and construct the Hamiltonian, $H(\gamma_{ij}, \pi_{ij}, N, N^i) = \pi_{ij}\dot{\gamma}^{ij} - L(\gamma_{ij}, \pi_{ij}, N, N^i)$, to arrive at Einstein's equations via the Hamiltonian equations of motion, Eq. (2.63). See Refs. [73, 125] for an explicit calculation. For our purposes, it suffices to consider the action (2.71) and observe that it is precisely of the form of Eq. (2.66).

While for most practical applications Eq. (2.71) is not very useful, it expresses a remarkable result: Only the six components of γ_{ij} along with their conjugate momenta π_{ij} appear as dynamical variables, while the lapse N and shift N^i [often summarised as $N^\mu = (N, N^i)$] are non-dynamical. Furthermore, even though we have not made any assumptions other than the ADM decomposition to exist, the N^μ appear exactly linearly in the action. Therefore, they act as Lagrange multipliers enforcing the constraint functions (2.72) to vanish, reducing the number of independent phase space variables by four. Using the gauge freedom, which reduces the number of phase space variables by another four, we see that GR propagates $12 - 4 - 4 = 4$ phase space, or two physical DOF – as expected.[8]

Let us now go one small step beyond GR, and expand the 'generalised' Fierz-Pauli mass term in Eq. (2.3) in the ADM manner [29, 54]:

$$\begin{aligned}\left(h_{\mu\nu}h^{\mu\nu} - a(h^\mu{}_\mu)^2\right) = -\Big(&h_{ij}h^{ij} - a(h^i{}_i)^2 - 2\delta^{ij}N_iN_j + 2a\underbrace{(1 - N^2 + N_i\gamma^{ij}N_j)h^i{}_i}_{\simeq -2\delta N\, h^i{}_i} + \\ &+ (1-a)(1 - N^2 + N_i\gamma^{ij}N_j)^2\Big)\,.\end{aligned} \tag{2.73}$$

[8] In decomposing the metric as in Eq. (2.69) we have not fixed any gauge. This becomes obvious when counting DOF: The symmetric rank-2 tensor $g_{\mu\nu}$ has 10 independent components, while γ_{ij} contains only six of these. The remaining four are the N^μ. Here, we have simply made use of the reparametrisation invariance of the action [125].

Here, we used the notation $h_{ij} \equiv \gamma_{ij} - \delta_{ij}$ for the spatial metric perturbation. Noting that the second-to-last term contains terms cubic in the perturbations $\delta N \equiv N - 1$ and $\delta N_i = N_i$ which we neglect at this order, only the last term is troublesome. It gives rise to contributions which are quadratic in the shift and the lapse, such that they no longer serve as Lagrange multipliers removing unwanted DOF. Only the Fierz-Pauli form of the mass term will avoid this illustrating once again its special structure. Note that this is analogous to what we discussed below Eq. (2.8): The higher-order time derivatives that appear in Eq. (2.6) give rise to a sixth propagating DOF with unbounded, negative energy. This is precisely the DOF that is removed by the remaining constraint in Eq. (2.73). See also Ref. [53] for a discussion.

Even with the special Fierz-Pauli choice $a = 1$, the δN_i no longer appear linearly thereby enforcing constraints; only the lapse function δN remains linear and reduces the number of phase space variables by two. Instead of two, the (linearised) theory now propagates $12 - 2 = 10$ phase space variables, corresponding precisely to the five helicity states expected for a massive spin-2 field. However, this prediction is already lost at the cubic order, where the lapse function reenters non-linearly. We could now introduce new terms in order to cancel these new inconsistencies from the action; however, the work of Boulware and Deser seemed to indicate that this approach is doomed to fail [29, 30]. It was pointed out in Refs. [37, 39] that the condition for the lapse to act as Lagrange multiplier is, in fact, weaker than the action being linear in the lapse, e.g. if this can be achieved by a field redefinition [54]. While it is a matter of taste how to approach this, we believe that the vielbein language highlights this much more transparently. We therefore proceed in this language.

Evading the appearance of the BD ghost. The interaction terms (2.52) have a remarkable feature: Due to the totally antisymmetric structure, only one independent temporal component can appear in each interaction term, such that the lapse and shift functions will appear *linearly* in the action. As noted in Ref. [50], this is even true for the case of N metrics in d dimensions! We will not provide the full proof of the absence of the BD ghost, but outline the idea following closely Refs. [44, 50], which also work in the vielbein language. The reader interested in a full proof is referred to Refs. [36–45, 49].

For the sake of making contact with the above observation, let us revert to the vielbein formulation, where the ADM decomposition analogous to that of the metric reads [50]

$$\widehat{E}^{(I)A}{}_{\mu} = \begin{pmatrix} N^{(I)} & N^{j(I)} e^{(I)}{}_{j}{}^{a} \\ 0 & e^{(I)}{}_{j}{}^{a} \end{pmatrix}, \quad \widehat{E}^{(I)}{}_{A}{}^{\mu} = \begin{pmatrix} 1/N^{(I)} & 0 \\ -N^{j(I)}/N^{(I)} & e^{(I)j}{}_{a} \end{pmatrix}, \tag{2.74}$$

where we have introduced a capital E to make it more easy to distinguish the 4D vielbein from its spatial part, which is defined via $\gamma^{(I)}_{ij} = e^{(I)a}{}_{i} e^{(I)b}{}_{j} \delta_{ab}$. Plugging this ansatz into the defining equation of the vielbein (2.35), one recovers the ADM decomposition for each metric:

$$g^{(I)}_{\mu\nu} = \widehat{E}^{(I)A}{}_{\mu} \widehat{E}^{(I)B}{}_{\nu} \eta_{AB} = \left(-N^{(I)2} - N^{(I)}_{k} N^{k(I)}\right) \mathrm{d}t^2 + N^{(I)}_{j} \mathrm{d}x^j \mathrm{d}t + \gamma^{(I)}_{jk} \, \mathrm{d}x^j \mathrm{d}x^k \,. \tag{2.75}$$

However, as we had noted below Eq. (2.35), the choice of vielbein is unique only up to

a Lorentz transformation. Thus, the most general form of Eq. (2.74) is actually $E^A_{\ \mu} = \Lambda(\vec{k})^A_{\ B}\widehat{E}^B_{\ \mu}$, where $\vec{k}$ is the momentum that parametrises the Lorentz boost

$$\Lambda(\vec{k})\begin{pmatrix}1\\ \vec{0}\end{pmatrix} = \begin{pmatrix}\sqrt{1-\vec{k}\cdot\vec{k}}\\ \vec{k}\end{pmatrix}. \tag{2.76}$$

As was shown in Ref. [115], we can go from the metric to the vielbein language by simply writing the action in the form suggested there [$R^\mu \equiv (R^0, R^i)$],

$$S_{\rm EH} = \int \mathrm{d}^4x\ \left[p_{a\,i}\,\dot{e}^{a\,i} + N_\mu(e)R^\mu(g(e),\pi(e,p))\right] \tag{2.77}$$

with the canonical momentum variable $p^{a\,i}$ related to the metric equivalent as $\pi^{ij} = \frac{1}{4}(p^{a\,i}e_a{}^j + p^{a\,j}e_a{}^i)$ [115]. However, this cannot be the correct form of the action for a simple reason: While the action (2.71) contains six (twelve) dynamical DOF (phase space variables) in the form of the six independent components of γ_{ij} (and π_{ij}), the nine independent spatial components of $e^a_{\ i}$ in Eq. (2.77) constitute too many independent variables (eighteen in phase space). Thus, we find that six phase space variables need to be removed by additional constraints. Following Deser and Isham [115], the correct constraints can be found by observing that $p_{a\,i}\,\dot{e}^{a\,i}$ is *not* invariant under local Lorentz transformations, $\Lambda^\mu_{\ \nu} = \Lambda^\mu_{\ \nu}(x)$,

$$e^{a\,i} \to \Lambda^a_{\ b}e^{b\,i},\ p_{a\,i} \to \Lambda_a{}^b p_{b\,i} \quad \Rightarrow \quad \dot{e}^{a\,i}p_{a\,i} \to \dot{e}^{a\,i}p_{a\,i} + e^{b\,i}p_{c\,i}\dot{\Lambda}^a_{\ b}\Lambda_a{}^c\,. \tag{2.78}$$

Noting that $\Lambda^a_{\ b}\Lambda_a{}^c = \delta_b{}^c$, we see that it is sufficient to demand that the antisymmetric part vanishes, $e^{[a}{}_i p^{b]\,i} = 0$. In conclusion, we find that the action (2.77) needs to be augmented by six constraints,

$$S_{\rm EH} = \int \mathrm{d}^4x\ \left[p_{a\,i}\,\dot{e}^{a\,i} + N_\mu(e)R^\mu[g(e),\pi(e,p)] + \lambda_{ab}e^{[a}{}_i p^{b]\,i}\right], \tag{2.79}$$

with precisely six antisymmetric Lagrange multipliers $\lambda_{ab} = -\lambda_{ba}$, removing the unwanted and spurious DOF.

Finally, we may write down the bigravity action (2.58) in vielbein language and ADM decomposition, and count the number of propagating DOF. Let us add the interaction term to Eq. (2.79). Using that the kinetic terms in Eq. (2.58) are independent of one another, we add for each site (I) one such kinetic term. What we obtain can be put in the compact form [50]

$$S_{\rm bi} = \int \mathrm{d}^dx \sum_I \left[p^{(I)}_{a\,i}\,\dot{e}^{(I)\,a\,i} - N^{(I)}_\mu\left(R^{(I)\,\mu} + R^{(I)\,\mu}_m\right) + \lambda^{(I)}_{ab}e^{(I)\,[a}{}_i\,p^{(I)\,b]\,i}\right], \tag{2.80}$$

making explicit that the shift and lapse appear *linearly* in the interaction terms, which we indicate by adding a subscript m.[9] The reason for this can be understood from Eq. (2.74): While the components $E^{(I)\ 0}_{\ \ \ \mu}$ are linear in lapse and shift, the $E^{(I)\ i}_{\ \ \ \mu}$ are independent

[9] One should bear in mind that the $R^{(I)\,\mu}_m$ may depend explicitly on all boost momenta $\vec{k}^{(J)}$.

of both lapse and shift [50]. This is a crucial observation and we wish to highlight once more that, in order to arrive at this result, it was of vital importance that we consider a interaction term as a function of $\mathbb{X} = (g^{-1}\tilde{g})^{1/2}$ (or equivalently a discretisation of the vielbein action). Any construction of a mass term founded on $g^{-1}\tilde{g}$ instead, is subject to the no-go theorem by Boulware and Deser.

Let us count the number of DOF in phase space for N metrics in a $(d+1)$-dimensional space-time:

- Our construction ensured that the action (2.80) is locally Lorentz invariant; however, the interaction terms remain only invariant if the metrics, or vielbeins, at different sites are rotated simultaneously, i.e. the diagonal subgroup of the N $SO(d,1)$ symmetries of the kinetic terms. Using this, we can eliminate the d-momentum $\vec{k}^{(1)}$ from the action, i.e. putting $E^{(1)}$ it in the form (2.74).

- Furthermore, we can use $N-1$ of the N shift constraints, arising from Eq. (2.80) upon invoking the $N_i^{(I)}$ EOM, in order to eliminate the remaining $d \times (N-1)$ momenta $\vec{k}^{(I)}$, leaving one shift, and N lapse constraints:

$$S_{\rm bi} = \int \mathrm{d}^d x \left\{ \sum_I \left[p^{(I)}_{a\,i}\, \dot{e}^{(I)\,a\,i} - N^{(I)} \left(R^{(I)} + R^{(I)}_m \right) + \lambda^{(I)}_{ab} e^{(I)\,[a}{}_i\, p^{(I)\,b]\,i} \right] - \right.$$
$$\left. - N^{(1)}_i \left(R^{(1)\,i} + R^{(1)\,i}_m \right) \right\}. \tag{2.81}$$

  At this point, we have used all the reparametrisations to arrive at the action in terms of the $N \times 2d^2$ ADM variables and a number of constraints:

- Eq. (2.81) contains $(d+1)$ shift and lapse constraints on site (1), and

- additionally $N-1$ lapse constraints for the remaining sites.

Balancing the contributions above, we find a total of [50]

$$\begin{aligned} &2\Big(N\,d^2 \quad - \quad N \times \underbrace{\frac{d}{2}(d-1)}_{\text{each } \lambda^{(I)}_{ab}} \quad - \quad \underbrace{(N+d)}_{N^{(1\ldots N)} \& N^{(1)}_i}\Big) \\ =&2\left(\left[\frac{d}{2}(d-1)-1\right] + (N-1)\left[\frac{d}{2}(d+1)-1\right]\right) \\ =&2\,(2+(N-1)\times 5) \quad \text{phase space DOF} \quad \text{for } d=3\,, \end{aligned} \tag{2.82}$$

which corresponds to one massless and $N-1$ massive spin-2 fields in $d+1$ dimensions. For example, bigravity in four dimensions comprises a total of $2 \times (2+5)$ phase space variables. In order to arrive at this result, it was crucial to have at hand the $N-1$ lapse constraints, which suffice to remove the expected $N-1$ BD ghosts [50].

We conclude our discussion of the absence of the BD ghost in multi-metric gravity with nearest neighbour interactions remarking that Ref. [50] also studied more general couplings, which are also ghost-free. The proof for the dRGT theory follows immediately, by observing that it corresponds to the decoupling limit of bigravity, i.e. $M_{\tilde{g}} \to \infty$. Furthermore, we remark that we have only considered the so-called primary constraints

here, i.e. those arising from integrating out the Lagrange multiplier functions, implicitly assuming that these give rise to secondary constraints, that remove another DOF in phase space.[10] While this has been discussed quite controversially at first, see e.g. [94, 126–128] and [129–132] for dRGT, or [133–136] for bigravity, the issue is now settled [39, 49, 137–141]. Notice that, we have not yet studied the perturbations of the metric that would allow us to conclude that the remaining modes are truly propagating. This is shown in Appendix A.3.

2.3 Solutions to the field equations of bigravity

In this section we apply the findings of the previous section to two important settings, namely a static, spherically symmetric vacuum solution of the field equations, which in GR leads to the Schwarzschild metric. Furthermore, we study a specific type of cosmological solution, which we will need in Chapter 3.

2.3.1 Central mass problem

In order to understand the implications the modified action (2.58) has on observations, we will need to understand the 'Newtonian' limit, i.e. the limit in which Newtonian gravity is recovered, if the mixing is chosen to reproduce GR. It turns out that the result is a potential that has a mixed Newtonian ($\sim 1/r$) and an exponentially decaying, Yukawa-type contribution ($\sim e^{-m_g r}/r$). This should not come as a surprise, given that both the counting of DOF of the previous section, as well as the study of linear perturbations in Appendix A.3 shows that the theory propagates two spin-2 force carrier fields, one massless and one massive.

In GR Birkhoff's theorem tells us that any spherically symmetric vacuum solution of the field equations is static and asymptotically flat, leading to the Schwarzschild metric. This no longer applies in a bimetric setup. Consequently, a more vivid landscape of BH solutions is found. Most notably, solutions exist where both tensors maintain a diagonal shape (bidiagonal BHs), as well as so-called non-bidiagonal BH solutions, where off-diagonal entries are relevant, too. This has been studied extensively in the literature; we refer the reader to Refs. [142–144] and references therein for an overview. For our purposes, it will suffice to consider solutions, which follow from the ansatz

$$g_{\mu\nu}\mathrm{d}x^\mu \mathrm{d}x^\nu = -e^{\nu_1(r)}\mathrm{d}t^2 + e^{\lambda_1(r)}\mathrm{d}r^2 + r^2\mathrm{d}\Omega^2\,, \tag{2.83a}$$

$$\tilde{g}_{\mu\nu}\mathrm{d}x^\mu \mathrm{d}x^\nu = -e^{\nu_2(r)}\mathrm{d}t^2 + e^{\lambda_2(r)}(r + r\mu(r))'^2\mathrm{d}r^2 + (r + r\mu(r))^2\mathrm{d}\Omega^2\,, \tag{2.83b}$$

which was first studied in Ref. [91]. Here, μ is a function of r and parametrises the non-linearities that will become important in solving the field equations. We refer the reader to Appendix A.2 for a step-by-step solution of the field equations, which is quite instructive to see the Vainshtein screening in operation and the emergence of GR in the small distance limit. Here, we merely summarise our result in a suggestive form that

[10] To remove one physical DOF, *two* phase space variables need to be removed. The secondary constraint can be obtained by demanding the primary constraint to be conserved in time, i.e. its Poisson bracket with the Hamiltonian vanishes [49, 124].

allows us to read off the Newtonian potential $\Phi(r)$:

$$2\Phi(r) = \nu_1(r) = \begin{cases} -\frac{r_S}{r} - r^2\,\frac{\Lambda_{\rm eff}}{3}\,, & r \ll r_V = \sqrt[3]{\frac{r_S}{m_g^2}} \\ -\frac{r_S}{r}\left[\alpha(\theta) + \beta(\theta) e^{-m_g r}\right] - r^2\cos^2(\theta)\,\frac{\Lambda_{\rm eff}}{3}\,, & r \gg r_V = \sqrt[3]{\frac{r_S}{m_g^2}}\,, \end{cases} \tag{2.84}$$

where $\alpha(\theta) \equiv \cos^2(\theta)\left[1 + \frac{2}{3}\sin^2(\theta)\right]$ and $\beta(\theta) \equiv \frac{2}{3}\sin^2(\theta)\left[1 + 2\sin^2(\theta) + \frac{\Lambda_{\rm eff}}{m_g^2}\right]$. The Schwarzschild radius is related to the point mass M via $r_S \equiv 2\,G_{\rm N}M$, and the effective CC, $\Lambda_{\rm eff} = m^2\sin^2(\theta)(\beta_0 + 3\,\beta_1 + 3\,\beta_2 + \beta_3)$, as well as the physical spin-2 mass, $m_g^2 = m^2(\beta_1 + 2\,\beta_2 + \beta_3)$, are derived in Appendix A.2 and coincide with the expression obtained from a cosmological solution considered in the next section. Interestingly, both $\Lambda_{\rm eff}$ and m_g are proportional to m, the naturally small mass parameter in the action (2.58).

Discussion. Eq. (2.84) has several interesting features that we wish to highlight at this point. First, there are two regimes that reproduce the result obtained in standard GR: One, where we take the mixing angle to vanish, i.e. $\theta \to 0$ and $\alpha(\theta) \to 1$, or equivalently $M_{\tilde{g}} \ll M_g$, different from the naive limit where the physcal graviton mass $m_g \to 0$. As we discussed above, this latter limit is plagued by the vDVZ discontinuity in the linear regime. The other interesting regime is the Vainshtein regime defined by a critical radius $r_V = (r_S/m_g^2)^{1/3}$. This defines a sphere inside which the potential looks identical to the weak-field limit of GR. At first sight this may come as a surprise; however, we have already argued that this is in fact a generic feature of massive spin-2 fields, that can be linked to the onset of strong coupling of the helicity-0 mode [78]. This has been found to be a general feature in massive gravity, see Refs. [74, 79–84, 86, 91, 92], and was also confirmed via numerical studies for massive and bimetric gravity [145, 146].

Second, going to the opposite limit, namely that of massive gravity ($M_{\tilde{g}} \gg M_g$), $\theta \to \pi/2$ and therefore $\cos(\theta) \to 0$ and $\beta(\theta) \to \frac{2}{3}\left[3 + \frac{\Lambda_{\rm eff}}{m_g^2}\right]$, we see that the CC term we have included in our calculations vanishes outside the Vainshtein radius. This is an effect known as degravitation, cf. Refs. [147–149]. The general idea behind this mechanism is that one may be able to resolve the CC problem by a screening mechanism. More concretely, instead of tuning its value to the observed, *small* value, the vacuum energy is decoupled from gravity at large distances.[11] As Eq. (2.84) indicates, coupling vacuum energy to a massive spin-2 field is a possible realisation of such a screening mechanism. However, by observing that inside the Vainshtein regime the CC is still present, cf. Eq. (2.84), there is still some severe tuning required: From the precession of the perihelion of Mercury a bound on the effective CC $\Lambda_{\rm eff} = \rho_{\rm vac}/M_{\rm Pl}^2$ can be obtained in terms of the vacuum energy density $\rho_{\rm vac} < (14\,{\rm eV})^4$ [150], while cosmological late time acceleration indicates that $\rho_{\rm vac}^{\rm obs} = (2\cdot 10^{-3}\,{\rm eV})^4$. This is still a large discrepancy, but it can be brought into agreement with a mixing angle that brings us close to massive gravity, $\cos(\theta) \gtrsim 10^{-8}$, if the bound is saturated. While this still requires the tuning of the vacuum energy density to be in agreement with solar system tests, it is less severe than the tuning required to cancel the contributions from the electroweak $\rho_{\rm vac}^{\rm EW} \sim (100\,{\rm GeV})^4$ or the QCD phase

[11] In Ref. [149] this is referred to as a high-pass filter, as only high frequency modes are allowed to couple to gravity, while the low frequency modes (with wave lengths outside the Vainshtein regime) are decoupled.

transition $\rho_{\text{vac}}^{\text{QCD}} \sim (100\,\text{MeV})^4$ to achieve the observed value. See also Ref. [151] for a discussion in massive gravity alone.

Furthermore, even away from this limit, i.e. without such a screening mechanism at work, the induced CC is proportional to the mass oparameter m, which is *naturally small* by virtue of the arguments given in Sec. 2.2.2.

Finally, in the massive gravity limit, $\cos(\theta) \to 0$, and in the regime where $r_V < r < m_g^{-2}$, the strength of the gravitational force is enhanced by a factor of 2 compared to the region $r < r_V$. We will return to this observation and put it to test in Chapter 4.

2.3.2 Cosmological solution

It is a natural question to ask if the field equations admit solutions of the Friedman-Lemaître-Robertson-Walker (FLRW) type, and whether they are phenomenologically viable. Before deriving such a cosmological solution, we emphasise that dRGT massive gravity, i.e. the version of Eq. (2.58) with no kinetic term for $\tilde{g}$, does not seem to possess stable, FLRW type cosmological solutions as discussed in Refs. [151–158]. Given that this shortcoming is alleviated as $\tilde{g}$ becomes dynamical itself can be seen as an incentive to study instead the bimetric case, beyond our argument coming from the 5D derivation of the action. Such bimetric cosmologies have been studied extensively in the past years [159–170].

In principle, there is no reason why both metrics should be perturbed around one and the same background. However, given our knowledge that the Universe is flat, homogeneous and isotropic on large scales [12], and on the other hand we assume the hidden sector to be devoid of matter, an FLRW-like background is a reasonable assumption for both $\tilde{g}$ and g (see Ref. [159] for more exotic ansätze, which however turn out to yield decoupled, GR-like solutions [54]).

Using conformal time η, we can parametrise the respective line elements as was first done in Refs. [159–161]

$$\begin{aligned} \mathrm{d}s^2 &\equiv g_{\mu\nu}\mathrm{d}x^\mu \mathrm{d}x^\nu = a(\eta)^2(-\mathrm{d}\eta^2 + \mathrm{d}\vec{x}^2)\,, \\ \mathrm{d}\tilde{s}^2 &\equiv \tilde{g}_{\mu\nu}\mathrm{d}x^\mu \mathrm{d}x^\nu = b(\eta)^2(-\tilde{c}(\eta)^2\,\mathrm{d}\eta^2 + \mathrm{d}\vec{x}^2)\,, \end{aligned} \tag{2.85}$$

where we assume that the spatial part takes the form $\mathrm{d}\vec{x} = \frac{\mathrm{d}r^2}{1-\kappa r^2} + r^2(\mathrm{d}\theta^2 + \sin^2(\theta)\mathrm{d}\phi^2)$.[12] The EMT is assumed to be compatible with homogeneity and isotropy, i.e. $T^\mu{}_\nu = \mathrm{diag}(\rho, P, P, P)$, with the energy density ρ and pressure P related by the equation of state $P = w\,\rho$ for the matter component under consideration. With this ansatz, the task that lies ahead is solving the field equations for the the functions $a(\eta)$, $b(\eta)$, and $\tilde{c}(\eta)$. Consequently, we plug the ansatz into Eqs. (2.60) and find

$$\frac{3}{a^2}\left(H^2 + \kappa\right) - m^2\sin^2(\theta)\left[\beta_0 + 3\beta_1 y + 3\beta_2 y^2 + \beta_3 y^3\right] = \frac{\rho}{M_g^2}, \tag{2.86a}$$

$$\frac{3}{b^2}\left(J^2/\tilde{c}^2 + \kappa\right) - m^2\cos^2(\theta)\left[\beta_1 y^{-3} + 3\beta_2 y^{-2} + 3\beta_3 y^{-1} + \beta_4\right] = 0. \tag{2.86b}$$

[12] One might wonder if the two sectors may have different curvatures κ, but it turns out that this is not viable, cf. Ref. [161].

Here, a prime denotes a derivative w.r.t. η, $y \equiv b/a$, and $\mathcal{H} = a'/a$, $\mathcal{J} = b'/b$. The latter two are the Hubble parameters for both metrics in conformal time, related to the Hubble rate in proper time ($\mathrm{d}t = a(\eta)\,\mathrm{d}\eta$) via $H(t) = a(t)^{-1}\mathcal{H}(t)$ and $J(t) = b(t)^{-1}\mathcal{J}(t)$.

The conservation of energy implies $\rho' = 3\mathcal{H}(1+w)\rho$ [159], and the Bianchi constraints (2.61) yield

$$(\tilde{c}\,\mathcal{H} - \mathcal{J})\underbrace{\left[\beta_1 y + 2\beta_2 y^2 + \beta_3 y^3\right]}_{\equiv\Gamma(y)} = 0\,. \tag{2.87}$$

Below and in later chapters, we will study the linearised equations of motion, where it turns out that the asymptotic limit of the expression named Γ is proportional to the mass of the heavy spin-2 field. Therefore, the solution to Eq. (2.87) with $\Gamma = 0$ is not viable: it seems that the massive mode is, in fact, massless and this branch is identical to GR (at the linearised level). However, it has been argued that the missing DOF will reenter non-perturbatively as a pathological ghost [168, 171]. Therefore, we choose the branch $\mathcal{J}(\eta) = \tilde{c}(\eta)\mathcal{H}(\eta)$. Using this and subtracting Eq. (2.86a) from Eq. (2.86b), we obtain an algebraic equation for y:

$$\begin{aligned}\beta_1\cos^2(\theta)y^{-1} + [3\beta_2\cos^2(\theta) - \beta_0\sin^2(\theta)] + [3\beta_3\cos^2(\theta) - 3\beta_1\sin^2(\theta)]y + \\ + [\beta_4\cos^2(\theta) - 3\beta_2\sin^2(\theta)]y^2 - \beta_3\sin^2(\theta)y^3 = \frac{\rho}{M_g^2 m^2}.\end{aligned} \tag{2.88}$$

By assumption, ρ is the density of a perfect fluid with $w \geq -1$:

$$\rho(\eta) = \rho_0 \begin{cases} 1 & \text{if } w = -1, \\ \left(\frac{a(\eta)}{a(\eta_0)}\right)^{-3(1+w)} & \text{if } w > -1\,. \end{cases} \tag{2.89}$$

Therefore, any fluid of type $w > -1$ dilutes, i.e. $\rho \to 0$ for $\eta \to \infty$. We note that, since a CC-type of matter with $w = -1$ is already build into the theory via the potential term β_0, we may disregard such types of matter in the following. Hence, if we are interested in late times, the solution to Eq. (2.88) will approach a constant value y_*, for $\rho = 0$. In fact, the exact value of y_* is irrelevant, since it can be absorbed via a redefinition of the parameters. To proceed, we linearise around the constant solution $y = y_* + \delta y$ and find

$$\delta y(\eta) = -\frac{\rho(\eta)}{3m^2 M_g^2}\,\frac{y_*^3}{\Gamma_*(\cos^2(\theta) + y_*^2\sin^2(\theta)) - \frac{2\,\widetilde{\Lambda}\,y_*^4}{3\,m^2}}, \tag{2.90}$$

with $\Gamma_* \equiv \Gamma(y_*)$ and $\widetilde{\Lambda} \equiv m^2\cos^2(\theta)\left(\beta_1 y_*^{-3} + 3\beta_2 y_*^{-2} + 3\beta_3 y_*^{-1} + \beta_4\right)$ an effective cosmological constant for the hidden sector. Combining the findings so far, we find the cosmic evolution in the visible sector obeys

$$a(\eta)^{-2}(\mathcal{H}(\eta)^2 + \kappa) = \tfrac{1}{3}\Lambda + \frac{\rho(\eta)}{3M_{\mathrm{Pl}}^2}\,, \tag{2.91}$$

which coincides with the evolution of ΛCDM [172]. Here, the effective CC is found to be $\Lambda \equiv m^2\sin^2(\theta)\left(\beta_0 + 3\beta_1 y_* + 3\beta_2 y_*^2 + \beta_3 y_*^3\right)$ and we have defined the physical Planck

mass

$$M_{\rm Pl}^2 \equiv M_g^2 \frac{\cos^2(\theta) + y_*^2 \sin^2(\theta) - \frac{2\widetilde{\Lambda}\, y_*^4}{3\, m_g^2}}{\cos^2(\theta) - \frac{2\widetilde{\Lambda}\, y_*^4}{3\, m_g^2}} \,. \tag{2.92}$$

Notice that $M_{\rm Pl}^2 \to M_g^2 \left(1 + y_*^2 \tan^2\theta\right)$, as $\widetilde{\Lambda} \to 0$, in agreement with Refs. [173, 174]. Moreover, we have introduced the graviton mass (cf. Appendix A.3)

$$m_g^2 \equiv m^2 \Gamma_* = m^2 \left[\beta_1 y_* + 2\beta_2 y_*^2 + \beta_3 y_*^3\right] . \tag{2.93}$$

Finally, we may use that $y' = \left(\frac{b}{a}\right)' = y(\mathcal{J} - \mathcal{H})$ and $\mathcal{J} = \tilde{c}\,\mathcal{H}$ to find that,

$$\tilde{c}(\eta) = 1 + \frac{y'}{y\mathcal{H}} \simeq 1 + \frac{\delta y'}{y_*\mathcal{H}} \simeq 1 - (1+w)\frac{\rho(\eta)}{m_g^2\, M_{\rm Pl}^2} \frac{y_*^2}{\cos^2(\theta) - \frac{2\widetilde{\Lambda}\, y_*^4}{3\, m_g^2}}, \tag{2.94}$$

where the continuity equation, $\rho' = 3\mathcal{H}(1+w)\rho$, was used in the last step. This allows us to define precisely what we mean by 'late times': When the quantity $\frac{\rho(\eta)}{M_{\rm Pl}^2 m_g^2} \ll 1$, we can take $\tilde{c}(\eta) = 1$ to a good approximation. For example, using the energy density of the CMB today, $\rho^0 = T_{\rm CMB} k_B \simeq 2.4 \cdot 10^{-4}\,\text{eV}$, the critical redshift z_* is found by solving

$$\frac{\rho(z_c)}{m_g^2\, M_{\rm Pl}^2} = \frac{(2.4 \cdot 10^{-4}\,\text{eV})^4\, z_*^4}{m_g^2 M_{\rm Pl}^2} \stackrel{!}{=} 1 \quad \Rightarrow \quad z_* \simeq 13 \times \left[\frac{m_g}{10^{-33}\,\text{eV}}\right]^{\frac{1}{2}} , \tag{2.95}$$

where we used that radiation scales with the cosmological redshift as z^4, with $1 + z \equiv a(t_0)/a(t)$ and t_0 is today. Moreover, $m_g = 10^{-33}\,\text{eV} = H_0 \equiv H(t_0)$ corresponds to the lowest observable mass: Any lower mass would only yield effects observable at scales outside the Hubble radius.

Discussion. Cosmological solutions in massive gravity, and even more so in bigravity, have a couple of remarkable features that should be emphasised at this point. At the same time we wish to highlight some of the shortcomings of these cosmological solutions. To begin with, it can be seen from the cosmic evolution equations (2.86), cast into the form (2.91), that late-time acceleration is *built into the model*, even in the absence of a bare CC (absorbed into β_0), if the parameter m is of the order of the Hubble rate today. This remains true even if quantum corrections are included, i.e. the small mass parameter required for this is *technically natural* in 't Hooft's sense [175], as was shown in Ref. [123]. At the same time, the evolution is such that it resembles GR without a CC at early times, where $y \to 0$ if $\beta_1 \neq 0$, cf. Eq. (2.88) and Ref. [162].

Next, we remark without going into the details, that in cosmological solutions of massive gravity, one often encounters yet another instability, first found by Higuchi, and hence referred-to as the Higuchi ghost [176]. Similar to the BD ghost, this scalar instability arises in the helicity-0 mode of a massive spin-2 field propagating on a de Sitter background, i.e. a metric whose curvature satisfies $R_{\mu\nu} = \Lambda g_{\mu\nu}$ [54]. There, the helicity-0 mode comes with a kinetic term proportional to $(\tilde{m}^2(H) - 2H^2)$ [157, 169], where the *dressed* mass

parameter of Ref. [177] has to satisfy [cf. also Eq. (A.38)][13]

$$\tilde{m}^2(H) \equiv m^2 \frac{H}{J}\left(\beta_1 + 2\beta_2 \frac{H}{J} + \beta_3 \frac{H^2}{J^2}\right) \geq 2H^2\,, \tag{2.96}$$

in order for the helicity-0 mode to be stable. Indeed, it turns out that one cannot satisfy this bound, and at the same time invoke a self-accelerated solution of the type (2.85) [151–158]. In principle, however, one might conceive more exotic cosmological solutions to resemble the observations at late times see e.g. Ref. [152]. We do not consider this possibility here, but instead emphasise that the bound (2.96) is modified in bigravity [177]:

$$\tilde{m}^2(H)\left[H^2 + J^2 \frac{M_g^2}{M_{\tilde{g}}^2}\right] \geq 2H^4\,. \tag{2.97}$$

Thus, choosing the parameters such that $\tan\theta = \frac{M_{\tilde{g}}}{M_g} \ll J/H$, the modified bound (2.97) is easily evaded, see also Refs. [53, 54] for further discussions.

Finally, a number of authors have considered perturbations on FLRW backgrounds, see Refs. [166, 169–171, 178–186]. It is generally found that some branches of solutions involve exponentially growing scalar and/or tensor modes that render perturbative predictions non-trustworthy and raise questions about the viability of these scenarios – or at least require to extend the scenario at early times. It seems that including an inflationary phase would be sufficient to obtain suitable initial conditions to avoid these growing modes [187]. Alternatively, this could also be avoided if a hidden matter sector is included [171]. Conversely, it has also been argued by some authors that these instabilities could actually serve as seeds for structure formation by virtue of the Vainshtein mechanism that is expected to set in when these instabilities lead to large overdensities [169, 188].

In any case, the cosmology in bigravity has a very rich spectrum and remains an ongoing field of research; e.g. recently there has been a growing interest in so-called doubly coupled cosmologies, where matter is coupled to a composite metric. This seems to help alleviate some of these instabilities, see Refs. [120–122] for the construction and [189–193] for the cosmological phenomenology.

[13] In terms of the physical Hubble parameters, the Bianchi constraint yields $\mathcal{J}/\mathcal{H} = y^2 J/H = y^2\tilde{c} \simeq y^2$. Thus, the mass (2.96) coincides with that in Eq. (2.93).

Chapter 3

Gravitational Wave Oscillations

This chapter is dedicated to the analysis of the modified propagation of GWs and the implications for the induced signals in a detector. It turns out that one can draw a very close analogy to neutrino oscillations – the dynamical conversion among neutrino generations – which one can consult to get some intuition about the expected observable effects. Neutrinos are produced in weak interactions and therefore in the flavour basis of the SM, (e, μ, τ). However, in this basis the mass matrix of neutrinos is not diagonal. Therefore, an electron-neutrino ν_e, produced e.g. in a nuclear reaction, is a QM superposition of mass eigenstates which propagate with different phase velocities. As it propagates, the interference of the mass eigenstates changes the initial state's composition in terms of flavours, until the neutrino is detected via another weak interaction. The same picture is true in bigravity: The metric perturbations of g, the tensor that couples to matter, is a superposition of massive and massless spin-2 modes. Both the production and the detection of GWs occur in the matter sector, e.g. a merging binary BH system producing GWs which are detected in the advanced LIGO detectors. Thus, a superposition of massive and massless GW is produced and an oscillation pattern is expected. For certain parameter choices, the wave packets corresponding to different mass eigenstates will overlap, and one will be able to observe an interference pattern due to the distinct phase velocities of massive and massless modes. On the contrary, in the regime where the wave packets no longer overlap, one will see a reduced overall signal strength in the detector. This will lead to a distortion of the redshift-dependent event rate. Both effects can be used to place constraints on the parameter space of bigravity and related frameworks, as we discuss in detail in this chapter.

In practice, the detection of GWs is achieved by an L-shaped laser interferometer, such as the two advanced LIGO detectors in the United States, the GEO600 detector in Germany, and the Virgo detector in Italy. If a GW passes through the array, the perpendicular arms are stretched and contracted, which leads to an observable interference pattern in the detector. The measured quantity is the *strain* projected onto the detector area, h, which is measured as the difference in the arm lengths induced by a passing GW, i.e. $\delta L(t) = \delta L_x - \delta L_y = h(t)L$ [56]. By increasing the arm length and using multiple reflections in the interferometer, displacements that are fractions of the wave length of the laser can be measured. Currently, the two LIGO detectors with their 4 km long arms located in Livingston, Louisiana and Hanford, Washington, achieve a remarkable strain

sensitivity of $10^{-23}/\sqrt{\text{Hz}}$ for frequencies in the range $50\,\text{Hz} \leq \nu \leq 300\,\text{Hz}$ [194, 195].

Thus far, the LIGO/Virgo collaborations have observed a total of six events from merging binary systems, five BH-BH mergers [56–60] and one binary neutron star (NS) merger event [61]. While the former necessarily produce a BH final state, it remains unclear which final state the latter produce, see Refs. [196, 197] for some recent work. In addition, there is a tentative signal, dubbed LVT151012 as it was only observed by the Livingston detector at much lower significance [198]. All seven have been determined to lie at redshifts well below $z = 1$, e.g. the first event GW150914 is associated with a redshift $z \approx 0.09$, while the most distant event is GW170104 at $z \simeq 0.2$. Furthermore, there is, as of yet, no measurement of stochastic [199] or periodic [200] background GW signals.

The first mention of GW oscillations in analogy to neutrinos can be found in Ref. [201]; however, in a very different and rather exotic setup which entails Lorentz violation. Ref. [202] first discussed this possibility in bigravity. However, it was not until the work of Refs. [173, 174] that the phenomenon was considered quantitatively in the bimetric framework. These references find that the effect is proportional to the deviation of the hidden metric background propagation speed from one, i.e. $[\tilde{c}(\eta) - 1]$ in the language of Sec. 2.3.2. Given the arguments there, one might be led to the conclusion that the effect should be negligible for late times, and even more so for the relevant redshifts $z < 1$. After the measurements of GW150914 and GW151226, Refs. [2, 3] reexamined the phenomenon, using the recently available data. Furthermore, it is found there that the leading effect persists even if $\tilde{c}(\eta) = 1$. Here, we begin with a discussion of the quadratic action which can be derived from the full action (2.58). Following our work in Refs. [2, 3], we will then see how the oscillation of GWs arises and which implications this has.

3.1 Quadratic action

In order to study the propagation of GWs, we need to expand the EOM around a suitable background. In Chapter 2 we have already studied a cosmological solution, which we will employ as the background solution for our analysis in the present chapter. Remarkably, we had found there that for late times, i.e. for $z < z_c \simeq 13 \times \left[\frac{m_g}{10^{-33}\,\text{eV}}\right]^{1/2}$, the cosmological background approaches that of ΛCDM with a dynamically generated CC if $m_g \sim H_0$. While this is interesting from a conceptual point of view, we do not solely focus on such small masses, but allow the mass to span several orders of magnitude, and only then draw our conclusions on viable mass ranges. Clearly, such larger masses invalidate the solution to correctly describe late-time acceleration. As we have argued in Sec. 2.3.1, degravitating the CC would be one alternative, albeit at the expense of some fine-tuning.

Tensor perturbations. Given that none of the observed GW events exceeds a redshift of $z = 0.2$, we may safely neglect the corrections to the constant solution of Eq. (2.88) and take $\tilde{c}(\eta) = 1$. Furthermore, the scale factor can be taken as constant, since at the redshifts of interest $a(\eta) = \frac{1}{1+z} = 1 + \mathcal{O}(.1)$. One last simplification that is justified is that we consider only the *vacuum* propagation of GWs, since at the time of production the Vainshtein screening will be in effect. This means that the production of the GW

signal is described correctly in the GR framework.[1]

For the cosmological background (2.85), a suitable choice to parametrise the perturbations is given by [171]

$$g_{\mu\nu} = a^2(\eta)\left(\eta_{\mu\nu} + \frac{h_{\mu\nu}(\eta,\vec{x})}{M_g}\right), \quad \tilde{g}_{\mu\nu} = b^2(\eta)\left(\eta_{\mu\nu} + \frac{\tilde{h}_{\mu\nu}(\eta,\vec{x})}{M_{\tilde{g}}}\right), \tag{3.1}$$

where $\eta_{\mu\nu}$ is the flat Minkowski metric. It is certainly not too far-fetched to guess that the linearised EOM for $h_{\mu\nu}$ and $\tilde{h}_{\mu\nu}$ will take the Fierz-Pauli form (2.2). Nevertheless, we discuss in detail how the linearised EOM are obtained from the action in Appendix A.3. Indeed, the resulting EOM can be derived from an action of the form (2.1):

$$S^{(2)}_{\rm bi} \supset -\frac{m_g^2 M_{\rm eff}^2}{8}\int d^4x\, a^4 \left(\frac{\tilde{h}^{\rm TT}_{\mu\nu}}{M_f} - \frac{h^{\rm TT}_{\mu\nu}}{M_g}\right)^2, \tag{3.2}$$

where $m_g^2 \equiv m^2\,\Gamma_* = y_* m^2(\beta_1 + 2y_*\beta_2 + y_*^2\beta_3)$, and we have chosen to show only the TT tensor components for both metrics, i.e. those that satisfy $\partial^\mu h^{\rm TT}_{\mu\nu} = 0 = \eta^{\mu\nu} h^{\rm TT}_{\mu\nu}$. These correspond to two helicity-2 excitations for each metric.[2] Thanks to this choice, the resulting EOM are cast into a very suggestive form, as derived in Appendix A.3:

$$\Box h^{\rm TT}_{\mu\nu} + 2\mathcal{H} h'^{\rm TT}_{\mu\nu} - m_g^2\, a^2 \sin(\theta)\left[\sin(\theta)\, h^{\rm TT}_{\mu\nu} - \cos(\theta)\,\tilde{h}^{\rm TT}_{\mu\nu}\right] = 0\,, \tag{3.3a}$$

$$\Box \tilde{h}^{\rm TT}_{\mu\nu} + 2\mathcal{H} \tilde{h}'^{\rm TT}_{\mu\nu} - m_g^2\, a^2 y^{-2} \cos(\theta)\left[\cos(\theta)\,\tilde{h}^{\rm TT}_{\mu\nu} - \sin(\theta)\, h^{\rm TT}_{\mu\nu}\right] = 0\,, \tag{3.3b}$$

where primes denote derivatives w.r.t. conformal time η and $\mathcal{H} = Ha(\eta)$, cf. Sec. 2.3.2. Upon diagonalisation via a generalised rotation,

$$\begin{pmatrix} h \\ \tilde{h} \end{pmatrix} \equiv \begin{pmatrix} \cos(\theta) & -y^2\sin(\theta) \\ \sin(\theta) & \cos(\theta) \end{pmatrix} \begin{pmatrix} h^{(1)} \\ h^{(2)} \end{pmatrix}, \tag{3.4}$$

these equations are decoupled,

$$\Box h^{(1),\rm TT}_{\mu\nu} + 2\,\mathcal{H}\, h'^{(1),\rm TT}_{\mu\nu} = 0\,, \tag{3.5a}$$

$$\Box h^{(2),\rm TT}_{\mu\nu} + 2\,\mathcal{H}\, h'^{(2),\rm TT}_{\mu\nu} - a^2(\eta)\,\frac{m_g^2}{y^2}\, h^{(2),\rm TT}_{\mu\nu} = 0\,. \tag{3.5b}$$

[1] This assumption is easily justified by realising that in order to satisfy solar system tests, the Vainshtein radius of the solar system must be larger than the solar system itself, which contains roughly $1\,M_\odot$. The binary systems quoted above comprise masses of the order $10\,M_\odot$ while being spatially much more compact, separated only by a few hundred kilometres when merging [56, 203]. Therefore, it is easy to see that they will safely lie inside the Vainshtein volume, if the solar system tests are passed.

[2] For the purely massive mode, the transverse-traceless condition is always true because it is a gauge invariant quantity, cf. Eq. (2.2) and Ref. [54]. Furthermore, the helicity-1 modes do not couple to the EMT, while the Vainshtein mechanism ensures that the helicity-0 modes are screened at production [53].

To solve these equations, we go to Fourier space,

$$h^{(j)}(\eta,\vec{x}) = \int \frac{\mathrm{d}^4k}{(2\pi)^4}\, e^{-i\omega\eta + i\vec{k}\cdot\vec{x}}\, \hat{h}^{(j)}(\omega,\vec{k})\,, \qquad j=1,2\,, \tag{3.6}$$

which gives

$$-\omega^2\, h^{(1),\mathrm{TT}}_{\mu\nu} + k^2\, h^{(1),\mathrm{TT}}_{\mu\nu} - 2\,\mathcal{H}\, i\omega\, h^{(1),\mathrm{TT}}_{\mu\nu} = 0\,, \tag{3.7a}$$

$$-\omega^2\, h^{(2),\mathrm{TT}}_{\mu\nu} + k^2\, h^{(2),\mathrm{TT}}_{\mu\nu} - 2\,\mathcal{H}\, i\omega\, h^{(2),\mathrm{TT}}_{\mu\nu} - a^2(\eta)\,\frac{m_g^2}{y^2}\, h^{(2),\mathrm{TT}}_{\mu\nu} = 0\,, \tag{3.7b}$$

where the hat has been omitted and $k \equiv |\vec{k}|$. While these expressions are exact as far as linear perturbations are concerned, we will now make a number of sensible assumptions that will allow us to find a simple analytic solution to the problem. To this end, we apply the late-time approximation $y = y_* = \text{const}$, together with the assumption that the Hubble rate is much less than the typical wave vector, $H \ll k$. The resulting equations allow simple plane wave solutions. Since we will be interested in redshifts $z < 1$, we may also safely set $a = 1$ (whereby $\eta = t$) to find

$$h^{(1)}_{\mu\nu}(t,\vec{x}) \propto \exp(-ik\,t + i\vec{k}\cdot\vec{x})\,, \tag{3.8a}$$

$$h^{(2)}_{\mu\nu}(t,\vec{x}) \propto \exp\left(-i\sqrt{k^2+m_g^2}\,t + i\vec{k}\cdot\vec{x}\right) \simeq \exp(-ik\,t + i\vec{k}\cdot\vec{x})\exp\left(-i\left[\frac{m_g^2}{2k}\right]t\right), \tag{3.8b}$$

where in the limit $k^2 \gg m_g^2$, the massive mode exhibits two distinct frequencies: the plane wave frequency $\omega_0 \equiv k$ and a dispersive modulation with frequency $\delta\omega \equiv \frac{m_g^2}{2\omega_0}$. Finally, the rotation (3.4) indicates the composition of the matter basis waves in terms of the mass eigenstates:

$$h_{\mu\nu} = \cos(\theta)\, h^{(1)}_{\mu\nu} - y_*^2 \sin(\theta)\, h^{(2)}_{\mu\nu}\,, \tag{3.9a}$$

$$\tilde{h}_{\mu\nu} = \sin(\theta)\, h^{(1)}_{\mu\nu} + \cos(\theta)\, h^{(2)}_{\mu\nu}\,. \tag{3.9b}$$

From hereon, we set $y_* = 1$, which can always be achieved by an appropriate rescaling of the mass parameter and the $\beta_{1,2,3}$: e.g. $m^2\, y_* \to \tilde{m}^2\, 1$, such that the physical mass remains invariant, $m_g^2 \to m_g^2 = \tilde{m}^2(\beta_1 + 2\tilde{\beta}_2 + \tilde{\beta}_3)$. These equations form the basis of our analysis, in which we discriminate two phenomenologically distinct regimes. In one regime, the two solutions, superimposed to form a spatially confined wave packet, will overlap and produce a frequency-dependent suppression of the strain and thereby modulate the signal shape. Depending on the choice of parameters, this can be quite drastic as we will see. Furthermore, the above plane wave solutions disregard the finite size of the physical wave packets that propagate in space-time. Due to the different propagation speeds of massive and massless mode, the signals will no longer overlap after they have travelled for a certain distance, resulting in a global suppression of the signal instead of interference. Combining the two regimes allows us to draw some interesting conclusions about the viable regions of the parameter space.

3.2 Oscillating gravitational waves

Let us first consider the regime in which the produced GWs interfere coherently, as required to produce an oscillatory phenomenon. At production, matter in the form of a BH or a NS binary system will produce g-type waves as it only couples to the g-metric, cf. the action (2.58), i.e. $h(t=0) = h_0$, while $\tilde{h}(t=0) = 0$. Following the calculations of Appendix A.3, wee see that this will excite a linear combination of massive and massless modes given by $h^{(1)}(t=0) = h_0 \cos(\theta)$ and $h^{(2)}(t=0) = h_0 \sin(\theta)$, cf. Eqs (A.41). Notice that the modifications discussed here have no implications on the polarisation states and we may disregard the index structure. Moreover, we discard the spatial dependence, and we set the initial value $h_0 = 1$ as it will be determined later. Combining everything we find the plane waves

$$h(t) = \cos^2(\theta)\, \exp(-i\,\omega_0\, t) + \sin^2(\theta)\, \exp(-i\,\omega_0\, t) \exp(-i\,\delta\omega\, t)\,, \tag{3.10a}$$

$$\tilde{h}(t) = \sin(\theta)\cos(\theta)\, [\exp(-i\,\omega_0\, t) - \exp(-i\,\omega_0\, t) \exp(-i\,\delta\omega\, t)]\,, \tag{3.10b}$$

whose real part is plotted in Fig. 3.1. From this we see that the maximal effect is obtained when the slow variation $\delta\omega = \frac{m_g^2}{2\omega_0}$ induces a maximal phase shift of $\delta\omega T_* = \pi$, which is true if

$$T_* = \frac{2\pi\omega_0}{m_g^2}\,. \tag{3.11}$$

We note that this coincides with the expression found for the oscillation length in neutrino oscillations, when multiplied by the propagation speed, approximately equal to the speed of light. This is one manifestation of the analogy to neutrino oscillations that we had claimed earlier. It is, of course, not a surprise to find this analogy given that the equations (3.5) describing the dynamics are wave equations, just as the Schrödinger equation governing the propagation of the neutrino wave function. Furthermore, the limit of small masses compared to the typical energies, $m_g \ll \omega_0$, is equally applicable to both phenomena. The crucial difference lies in the interpretation. We interpret the perturbation $h_{\mu\nu}$ as a physical quantity that induces a displacement of the laser beams in the GW detector leading to an interference pattern. The neutrino wave function, in contrast, has no physical interpretation; only its squared modulus can be interpreted as a probability density for the neutrino's flavour composition and location.

It should be noted that Eqs. (3.10) comprise two distinct effects. One is exclusively due to the modified dispersion relation of the massive spin-2 field and has already been studied in Refs. [56, 204], which are founded on the earlier work of Ref. [205]. There, the signal is distorted because different frequency modes of the signal propagate at different velocities, i.e. the frequency modes of the GW receive a different phase shift $e^{-i\,\delta\omega\, t}$. In our study, we wish to discuss another effect, which crucially relies on the interference of the massive and massless mode. This can be seen in Fig. 3.1, where only one frequency mode is plotted. Due to the interference of massive and massless mode, we obtain a modulation of the amplitude *for each frequency mode*, which would be lost if the mixing was $\theta = \pi/2$ (massive spin-2 limit). Away from $\theta = \pi/2$ this turns out to be the dominant effect. To quantify this suppression factor, we may proceed in two ways. The first makes use of the neutrino analogy and quickly gives the desired results, because in the massive limit, the

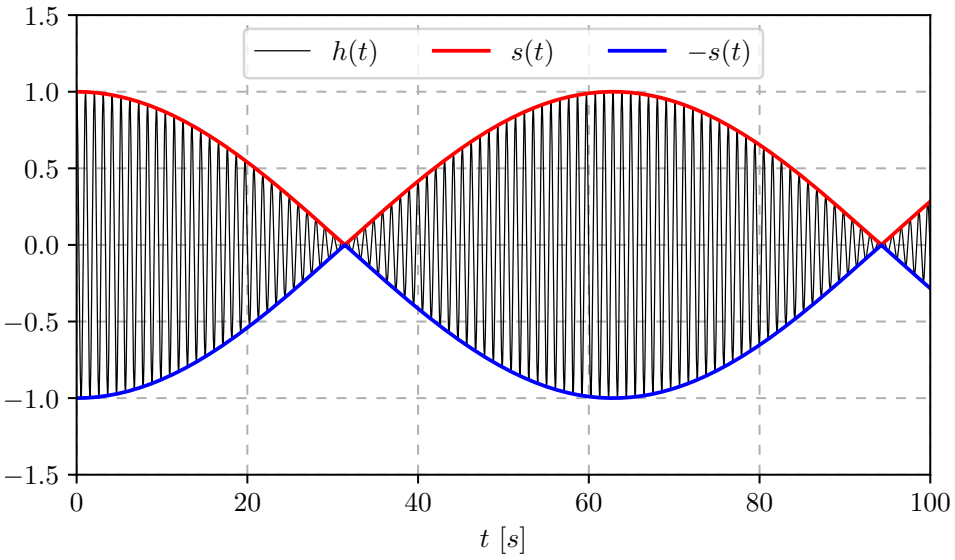

Figure 3.1.: Illustration of the averaging procedure. Shown in black is the real part of the solution (3.10a), given in Eq. (3.13a), and which upon applying the averaging procedure in Eqs. (3.15) gives the modulation (3.18). We denote $s(t) = \sqrt{s^2(t)}$. Notice the very fast oscillation with $\omega_0 = 6\,\mathrm{Hz}$ (black line) superimposed with a slow modulation with $\delta\omega = 0.1\,\mathrm{Hz}$ (coloured lines). The mixing is chosen maximal, $\theta = \pi/4$.

modified dispersion relation of the massive mode gives merely a global phase. Conversely, the second approach will highlight the physical assumptions we make in discarding the dispersion of the signal due to a massive spin-2 mode. The agreement of both approaches is yet another, *a posteriori* manifestation of the analogy.

In the former approach, we treat $h(t)$ as if it were the neutrino wave function. Squaring this quantity yields

$$s^2(\delta\omega t) \equiv |h(t)|^2 = h(t)h^*(t) = \cos^4(\theta) + 2\cos^2(\theta)\sin^2(\theta)\cos(\delta\omega t) + \sin^4(\theta)\,, \tag{3.12}$$

where the global phase $e^{-i\omega_0 t}$ has dropped out. This is the frequency dependent suppression factor that needs to be convolved with the signal strain, as discussed below.

The latter approach makes use of a real solution of Eqs. (3.5), which reads

$$h(t) = \cos^2(\theta)\,\cos(\omega_0\, t) + \sin^2(\theta)\,\cos\left([\omega_0 + \delta\omega]\, t\right), \tag{3.13a}$$

$$\tilde{h}(t) = \sin(\theta)\cos(\theta)\left[\cos(\omega_0\, t) - \cos\left([\omega_0 + \delta\omega]\, t\right)\right]. \tag{3.13b}$$

With Fig. 3.1 in mind, we wish to identify the slowly modulating envelope function s that multiplies each frequency mode of the zero-mass result $h \sim \cos(\omega_0 t)$ (the fast oscillations in Fig. 3.1). Thus, once convolved with a GR signal, this yields the corresponding waveform in bigravity without the need of a full-fledged numerical simulation. To do so, we make use of the trigonometric identity

$$\cos([\omega_0 + \delta\omega]t) = \cos(\omega_0\, t)\cos(\delta\omega\, t) - \sin(\omega_0\, t)\sin(\delta\omega\, t)\,, \tag{3.14}$$

and average out the fast oscillations to retain only the strain modulation s. In order to do so, we square the above expression for $h(t)$, and apply an averaging scheme over a time scale T which should be thought of as the propagation time of the GW. This time scale exceeds the period $T_0 = 2\pi/\omega_0$ by many orders of magnitude, but is much smaller than the oscillation time T_*, i.e. $T_0 \ll T \ll T_*$. Thus, we obtain

$$\langle \sin(\omega_0\, t)\rangle_{T_0\ll T\ll T_*} \equiv \frac{1}{T}\int_0^T \sin(\omega_0\, t)\mathrm{d}t = 0 = \langle \cos(\omega_0\, t)\rangle_{T_0\ll T\ll T_*}\,, \tag{3.15a}$$

$$\langle \sin^2(\omega_0\, t)\rangle_{T_0\ll T\ll T_*} = \langle \cos^2(\omega_0\, t)\rangle_{T_0\ll T\ll T_*} = \frac{1}{2}\,, \tag{3.15b}$$

$$\langle \sin(\delta\omega\, t)\rangle_{T_0\ll T\ll T_*} \equiv \frac{1}{T}\int_0^T \sin(\delta\omega\, t)\mathrm{d}t \simeq \sin(\delta\omega\, T)\,, \tag{3.15c}$$

$$\langle \cos(\delta\omega\, t)\rangle_{T_0\ll T\ll T_*} \equiv \frac{1}{T}\int_0^T \cos(\delta\omega\, t)\mathrm{d}t \simeq \cos(\delta\omega\, T)\,. \tag{3.15d}$$

Using these expressions, we eventually find the *envelope* of the strain (see also Fig. 3.1)

$$s(\delta\omega T)^2 = 2\times\langle h(\omega,t)^2\rangle_{T_0\ll T\ll T_*} = \cos^4(\theta)\left[1+\tan^4(\theta)+2\tan^2\theta\cos(\delta\omega\, T)\right], \tag{3.16}$$

which needs to be rescaled by a factor 2 because the unmodulated Fourier mode is simply $\cos(\omega_0 t)$, which, upon squaring, averages to $1/2$. As advocated, this agrees with Eq. (3.12) and establishes the analogy to neutrino oscillations. In this expression T should be understood as the time travelled, and can be expressed in terms of the cosmic redshift by reintroducing the scale factor for late times in coordinate time,

$$\left.\begin{aligned} a(T) &= a(t_0)e^{H_0\, T}\\ 1+z &\equiv \frac{a(t_0)}{a(T)}\end{aligned}\right\} \Rightarrow \quad T = -\frac{1}{H_0}\log(1+z)\,, \tag{3.17}$$

where $H_0 \simeq 70\frac{\mathrm{km}}{\mathrm{s\,Mpc}}$ is the Hubble rate today. Notice that this is in fact in contrast with our previous assumption that $a = \text{const}$, and therefore is valid only for small $z < 1$.[3] Finally, we obtain for a given redshift a frequency modulation of the form

$$s^2(\omega_0, z) = \cos^4(\theta)\left[1+\tan^4(\theta)+2\tan^2(\theta)\cos\left(\frac{m_g^2}{2\omega_0}\frac{\log(1+z)}{H_0}\right)\right]. \tag{3.18}$$

Given that we do not assume any modification of the production process by virtue of the Vainshtein mechanism, we can use the binary system parameters as inferred from the events GW150914 and GW151226 by the LIGO detector array. These serve as input values for the publicly available numerical code, the Einstein Toolkit, that we use to generate a GR waveform [206–215]. The resulting waveform should now be convolved with the frequency dependent modulation s, which in practice is implemented by multiplication

[3] In general, the Hubble rate is given by $H(z) = H_0\sqrt{\Omega_m(1+z)^3+\Omega_r(1+z)^4+\Omega_k(1+z)^2+\Omega_\Lambda}$, with energy densities for non-relativistic matter Ω_m, radiation Ω_r, curvature Ω_k, and dark energy Ω_Λ. Using this and the best fit values of Ref. [12], one can find that the transition to an accelerated expansion occurs for redshifts $z \lesssim 0.6$, which is true for all observed LIGO/Virgo events.

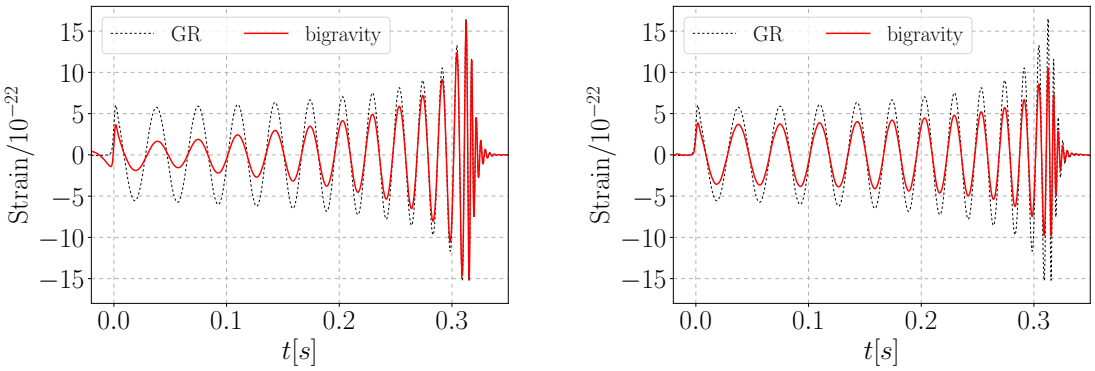

(a) $m_g = 10^{-22}\,\mathrm{eV}$ **(b)** $m_g = 10^{-19}\,\mathrm{eV}$

Figure 3.2.: Waveform modulation in bigravity for different graviton masses m_g. The mixing angle has been chosen such as to maximise the visible effect, $\theta = \pi/4$. Figures adapted from Ref. [2].

in Fourier space. Concretely, we start with a simulated strain $h^{\mathrm{GR}}(t)$, and obtain the bigravity strain via

$$h^{\mathrm{bi}}(t) = \int \mathrm{d}\omega\, e^{i\omega t} s(\omega, z)\, \hat{h}^{\mathrm{GR}}(\omega) = \int \mathrm{d}\omega\, e^{i\omega t}\, s(\omega, z) \int \frac{\mathrm{d}\tau}{2\pi}\, e^{-i\omega\tau} h^{\mathrm{GR}}(\tau)$$
$$= \int \mathrm{d}\tau \tilde{s}(t-\tau, z) h^{\mathrm{GR}}(\tau)\,, \tag{3.19}$$

where $\tilde{s}(t, z)$ is the Fourier transform of $s(\omega, z)$ w.r.t. ω. The resulting waveform is shown in Fig. 3.2 for two different benchmark models. We observe that the resulting signal (solid red line) can be extremely distorted compared to GR (dashed line), as Fig. 3.2a illustrates. We remark that the parameters have been chosen in order to maximise the effect for illustrative purposes.

Another important result can be seen in Fig. 3.2b, where the signal shape is modulated *independently* of the frequency. It appears that all frequency modes receive a constant suppression. This signals that for the chosen parameters, one has entered the regime of decoherence, which we will discuss closer in the next section.

Finally, we can analyse the waveform, which we allow to be rescaled by a global factor in order to lie within the error bands. This would be interpreted as a merger event at larger distance, as we will discuss shortly. The result of this analysis is shown in Fig. 3.3, where we used a simple χ^2 estimator to draw the 95% C.L. exclusion limits (cf. Appendix B.2 for details). Clearly, this does not capture the entire picture in the regime of larger masses, where the suppression will become constant and independent of frequency. Nevertheless, it gives us a simple and reliable way to rule out masses and mixing angles that heavily modulate the signal as in Fig. 3.2a.

We have also included the most stringent, model-independent bound on the graviton mass available in the literature, namely the one from tests in our solar system: $m_g < 7.2 \cdot 10^{-23}\,\mathrm{eV}$ [205, 216]. Since we smoothly approach GR in the limit where $\theta \to 0$, by

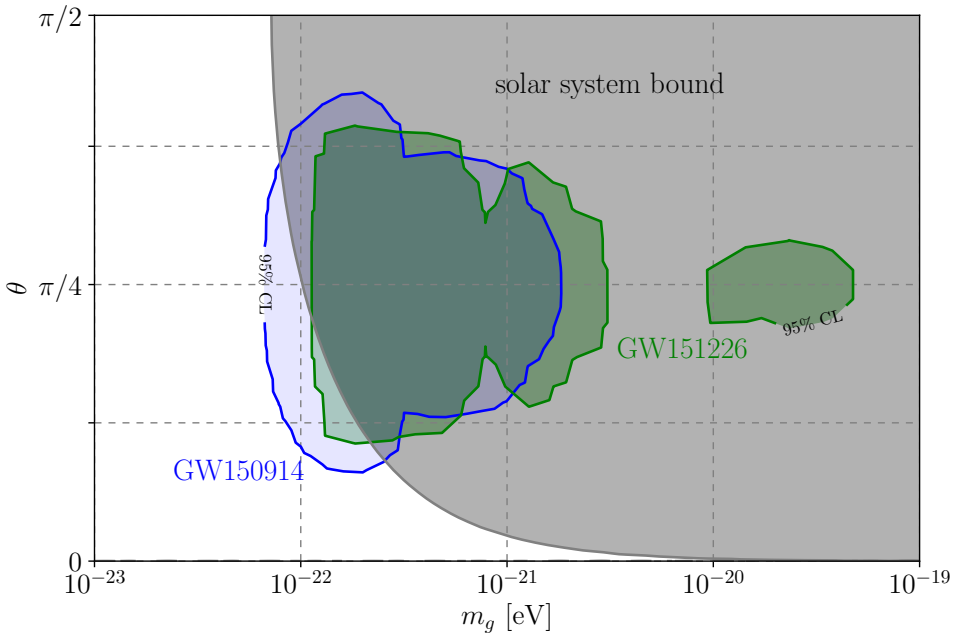

Figure 3.3.: Excluded region from GW oscillations. Recall that the mixing angle is defined such that $\theta = 0$ reproduces GR and $\theta = \pi/2$ corresponds to gravity mediated by a massive spin-2 field alone. The case of maximal mixing, $\theta = \pi/4$, yields the strongest bound. Figure adapted from Ref. [2].

decoupling the heavy spin-2 state, we rescale this bound by a factor $\sin^{-1}(\theta)$. This is consistent with considerations concerning the Newtonian limit of bigravity, see Eq. (2.84).[4]

3.3 Gravitational waves in the decoherence regime

In order to better understand the regime where the suppression becomes independent of the frequency, or equivalently independent of the distance [cf. Eq. (3.11)], we calculate the average strain w.r.t. GR for various masses and mixing angles in Fig. 3.4. There we see that the squared strain averaged over the signal time, and plotted as a function of redshift, receives a constant suppression depending on the mixing angle, see Fig. 3.4a. The critical redshift where this decoherence occurs is, in turn, a function of the mass m_g as we conclude from Fig. 3.4b. Let us now specify under which conditions this phenomenon occurs and which observable consequences this would have. Suppose a source produces a GW strain of given functional form, which is decomposed into massless and massive contributions according to Eqs. (3.10), $\hat{h} = \cos^2(\theta)\,\hat{h}_1 + \sin^2(\theta)\,\hat{h}_2$. This corresponds to a

[4] To see this, notice that the solar system bound is obtained from the modification of the force, which is given by $-\frac{\partial V}{\partial r} = \frac{r_S}{r^2}(1 + m_g\, r)e^{-m_g\, r} = \frac{1}{r^2}\left[1 - \frac{1}{2}\,(m_g\, r)^2 + \mathcal{O}\left((m_g\, r)^4\right)\right]$ [205]. Thus, the bound applies to $m_g^2 \times \sin^2(\theta)$.

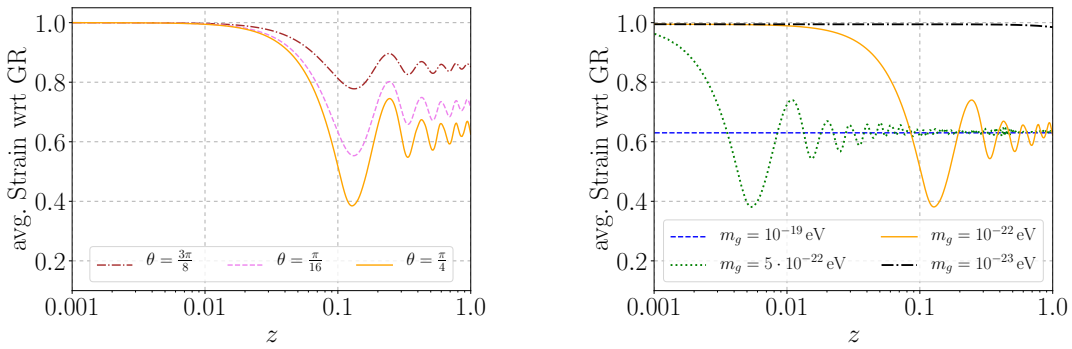

(a) $m_g = 10^{-22}\,\mathrm{eV}$ **(b)** $\theta = \pi/4$

Figure 3.4.: Suppression factor as a function of redshift for fixed graviton mass (*left*) and mixing angle (*right*). For large redshift the oscillation averages out and we enter the decoherence regime, where the suppression is no longer redshift (frequency) dependent. The level of suppression is determined by the mixing angle θ, while the onset of the decoherence regime is determined by the mass m_g.

GW strain

$$h(t,\vec{x}) = \cos^2(\theta)\int \frac{\mathrm{d}^3k}{(2\pi)^3}\frac{e^{-i\omega_1(k)t+i\vec{k}\cdot\vec{x}}}{2\omega_1(\vec{k})}\hat{h}_1(\omega_1(\vec{k}),\vec{k}) + \\ + \sin^2(\theta)\int \frac{\mathrm{d}^3k}{(2\pi)^3}\frac{e^{-i\omega_2(k)t+i\vec{k}\cdot\vec{x}}}{2\omega_2(\vec{k})}\hat{h}_2(\omega_2(\vec{k}),\vec{k})\,, \tag{3.20}$$

where $\omega_1(k) = k = \omega_0$ and $\omega_2(k) = \sqrt{m_g^2 + k^2} \simeq \omega_0 + \frac{m_g^2}{2\omega_0} = \omega_0 + \delta\omega$. While the massless mode will travel with a group velocity equal to the speed of light,

$$v_{g,1} = \frac{\mathrm{d}\omega_1(k)}{\mathrm{d}k} = 1\,, \tag{3.21}$$

the massive mode will travel with a dispersive and lower group velocity,

$$v_{g,2} = \frac{\mathrm{d}\omega_2(k)}{\mathrm{d}k} = \frac{k}{\omega_2} \simeq 1 - \frac{m_g^2}{2\omega_0^2}\,. \tag{3.22}$$

Consulting Fig. 3.5 for some physical intuition, we see that after a time of flight T yet to be determined, the centre of the wave packets will be separated by a distance $\Delta L = \Delta v_g\, T = \frac{m_g^2\, T}{2\omega_0^2}$. If this separation exceeds the width of the wave packets, say σ_x, any interference pattern will be lost, i.e. if

$$T > T_{\mathrm{coh}} \equiv \frac{2\sigma_x\omega_0^2}{m_g^2}, \tag{3.23}$$

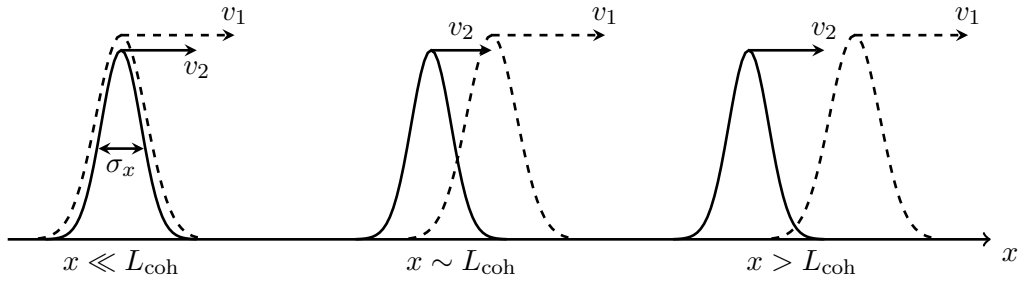

Figure 3.5.: Separation of wave packets with different group velocities $v_1 > v_2$, and widths σ_x. Once the distance travelled exceeds the coherence length, the wave packets no longer overlap and therefore no interference is possible. For large enough distances two signals can be observed in principle. See also Refs. [217, 218] for discussions in the context of neutrino wave packets.

or equivalently if the distance of the GW source is more distant to the detector than

$$L_{\rm coh} \approx 0.1\,{\rm s} \cdot c\,\frac{2\omega_0^2}{m_g^2} \approx 1\,{\rm Gpc}\,\left(\frac{\sigma_x}{0.1\,{\rm s}}\right)\,\left(\frac{10^{-22}\,{\rm eV}}{m_g}\right)^2\,\left(\frac{\nu}{30\,{\rm Hz}}\right)^2\,, \tag{3.24}$$

where we have estimated the signal width with $\sigma_x/c = 0.1\,{\rm s}$, and used that the frequency is $\nu = \omega_0/2\pi$. Finally, we remark that an exact determination of σ_x would require a simulation of the signal at production, which is computationally very costly. However, the argument can be turned around by using a fixed distance, say $L = 100\,{\rm Mpc}$ or $z = 0.02$, and a frequency $\nu = 30\,{\rm Hz}$, which is on the lower end of the observed frequency spectra. With these numbers, we find that the mass must be larger than $5 \cdot 10^{-22}\,{\rm eV}$ in order for that specific frequency mode to decohere entirely. This is in qualitative agreement with Fig. 3.4b. We content ourselves with this estimate, but emphasise that a future, possibly numerical treatment of this phenomenon should improve on this uncertainty.

With the understanding of the requirement for the two wave packets corresponding to massive and massless components of the GW signal to be non-overlapping, we can now consider the phenomenological consequences. Assuming to be in the decoherence regime, i.e. $L > L_{\rm coh}$ for all frequencies, a source at a distance L will induce *two* signals in the detector, separated by a time

$$\Delta T = L(v_{g,\,2}^{-1} - v_{g,\,1}^{-1}) \simeq L\frac{\Delta v_g}{v_{g,\,1}^2}\,. \tag{3.25}$$

According to Eqs. (3.10), the first signal will be suppressed by a factor $\cos^2(\theta)$, the second one by a factor $\sin^2(\theta)$, which is confirmed by Fig. 3.4.

The key observation underlying our analysis is that the luminosity distance of a GW source is derived from the assumption that, as the wave propagates isotropically away from the production site, its strain is reduced as $1/d_L$ [219], where

$$d_L(z) = c\,(1+z)\int H(z')^{-1}{\rm d}z' \tag{3.26}$$

is the luminosity distance. Thus, the decohered signals would be interpreted as lying at

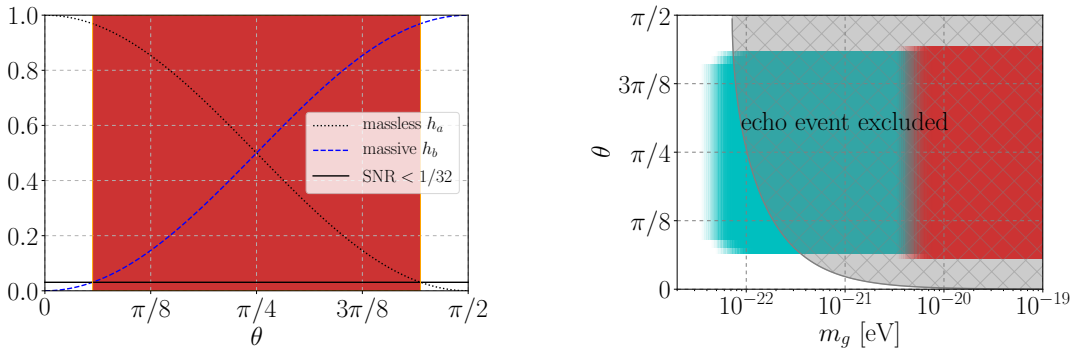

(a) suppression factor **(b)** echo event constraints

Figure 3.6.: *Left*: Modulation of the suppression factor as a function of the mixing angle θ and excluded range of angles from the non-observation of an echo for GW170817 (red). *Right*: Summary of excluded parameter regions due to the non-bservation of GW echoes in the available LIGO/Virgo data for BH merger events (turquoise) and the NS merger GW170817 (red). The turquoise region is overlain by the red region for better visibility. Figures adapted from Ref. [3].

larger luminosity distance, or redshift $z_{\rm obs}$:

$$\cos^2(\theta)/d_L(z) = 1/d_L(z_{\rm obs}^{m=0})\,, \quad \sin^2(\theta)/d_L(z) = 1/d_L(z_{\rm obs}^{m\neq 0})\,. \tag{3.27}$$

It is then a matter of interpretation if we study individual events and their *echoes*, or the distribution of merger events as a function of redshift, where each event would be double counted. We will discuss both approaches in more detail now.

3.3.1 Echo events in the gravitational wave detector

First, we take the point of view that the secondary signal, h_b, which is suppressed by $\sin^2(\theta)$, would be seen as an *echo* of the first signal, h_a. For the available GW signals, we display in Fig. 3.6 how constraints on the parameter space arise from the *non-observation* of such echo events. The left panel shows an example for the NS merger event GW170817, which is the event with the largest signal-to-noise ratio (SNR) (SNR = 32). The red region is excluded, because inside it the echo event would be observable above the background noise ($\sin^2(\theta) > {\rm SNR}^{-1}$).[5] The range of mixing angles that can be excluded by this procedure is then transformed into an exclusion region in the right panel of Fig. 3.6 by demanding the mass m_g to be sufficiently large for the entire signal to be in the decoherence regime. Note that the shading indicates the onset of decoherence via Eq. (3.24). This yields the red region, while the turquoise regions correspond the available binary BH merger events. Notice that these exclude a smaller range of angles – due to the smaller SNR – however, probing smaller masses owing to the larger distance of the event sources.

[5] Notice that conventionally a threshold SNR > 8 is adopted for a detection [220]. However, a dedicated search for echo events could make use of the primary signal waveform and thereby effectively lower the threshold.

event name	d_L [Mpc]	min. ν [Hz]	time scale [s]	max. SNR	reference
GW150914	420	35	0.1	24	[56]
GW151226	440	35	1.0	13	[57]
GW170104	880	35	0.1	13	[58]
GW170608	340	35	1.0	13	[59]
GW170814	540	35	0.1	18	[60]
GW170817	40	40	10.0	32	[199]

Table 3.1.: Parameters of the BH and NS binary merger events. Time scales are order-of-magnitude estimates from the total duration of the events. For updated values see also Ref. [198].

We have summarised the relevant parameters of the LIGO GW events in Tab. 3.1, from which we can draw the conclusions shown in Fig. 3.6b.

3.3.2 Modified merger distribution

Next, one may study what can be learnt from a larger set of binary merger events. Given that a signal is misplaced to larger redshift, we expect the annual merger rate as a function of redshift to be modified compared to the standard prediction. More specifically, one should expect *less* events at small redshift, and simultaneously *more* events at larger redshift, when compared to the GR prediction. Let us make the assumption that $z_{\rm obs}^{m\neq 0} > z_{\rm obs}^{m=0}$, i.e. the primary signal is due to an undistorted, massless spin-2 wave, which effectively restricts the mixing angle to be $0 \leq \theta < \pi/4$. The regime $\pi/4 \leq \theta \leq \pi/2$ is straightforwardly obtained from this; however, there is an additional complication because the signal is distorted due to the modified dispersion relation, cf. [205], which we discard in our analysis. While future surveys can easily implement this numerically, we try to isolate the present phenomenon and study it analytically.

Given a BH binary merger rate R, we follow Ref. [220] and parametrise the differential merger rate per unit redshift as

$$\frac{dN}{dz} = 4\pi\, R\, \chi(z)^2 (1+z)^{(R_b-1)} \frac{c}{H(z)}\,, \tag{3.28}$$

with the co-moving distance $\chi(z)$ and a free parameter R_b. Ref. [220] finds the best fit value $R_b = 2$ and remarks that the result is valid for $z < 10$. From the O1 run of advanced LIGO (GW150914, LVT151012, GW151226), it can be inferred that the merger rate is[6] [198]

$$R = 55\,^{+103}_{-41}\,\mathrm{Gpc}^{-3}\,\mathrm{yr}^{-1}\,. \tag{3.29}$$

While the errors on this number are still large, it is expected that in the near future, with more events available and advanced LIGO running at design sensitivity probing redshifts

[6] This number is obtained by an event based mass distribution disregarding astrophysical population models. Note, however, that this number changes significantly when astrophysically motivated mass distributions are assumed. More conservatively, the LIGO/Virgo collaborations quote a range of $R = 9 \ldots 240\,\mathrm{Gpc}^{-3}\,\mathrm{yr}^{-1}$, which is the lowest and the largest R found from various priors and mass distributions, cf. Ref. [198]. This range is consistent with later events at larger redshift, namely GW170104 at $z = 0.18$ [58].

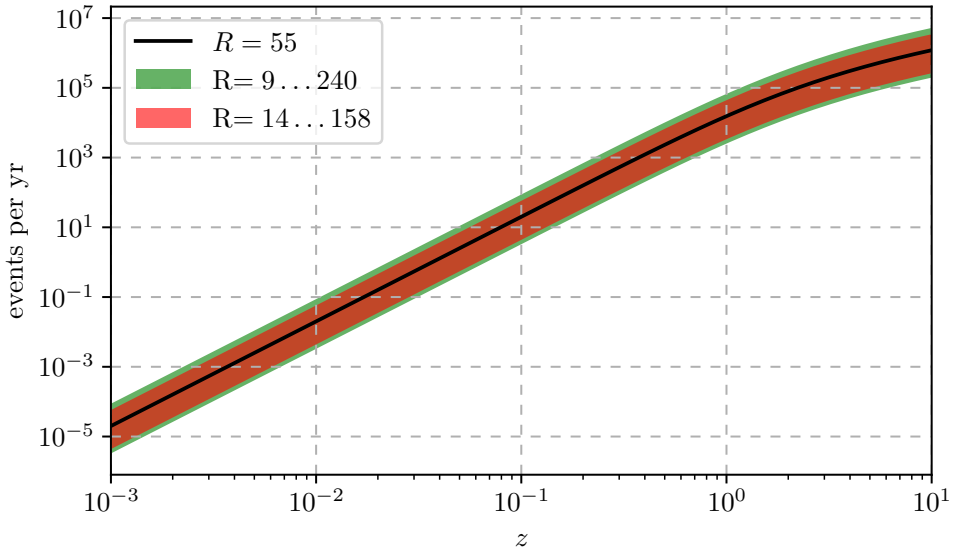

Figure 3.7.: Integrated annual BH merger rate as a function of redshift and for different merger rate constants taken from Ref. [198].

$z \lesssim 1$ [195, 221], the error bars could come down to about 10% [220]. We remark that with the envisioned Einstein Telescope, redshifts as large as $z \lesssim 10$ could be probed [222–224].

Integrating Eq. (3.28) up to a redshift $z \approx 0.1$, yields a total of 20^{+50}_{-15} observable events per year; not all of which induce a strain large enough to be actually detected.[7] This is shown in Fig. 3.7, where one can see that increasing the sensitivity, such that redshifts $z = 1$ can be probed, may increase this number by a factor 10^3.

It is now straightforward to solve Eq. (3.27), and thereby determine the differential merger rate for a given, observed redshift $z_{\rm obs}$. Demanding that the event lies entirely in the decoherence regime, yields a *lower* bound on m_g, cf. Eq. (3.24). Combing this with the *upper* bound from solar system tests, $m_g \sin(\theta) \leq 7.2 \cdot 10^{-23}\,\mathrm{eV}$, we finally obtain a necessary condition

$$\begin{aligned} d_L(z) > L_{\rm coh} &> 1.0\,\mathrm{Gpc} \left(\frac{\sigma_x}{0.1\,\mathrm{s}}\right) \left(\frac{\nu}{30\,\mathrm{Hz}}\right)^2 \left(\frac{10^{-22}\,\mathrm{eV}}{m_g}\right)^2 \\ &> 2.4\,\mathrm{Gpc} \left(\frac{\sigma_x}{0.1\,\mathrm{s}}\right) \left(\frac{\nu}{30\,\mathrm{Hz}}\right)^2 \times \sin^2(\theta)\,. \end{aligned} \tag{3.30}$$

In Fig. 3.8 we show the result of this procedure for various mixing angles, using both the current and future merger rate intervals. Notice that we have indicated the necessary condition (3.30) by dashed lines. The fading of the shaded areas indicates that this is only an estimate and the bounds cannot be fully trusted already in the shaded region which indicates the onset of decoherence.

Generally speaking, the reduction of the strain leads to the mislocation of events to

[7] Using the merger rate $R = 9 \ldots 240\,\mathrm{Gpc}^{-3}\,\mathrm{yr}^{-1}$ quoted in Footnote 6, and integrating up to the redshift of GW170104, $z = 0.18$, we find instead a range of $26 \ldots 693$ merger events per year.

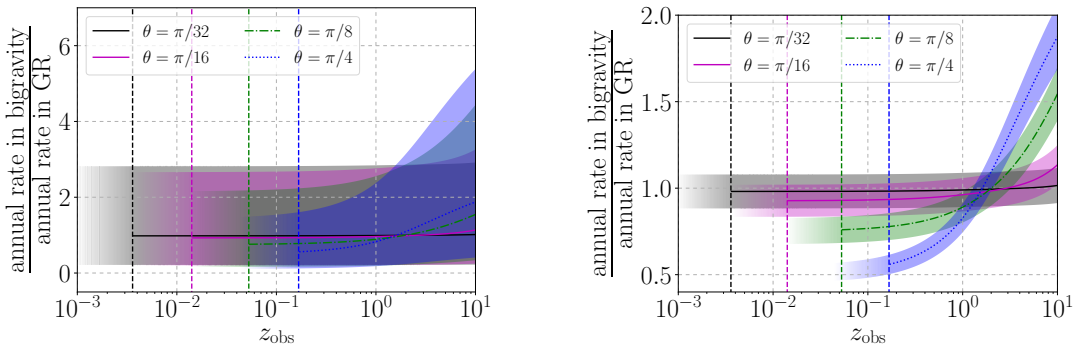

(a) present uncertainty **(b)** future uncertainty

Figure 3.8.: Annual merger rates in bigravity modulated according to the individual event assumption with current (*left*) and projected (*right*) uncertainties. The dashed lines indicate the onset of decoherence. Figures adapted from Ref. [3]

lie at larger redshift. Therefore, the event rate relative to GR is less than one for small redshifts, with the reduction increasing with the mixing angle, and reaching its maximum for $\theta = \pi/4$. Consequently, we find more events at larger redshifts than expected in GR.

Due to the presently large error bars, all values of θ are compatible with the GR prediction and we cannot draw any conclusions, as we see from the left panel. However, with the current experiments reaching design sensitivity and more data being collected (cf. Fig. 3.8, right panel), scenarios with large mixing ($\theta \gtrsim \pi/8$) can be probed.

3.4 Discussion and outlook

We have presented the phenomenon of GW oscillations, an effect reminiscent of neutrino oscillations, which originates from the presence of multiple spin-2 fields of different masses that couple non-diagonally to matter. We have studied two regimes, where in the first the wave packets interfere coherently allowing us to immediately constrain the parameter space. Interestingly, the resulting bounds are of similar order as the solar system tests. The second regime is reached when the two wave packets are separated due to different group velocities and no longer interfere. This leads to a frequency-independent reduction of the strain and a misinterpretation of the event to be more distant, if GR is assumed. While an 'echo event' would be a striking signature of bi- or multi-metric models, one can even learn about the existence of such events from the binary BH merger distribution, given that the secondary event is interpreted to lie at a redshift beyond the sensitivity of the detector. Therefore, if after a few years of recording BH merger events, the rate of such events turns out to be lower than expected at low redshift, this might hint towards GW echoes. It would also be interesting to consider instead of BH binaries, NSs which would additionally produce an electromagnetic signal. This could be used to compare the population of binary NS systems deduced from optical signals to those inferred from GW measurements. However, at present only one binary NS event is available and this is left

for future work.

In fact, there are claims of such echo events in the literature (cf. Refs. [225–227]), but this interpretation is subject to debate [228–230]. However, we would like to point out that while such echoes are usually interpreted in the context of so-called exotic compact objects [231–233], an echo is also expected if the massless mediator of gravity can oscillate into massive spin-2 states. Our aim was to gain an analytic understanding of the phenomenon of GW oscillations. In order to to so, we have made a number of approximations that allowed an analytic treatment. Nevertheless, the results are straightforwardly generalised and can be implemented in a numerical survey taking into account all effects.

A direct generalisation of the approach outlined in this chapter is to study different matter couplings such as those in doubly-coupled bigravity [120–122], whose background solutions have been studied in Refs. [190, 191, 234–236]. This has already been done in Ref. [237], where the authors find that the main effect is a modified GW speed different from the speed of light, and no interference pattern seems to arise.

A final remark is in order at this point. The inclined reader may have noticed that some of our early results deviate from the expressions found in Ref. [2]; however, physically observable results agree, most importantly the modulation factor in Eq. (3.18). The reason for the initial disagreement is that in the reference, non-canonically normalised states were considered. While it is irrelevant to the final result, canonically normalised states should always be given preference, especially in the light of a particle interpretation.

Chapter 4

Astrophysical Implications of Bigravity

Rotation curves of galaxies, i.e. the circular velocity of the visible contents of a galaxy around its centre, are considered one of the evidences for the existence of DM. While observations of galaxy clusters, the CMB, and structure formation simulations support this hypothesis, the properties and origin of the DM remain among the greatest mysteries of modern physics. Modified gravity models such as modified Newtonian dynamics (MOND) have prominently been used to argue that DM is obsolete [238]. However, there is little to no evidence that such theories describe the phenomenon correctly on all length scales [239–241].[1] This can be seen from a very simple argument: Cold DM – the 'CDM' in ΛCDM – is a non-relativistic fluid which forms haloes of various sizes and mass. It is found that the mass of these haloes approximately scales with the third power of the characteristic radius, $M \propto r_c^3 \sim V_c$, over a vast range of halo sizes [244]. This yields the correct behaviour in order to explain dynamics on galactic and extragalactic (galaxy cluster) scales. MOND, on the other hand gives rise to a critical scaling incompatible with these observations. This is because MOND modifies the gravitational force at a critical *acceleration* $a_c = F_c/m \propto M/r_c^2$. Thus, one finds that $V_c \sim r_c^3 \propto M^{3/2}$, and it is impossible to explain all observed phenomena with a single MOND-type acceleration or length scale. This is different for modifications that invoke the Vainshtein screening mechanism, such as the present bimetric framework. Here, the modifications occur at the Vainshtein radius $r_V \propto \sqrt[3]{M}$ [cf. Eq. (2.84)], and therefore one obtains a critical scaling *identical* to that of DM. This argument, due to J. Smirnov [4], raises the question how the modifications that arise due to the presence of multiple spin-2 fields affect the DM phenomenon. This will be the subject of the present chapter.

Historically, it is not a new idea to apply modified gravity frameworks to galaxy dynamics. However, it is often implied that the modifications should *replace* the DM component in the galaxies. For example, many studies of modified gravity models tried to argue that DM is obsolete, in the spirit of the early work of Ref. [245]. These references often considered only individual examples, or argued on the basis of feasibility [246–249]. Nev-

[1] Recently, it has been found that a single-scale modification cannot even successfully explain the dynamics on various galactic scales [242, 243].

ertheless, a few of these studies considered more data sets of galaxies [250, 251], some even including galaxy clusters [252, 253]. There are indeed examples of studies that considered a DM component [254, 255], and yet others quantified the observational bias due to the assumption of a Newtonian potential in favour of a modified Yukawa potential [256]. A more recent idea was put forward in Ref. [257], where the authors included for the first time the Vainshtein screening effect. However, this is done on the rather simplistic argument that the galaxy should be contained in its own Vainshtein radius – disregarding potential positive effects this might have. Moreover, dRGT massive gravity and its implications for galactic dynamics was recently explored in [258]; however, only in a specific parameter regime and neglecting the Vainshtein mechanism. Finally and most recently, Ref. [259] assumed generic Yukawa-type modifications of the gravitational potential and explored their impact on galaxy rotation curves – once more disregarding the Vainshtein effect and considering modifications in the DM sector only.

Here, we do not pursue to replace DM, but rather ask what implications does the presence of a massive spin-2 field – in addition to the massless spin-2 mediator of gravity – have on the DM phenomenology. Nevertheless, we do highlight when improved fits can be obtained. In this manner, we believe to present an unbiased analysis of potential benefits and shortcomings of the model at hand. To this end, the expression for the deflection angle of light in bigravity is derived and put to test on a galaxy cluster. While this is only meant as a proof of principle, it can be directly applied to large surveys involving many such clusters. We continue with the study of galactic dynamics, derive the matter potentials for gas, baryonic matter and DM components, and finally apply the findings to galaxy rotation curves. The results of this chapter have been published in Ref. [4].

4.1 General procedure

Newtonian Gravity. The starting point for our discussion is Poisson's equation for Newtonian gravity, which determines the potential Φ in terms of a mass density ρ,

$$\Delta\Phi(\vec{r}) = 4\pi\, G_{\rm N}\, \rho(\vec{r})\,, \tag{4.1}$$

where $\Delta = \sum_i \partial_i^2$ is the Laplace operator. This is easily solved by the Green's function method,

$$\Phi(\vec{r}) = -G_{\rm N} \int \mathrm{d}^3\vec{r}\,' \, \frac{\rho(\vec{r}\,')}{|\vec{r} - \vec{r}\,'|}\,. \tag{4.2}$$

Let us assume spherical symmetry such that $\rho(\vec{r}) = \rho(|\vec{r}|)$. Orienting the primed coordinates such that the polar angle θ' is the angle between $\vec{r}$ and $\vec{r}\,'$, we can carry out the angular integrations,

$$\Phi(|\vec{r}| = r) = -2\pi G_{\rm N} \int \mathrm{d}\cos\theta'\, \mathrm{d}r\, r'^2 \frac{\rho(r')}{\sqrt{r^2 - 2\cos\theta' r\, r' + r'^2}}$$

$$
\begin{aligned}
&= 2\pi G_{\rm N} \int {\rm d}r'\, \rho(r') \frac{r'}{r}\, \sqrt{r^2 - 2\cos\theta' r\, r' + r'^2}\Big|^1_{\cos\theta'=-1} \\
&= -2\pi G_{\rm N} \Bigg\{ \int_{r'<r} {\rm d}r'\, \rho(r') \frac{r'}{r} \left[(r+r') - (r-r')\right] + \\
&\qquad\qquad + \int_{r'>r} {\rm d}r'\, \rho(r') \frac{r'}{r} \left[(r+r') - (r'-r)\right] \Bigg\} \\
&= -4\pi \frac{G_{\rm N}}{r} \underbrace{\int_{r'<r} {\rm d}r'\, \rho(r') r'^2}_{=M(r)/4\pi} + r\text{-independent terms}, \qquad (4.3)
\end{aligned}
$$

where $r' = |\vec{r}\,'|$. Thus, we find for a Newtonian potential a mass-velocity relation of the form[2]

$$
v^2(r) = r \frac{{\rm d}\Phi}{{\rm d}r} \overset{\rm GR}{=} \frac{G_{\rm N} M(r)}{r}\,. \qquad (4.4)
$$

Massive gravity. For the case of a massive mediator, the Poisson equation is modified to include a mass term, cf. [260]

$$
(\Delta - m^2)\tilde{\Phi}(\vec{r}) = 4\pi G_{\rm N} \rho(\vec{r})\,, \qquad (4.5)
$$

which is responsible for the Yukawa potential, with its exponential fall-off for $r > m_g$,

$$
\tilde{\Phi}(\vec{r}) = -G_{\rm N} \int {\rm d}^3\vec{r}\,'\, \rho(\vec{r}\,') \frac{e^{-m_g|\vec{r}-\vec{r}\,'|}}{|\vec{r}-\vec{r}\,'|}\,. \qquad (4.6)
$$

The radial integral in this potential cannot be decomposed as we had done before, and the mass distribution contributes also for $r' > r$ – however, exponentially suppressed. This leads to a modification in the relation between the radius and (circular) velocity distribution. Thus, the validity of Eq. (4.4) is lost, and we have to revert to the integration of the potential,

$$
v^2(r) = r \frac{{\rm d}\tilde{\Phi}}{{\rm d}r} \neq \frac{G_{\rm N} M(r)}{r}\,. \qquad (4.7)
$$

Nevertheless, it should be remarked that the exponential fall-off is negligible if the mass distribution is well inside the Compton radius of the massive mediator, i.e. $r_0 \ll \lambda_c \equiv m_g^{-1}$. Here, r_0 is the length scale of the mass density, in the sense that $\rho(r) \to 0$, as $r_0/r \to 0$, and λ_c is the Compton wavelength of the graviton. In this limit the exponent is close to unity and the Yukawa modification becomes irrelevant: $\exp(-m_g\, r) \sim 1$ for all $r \leq r_0 \ll \lambda_c$.

Bigravity. One may now assemble the pieces of the previous paragraphs and the study of the central mass problem in Sec 2.3.1. Owing to the linearity of Poisson's equation, the potential generated by two spin-2 mediators – one massless and one massive – is given by

[2] In computing the derivative, it should be noted that in the second to last line, differences in the integration boundaries cancel and can therefore be ignored. Thus, there is no $\frac{{\rm d}M}{{\rm d}r}$ term.

the superposition (see also Eq. (2.84) for a point mass)

$$\Phi(\vec{r}) = -G_{\rm N} \int \mathrm{d}^3\vec{r}\,'\ \rho(\vec{r}\,') \left[\frac{\alpha(\theta)}{|\vec{r}-\vec{r}\,'|} + \frac{\beta(\theta) e^{-m_g|\vec{r}-\vec{r}\,'|}}{|\vec{r}-\vec{r}\,'|} \right]. \tag{4.8}$$

This, together with the relation $v^2(r) = r\frac{\mathrm{d}\Phi}{\mathrm{d}r}$, fully determines the velocity profile of the galaxy under consideration once the mass density is specified.

At this point, one should highlight the importance of the Vainshtein mechanism in massive and bimetric gravity. We have seen in Chapter 2, that the longitudinal mode becomes non-dynamical if the gravitational potential is evaluated for distances $r < r_V$, where the Vainshtein radius is found to be

$$r_V = \sqrt{\frac{r_S}{m_g^2}}\,. \tag{4.9}$$

Here, one needs to take into account that the mass distribution itself becomes a function of the radial coordinate r, and thereby also the Vainshtein radius r_V via the Schwarzschild radius $r_S(r) = 2G_{\rm N}M(r)$.

Given that this effect is of non-linear nature and that, in general, one cannot evaluate the true potential for all values of parameters efficiently, we choose a phenomenological approach to account for this effect. This is done via the mixing angle as it allows an interpolation between the massive and the massless, i.e. GR, regimes. We introduce the effective mixing angle,

$$\theta_{\rm eff} \equiv \frac{\theta}{2}\left[1 + \tanh\left(\frac{r - r_V}{\Delta r_V}\right)\right], \tag{4.10}$$

which replaces the mixing angle θ in the numerical evaluation of all expressions that we use in this chapter, even if not stated explicitly. This expression smoothly interpolates between a linear regime where $\theta_{\rm eff} = \theta$, for $r \gg r_V$, and the non-linear regime, where $\theta_{\rm eff} = 0$, for $r \ll r_V$. The width of the intermediate regime, Δr_V, is taken to be a free parameter, although this will not be strictly speaking true in a fully non-linear analysis. There, one would find that the transition regime is fully determined dynamically. Given that we are interested in a physical picture rather than an exact treatment to all orders, we believe that such a phenomenological approach is well justified. We proceed with the analysis of gravitational lensing and subsequently discuss galactic rotation curves in Sec. 4.3.

4.2 Gravitational lensing

The bending of light is one of the most important predictions of GR, and considered one of the earliest successful tests of Einstein's theory of gravity by the measurements of Eddington and Dyson during the solar eclipse of 1919 [261]. However, the phenomenon is not unique to GR. Indeed, it is a generic feature of metric formulations of gravity, in

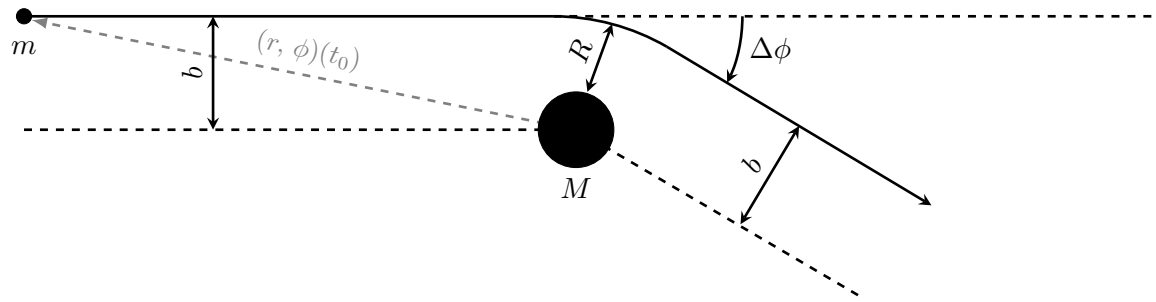

Figure 4.1.: Sketch of the light deflection geometry.

which a test mass follows a geodesic.[3] Thus, it seems rather natural to ask how light is deflected in a modified theory of gravity, like the present bimetric theory. To the best of our knowledge, this result has not been obtained consistently in the literature, and was recently presented in Ref. [4]. In the following we derive the light deflection angle in bigravity and study some observational implications for the parameter space of the theory.

4.2.1 Bending of light in bigravity

To study the effects massive spin-2 extensions have on the propagation of light, we follow the derivation of Ref. [111]; however in a general, spherically symmetric and static metric ansatz inspired by the study of BH solutions in bigravity, (cf. Ref. [144] and Sec. 2.3.1)

$$ds^2 = e^{\nu}\mathrm{d}t^2 - e^{\lambda}\mathrm{d}r^2 - r^2\mathrm{d}\Omega^2\,, \quad \text{with} \tag{4.11}$$
$$\nu(r) = -\frac{r_S}{r}\left(\alpha(\theta) + \beta(\theta)e^{-m_g r}\right), \quad \lambda(r) = \frac{r_S}{r}\left(\alpha(\theta) + \frac{\beta(\theta)(1+m_g r)}{2}e^{-m_g r}\right),$$
$$\text{and} \;\; \alpha(\theta) = \cos^2(\theta)\left[1 + \frac{2}{3}\sin^2(\theta)\right], \quad \beta(\theta) = \frac{2}{3}\sin^2(\theta)\left[1 + 2\sin^2(\theta)\right],$$

where $0 \leq \theta \leq \pi/2$. Light, by construction, follows null-geodesics corresponding to $\mathrm{d}s^2 = 0$. To avoid confusion with the mixing angle θ, we take light to propagate in a plane characterised by the coordinates (r, ϕ) and time t, perpendicular to the conserved angular momentum; see Fig. 4.1 for the geometry. Since the metric components are independent of t and ϕ, we expect that we can construct at least two constants of the motion [110]. Indeed, the total energy and the angular momentum of a test particle moving in space-time (4.11) are conserved. Each conserved quantity corresponds to a Killing vector field oriented in the corresponding direction, i.e.

$$\xi_1{}^{\mu} = (1,0,0,0)^T \quad \text{and} \quad \xi_2{}^{\mu} = (0,0,1,0)^T\,, \tag{4.12}$$

[3] If gravity were described by a scalar instead of a tensor field, it could only couple to the trace of the energy-momentum tensor, which vanishes for light. Therefore, the measured bending of light implies that gravity is described by a tensor field, whose quantum fluctuations would be associated with a spin-2 particle.

for which the Killing equation holds [110],

$$0 \overset{!}{=} (\mathcal{L}_{\xi_i} g)_{\alpha\beta} \equiv \xi_i{}^{\mu} \underbrace{\nabla_\mu g_{\alpha\beta}}_{=0} + (\nabla_\alpha \xi_i{}^{\mu}) g_{\mu\beta} + (\nabla_\beta \xi_i{}^{\mu}) g_{\alpha\mu} = \nabla_\alpha \xi_{i\beta} + \nabla_\beta \xi_{i\alpha} \,, \tag{4.13}$$

where $\mathcal{L}_{\xi_i}$ is the Lie derivative w.r.t. the vector field ξ_i and ∇ is the covariant derivative. Moreover, we used that the metric is covariantly constant, $\nabla_\alpha g_{\mu\nu} = 0$. Combining Eq. (4.13) and the geodesic equation $\nabla_\mu U^\nu = 0$, we obtain two conservation equations [110],

$$\frac{\mathrm{d}}{\mathrm{d}\tau} (\xi_i{}^{\mu} U_\mu) = \xi_i{}^{\mu} U^\nu \underbrace{\nabla_\nu U_\mu}_{=0} + U^\mu U^\nu \nabla_\nu \xi_{i\mu} \overset{(4.13)}{=} U^{(\mu} U^{\nu)} \nabla_{[\mu} \xi_{i\nu]} = 0 \,, \quad i = 1, 2. \tag{4.14}$$

The meaning of these equation is that the scalar product $\xi_i{}^{\mu} U_\mu$ is conserved along the geodesic with tangent vector U^μ. Thereby, we obtain two conserved quantities, expressed in terms of the proper time τ as

$$g_{00} \frac{\mathrm{d}t}{\mathrm{d}\tau} \equiv \frac{E}{m} \,, \qquad g_{\phi\phi} \frac{\mathrm{d}\phi}{\mathrm{d}\tau} \equiv \frac{J}{m} \,. \tag{4.15}$$

These, in turn, correspond to the energy E and the angular momentum J of a test particle of mass m, and allow us to compute the null geodesic directly from the metric (4.11):

$$0 = \left(\frac{\mathrm{d}s}{\mathrm{d}\tau}\right)^2 = e^\nu \left(\frac{\mathrm{d}t}{\mathrm{d}\tau}\right)^2 - e^\lambda \left(\frac{\mathrm{d}r}{\mathrm{d}\tau}\right)^2 - r^2 \left(\frac{\mathrm{d}\phi}{\mathrm{d}\tau}\right)^2 \,, \tag{4.16}$$

from which it follows that

$$\left(\frac{\mathrm{d}r}{\mathrm{d}\tau}\right)^2 = e^{-\lambda} \left[e^{-\nu} \frac{E^2}{m^2} - r^{-2} \frac{J^2}{m^2} \right] . \tag{4.17}$$

This can be simplified further by using the identity

$$\frac{\mathrm{d}r}{\mathrm{d}\tau} = \frac{\mathrm{d}\phi}{\mathrm{d}\tau} \frac{\mathrm{d}r}{\mathrm{d}\phi} = \frac{1}{r^2} \frac{J}{m} \frac{\mathrm{d}r}{\mathrm{d}\phi} \,. \tag{4.18}$$

Noting that the mass has dropped out and can be set to $m = 0$ (as it should), we finally arrive at the light geodesic[4]

$$\left(\frac{1}{r^2} \frac{\mathrm{d}r}{\mathrm{d}\phi}\right)^2 = \frac{e^{-(\lambda+\nu)}}{b^2} - \frac{e^{-\lambda}}{r^2} \,. \tag{4.19}$$

This equation can be recast into a more useful form by introducing the dimensionless variable $u \equiv \frac{R}{r}$. Here, $\frac{\mathrm{d}r}{\mathrm{d}\phi}\Big|_{r=R} = 0$ defines the radius of closest approach, R, which is

[4] One may object that the procedure shown here is inconsistent, since the previously introduced mass is now set to zero. However, the result is the same as one would have obtained from solving the set of geodesic equations, which involves a tedious computation of the Christoffel symbols, see e.g. Ref. [111].

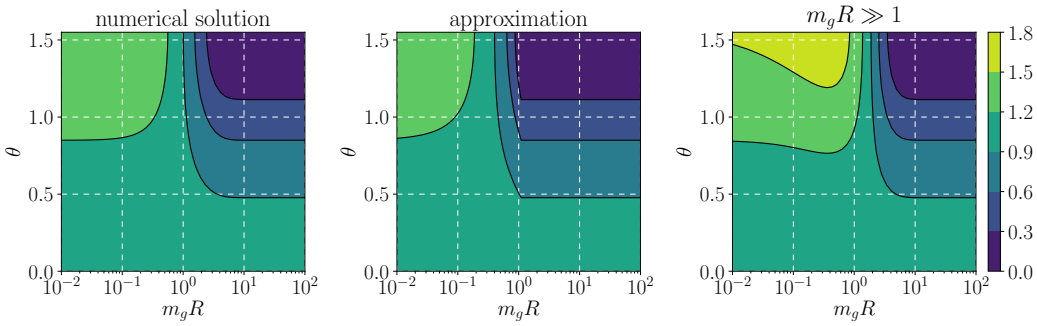

Figure 4.2.: The light deflection angle in bigravity normalised to the GR value, $\Delta\phi_{\rm GR} = 2\,r_S/R$, obtained from solving the integral (4.22), and the two approximate solutions (4.23) and (4.24). All expressions agree when $m_gR \gg 1$; however, only Eq. (4.23) approximates $\Delta\phi$ well when $m_gR < 1$. Figures adapted from Ref. [4].

related to the impact parameter $b \equiv J/E$ via

$$\frac{1}{b^2} = \frac{e^{\nu(R)}}{R^2}\,. \tag{4.20}$$

Notice that for $R \leq r < \infty$ we obtain $0 < u \leq 1$. Conventionally, the geodesic equation is expanded in powers of r_S/R to simplify the exponentials,

$$\left(\frac{\mathrm{d}u}{\mathrm{d}\phi}\right)^2 = \big[1 - \lambda(r = R/u)\big](1 - u^2) + \nu(R) - \nu(r = R/u)\,. \tag{4.21}$$

In GR, we find that $e^{\nu}\,e^{\lambda} = 1$ and this equation can be solved analytically. In bigravity however, $e^{\nu}\,e^{\lambda} \sim e^{-m_g r}$, such that the exponentials carry non-trivial information about the massive spin-2 modification. In order to obtain the total deflection angle [111],

$$\Delta\phi = 2\int \mathrm{d}\phi = 2\int_0^1 \mathrm{d}u\,\frac{\mathrm{d}\phi}{\mathrm{d}u}\,, \tag{4.22}$$

we plug Eq. (4.19), expressed in u, into Eq. (4.22) and only then expand in powers of r_S/R.

The resulting integral, however, cannot be given in closed form due to the u-dependence of λ and ν. Nevertheless, an approximation to the numerically integrated result can be found: On the one hand, terms of the form $e^{-m_g\,R/u}$ can be disregarded when $m_g\,R \gg 1$, as $0 < u \leq 1$. On the other hand, when $m_g\,R < 1$, we see that $e^{-m_g\,R/u} \to e^{-m_g\,R} \simeq 1$ for $u \to 1$, and $e^{-m_g\,R/u} \to 0$ for $u < m_gR$. This can be implemented into Eq. (4.22) by replacing the exponential factors as $e^{-m_g\,R/u} \to e^{-m_g\,R}$, while simultaneously shifting the lower integration boundary to $u = m_g\,R$. This yields

$$\Delta\phi \simeq 2\frac{r_S}{R}\left[\alpha(\theta) + \frac{1}{4}\beta(\theta)e^{-m_gR}\left((3 + m_gR)\sqrt{\frac{1 + m_gR}{1 - m_gR}} + m_gR\,\arccos\left(m_gR\right)\right)\right]. \tag{4.23}$$

Some care is required when using this equation, as for $m_g R > 1$ the arccos function will develop an imaginary part. However, in this regime one can simply drop the piece proportional to $e^{-m_g R}$, as it quickly goes to zero (cf. Fig. 4.2).

An even simpler, but less general approximation is to take $m_g R \gg 1$, and retain only the global exponential factor in Eq. (4.23),

$$\Delta\phi \simeq 2\frac{r_S}{R}\left[\alpha(\theta) + \frac{3}{4}\beta(\theta)e^{-m_g R}\right]. \tag{4.24}$$

The three different solutions to $\Delta\phi$ (numerical, approximation, and the simple approximation '$m_g\, R \gg 1$') are compared in Fig. 4.2. One can see that Eq. (4.23) is in good agreement with the numerical solution away from the point where $m_g\, R = 1$. Eq. (4.24), on the contrary, works only for the regime $m_g R \gg 1$, as one expects from the assumptions.

4.2.2 Mass estimates from gravitational lensing

As we have just seen, the deflection angle of light in bigravity changes compared to GR depending on the graviton mixing angle θ according to

$$\Delta\phi \to \Delta\phi\, f_{\rm GL}(\theta)\,, \tag{4.25}$$

where $f_{\rm GL}(\theta)$ is found by performing the integral in Eq. (4.22), and is well approximated by Eq. (4.23), which yields

$$f_{\rm GL}(\theta) = \alpha(\theta) + \frac{1}{4}\beta(\theta)e^{-m_g R}\left((3 + m_g R)\sqrt{\frac{1+m_g R}{1-m_g R}} + m_g R\, \arccos\left(m_g R\right)\right). \tag{4.26}$$

Since this function does not depend on the radial variable r, but only on the radius of closest approach R, derivatives of the deflection angle/ will change by the same factor $f_{\rm GL}$.[5] Mass estimates from gravitational lensing will hence change as

$$M_{\rm lens} \to \frac{M_{\rm lens}}{f_{\rm GL}(\theta)}\,. \tag{4.27}$$

Thus, observing the strength of the lensing effect, we can reconstruct the lensing mass responsible for the light bending $M_{\rm lens}$, which depends on the bigravity parameters m_g and θ. We will now outline an independent method to reconstruct the gravitational potential in a cluster, namely by X-ray observations. This will give us a handle on the model parameters of bigravity.

4.2.3 Mass estimates from X-ray emission of galaxy clusters

In Ref. [262] the Planck collaboration analysed 439 galaxy clusters which are identified via the thermal Sunyaev–Zel'dovich (SZ) effect, where CMB photons scatter off high-

[5] Strictly speaking this is only true if the radius of closest approach, R, lies outside the mass distribution under consideration. However, if $m_g\, r \gg 1$ the resulting expression is independent of r; while for $m_g\, r \ll 1$ the Vainshtein screening will take effect. In the intermediate regime one should revert to the numerical procedure, which we leave for future work.

energetic electrons inside the clusters via inverse Compton scattering [263]. On average, this transfers energy from the electrons to the photons, reducing the number of low energetic CMB photons in favour of high-energy photons. This leaves a characteristic signature on the CMB and can be used to identify and probe galaxy clusters [264, 265]. As it turns out, less clusters are observed than expected, which could be related to the gas inside the cluster having a lower temperature than expected (hence fewer high-energy electrons), or a deviation from the assumption of hydrostatic equilibrium, which is typically assumed. This is quantified by the so-called hydrostatic bias factor, which will be defined below, and which is found to be smaller than unity, $R_M = 0.6 \ldots 0.99$ (depending on the prior distribution chosen) this gives a tension of up to 3.7σ with other CMB measurements [262]. As we will see shortly, the modifications implied by the present framework, indeed imply such a deviation from the prediction $R_M = 1$. Let us now outline the procedure to obtain the mass estimate from X-ray emissions that we will need to properly define R_M.

In order to obtain an analytic expression, we assume that the mass of the galaxy cluster is dominated by the DM contained in it. With this assumption, the hydrodynamics of the gaseous cloud emitting X-rays is therefore determined by an *independent* DM potential. Following Ref. [265] and assuming a static, spherically symmetric configuration, the hydrodynamical equation describing this situation reduces to

$$\frac{\vec{\nabla} P_{\rm gas}}{\rho_{\rm gas}} = -\vec{\nabla}\Phi_{\rm DM}\,. \tag{4.28}$$

Taking the divergence and employing Poisson's equation [see Eq. (4.1)], this yields

$$\vec{\nabla}\left[\frac{\vec{\nabla} P_{\rm gas}}{\rho_{\rm gas}}\right] = -4\pi G_{\rm N}\rho_{\rm DM}\,. \tag{4.29}$$

Finally, this equation can be integrated to yield a mass estimate for the dominant dark component:[6]

$$\begin{aligned} G_{\rm N}\, M_{\rm DM}(r) = 4\pi G_{\rm N}\int_0^r {\rm d}r'\, r'^2 \rho_{\rm DM}(r') &= -\int_0^r {\rm d}r' \partial_{r'}\left[\frac{r'^2}{\rho_{\rm gas}(r')}\partial_{r'} P_{\rm gas}(r')\right] \\ &= -\frac{r^2}{\rho_{\rm gas}(r)}\partial_r P_{\rm gas}(r)\,, \end{aligned} \tag{4.30}$$

where spherical symmetry was assumed to hold. Furthermore, taking the gas to be ideal, the equation of state relating its pressure $P_{\rm gas}$ to the particle number density $n = \rho_{\rm gas}/m$ and temperature T for a gas particle of mass m is $P_{\rm gas} = n k_B T = \frac{\rho_{\rm gas}}{m} k_B T$, where k_B is Boltzmann's constant. Thus, the mass of the DM component within the cluster, which was

[6] Here, we use the gradient and Laplace operators in spherical coordinates:

$$\begin{aligned} \vec{\nabla}\left[f(r)\vec{\nabla}g(r)\right] &= \left(\vec{\nabla}f(r)\right)\cdot\left(\vec{\nabla}g(r)\right) + f(r)\Delta g(r) = (\hat{e}_r\partial_r f(r))\cdot(\hat{e}_r\partial_r g(r)) + f(r)\frac{1}{r^2}\partial_r\left(r^2\partial_r g(r)\right) \\ &= (\partial_r f(r))(\partial_r g(r)) + f(r)\frac{1}{r^2}\partial_r\left(r^2\partial_r g(r)\right) = \frac{1}{r^2}\partial_r\left(f(r)r^2\partial_r g(r)\right). \end{aligned}$$

assumed to dominate the mass distribution, is found to be linked to the thermodynamical quantities T and $\rho_{\rm gas}$ as

$$M_{\rm DM}(r) = -\frac{r\,k_{\rm B}T}{m\,G_{\rm N}}\left(\frac{{\rm d}\log(\rho_{\rm gas})}{{\rm d}\log r} + \frac{{\rm d}\log(T)}{{\rm d}\log r}\right). \tag{4.31}$$

This is the mass estimate we obtain from X-ray observations via the measurement of the right-hand side of this equation, cf. Ref. [266]. Let us now discuss how this mass estimate is modified in a theory with additional spin-2 DOF.

From the metric in Eq. (4.11) (or the more detailed discussion in Sec. 2.3.1) we deduce that the gravitational potential of a point source is modified as[7]

$$\Phi(r) \to \Phi(r)\, f_{\rm pot}(\theta, r)\,, \tag{4.32}$$

where the function $f_{\rm pot}$ reads [cf. Eq. (2.84)]

$$f_{\rm pot}(\theta, r) \equiv \alpha(\theta) + \beta(\theta)\, e^{-m_g\, r}\,. \tag{4.33}$$

Therefore, the above argument is modified only on the right-hand side of Eq. (4.28):

$$\frac{\vec{\nabla} P_{\rm gas}}{\rho_{\rm gas}} = -\vec{\nabla}\Phi \to -\vec{\nabla}\Phi\, f_{\rm pot} - \Phi\,\vec{\nabla} f_{\rm pot}\,. \tag{4.34}$$

Since the right-hand side of Eq. (4.31) is measured, we see that with the above modification, the inferred *kinetic* mass is altered as

$$M_{\rm kin}(r) \to \frac{M_{\rm kin}(r)}{\alpha(\theta) + \beta(\theta)\,(1 + m_g\, r)e^{-m_g\, r}}\,, \tag{4.35}$$

such that the ratio of masses inferred from lensing and X-rays becomes

$$\frac{M_{\rm kin}(r)}{M_{\rm lens}(r)} \to \frac{M_{\rm kin}(r)}{M_{\rm lens}(r)}\,\frac{f_{\rm GL}(\theta)}{\alpha(\theta) + \beta(\theta)\,(1 + m_g\, r)e^{-m_g\, r}} \equiv R_M(m_g, \theta)\,\frac{M_{\rm kin}(r)}{M_{\rm lens}(r)}\,, \tag{4.36}$$

where $f_{\rm GL}$ is given in Eq. (4.26).

The ratio R_M is plotted in the $m_g - \theta$ plane in Fig. 4.3, where we have replaced $\theta \to \theta_{\rm eff}$ [cf. Eq.(4.10)], in order to phenomenologically implement the Vainshtein mechanism as discussed above. This is manifest in the contour plot, as for small m_g (corresponding to large $r_V = (r_s m_g^{-2})^{1/3}$) the entire cluster is contained inside the Vainshtein sphere below $10^{-31}\,$eV, recovering the predictions of GR, i.e. $R_M = 1$ under the specified assumptions. Note that we fixed the radial coordinate to a typical galaxy cluster size of approximately 5 Mpc. What we learn from Fig. 4.3 can be summarised quite briefly: For a mass range $10^{-31}\,{\rm eV} \leq m_g \leq 10^{-28}\,{\rm eV}$, and sizeable mixing angles, $\theta \gtrsim \pi/4$, a reduction of the *total* cluster mass ratio is expected. In fact, as we approach the massive gravity limit

[7] We remark that this is strictly speaking only true if the mass distribution is confined inside a sphere $r < r_0$ and $m_g\, r_0 \ll 1$ such that the exponential can be ignored. Otherwise a more complicated procedure has to be applied, as the one outlined in Appendix C.1. However, it turns out that for most of the parameter points considered here, this is a good approximation.

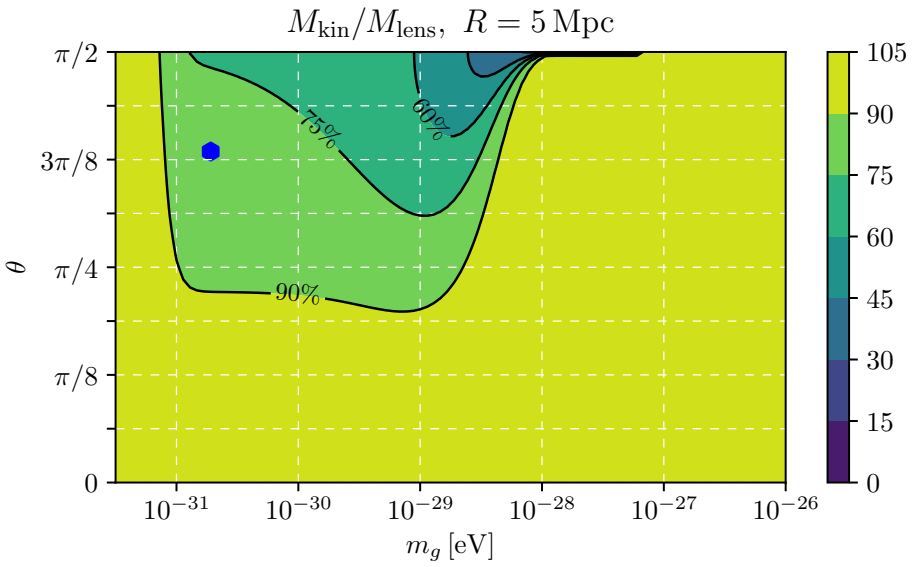

Figure 4.3.: Mass ratio R_M relative to the GR value for a typical cluster size $R = 5\,\mathrm{Mpc}$. The blue hexagon indicates the best fit point from the analysis of the MACS cluster J1206.2-0847, cf. Fig. 4.4a. Adapted from Ref. [4].

($\theta \to \pi/2$), the ratio goes to zero for masses $m_g \gtrsim 10^{-28}\,\mathrm{eV}$. This is an interesting observation, as CMB cluster surveys indicate that the ratio R_M might deviate from one, as mentioned above. While it is still an interesting observation that the modification drives the ratio into the seemingly correct direction, we emphasise once again that this could be explained more economically, and within GR.

4.2.4 Application to a specific cluster

Let us apply the above findings to a concrete example: the MAssive Cluster Survey (MACS) galaxy cluster J1206.2-0847, which was identified at redshift $z = 0.44$ [267–270]. This cluster was analysed in more detail in Ref. [271], determining its mass density profile. We have chosen this cluster as an appropriate example, because the latter reference contains precisely the required information about both the mass inferred from gravitational lensing, as well as the reconstructed mass from X-ray emission. These mass estimates for various radii are shown in Fig. 4.4a. We see that for this cluster the data are compatible with the GR prediction $R_M = 1$. Nevertheless, there appears to be a tendency for the ratio to decrease, as the radius at which it is evaluated is increased. Applying the χ^2 method outlined in App. B.2, we can now identify viable and non-viable parameter constellations, as shown in Fig. 4.4b. The red region obtained in this manner shows the parameter points that are excluded at the 95% confidence level (C.L.).

In the limit of massive gravity, $\theta = \pi/2$, we find that masses above $5 \cdot 10^{-31}\,\mathrm{eV}$ and below $10^{-25}\,\mathrm{eV}$ are excluded. This result is consistent with previous results obtained from cluster lensing [272]. As the mixing angle decreases, this bound slightly relaxes and more viable mass ranges emerge. Conversely, for the region $\theta < \pi/4$, virtually no

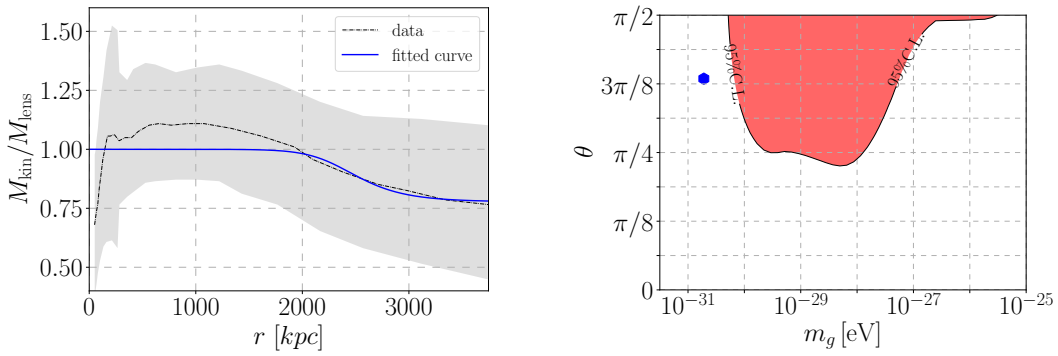

(a) Mass ratio R_M as function of the radius

(b) parameter scan

Figure 4.4.: *Left:* Fit of the bigravity modification $R_M(m_g, \theta)$ to the cluster data. We find the best fit for $m_g = 2 \cdot 10^{-31}\,\text{eV}$, $\theta = 1.2$, $\Delta r = 0.23\, r_V$. *Right:* Parameter scan of R_M in the (m_g, θ) plane. The best fit point is indicated as a blue hexagon. Adapted from Ref. [4].

constraints arise, because the ratio $M_{\rm kin}/M_{\rm lens}$, that we take to be of purely non-GR origin, approaches $R_M \to 1$, while at the same time the errors are quite large. Finally, there is a parameter point, where a reduction of the χ^2 compared to the hypothesis $R_M = 1$ is possible. This is shown in Fig. 4.4a by the blue line, and marked with a blue hexagon in Fig. 4.4b. Remarkably, this point corresponds to a small mass $\sim 10^{-31}\,\text{eV}$ but large, almost maximal, mixing angle, and it achieves precisely what the tentative deviation from $R_M = 1$ seems to indicate: The mass ratio is close to $R_M = 1$ for small radii, while it decreases for larger r, starting at a radius $r \sim 2\,\text{Mpc}$ and reaching a reduction of up to $R_M = 0.8$ for $r = 4\,\text{Mpc}$. This can be easily understood from the cluster mass function which was found in Refs. [270, 271] to be well approximated by

$$M(r) = M_{200} \frac{\log\left(1 + \frac{r}{r_0}\right) - \frac{r}{r+r_0}}{\log\left(1 + c_{200}\right) - \frac{c_{200}}{1+c_{200}}}\,, \tag{4.37}$$

with parameters M_{200}, r_0, and c_{200} determined therein. Thus, we see that the mass grows slower than linearly with the radius, such that the Vainshtein radius grows slower than $r^{1/3}$. Starting inside the Vainshtein sphere and increasing r, one is therefore bound to leave it at some radius determined by the spin-2 mass m_g, and the reduction sets in. With this observation, we conclude our discussion of galaxy cluster lensing and turn to the discussion of galaxy rotation curves.

4.3 Galaxy rotation curves

Since the early days of astronomy, the dynamics of galaxies have been used to infer the macroscopic properties of DM. In this section, we discuss how these dynamics are modified in the bigravity framework. In doing so we follow Ref. [249], where the authors studied the galaxy ESO138-G014 both with a DM halo and without one, instead using the MOND paradigm. There it is found that MOND provides a worse fit than the DM halo models.

4.3.1 Components of a spiral galaxy

Spiral galaxies, such as the Milky Way, are usually understood to be composed of three distinct matter components: a gaseous cloud consisting mostly of hydrogen, a stellar disk, and a DM halo. For each class of matter one assumes a separate density profile, which, by virtue of the linear Poisson equations (4.1) and (4.5), can be added linearly to obtain the total mass density. While some galaxies also exhibit a so-called bulge, a spherical region of stars near the centre, we focus here on examples that are (mostly) devoid of such bulges. Most of the galaxies we consider are so-called low surface brightness (LSB) galaxies which, as the name suggests, have a low light emission, and are thus assumed to be DM dominated [273], making them ideal laboratories to explore the properties of DM on galactic scales. In order to draw conclusions for the mass of a galaxy from its light emission, it is assumed that the stellar mass is proportional to the brightness, where the proportionality factor is given by the mass-to-light ratio, which is treated as a free parameter in our study. We emphasise that the present analysis is merely a first step towards a comprehensive understanding of the phenomena bigravity would induce in galaxies.

The gas component is modelled according to the hydrogen 21cm line emission, and is assumed to have an exponentially decreasing surface density,

$$\Sigma(r) = \Sigma_0 e^{-r/r_0} \;\Rightarrow\; M_{\rm gas}(r) = L\,\Sigma_0 \times \int_0^r \mathrm{d}r'\,\Sigma(r') = L\,\Sigma_0\left(r_0 - (r+r_0)e^{-r/r_0}\right), \tag{4.38}$$

with the mass-to-light ratio L. The radius r_0, which characterises the size of the gaseous cloud, is used as an input parameter for the stellar disk, whose mass distribution reads [274, 275]

$$M_{\rm disk}(x) = 0.5 M_D^0 (3.2x)^3 (I_0K_0 - I_1K_1), \tag{4.39}$$

with $x \equiv r/R_{\rm opt}$ and $R_{\rm opt} \equiv 3.2\,r_0$. The modified Bessel functions $I_{0/1}$ and $K_{0/1}$ are evaluated at $1.6\,x$, respectively. Notice that assuming an axisymmetric mass density instead of a spherically symmetric mass density leads to some difficulties; most notably, we cannot simply integrate the potential analytically for most cases. We discuss this issue in Appendix C.1, but remark here that the the outcome is rather insensitive to a change in the procedure.

Finally, we include a DM halo, taken to have a density profile as proposed by Navarro, Frenk, and White (NFW) in Ref. [244],

$$\rho_{\rm NFW}(r) = \frac{M^0_{\rm DM}}{r\,(r+r_h)^2} \quad\Rightarrow\quad M_{\rm DM}(r) = M^0_{\rm DM}\left[\log\left(1+\frac{r}{r_h}\right) - \frac{r}{r+r_h}\right], \tag{4.40}$$

with the free parameters $M^0_{\rm DM}$ and r_h.

We emphasise once again that the relation $v^2(r) = G_{\rm N}M(r)/r$ *does not hold in general*. In order to obtain consistent results, we have to employ Eq. (4.7) wherever possible. Unfortunately, the resulting expressions are not very compact and thus not shown here. The reader interested in the full expressions for the velocities $v(r)$ for the individual components is referred to Appendix C.1.

Having fixed the characteristic radius r_0 from the HI emission, we are left with a total

of five free parameters (per galaxy) to fit the rotation curve data. Turning on bigravity adds another three parameters to this, yielding an eight-dimensional parameter space. It is certainly not impossible but also not very insightful at this point to perform a *global* fit of the parameter space. This would require a maximisation of the likelihood as a function of these eight parameters, cf. Appendix B.2. Here, we are only interested in a first picture of the compatibility of bigravity with the data, which for our purposes can be parametrised by the mass parameter m_g and the mixing angle θ. Therefore, we choose a hybrid approach in which we compute for a given pair of values (m_g, θ) the best fit to the data via a least squares algorithm. This approach also makes sense from a physical point of view: While the masses and characteristic radii of the galactic matter components are properties of that individual system, the values of m_g and θ would be considered natural constants, if Nature was to be described *bimetrically*. Therefore, we believe that it is justified to treat these sets of parameters on different footings.[8] Let us now exemplify this approach for a particular galaxy.

4.3.2 In-depth fitting of a rotation curve

Now that we have a model of a spiral galaxy, let us consider an example to illustrate our procedure. To this end we use data of the spiral galaxy ESO138-G014, located at a distance of 18.57 Mpc [276, 277]. As stated in Ref. [249], this galaxy has a number of favourable properties that make it an ideal example: HI brightness measurements over the entire visible disk, no significant bulge component, large number of data points with small errors, and finally the fact that its distance is well determined.

We assume that the HI-emission brightness of the galaxy is directly proportional to the mass of the gaseous component, and therefore, this fit is easily obtained, cf. Fig. 4.5a. In order to perform the fit, we utilise a least-squares routine of the Python SciPy library. Thereby, we find for the gas component that $M_{\mathrm{HI}}(20\,\mathrm{kpc}) = 6.4 \cdot 10^9 M_\odot$, in concordance with Ref. [249].

Disregarding at first the modifications induced by the presence of a massive spin-2 field, we obtain a fit to the observed velocities under the GR hypothesis. This is shown in Fig. 4.5b, where one can observe two important features: One is the well-known decrease of the visible matter components' contribution (green, dotted line labelled 'disk+gas'). This is to be expected as towards the edge of a galaxy the mass is approximately constant, $M(r > r_0) = \text{const}$, which by virtue of Eq. (4.4) leads to $v(r > r_0) \sim 1/\sqrt{r}$. This behaviour needs to be counteracted by a DM halo, which dominates the mass of the galaxy, constituting the second important observation. The DM dominance is evident from the dashed, magenta curve in Fig. 4.5b.

Using the χ^2 estimator introduced in Appendix B.2, we can repeat this procedure for each point on a grid in the (m_g, θ) plane. What we obtain is summarised in Fig. 4.6. In the left panel of this figure, we show in red the region that is excluded at the 95% C.L., while the red hexagon indicates the point in the (m_g, θ) plane which yields the best fit. The velocity profile obtained from this set of model parameters is shown in Fig. 4.5c.

[8] A future survey might want to improve on this, and we refer the inclined reader to Ref. [259], where this approach was chosen. However, another simplification was made in that reference by assuming the modification of the potential to occur exclusively in the dark sector. At the same time no Vainshtein effect was considered.

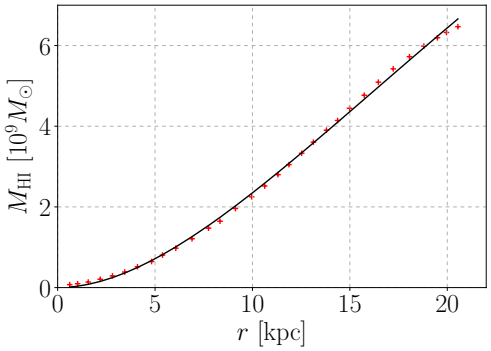

(a) gas mass fit

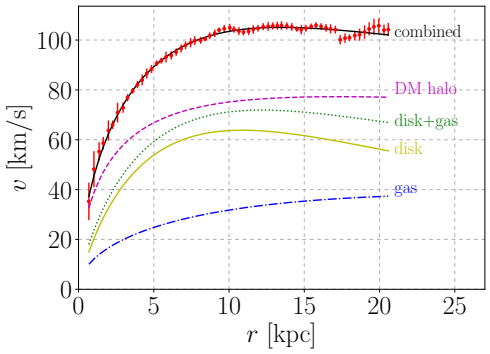

(b) GR, $\theta = 0$

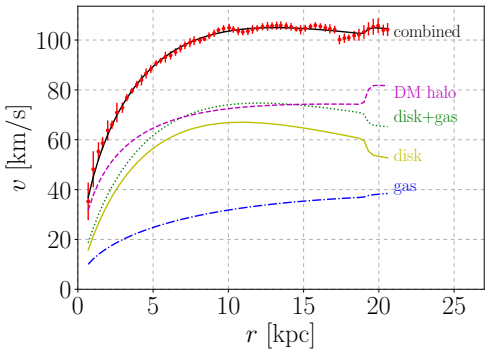

(c) $(m_g, \theta, \Delta r/r_V) = (1.4 \cdot 10^{-30}\,\text{eV}, 0.7, 0.5)$

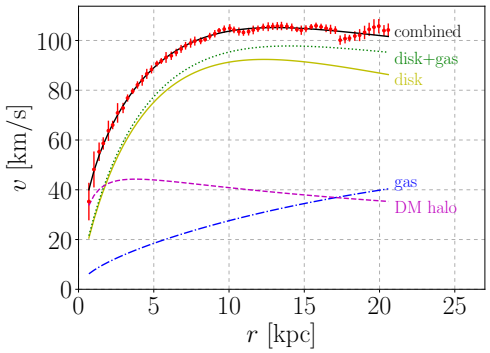

(d) $(m_g, \theta, \Delta r/r_V) = (2 \cdot 10^{-27}\,\text{eV}, 1.2, 0.04)$

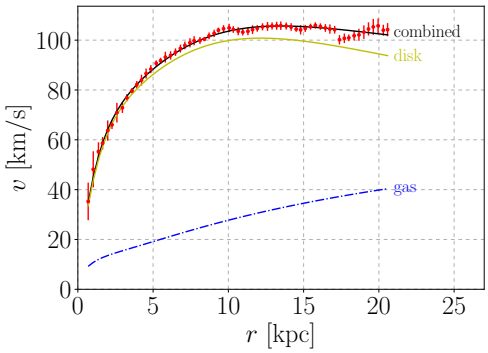

(e) $(m_g, \theta, \Delta r/r_V) = (2 \cdot 10^{-29}\,\text{eV}, 1.0, 0.4)$

Figure 4.5.: Rotation curve of ESO138-G014 in GR and bigravity. *Top*: Fit to the gas mass of ESO138-G014. The total mass contained in the fiducial volume is $M_{\rm HI}(20\,\text{kpc}) = 6.4 \cdot 10^9 M_\odot$, as found in Ref. [249]. *Centre*: Panel (b) shows the GR fit to the data with error bars, and the three components making up the galaxy ($\chi_0^2 = 26$). Panel (c): best fitting point found in our analysis for which $\Delta\chi^2 \equiv (\chi_0^2 - \chi^2) = 4.3$. This corresponds to a mild 1.5σ improvement. *Bottom*: Rotation curves fitted with lowest possible DM mass fraction (d) and no DM component (e). We find $\Delta\chi^2 = 0.7$ and $\Delta\chi^2 = -6.2$, respectively. Therefore, the bigravity without DM scenario is excluded at the 95% C.L., while the minimal DM scenario yields a fit of equal quality than the GR fit to the data. Figures Adapted from Ref. [4].

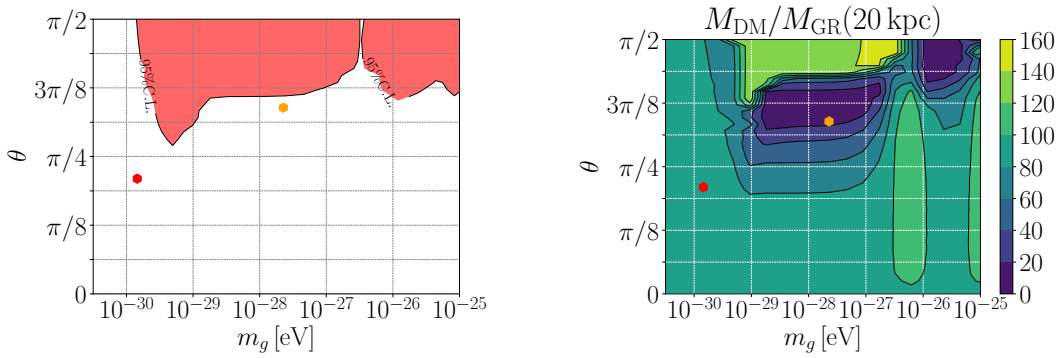

(a) rotation curve parameter scan

(b) ratio of dark matter to total mass

Figure 4.6.: *Left*: Parameter scan for the bigravity parameters (m_g, θ). The best fit point is marked in red, while the parameter point with the least DM content is marked in orange. *Right*: Mass ratio $M_{\rm DM}/M_{\rm tot}(20\,{\rm kpc})$ with the central region of the galaxy. Figures adapted from Ref. [4].

We may also want to ask if the amount of DM needed to fit the rotation curve is reduced compared to GR. To this end we need to quantify the amount of DM contained in the galaxy. This is in principle not a simple question to answer because we can only infer the DM mass distribution from the visible part of the galaxy. For our purposes it suffices to consider the ratio $M_{\rm DM}/M_{\rm tot}(20\,{\rm kpc})$, i.e. the amount of DM mass relative to the total mass inside a fiducial volume bounded by the radius $r = 20\,{\rm kpc}$. This should not be confused with the total DM mass, which could be much larger. This is shown in Fig. 4.6b, and we see that a significant reduction of the DM mass is feasible for a set of parameters that are not ruled out, cf. the orange hexagon.

For the best fit point, we observe that the DM halo mass is *slightly* reduced compared to the GR fit, while the χ^2 is slightly improved compared to GR thanks to the Vainshtein mechanism which sets in towards the outer edge of the galaxy, allowing the model to better fit certain features in the data. In contrast, the orange hexagon in Fig. 4.6b marks the parameter values which minimise the DM mass needed to fit the rotation curve. This is shown in Fig. 4.5d, where the DM mass is reduced by a factor 15 compared to GR, while simultaneously a fit as good as the GR fit is found ($\chi^2_0 - \chi^2 = 0.7$). Finally, we can ask if the data can be fitted without any DM component. The result is depicted in Fig. 4.5e and gives a worse fit than GR ($\chi^2 - \chi^2_0 = -6.2$).

In conclusion, we find that for sufficiently small mixing angles, we cannot exclude any mass range as of yet. However, when the mixing angle becomes large, $\theta \gtrsim \pi/4$, a stringent limit $m_g \lesssim 10^{-30\cdots-29}\,{\rm eV}$ can be deduced. The origin of this disagreement with the data lies in the Yukawa-nature of the bigravity potential, induced by the presence of a massive spin-2 field. Too large graviton masses induce a strong, exponential suppression of the potential, schematically $v^2(r) \sim M(r)/r(1 + m_g\, r)e^{-m_g\, r}$. This, in turn, makes it necessary to add more mass in the form of DM to the galaxy model, in disagreement with the data at smaller distances from the centre, where the exponent approaches unity and/or the Vainshtein screening sets in. For masses $m_g > 10^{-25}\,{\rm eV}$, it turns out that the entire galaxy suffers from this exponential suppression, and one must allow for a larger

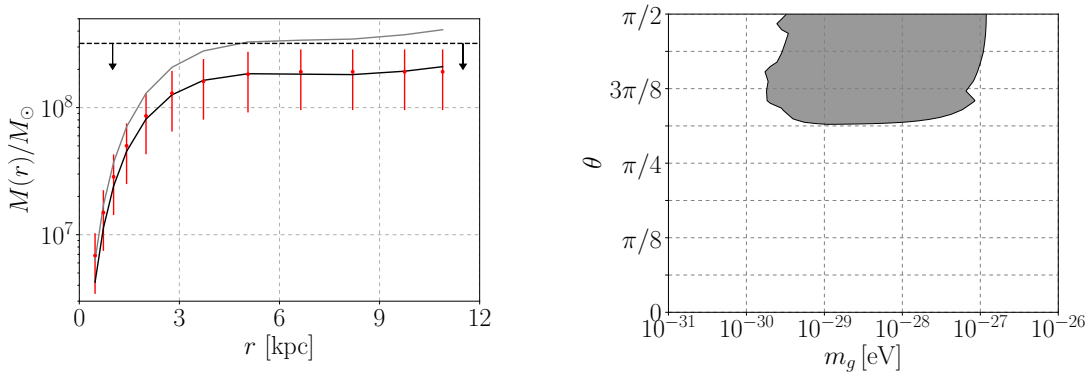

(a) Mass distribution of NGC1052-DF2 and limit; $(m_g,\, \theta) = (3 \cdot 10^{-29}\,\text{eV}, \pi/2)$

(b) grey: excluded parameter space

Figure 4.7.: Mass profile of NGC1052-DF2 (*left*) and exclusion region (*right*) derived from our analysis and the data in [278].

mass-to-light ratio in order to comply with the data. We have therefore excluded this region, which critically depends on this choice, from Fig. 4.6a. Conversely, in the mass range $m_g \ll 10^{-30}\,\text{eV}$ the galaxy is contained in the Vainshtein sphere and no modification arises, cf. Fig. 4.6.

These non-trivial results highlight the importance of the interplay between the mixing of the two modes, the Vainshtein screening and the specific form of the modification of the potential. This is confirmed by the study of a set of LSB galaxies, whose fits are shown in Appendix C.2.

4.3.3 A galaxy lacking dark matter

Finally, we wish to discuss a rather recent observation. In March 2018, astronomers announced the discovery of the galaxy NGC1052-DF2, whose dynamics suggest that it contains very little or no DM, see Ref. [278]. Clearly, the absence of a significant DM component in NGC1052-DF2 severely challenges models that try to replace the DM by an altered gravitational law on galactic scales. In these models, e.g. MOND, one would always expect to see an effect once the system under consideration is sufficiently massive and large. We note that this is the subject of an ongoing discussion, cf. Refs. [279–281].

For the present study, we use the data from Ref. [278] to calculate the mass contained in the galaxy. We then impose the 90% C.L. upper limit quoted in this reference, $M_{\text{tot}} < 3.2 \cdot 10^8 M_\odot$, as illustrated in Fig. 4.7a. The red points are data inferred from the dynamics of NGC1052-DF2 which were translated into a mass via the Newtonian relation $v^2(r) = G_{\text{N}} M(r)/r$. One can fit the velocity data as before, and then translate back to the mass; however, this time using the relation for the mixed Newton-Yukawa potential, Eq. (4.8). This yields the grey curve which should remain below $3.2 \cdot 10^8 M_\odot$ for all r. The example shown is therefore ruled out! Finally, the right panel of Fig. 4.7 shows the exclusion region obtained by repeating this procedure in the (m_g, θ) plane. In conclusion, the 'ultra-diffuse galaxy' reported in Ref. [278] provides some constraints on a range of masses

$10^{-30}\,\mathrm{eV} \leq m_g \leq 10^{-27}\,\mathrm{eV}$ and mixing angles $\theta > \pi/3$ of the spin-2 fields. Nevertheless, it is not able to rule out significant parts of the parameter space, as one might have suspected.

4.4 Discussion

In the study of weak gravitational lensing of galaxy clusters and rotation curves of galaxies in bigravity, we have found important constraints on the model's parameter space. While we have adapted a phenomenological approach to the Vainshtein mechanism, it turns out that this is a crucial ingredient to the phenomenology of massive spin-2 fields on astrophysical scales. Given that the radius r_V, below which the predictions of GR are restored, is a function of the enclosed mass, systems of very different scales can yield similar constraints on the spin-2 mass. For example, we have studied the weak lensing induced by a cluster with a total mass of the order of $10^{15} M_\odot$, and the rotation curve of a galaxy with a mass of roughly $10^{10} M_\odot$. Both systems, although very different in size and mass, give strong constraints of the mass parameter of approximately $m_g \lesssim 10^{-31\ldots-30}\,\mathrm{eV}$ when the mixing angle θ is large, i.e. when gravity is mediated mostly by a massive spin-2 field. While our analysis method is rather rudimentary, and the details of the results are subject to slight changes, the complementarity of systems of different size and mass is the key result of this chapter. The results encourage further investigations, in which the Vainshtein mechanism should be taken into account numerically in order to fully capture its phenomenological consequences.

Chapter 5

Discussion and Outlook

Let us put the results of the previous chapters into perspective and highlight how future work could tie in with them. First, we recapitulate the constraints that were obtained and summarise them in a single summary plot, Fig. 5.1. Next, we discuss which other bounds on massive spin-2 fields exist and which conceptual flaws such models yet have to overcome. We give an outlook on future work, where we highlight possible connections to current research in particle physics. Finally, we speculate about a possibility to find an ultraviolet completion of bimetric gravity. From this, one can appreciate that the bigravity framework is generic enough to represent a sizeable class of models that give rise to massive spin-2 fields at low energies, while being sufficiently specific in order to reduce the complexity of the available parameter space to the massive graviton's mass m_g and the mixing angle with the massless graviton θ. This angle is defined such that $\theta = 0$ yields GR, while $\theta = \pi/2$ corresponds to a theory of gravity being mediated by a massive spin-2 field alone. Hence, any intermediate value represents a theory where gravity is mediated by an admixture of both massive and massless spin-2 fields. We remark that this is a convenient parametrisation for the purposes of this thesis, because the relevant constrains arise when the mixing angle is large. However, there is no *a priori* reason for the ratio of the masses $M_{\tilde{g}}/M_g = \tan(\theta)$ to be of order unity, such that a large part of the parameter space with $\tan(\theta) \ll 1$ remains viable. Interestingly, this is also the regime where most of the conceptual flaws of massive gravity can be evaded.

5.1 Discussion

In Fig. 5.1 we present the collection of constraints on the parameter space in the $m_g - \theta$ plane, which have been obtained in the course of this thesis. In the following we discuss these bounds beginning with higher masses and then going towards lower masses.

First, we should remark that the grey, hatched region in Fig. 5.1 represents the constraint on the graviton mass derived from solar system tests, $m_g < 7.2 \cdot 10^{-23}\,\mathrm{eV}$ [216], which has been known for quite some time. Nevertheless, we have decided to include it in our summary plot, since it represents the strongest model-*independent* bound on the spin-2 mass, relying exclusively on the planetary orbits in our solar system [205]. As explained in Sec. 3.2, we have adapted it to the case of non-zero mixing as $m_g \times \sin(\theta) < 7.2 \cdot 10^{-23}\,\mathrm{eV}$.

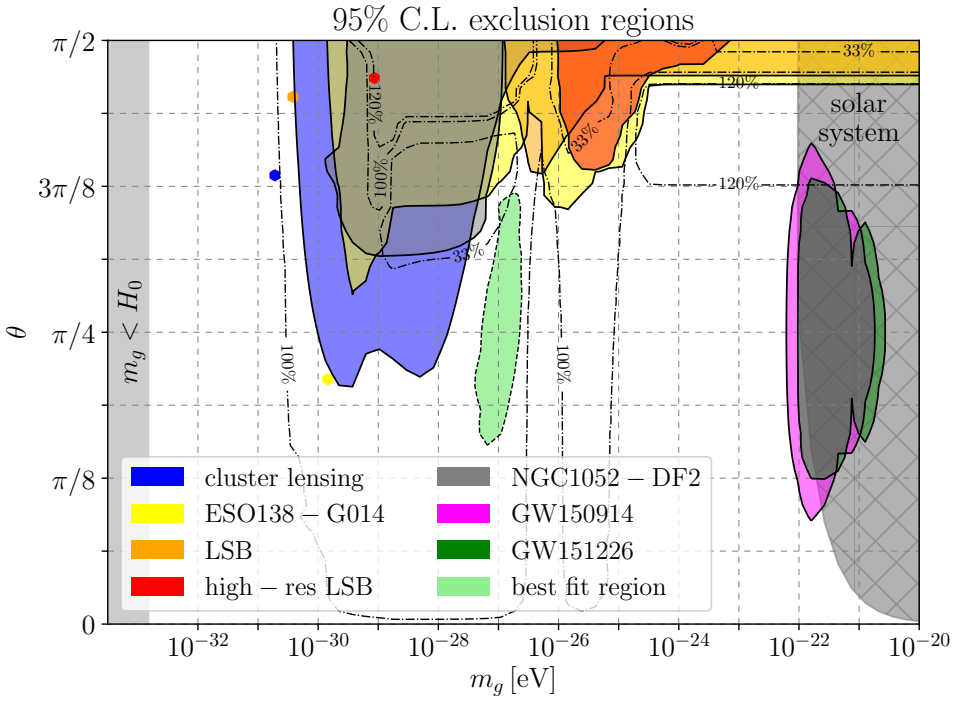

Figure 5.1.: Summary of the constrains derived in this work. We also indicate the best fit points and a global best fit region obtained from a combination of all the data ($\Delta\chi^2 \equiv \chi^2_0 - \chi^2 > 1$; light green region bounded by a dashed line). Furthermore, the contours of the DM mass of the ESO138-G014 galaxy relative to the GR value (cf. Fig. 4.6b) are included to highlight which regions tend to require less DM than under the GR hypothesis.

Moreover, the emergence of GW astronomy has sparked new ways to test GR in its strong-field and relativistic regime, which previously could only be done indirectly, e.g. by studying the energy-loss due to GW emission of pulsars, see e.g. Refs. [282–284]. This is not only of conceptual interest, but as we can see from the green and magenta regions in Fig. 5.1, it allows to probe parameter regions that are neither accessible by astrophysical observations, nor solar system tests. As we discussed in Chapter 3, the presence of multiple spin-2 fields leads to interference effects similar to the phenomenon of neutrino oscillations. It is interesting to observe further that it is this class of constraints that probes the lowest mixing angles, down to roughly $\theta \simeq 0.25$. While the discussion of decoherence did not yield any reliable bound at present, we have pointed out that the observation of a GW echo could find an interpretation in this picture. We refer the reader to Chapter 3 for more details.

Next, the red ('high-res LSB'), orange ('LSB'), and yellow ('ESO138-G014') regions are found from the study of galaxy dynamics. Studying rotation curves of spiral galaxies allows one to determine areas in parameter space where a massive spin-2 field disrupts the galactic dynamics so violently, that no satisfactory fit to the data can be found due to the strong exponential suppression of the Yukawa potential, cf. Sec. 4.3. Furthermore, the recent detection of the galaxy NGC1052-DF2, which seems to be devoid of DM [278], can

be employed to derive the grey shaded area at the upper centre of Fig. 5.1. Furthermore, the bounds represented by the blue region are of extragalactic origin, namely due to weak lensing of a galaxy cluster, and yield the strongest bound on the graviton mass obtained in this work, $m_g < 5 \cdot 10^{-31}\,\mathrm{eV}$ for $\theta = \pi/2$. This is discussed in Sec. 4.2 alongside the derivation of the light deflection angle in bigravity.

Finally, we have restricted the mass to lie above $1.6 \cdot 10^{-33}\,\mathrm{eV}$, the mass scale which corresponds to the Hubble constant today, $H_0 \approx 70 \frac{\mathrm{km}}{\mathrm{s\,Mpc}}$ [12]. While this is indeed a strict, theoretical limit in the case where gravity is mediated by a massive field ($\theta = \pi/2$), this bound, dubbed Higuchi bound, is relaxed if the second tensor becomes dynamical, cf. the discussion in Sec. 2.3.2. It is still included in Fig. 5.1 as a phenomenological bound, as lower spin-2 masses would not have any consequences within the observable Universe.

An interesting conclusion can be drawn from Fig. 5.1: Naively, one would assume a massive but light field to modify the force laws at a scale $l \sim 1/m$, where m is its mass. However, the Vainshtein mechanism adds yet another scale to the problem. Most notably, this scale depends on the enclosed mass, and is thereby intrinsic to the physical system itself. This allows one to probe a certain mass scale in the parameter space, say $10^{-29}\,\mathrm{eV}$ by physical systems of various sizes, e.g. galaxy dynamics and gravitational lensing due to galaxy clusters, as is evident from the yellow and blue regions in Fig. 5.1. This complementarity is an important means to derive robust bounds on the parameter space and a key result of this thesis.

As an exercise for future work, we also include a best fit region. It should be emphasised though that in this region the fits improve only slightly ($\chi_0^2 - \chi^2 > 1$), and we are *not* led to the conclusion that GR should be rejected. Already at the 1σ level, we find that the green region spans most of the remaining viable parameter space. Interestingly, while the individual best fit points prefer lower masses, the combined data seem to exhibit a preference for larger masses around $10^{-27}\,\mathrm{eV}$. This is also in agreement with the recent investigations of Ref. [259], which found a preferred mass region around $10^{-25}\,\mathrm{eV}$ from the study of a set of galaxy rotation curves. This value, although some two orders of magnitude larger than the best fit region found here, is by no means in conflict with our analysis. Apart from the low significance we have found, there are also systematic differences in the analyses, namely the inclusion of the Vainshtein mechanism, which was not included there. Furthermore, we studied a modification of the gravitational potential relating the strength of the Newton and Yukawa forces via the mixing angle θ [cf. Eq. (4.8)], instead of a generic, dark sector modification only. We believe that these results should be understood as a motivation to conduct further research in this direction, refine the analysis method, and include more data samples. An interesting observation is that the best fit region seems to require less DM mass than the GR hypothesis ($\theta \to 0$) indicated by the dash-dotted contour lines.

A final question we would like to address is how far the grey, hatched region in Fig. 5.1 extends towards the right. Laboratory experiments that use a torsion balance to test gravitational interactions suggest that gravity follows the laws of GR on scales as low as $85\,\mu\mathrm{m}$, or energy scales up to approximately $10\,\mathrm{meV}$ [285]. At the same time, the bound becomes weaker as the Yukawa potential's prefactor is decreased [285] (in our language the mixing angle $\theta \to 0$). This tells us that above $10^{-2}\,\mathrm{eV}$, no significant bounds exist and we enter a viable, heavy spin-2 regime for $m_g \gtrsim 10\,\mathrm{meV}$. However, the exact shape of the exclusion region is not known for bigravity. In fact, it has been argued that for a

mass $m_g \gtrsim 1\,\mathrm{TeV}$ the heavy spin-2 state could constitute a weakly interacting massive particle (WIMP)-type DM candidate, if the mixing is very small in order to be stable against decay [286–288]. This interesting idea remains phenomenologically viable in the context of our survey, as it does not affect gravity on (extra-)galactic scales.

5.1.1 Other graviton mass bounds

While we have considered a number of constraints on massive spin-2 fields here, the list of available bounds is clearly not exhausted, see Ref. [76] for a compilation of various bounds. For the case of gravity being mediated by a massive spin-2 field alone (i.e. dRGT gravity), very strong constraints apply, most notably by gravitational lensing, $m_g < 6 \cdot 10^{-32}\,\mathrm{eV}$ [272]. However, we have seen that lowering the mixing between a massive spin-2 field and the massless mediator of gravity, the bounds can be evaded. This is also true for the solar system tests $m_g < 7.2 \cdot 10^{-23}\,\mathrm{eV}$ [216], and pulsar timing constraints $m_g < 7.6 \cdot 10^{-20}\,\mathrm{eV}$ [289], the latter of which have not been included in this work.

Furthermore, CMB B-mode polarisations, once measured, would display a plateau at low multipoles, $\ell \lesssim 100$, with a high sensitivity to the spin-2 mass [290, 291]. Thus, a deviation from the GR prediction could be seen as a smoking gun for a massive spin-2 field, or would yield strong constraints of the order $m_g \sim 10^{-30}\,\mathrm{eV}$ [290]. See also Refs. [292–295] for related work in bigravity and beyond. Complementary to this, a peak in the stochastic GW background would be expected in this case, as was studied for a generic time-varying spin-2 mass in Refs. [187, 291].

Lastly, it should be mentioned that many theories of modified gravity predict GW propagation speeds different from the speed of light. In such theories the cosmological background solution acts as a diffractive medium [296]. This is different in the present setting, where the background medium is such that at late times we obtain $\tilde{c} = 1$, cf. Sec. 2.3.2. Here, the only modification is the dispersion relation of the massive mode that propagates and mixes with the massless mode. Theories with such an effective background medium do not easily withstand the joint observation of GW170817 and GRB170817A [297], a short gamma-ray burst that could be associated with the merger of a NS binary system, which led to the former GW signal [298]. As discussed at length in Refs. [299–302], this renders many such models non-viable under the assumption of simultaneous or delayed emission of GWs and their electromagnetic counterpart. For a modified dispersion relation, these observations imply a mass bound, which is similar to, but independent of the solar system bound, $m_g < 1 \cdot 10^{-22}\,\mathrm{eV}$ [303].

We have summarised the existing and presently obtained bounds in Tab. 5.1. While solar system tests clearly give the least model dependent bound, it is quite remarkable to observe that our bound for the graviton mass at maximal mixing ($\theta = \pi/4$) derived from oscillations of GWs is very competitive highlighting once more the importance of GW astronomy. Furthermore, this bound is due to a modification of the propagation of GWs and therefore an important complementarity test, as a force mediated by an admixture of a massless and a massive spin-2 field is expected to display both a modified potential, and a modified dispersion relation. In this sense, the projected bounds from the CMB B-modes would constitute an important cross-check for the bounds derived from weak lensing and rotation curves.

Yukawa potential		
m_g [eV]	description & comments	references
$\mathbf{7.2 \cdot 10^{-23}}$	solar system tests (Mercury)	[205, 216]
$\mathbf{6 \cdot 10^{-32}}$	weak lensing of a cluster at redshift $z = 1.2$	[272]
$5 \cdot 10^{-31}$	weak lensing of a cluster at $z = 0.44$ ($\theta = \pi/2$)	Sec. 4.2.4
$3 \cdot 10^{-30}$	ESO138-G014 rotation curve ($\theta = \pi/2$)	Sec. 4.3.2
$5 \cdot 10^{-30}$	NGC1052-DF (galaxy without DM; $\theta = \pi/2$)	Sec. 4.3.3
$4 \cdot 10^{-27}$	LSB galaxies ($\theta = \pi/2$)	App. C.2

Modified propagation		
m_g [eV]	description & comments	references
$\mathbf{7.7 \cdot 10^{-23}}$	GW170104 with a modified dispersion relation	[58, 205]
$\mathbf{1 \cdot 10^{-22}}$	coincidence of GW170817 and GRB170817A	[303]
$\mathbf{7.6 \cdot 10^{-20}}$	pulsar timing (PSR B1913+16 & PSR B1534+12)	[289]
$6 \cdot 10^{-23}$	GW oscillations of GW150914 (max. mixing: $\theta = \pi/4$)	Sec. 3.2
$\mathit{10^{-30}}$	B-mode polarisation in the CMB	[290]
$\mathit{10^{-26}}$	$10^4 \ldots 10^7 M_\odot$ binary merger (eLISA)	[205]
$\mathit{10^{-23}}$	pulsar timing array (100 ns accuracy, 10 yr observation)	[304]
$\mathit{10^{-20}}$	combined gamma ray and GW Supernova observation	[305]

Table 5.1.: Summary of existing upper graviton mass bounds (boldface) and some projected constraints (italic) in comparison to our work. If not stated otherwise, these apply to the case of massive gravity ($\theta = \pi/2$). For a more exhaustive list see Ref. [76].

5.1.2 Persisting issues of massive gravity

We have already commented on some of the conceptual questions that remain to be clarified in the context of massive spin-2 fields, cf. Sec. 2.3.2. Most of these issues arise in the context of cosmology, such as the Higuchi instability, which can be remedied by considering the bimetric setup, as was done here. Furthermore, stable cosmological solutions seem to exist only for fine-tuned initial condition, as pointed out in Ref. [184].

Further, the scale $\Lambda_3 = (m_g^2 M_{\rm Pl})^{1/3}$ in Eq. (2.21), which characterises the onset of strong coupling, can be very low. At the same time it is indispensable to the emergence of the Vainshtein regime, as we discussed in Chapter 2. While some authors have used this to find *lower* bounds on the spin-2 mass from the validity of the effective field theory, see e.g. [306–308], others pointed out that this scale is not to be understood as a cut-off limiting the theory's validity, but merely a strong coupling scale, above which perturbation theory breaks down [309–312]. Whether the two coincide or not is then a question of the nature of the high-energy completion of the effective theory, see Sec. 10 of Ref. [53], which contains a discussion of these and related questions. This issue, too, can be cured by considering the bimetric setup close to GR. There, the strong coupling scale is found to be $\Lambda_3 / \tan^{1/3}(\theta)$, which can be made large by taking the $\theta \to 0$ limit [168].

Finally, some authors have raised the concern that the theory might be acausal, because

it, in principle, admits superluminal propagation [313–318]. However, it is not clear which type of velocity is considered, and if, indeed, information is propagating superluminally. If this were the case, one could construct closed time-like curves in violation of causality. However, it has been shown that *local* closed time-like curves cannot be constructed in the perturbative regime [319], while the strong coupling regime is believed to restore GR, and that some of the constructions relied on unphysical backgrounds [320]. We remark that in a bimetric framework, the null surfaces of the hidden sector could be space-like w.r.t. the physical metric g. However, these superluminalities w.r.t. the g light cone do not necessarily imply acausality, if the field equations allow a well-posed initial value problem [321], see also Ref. [322] (note especially Figs. 1 and 2 of this reference). Of course, if acausalities do arise in the theory, its viability is strongly challenged, but as of writing of this manuscript no conclusive verdict has been reached. The reader is referred to Sec. 10.6 of Ref. [53] for a thorough confrontation of arguments.

In conclusion, we see that while some issues yet need to be resolved, many conceptual obstacles can be overcome by giving dynamics to the hidden sector tensor field. This observation was our initial motivation to study a bimetric setup in favour of the dRGT framework, which can be obtained as a limit of bigravity.

5.2 Outlook

This work, in accord with most of the literature, has found that the Yukawa-type modifications of the gravitational law on galactic scales is not apt to render a DM component obsolete. Therefore, it is of great importance to investigate how particle DM could be realised in bigravity. This is, indeed, a very active field of research, and the proposed models range from very light spin-2 DM candidates considered in [323, 324], via intermediate masses [325–328], to the aforementioned TeV-scale models [286–288].

Instead of considering spin-2 DM, one could speculate about a hidden matter sector coupling exclusively to the hidden sector tensor as its metric. This would allow one to construct a model of ordinary particle DM along the lines of WIMPs, and at the same time evade the notorious hierarchy problem of SM extensions that involve heavy particles. Recently, there has been some interest in particle DM models, which couple to the SM only via their gravitational interactions, see e.g. Ref. [329]. While it is certainly no necessity to incorporate such a setup into a bimetric framework, this could have some interesting consequences, both for the DM phenomenology and possibly improve the stability of the cosmic evolution [171]. Furthermore, such a setting would immediately follow from our approach to the action from a discretised extra dimension, as outlined in Chapter 2.

Lastly, let us speculate about possible high-energy extensions of bigravity and related theories. Continuous, periodic extra dimensions give rise to an infinite tower of massive excitations, dubbed the Kaluza-Klein tower [330, 331]. It was shown in Ref. [113], that the deconstruction of an extra space-like dimension is equivalent to a truncation of that tower at a given order. Therefore, we might think of bi- or multi-metric theories simply as an effective field theory of models that introduce compact extra dimensions. Moreover, it is a well-established idea to restrict matter to a slice of the higher-dimensional space-time, a so-called *brane*, in order for the extra dimension to be large. Effectively this is done via

a delta-function, see e.g. Refs. [31–35],

$$S = \int \mathrm{d}^4x \int \mathrm{d}y \left(\sqrt{-\det G} \frac{M_5^3}{2} R_g^{(5)} + \sqrt{-\det g}\, \delta(y)\, \mathcal{L}_{\mathrm{SM}} \right), \tag{5.1}$$

where G is the 5D metric and g its physical $d = 4$ components. This is interesting because in this setting the 4D Planck mass emerges from the higher dimensional Planck mass, say in $d = 5$, as $M_{\mathrm{Pl}}^2 = M_5^3 \times \ell$, where ℓ is the 'volume' of the extra dimension. In Eq. (2.48), we had found that $\ell = m^{-1}$. Thus, a large volume, or small m, can be used to explain the weakness of gravity compared to the other known forces in Nature. While a dynamical mechanism to stabilise the matter brane by means of a bulk scalar field is known in these settings [332], it is found that its backreaction onto gravity is negligible [333]. Interestingly, the low-energy phenomenology of such frameworks is similar to what was found here, cf. Refs. [32, 334]. To dynamically discretise the entire action including the curvature, one would have to find a way to let $\delta(y)$ emerge dynamically and have it react back onto gravity. This could be done, e.g. via an approximation of the kind $\delta_\varepsilon(y) \equiv \frac{1}{\varepsilon} e^{-y^2/(2\varepsilon)}$, which approximates $\delta(y)$ as $\varepsilon \to 0$. If a mechanism can be conceived in which such a term emerges from the 5D action, e.g. from the determinant, and where one could think of ε as time dependent or depending on a (bulk) field, the action would be dynamically deconstructed at late times. Whether such a mechanism exists or not, is unknown to us, and we leave this for future work.[1]

A final remark we would like to make is a possible connection of conformal gravity to bimetric gravity [335]. Interestingly, the former is found to propagate six DOF (cf. footnote 5 of Ref. [336]), which can be thought of as the massless and massive spin-2 fields of linearised bimetric theory with a non-propagating scalar mode – a phenomenon known as partial masslessness [337]. While conformal gravity can address the issue of the non-renormalisabilty of GR, it turns out that the massive mode is tachyonic [336]. Conversely, in a linearised theory one can decouple the helicity-0 mode on a de Sitter background by saturating the Higuchi bound (2.96), $m_g^2(H^2) = 2H^2$ [335]. This is interesting because it relates the CC to the mass scale which turns out to be protected by a symmetry in this limit, and can thus be as small as observed. To date, it is unknown if one can construct a non-linear theory that keeps this scalar mode non-dynamical and cure the tachyonic states in conformal gravity, as discussed at length in the reviews [53, 54].

[1] I would like to thank Kevin Max for many interesting discussions about this mechanism and acknowledge contributions to attempts at its implementation.

Chapter 6

Conclusions

In this work we examined the phenomenological implications of massive spin-2 fields present in addition to the massless spin-2 field predicted in general relativity (GR). We have taken a point of view inspired by particle physics, where the standard model of particle physics (SM) successfully describes most interactions observed in experiments, but suffers from some conceptual and observational shortcomings such as non-zero neutrino masses, the identity of dark matter (DM), late-time acceleration, and the gauge hierarchy problem. In addressing one or several of these lapses, phenomenologists are challenged to bring these extensions of the SM into agreement with observations, i.e. evade experimental bounds arising from the non-observation of new physics.

In this very spirit we have considered bimetric gravity, or simply bigravity, a framework which in the present form dates back to the years 2010/11 and which describes precisely the above: two interacting spin-2 fields, one massive and one massless. While the interaction term is chosen to comply with consistency criteria – also at the non-linear level – it induces very interesting phenomenological effects, both at the linear level and beyond:

- Cosmological solutions encompass late time acceleration if the mass of the heavy spin-2 field is of the order of the Hubble rate today. Such small values have been found to be technically natural as they do not suffer from large quantum corrections.

- If the mass of the heavy spin-2 field is some ten orders of magnitude larger than the Hubble rate, it presents an interesting alternative to light scalar or vector DM models.

- However, the mass might even be allocated in the TeV scale, which allows one to construct a DM candidate along the lines of weakly interacting massive particles (WIMPs).

- Alternatively, it naturally allows the introduction and *gravitational decoupling* of a hidden matter sector, thereby evading the notorious hierarchy problem of many models beyond the SM.

These rather favourable features should be contrasted with some of the persisting issues that remain to be addressed. Among them is the question of causality, which arises

because the framework seems to allow parameter choices that induce superluminal propagation. However, one might object that the SM allows a scalar potential that is unbounded from below if the Higgs self-coupling were negative. Clearly, Nature does not choose such unphysical parameters. Furthermore, the limit where the hidden sector tensor field becomes non-dynamical, cosmological solutions no longer admit solutions that entail late-time acceleration since new tachyonic instabilities arise. This is, in fact, remedied by giving dynamics to the second tensor field, as we have assumed throughout the present manuscript. Nevertheless, cosmological perturbations appear to generally induce non-perturbative behaviour, either at late or at early times in cosmic history. While the former is, of course, ruled out, the latter option is an interesting observation that needs further attention as it could seed and/or affect structure formation, or the formation of primordial black holes. These, in turn, could serve as the observed DM in the Universe, or at least a fraction of it. Another open question is the issue of matter couplings. We have mostly evaded this discussion by an extra-dimensional *top-down* derivation of the action that immediately leads to a diagonal matter coupling, i.e. each matter Lagrangian couples to its own metric tensor. However, choosing instead a *bottom-up* approach, other matter couplings appear to be consistent, while others render the model unstable. This issue remains unsettled and the results of the present manuscript have no implications on this (maybe somewhat philosophical) question. In the end, this issue can only be settled by finding appropriate ultraviolet completions and testing them against each other phenomenologically, ruling out all of them or singling out a candidate theory.

The recent advent of gravitational wave (GW) astronomy has enabled us to discuss in detail how to probe the model via the modified propagation of GWs and allowed us to constrain the available parameter space of the model. Using these and existing bounds from solar system tests gives an upper bound for the viability of the low-mass regime considered here. Moreover, we have discussed how the distribution of merging black hole and neutron star binary systems could be affected by the modified propagation in the regime where the mass of the spin-2 field is sufficiently large for the wave packets to decohere such that any interference pattern is lost. At present, this does not yield reliable constraints on the parameter space. In the future, however, this could prove to be a valuable handle on the viability of the model. In an attempt to study the implications of the non-linear nature of the interactions present in this setting, we have phenomenologically implemented the Vainshtein screening mechanism, which restores GR predictions inside a sphere of a certain radius depending on the spin-2 mass and the enclosed mass distribution. This has interesting implications for the predictions on gravitational lensing, because the light deflection angle changes, and the gravitational interactions inside galaxies and clusters of galaxies. In our analysis, we have not found any preference for the bigravity framework over GR to better describe the data on galactic or extragalactic scales. Nevertheless, it does allow to address some tentative anomalies in cluster mass estimates that appear to systematically deviate depending on the assumptions. It is found that bigravity would induce precisely the required bias, lowering one mass estimate, while increasing the other. Nevertheless, this could very well be explained by the departure from the equilibrium assumptions that are made. However, at present, the data do not allow for a conclusive statement. Finally, we have also made contact with recent observations in astronomy by considering a galaxy whose discovery was reported in March 2018, and which appears to be devoid of DM. This provides additional constraints on the parameter space, as does

the study of other galaxies which do contain significant amounts of DM.

Our findings are summarised in Fig. 5.1, which contains all relevant constraints we have derived in Chapters 3 and 4. Furthermore, it states a lower bound on the graviton mass, which should be understood as a phenomenological bound, given that below it, no observable effects are expected. In concordance with the literature, we find that gravity with only one massive mediator is highly constrained and only masses well below $10^{-30}\,\mathrm{eV}$ are allowed. The situation changes dramatically when relaxing this assumption and introducing on top of the standard, massless graviton a massive graviton, allowing both to mix. While the region above $10^{-22}\,\mathrm{eV}$ remains to be excluded due to solar system tests and our analysis of GW oscillations, a vast region of the parameter space remains to be tested. In some regions, certain tentative anomalies can be explained, and a region, where the combined data yields a better fit emerges – albeit at very low statistical significance. It should be highlighted that this, by no means, complies with Occam's razor due to the many complications the description necessitates. Therefore, the standard model of cosmology (ΛCDM) and GR clearly survive our analyses as the preferred description of Nature on large scales. Finally, we wish to remark that while our analyses provide a first insight into the phenomenology of massive spin-2 extensions of ΛCDM, there remains plenty of work, both in theory and phenomenology, for future studies as we have highlighted in Chapter 5.

Appendices

Appendix A

Gravitational Field Equations in Bigravity

This appendix is dedicated to the detailed study of the field equations, similar to the Einstein equations in GR. Initially, we will present the exact form of these equations in such a manner, that enables the reader to directly implement these in a concrete calculation. This requires the derivation of the interaction terms $V^{(i)}(g)^{\mu}{}_{\nu}$ and $V^{(i)}(\tilde{g})^{\mu}{}_{\nu}$ from the action, which was given in Eq. (2.58). In a next step, we show an example how to solve these equations, stating from the ansatz (2.83). Finally, we discuss the linearisation of the field equations around an asymptotically flat, cosmological background. This will allow us to assess that, indeed, bigravity propagates seven DOF, and moreover will be the basis for our discussion in Chapter 3.

A.1 Field equations in bigravity

Let us derive the analogue of Einstein's field equations for the theory describing the interactions of two tensor fields g and $\tilde{g}$, starting from the action (2.58):

$$\begin{aligned} S_{\rm bi} = &\frac{M_g^2}{2}\int d^4x\sqrt{-\det g}\; R(g) + \frac{M_{\tilde{g}}^2}{2}\int d^4x\sqrt{-\det \tilde{g}}\; \tilde{R}(\tilde{g}) - \\ &- m^2 M_{\rm eff}^2 \int d^4x\sqrt{-\det g}\sum_{n=0}^{4}\beta_n e_n(\sqrt{g^{-1}\tilde{g}}) + \int d^4x\sqrt{-\det g}\;\mathcal{L}_{\rm matter}\,. \end{aligned} \tag{A.1}$$

The e_n are symmetric polynomials of the eigenvalues of the matrix $\mathbb{X} = \sqrt{g^{-1}\tilde{g}}$, i.e. they are defined via

$$e_n(\mathbb{X}) \equiv \sum_{i_1<i_2<\ldots<i_n} \lambda_{i_1}\lambda_{i_2}\cdots\lambda_{i_n}\,. \tag{A.2}$$

A more convenient way to express these for most practical purposes (avoiding the explicit calculation of the eigenvalues) reads

$$\begin{aligned} e_0(\mathbb{X}) &= 1\,, \quad e_1(\mathbb{X}) = [\mathbb{X}]\,, \quad e_2(\mathbb{X}) = \frac{1}{2}\left([\mathbb{X}]^2 - \left[\mathbb{X}^2\right]\right), \\ e_3(\mathbb{X}) &= \frac{1}{6}\left([\mathbb{X}]^3 - 3\,[\mathbb{X}]\left[\mathbb{X}^2\right] + 2\left[\mathbb{X}^3\right]\right), \quad e_4(\mathbb{X}) = \det \mathbb{X}\,, \end{aligned} \tag{A.3}$$

where we have used the notation $[\cdot] \equiv \mathrm{tr}\,(\cdot)$. The variation of the interaction potentials in the action (A.1) w.r.t. g will give us the interaction terms that enter the field equations of bigravity (2.60). Let us outline how these expressions are obtained from the action, Eq. (2.58). To this end we compute

$$\begin{aligned} \delta_g \sqrt{-\det g} &= -\frac{1}{2\sqrt{-\det g}}\,\delta_g \sqrt{-\det g} = \frac{1}{2\sqrt{-\det g}} \det g\,\mathrm{tr}\left(g^{-1}\delta g\right) \\ &= -\frac{1}{2}\sqrt{\det g}\,g_{\mu\nu}\,\delta g^{\mu\nu}\,, \end{aligned} \tag{A.4}$$

where we have invoked Jacobi's rule for the differential of a determinant, $\mathrm{d}\det A = \det A \mathrm{tr}\left(A^{-1}\mathrm{d}A\right)$, and the identity $\delta_g g^{-1} = -g^{-1}\delta g g^{-1}$, which follows from $\delta_g\left(g^{-1}g\right) = 0$. Moreover we need to vary the trace of the matrix $\mathbb{X} = \sqrt{g^{-1}\tilde{g}}$:

$$\begin{aligned} \delta_g \mathrm{tr}\left(\sqrt{g^{-1}\tilde{g}}\right) = \mathrm{tr}\left(\delta_g \sqrt{g^{-1}\tilde{g}}\right) &= \frac{1}{2}\mathrm{tr}\left(\left(\sqrt{g^{-1}\tilde{g}}\right)^{-1}\delta_g\left(g^{-1}\tilde{g}\right)\right) \\ &= -\frac{1}{2}\mathrm{tr}\left(\left(\sqrt{g^{-1}\tilde{g}}\right)^{-1} g^{-1}\delta g\,\left(g^{-1}\tilde{g}\right)\right) \\ &= -\frac{1}{2}\mathrm{tr}\left(\sqrt{g^{-1}\tilde{g}}\,g^{-1}\delta g\right) = \frac{1}{2}\mathbb{X}^{\mu}{}_{\alpha}\,g_{\mu\nu}\,\delta g^{\alpha\nu}\,, \end{aligned} \tag{A.5}$$

where we have used the linearity of the trace and the variation as a differential operation, the cyclicity of the trace, and the above identities. We are now ready to vary the polynomials $e_n(\mathbb{X})$ w.r.t. g. As an example, we compute the variation $\delta_g\sqrt{\det g}\,e_2(\mathbb{X})$:

$$\begin{aligned} &\left(\delta_g\sqrt{\det g}\right)e_2(\mathbb{X}) + \frac{1}{2}\sqrt{\det g}\,\delta_g\left(\mathrm{tr}\,(\mathbb{X})^2 - \mathrm{tr}\left(\mathbb{X}^2\right)\right) \\ &= -\frac{1}{2}\sqrt{\det g}\,e_2(\mathbb{X})\,g_{\mu\nu}\delta g^{\mu\nu} + \sqrt{\det g}\,\mathrm{tr}\,(\mathbb{X})\,\delta_g\mathrm{tr}\,(\mathbb{X}) - \frac{1}{2}\sqrt{\det g}\,\delta_g\mathrm{tr}\left(g^{-1}\tilde{g}\right) \\ &= -\frac{1}{2}\sqrt{\det g}\left\{e_2(\mathbb{X})\,g_{\mu\nu}\,\delta g^{\mu\nu} - \mathrm{tr}\,(\mathbb{X})\,\mathbb{X}^{\mu}{}_{\alpha}\,g_{\mu\nu}\,\delta g^{\mu\nu} - \mathrm{tr}\left(\left[g^{-1}\,\delta g\,g^{-1}\right]\tilde{g}\right)\right\} \\ &= -\frac{1}{2}\sqrt{\det g}\,g_{\mu\alpha}\left\{(\mathbb{X}^2)^{\alpha}_{\ \nu} - \mathrm{tr}\,(\mathbb{X})\,\mathbb{X}^{\alpha}_{\ \nu} + \frac{\delta^{\alpha}_{\ \nu}}{2}\left[\mathrm{tr}\,(\mathbb{X})^2 - \mathrm{tr}\left(\mathbb{X}^2\right)\right]\right\}\delta g^{\nu\mu}\,, \end{aligned} \tag{A.6}$$

where we used that $\mathbb{X}^2 = g^{-1}\tilde{g}$ by definition. Dividing by the conventional $\frac{1}{2}\sqrt{-\det g}$, we arrive at

$$\begin{aligned}
V^{(0)}(g)^{\mu}{}_{\nu} &= \delta^{\mu}{}_{\nu}\,, \quad V^{(1)}(g)^{\mu}{}_{\nu} = \operatorname{tr}(\mathbb{X})\,\delta^{\mu}{}_{\nu} - \mathbb{X}^{\mu}{}_{\nu}\,,\\
V^{(2)}(g)^{\mu}{}_{\nu} &= \left(\mathbb{X}^2\right)^{\mu}{}_{\nu} - \operatorname{tr}(\mathbb{X})\,\mathbb{X}^{\mu}{}_{\nu} + \frac{\delta^{\mu}{}_{\nu}}{2}\left[\operatorname{tr}(\mathbb{X})^2 - \operatorname{tr}\left(\mathbb{X}^2\right)\right],\\
V^{(3)}(g)^{\mu}{}_{\nu} &= -\left(\mathbb{X}^3\right)^{\mu}{}_{\nu} + \operatorname{tr}(\mathbb{X})\left(\mathbb{X}^2\right)^{\mu}{}_{\nu} - \frac{1}{2}\left[\operatorname{tr}(\mathbb{X})^2 - \operatorname{tr}\left(\mathbb{X}^2\right)\right]\mathbb{X}^{\mu}{}_{\nu} +\\
&\quad + \frac{\delta^{\mu}{}_{\nu}}{6}\left[\operatorname{tr}(\mathbb{X})^3 - 3\operatorname{tr}(\mathbb{X})\operatorname{tr}\left(\mathbb{X}^2\right) + 2\operatorname{tr}\left(\mathbb{X}^3\right)\right].
\end{aligned} \tag{A.7}$$

In order to derive the corresponding expressions for the $\tilde{g}$ tensor, we need to vary the action w.r.t. $\tilde{g}$. We observe that the variation of the $\sqrt{-\det g}$ term no longer contributes, such that the $\delta^{\alpha}{}_{\nu}$ terms in Eq. (A.7) must be dropped. Furthermore, the potentials $V^{(1,2,3,4)}(\tilde{g})$ will carry an additional minus sign, because we find that

$$\begin{aligned}
\delta_{\tilde{g}} \operatorname{tr}\left(\sqrt{g^{-1}\tilde{g}}\right) &= +\frac{1}{2}\operatorname{tr}\left(\left(\sqrt{g^{-1}\tilde{g}}\right)^{-1} g^{-1}\delta\tilde{g}\right)\\
&= -\frac{1}{2}\mathbb{X}^{\mu}{}_{\alpha}\,\tilde{g}_{\mu\nu}\,\delta\tilde{g}^{\alpha\nu}\,,
\end{aligned} \tag{A.8}$$

having used $\delta\tilde{g}^{-1} = -\tilde{g}^{-1}\,\delta\tilde{g}\,\tilde{g}^{-1}$. Therefore, one obtains after dividing by $\frac{1}{2}\sqrt{-\det\tilde{g}}$,

$$\begin{aligned}
V^{(1)}(\tilde{g})^{\mu}{}_{\nu} &= \mathbb{X}^{\mu}{}_{\nu}\,, \quad V^{(2)}(\tilde{g})^{\mu}{}_{\nu} = -\left(\mathbb{X}^2\right)^{\mu}{}_{\nu} + \operatorname{tr}(\mathbb{X})\,\mathbb{X}^{\mu}{}_{\nu}\,,\\
V^{(3)}(\tilde{g})^{\mu}{}_{\nu} &= \left(\mathbb{X}^3\right)^{\mu}{}_{\nu} - \operatorname{tr}(\mathbb{X})\left(\mathbb{X}^2\right)^{\mu}{}_{\nu} + \frac{1}{2}\left[\operatorname{tr}(\mathbb{X})^2 - \operatorname{tr}\left(\mathbb{X}^2\right)\right]\mathbb{X}^{\mu}{}_{\nu}\,,\\
V^{(4)}(\tilde{g})^{\mu}{}_{\nu} &= \delta^{\mu}{}_{\nu}\,,
\end{aligned} \tag{A.9}$$

where indices are raised and lowered using $\tilde{g}$.

A.2 Solving the bimetric field equations of a Schwarzschild-type black hole

We can now apply these findings to a practical problem. In order not to obscure the main message, we did not explicitly show the solution to the BH ansatz formulated in Eq. (2.83),

$$g_{\mu\nu}\mathrm{d}x^\mu\mathrm{d}x^\nu = -e^{\nu_1(r)}\mathrm{d}t^2 + e^{\lambda_1(r)}\mathrm{d}r^2 + r^2\mathrm{d}\Omega^2\,, \tag{A.10a}$$

$$\tilde{g}_{\mu\nu}\mathrm{d}x^\mu\mathrm{d}x^\nu = -e^{\nu_2(r)}\mathrm{d}t^2 + e^{\lambda_2(r)}(r + r\mu(r))'^2\mathrm{d}r^2 + (r + r\mu(r))^2\mathrm{d}\Omega^2\,. \tag{A.10b}$$

Will will now solve the resulting field equations, first in a linearised regime, and later confirm under which circumstances this assumption is valid. As it turns out, some of the linearity assumptions must be dropped when the radial coordinate becomes smaller than a certain critical radius, i.e. the Vainshtein radius.

Linear regime. Let us first consider the linearised equations, which will be justified *a posteriori*. To this end, we assume that the exponentials can be expanded in powers of λ and ν; furthermore, let us assume that $\mu \ll 1$. To obtain compact expressions, we define $\alpha_1 \equiv \beta_1 + 2\beta_2 + \beta_3$, $\alpha_2 \equiv 3\beta_1 + 3\beta_2 + \beta_3$, and $\alpha_3 \equiv \beta_2 + 2\beta_3$, and set $\beta_4 = 0$ for now. We will return to discussing this assumption below. Plugging our ansatz into Eqs. (2.60), we obtain the following set of linearised equations for the g-type functions:

$$\frac{\lambda_1}{r^2} + \frac{\lambda_1'}{r} = \Lambda_g + m_g^2\sin^2(\theta)\left[\frac{1}{2}(\lambda_2 - \lambda_1) + \left(3\mu + r\mu'\right)\right], \tag{A.11a}$$

$$\frac{\lambda_1}{r^2} - \frac{\nu_1'}{r} = \Lambda_g + m_g^2\sin^2(\theta)\left[\frac{1}{2}(\nu_2 - \nu_1) + 2\mu\right], \tag{A.11b}$$

$$\frac{1}{2}\left(\frac{\lambda_1'}{r} - \frac{\nu_1'}{r} - \nu_1''\right) = \Lambda_g + m_g^2\sin^2(\theta)\left[\frac{1}{2}(\lambda_2 - \lambda_1 + \nu_2 - \nu_1) + \left(2\mu + r\mu'\right)\right]. \tag{A.11c}$$

We have introduced the mass $m_g^2 \equiv m^2\alpha_1$ and the cosmological constant $\Lambda_g \equiv \Lambda + m^2\alpha_2\sin(\theta)^2$ for the g metric. Analogously, we find for the $\tilde{g}$-type functions:

$$\frac{\lambda_2}{r^2} + \frac{\lambda_2'}{r} = \Lambda_f + m_g^2\cos^2(\theta)\left[\frac{1}{2}(\lambda_1 - \lambda_2) - \left(3\mu + r\mu'\right)\right], \tag{A.12a}$$

$$\frac{\lambda_2}{r^2} - \frac{\nu_2'}{r} = \Lambda_f + m_g^2\cos^2(\theta)\left[\frac{1}{2}(\nu_1 - \nu_2) - 2\,\mu\right], \tag{A.12b}$$

$$\frac{1}{2}\left(\frac{\lambda_2'}{r} - \frac{\nu_2'}{r} - \nu_2''\right) = \Lambda_f + m_g^2\cos^2(\theta)\left[\frac{1}{2}(\lambda_1 + \nu_1 - \lambda_2 - \nu_2) - \left(2\mu + r\mu'\right)\right], \tag{A.12c}$$

with $\Lambda_f = m^2(\alpha_1 + \alpha_3)\cos^2(\theta)$. In addition, the constraints (2.61) give

$$\lambda^{(-)} - \frac{r}{2}\nu^{(-)\prime} = 0\,, \tag{A.13a}$$

$$\lambda^{(-)\prime} + \nu^{(-)\prime} - 8\mu' - 2r\mu'' = 0\,, \tag{A.13b}$$

abbreviating $\lambda^{(-)} \equiv \lambda_1 - \lambda_2$ and $\nu^{(-)} \equiv \nu_1 - \nu_2$. Integrating Eqs. (A.13b) and (A.13a) yields

$$\left(r^3\mu\right)' = \frac{r}{4}\left(r^2\nu^{(-)}\right)' + \frac{C_0\, r^2}{2}\,, \tag{A.14}$$

which we use to simplify the expressions in square brackets in Eqs. (A.11a) and (A.12a):

$$\mp\frac{1}{2}\lambda^{(-)} \pm \left(3\mu + r\mu'\right) = \mp\frac{r}{4}\nu^{(-)\prime} \pm \frac{1}{4r}\left(2r\nu^{(-)} + r^2\nu^{(-)\prime}\right) \pm \frac{C_0}{2} = \pm\frac{1}{2}\nu^{(-)} \pm \frac{C_0}{2}. \tag{A.15}$$

This allows us to combine the first lines of Eqs. (A.11, A.12) into a single differential equation:

$$\frac{1}{r^2}\left(r\lambda^{(-)}\right)' = \frac{1}{r^2}\left(\frac{r^2}{2}\nu^{(-)\prime}\right)' = \frac{m_g^2}{2}\nu^{(-)}\,, \tag{A.16}$$

where we used the integration constant C_0 to set

$$\Lambda + m^2\left(\alpha_1 C_0/2 + \sin^2(\theta)\alpha_2 - \cos^2(\theta)\left(\alpha_1 + \alpha_3\right)\right) = 0\,. \tag{A.17}$$

Eq. (A.16) is solved by

$$\nu^{(-)}(r) = \frac{C_2}{r}e^{-m_g\, r} \quad \Rightarrow \quad \lambda^{(-)}(r) = -\frac{C_2\left[1 + m_g\, r\right]}{2r}e^{-m_g\, r}\,. \tag{A.18}$$

Notice that we did not consider the unphysical exponentially growing type of solution. The orthogonal linear combination to $\lambda^{(-)}$ is $\lambda^{(+)} \equiv \cos(\theta)^2\lambda_1 + \sin^2(\theta)\lambda_2$, which obeys the differential equation

$$\frac{1}{r^2}\left(r\lambda^{(+)}\right)' = \cos(\theta)^2\left[\Lambda + m^2\sin^2(\theta)(\alpha_1 + \alpha_2 + \alpha_3)\right], \tag{A.19}$$

and is easy to solve ($\Lambda_{\text{eff}} \equiv \left[\Lambda + m^2\sin^2(\theta)(\alpha_1 + \alpha_2 + \alpha_3)\right]$),

$$\lambda^{(+)}(r) = \frac{C_1}{r} + \frac{r^2}{3}\cos(\theta)^2\Lambda_{\text{eff}} \;\Rightarrow\; \nu^{(+)}(r) = -\left[\frac{C_1}{r} + \frac{r^2}{3}\cos(\theta)^2\Lambda_{\text{eff}} - C_3\right], \tag{A.20}$$

for $\nu^{(+)} \equiv \cos(\theta)^2\nu_1 + \sin^2(\theta)\nu_2$. Going back to the original functions, let us summarise the results:

$$\nu_1(r) = -\left[\frac{C_1}{r} + \frac{r^2}{3}\cos^2(\theta)\Lambda_{\text{eff}}\right] + \sin^2(\theta)\left(\frac{C_2\, e^{-m_g\, r}}{r}\right) + C_3, \tag{A.21a}$$

$$\lambda_1(r) = \frac{C_1}{r} + \frac{r^2}{3}\cos^2(\theta)\Lambda_{\text{eff}} - \sin^2(\theta)\,\frac{C_2 e^{-m_g\, r}\left[1 + m_g\, r\right]}{2r}, \tag{A.21b}$$

$$\nu_2(r) = -\left[\frac{C_1}{r} + \frac{r^2}{3}\cos^2(\theta)\Lambda_{\text{eff}}\right] - \cos(\theta)^2\left(\frac{C_2\, e^{-m_g\, r}}{r}\right) + C_3, \tag{A.21c}$$

$$\lambda_2(r) = \frac{C_1}{r} + \frac{r^2}{3}\cos^2(\theta)\Lambda_{\text{eff}} + \cos(\theta)^2\frac{C_2\, e^{-m_g\, r}\left[1 + m_g\, r\right]}{2r}. \tag{A.21d}$$

By virtue of Eq. (A.14), we finally obtain

$$\mu(r) = \frac{C_2\, e^{-m_g\, r}\left[1 + m_g\, r + m_g^2\, r^2\right]}{4 m_g^2\, r^3} + \frac{m_g^2\, C_0}{6 m_g^2} + \frac{C_4}{r^3}\,. \tag{A.22}$$

As we had claimed earlier, this function blows up as $\frac{C_2}{m_g^2\, r^3}$ grows. Eventually, we will identify this with the onset of the Vainshtein screening and the restoration of (the Newtonian limit of) GR. To arrive at this conclusion we must include non-linear effects.

The non-linear regime. The crossing into the region, where $\mu \gtrsim 1$ signals that our approximations must be adopted. We could, of course, try to solve the full set of equations at the fully non-linear level, as was done in Refs. [145, 146]. However, the purpose of this section is to gain some physical insight into the solutions, and hence we make a minimal change to our assumptions, by relaxing the requirement $\mu \ll 1$. This yields a slightly more complicated set of equations, now including non-linear terms in μ:

$$\nu_1'(r) = \frac{r_S}{r^2} - \frac{2}{3}\Lambda_g r + \frac{1}{3} m^2 r \sin^2(\theta)\mu(r)\left[-3\alpha_1 + (\alpha_3 - \alpha_4)\mu(r)^2\right]\,, \tag{A.23a}$$

$$\lambda_1(r) = \frac{r_S}{r} + \frac{1}{3}\Lambda_g r^2 + \frac{1}{3} m^2 r^2 \sin^2(\theta)\mu(r)\left[3\alpha_1 + 3\alpha_4\mu(r) + (\alpha_3 - \alpha_4)\mu(r)^2\right]\,, \tag{A.23b}$$

$$\nu_2'(r) = -\left[\frac{2}{3}\Lambda_f\, r + m^2 r \cos^2(\theta)\mu(r)\left(\alpha_1 + 2\alpha_3 + 2\alpha_3\mu(r) + (\alpha_3 - \alpha_4)\mu(r)^2\right)\right] \times \\ \times \frac{(r + r\mu(r))'}{(1+\mu(r))^2}\,, \tag{A.23c}$$

$$\lambda_2(r) = \left[\frac{1}{3}\Lambda_f\, r^2 + m^2 \cos^2(\theta) r^2 \mu(r)\left(\alpha_3 + (\alpha_3 - \alpha_4)\mu(r)\right)\right]\frac{1}{1+\mu(r)}\,, \tag{A.23d}$$

while the independent constraint equation (2.61) gives

$$\frac{2\,(r + r\mu(r))'\,(\lambda_1(r) - \lambda_2(r))}{(r + r\mu(r))'\,\nu_1'(r) - \nu_2'(r)} = r\frac{\alpha_1 + 2\alpha_4\,\mu(r) + (\alpha_3 - \alpha_4)\mu(r)^2}{\alpha_1 + \alpha_4\,\mu(r)}\,. \tag{A.24}$$

Here, we have defined $\alpha_4 \equiv \beta_2 + \beta_3$ and take $\beta_4 = 0$. This last assumption is justified as β_4 can only influence the hidden sector directly, while the visible sector to which matter couples, is insensitive to β_4. We will comment on the effect of $\beta_4 \neq 0$ below. Following Ref. [91], the integration constants have been fixed according to the matching to the matter distribution with Schwarzschild radius $r_S \equiv 2\,G_{\rm N} M$, where M is the total mass. Combining Eqs. (A.23, A.24), one arrives at an *algebraic* equation for μ, which we do not show explicitly. We highlight that the equation can always be solved if $\alpha_3 = 0$ and $\alpha_4 = -\alpha_1$, which leads to $\mu = 1$. In fact, Ref. [91] shows that any other branch of solution with $\mu \neq 1$ can be compensated for by a simple redefinition of the physical quantities r_S and Λ. The simple branch of solution ($\mu = 1$) leads to the familiar result obtained in GR:

$$\nu_1(r) = -\lambda_1(r) = -\frac{r_S}{r} - \frac{r^2}{3}\Lambda_{\text{eff}}\,, \tag{A.25a}$$

$$\nu_2(r) = -\lambda_2(r) = -\frac{2}{3}\,\alpha_1 m^2 r^2 \cos^2(\theta)\,. \tag{A.25b}$$

A final step is the matching of both regimes by fixing the integration constants at $r = r_V$, a procedure which yields

$$\begin{aligned} C_1 &= r_S\,\cos^2(\theta)\left(1+\frac{2}{3}\sin^2(\theta)\right), \quad & C_2 &= -2\,r_S\frac{\Lambda + m^2\alpha_1 + m^2\sin^2(\theta)(3\alpha_1+\alpha_2)}{3m^2\alpha_1}\,, \\ C_3 &= -\cos^2(\theta) m\sqrt{\alpha_1}C_2, & C_4 &= r_S\frac{5\Lambda + 3\alpha_1 m^2 + m^2\sin^2(\theta)(7\alpha_1+5\alpha_2)}{6\alpha_1^2 m^4}, \end{aligned} \tag{A.26}$$

under the assumption that $r_V\, m_g \ll 1$. Notice that we have already assumed implicitly that $C_2 \sim r_S$, an assumption which is now justified by virtue of Eqs. (A.26) and (A.22).

We conclude this section by discussing the implications of non-zero β_4. At the level of the field equations, this amounts to a modification

$$\text{Eqs. (A.12)} \to \text{Eqs. (A.12)} + m^2\cos^2(\theta)\,\beta_4\left[\frac{1}{2}(\lambda_1-\lambda_2)+\frac{1}{2}(\nu_1-\nu_2)-\left(3\mu + r\mu'\right)\right]. \tag{A.27}$$

Subtracting these new Eqs. (A.12) from Eqs. (A.11) results in the same expression we had in Eq. (A.18), if we choose the integration constant C_0 appropriately. Finally, the (+) labelled functions need to be modified as

$$\widehat{\nu}^{(+)} \equiv \frac{\alpha_1+\beta_4}{\alpha_1}\cos(\theta)^2\nu_1 + \sin^2(\theta)\nu_2\,, \tag{A.28}$$

which in general will display both $1/r$ and Yukawa-like behaviour. More importantly, the solutions approach Eqs. (A.20) in the limit where $\cos(\theta) \to 0$.

A.3 Linearised interaction potentials in FLRW background

In order to derive the linearised EOM in bigravity, which allow us to deduce which of the DOF are propagating, we need to linearise the interaction terms presented in Appendix A.1. We consider the background solution (2.85) found in Sec. 2.3.2, but only at late times where $\tilde{c} = 1$ and $y = y_* = \text{const}$ (see Ref. [171] for a more general approach). This will be the case relevant for the discussion in Chapter 3. The expansion parameter is a small fluctuation around this background, where $\eta_{\mu\nu}$ is the flat Minkowski metric and $\eta^{\mu\nu}$ its inverse [171],

$$g_{\mu\nu} = a^2(\eta)\left(\eta_{\mu\nu} + \frac{h_{\mu\nu}(\eta,\vec{x})}{M_g}\right), \qquad g^{\mu\nu} = a^{-2}(\eta)\left(\eta^{\mu\nu} - \frac{h^{\mu\nu}(\eta,\vec{x})}{M_g}\right), \tag{A.29a}$$

$$\tilde{g}_{\mu\nu} = b^2(\eta)\left(\eta_{\mu\nu} + \frac{\tilde{h}_{\mu\nu}(\eta,\vec{x})}{M_{\tilde{g}}}\right), \qquad \tilde{g}^{\mu\nu} = b^{-2}(\eta)\left(\eta^{\mu\nu} - \frac{\tilde{h}^{\mu\nu}(\eta,\vec{x})}{M_{\tilde{g}}}\right), \tag{A.29b}$$

where indices are raised and lowered w.r.t. η. and we defined the inverse perturbation with an appropriate minus sign in order to ensure that $g^{\mu\alpha}g_{\alpha\nu} = \delta^\mu_{\ \nu}$ to linear order. Given that the interaction terms are functions of $\mathbb{X}$, defined to satisfy

$$\mathbb{X}^\mu_{\ \alpha}\mathbb{X}^\alpha_{\ \nu} = \left(g^{-1}\tilde{g}\right)^\mu_{\ \nu}, \tag{A.30}$$

we find that the naive expansion is a suitable choice:

$$\mathbb{X}^\mu_{\ \nu} = \sqrt{\frac{b^2}{a^2}}\left[\delta^\mu_{\ \nu} + \frac{1}{2}\left(\frac{\tilde{h}_{\mu\alpha}(\eta,\vec{x})}{M_{\tilde{g}}}\eta^{\alpha\nu} - \frac{h^{\alpha\nu}(\eta,\vec{x})}{M_g}\eta_{\mu\alpha}\right)\right], \tag{A.31}$$

which satisfies Eq. (A.30) linearly. For later convenience let us define

$$u^\mu_{\ \nu} \equiv \frac{1}{2}\left(\frac{\tilde{h}^\mu_{\ \nu}(\eta,\vec{x})}{M_{\tilde{g}}} - \frac{h^\mu_{\ \nu}(\eta,\vec{x})}{M_g}\right). \tag{A.32}$$

Let us now linearise the interaction terms (A.7):[1]

$$\begin{aligned}\beta_1 V^{(1)}(g)^\mu_{\ \nu} =& \beta_1\left[\mathrm{tr}\left(\mathbb{X}\right)\mathbb{1} - \mathbb{X}\right]^\mu_{\ \nu} = \beta_1 y\left[\mathrm{tr}\left(1+u\right)\mathbb{1} - (1+u)\right]^\mu_{\ \nu} \\ =& \beta_1 y\left[3\,\mathbb{1} + \mathrm{tr}\left(u\right)\,\mathbb{1} - u\right]^\mu_{\ \nu}, \end{aligned} \tag{A.33a}$$

$$\begin{aligned}\beta_2 V^{(2)}(g)^\mu_{\ \nu} =& \beta_2\left[\mathbb{X}^2 - \mathrm{tr}\left(\mathbb{X}\right)\mathbb{X} + \frac{\mathbb{1}}{2}\left(\mathrm{tr}\left(\mathbb{X}\right)^2 - \mathrm{tr}\left(\mathbb{X}^2\right)\right)\right]^\mu_{\ \nu} \\ =& \beta_2 y^2\Bigg[\mathbb{1} + 2u - (4+\mathrm{tr}\left(u\right))(1+u) + \\ & \qquad + \frac{\mathbb{1}}{2}\left((4+\mathrm{tr}\left(u\right))^2 - \mathrm{tr}\left(1+2u\right)\right)\Bigg]^\mu_{\ \nu} \\ =& \beta_2 y^2\left[3\,\mathbb{1} + 2\mathrm{tr}\left(u\right)\,\mathbb{1} - 2u\right]^\mu_{\ \nu}, \end{aligned} \tag{A.33b}$$

[1] $V^{(0)}$ only yields a CC contribution.

and after some algebra,

$$\beta_3 V^{(3)}(g)^{\mu}_{\ \nu} = \ldots = \beta_3 y^3 \left[\mathbb{1} + \mathrm{tr}\,(u)\ \mathbb{1} - u\right]^{\mu}_{\ \nu}\,, \tag{A.33c}$$

where we used the notation $y \equiv b/a$. Notice that the mass term naturally gives rise to a y-dependent CC $\Lambda(y) = m^2(\beta_0 + 3\beta_1\, y + 3\beta_2\, y^2 + \beta_3\, y^3)$, even in the absence of a bare CC $\sim \beta_0$.

For the corresponding $\tilde{g}$ equations, we make use of the following property of the interaction terms, which follows from Eq. (A.2) [48]:

$$\det \mathbb{X}\, e_n\left(\mathbb{X}^{-1}\right) = e_{4-n}(\mathbb{X})\,, \tag{A.34}$$

with

$$e_n\left(\mathbb{X}^{-\mathbb{1}}\right) = \sum_{i_1<i_2<\ldots<i_n} \frac{1}{\lambda_{i_1}\lambda_{i_2}\cdots\lambda_{i_n}}\,. \tag{A.35}$$

Thus, a more symmetric way to express the interactions in Eq. (2.60) is found to be [54]

$$R_{\mu\nu} - \frac{1}{2}g_{\mu\nu}R + m^2\sin^2(\theta)\sum_{n=0}^{3}\beta_n V^{(n)}(\mathbb{X})_{\mu\nu} = \frac{1}{M_g^2}T_{\mu\nu}\,, \tag{A.36a}$$

$$\tilde{R}_{\mu\nu} - \frac{1}{2}\tilde{g}_{\mu\nu}\tilde{R} + m^2\cos^2(\theta)\sum_{n=0}^{3}\beta_{4-n} V^{(n)}\left(\mathbb{X}^{-1}\right)_{\mu\nu} = 0\,, \tag{A.36b}$$

and we merely have to prepend a minus sign, and take into account a global factor y^{-4} relative to Eqs. (A.33). Omitting the CC, we end up with the following linearised set of equations:

$$\mathcal{E}^{\alpha\beta}_{\mu\nu}h_{\alpha\beta} + \frac{m_g^2}{2}\,a^2\sin(\theta)\left[\sin(\theta)\,(h_{\mu\nu} - h\,\eta_{\mu\nu}) - \cos(\theta)\,(\tilde{h}_{\mu\nu} - \tilde{h}\,\eta_{\mu\nu})\right] = \frac{\delta T_{\mu\nu}}{M_g}\,, \tag{A.37a}$$

$$\mathcal{E}^{\alpha\beta}_{\mu\nu}\tilde{h}_{\alpha\beta} + \frac{m_g^2}{2}\,a^2 y^{-2}\cos(\theta)\left[\cos(\theta)\,(\tilde{h}_{\mu\nu} - \tilde{h}\,\eta_{\mu\nu}) - \sin(\theta)\,(h_{\mu\nu} - h\,\eta_{\mu\nu})\right] = 0\,, \tag{A.37b}$$

where

$$m_g^2 \equiv m^2(\beta_1\, y + 2\beta_2\, y^2 + \beta_3\, y^3)\,, \tag{A.38}$$

in agreement with Refs. [54, 171, 202]. Further, we remark that we work with canonically normalised fields. These equations can be diagonalised by means of an modified rotation,

$$\begin{pmatrix} h \\ \tilde{h} \end{pmatrix} \equiv \begin{pmatrix} \cos(\theta) & -y^2\sin(\theta) \\ \sin(\theta) & \cos(\theta) \end{pmatrix}\begin{pmatrix} h^{(1)} \\ h^{(2)} \end{pmatrix}. \tag{A.39}$$

This is a true rotation only in the case $y = 1$; albeit we can define the inverse transformation as

$$\tilde{U} \equiv \begin{pmatrix} \cos(\theta) & y^2\sin(\theta) \\ -\sin(\theta) & \cos(\theta) \end{pmatrix}, \tag{A.40}$$

such that $U\tilde{U} = \tilde{U}U = \cos^2(\theta) + y^2\sin^2(\theta)$. This achieves precisely the sought after

diagonalisation of the mass terms:

$$\mathcal{E}^{\alpha\beta}_{\mu\nu} h^{(1)}_{\mu\nu} = \frac{\cos(\theta)}{M_g} \delta T_{\mu\nu} \,, \tag{A.41a}$$

$$\mathcal{E}^{\alpha\beta}_{\mu\nu} h^{(2)}_{\mu\nu} + a^2 \, \frac{m_g^2}{2y^2} \left(h^{(2)}_{\mu\nu} - h^{(2)} \, \eta_{\mu\nu} \right) = \frac{\sin(\theta)}{M_g} \delta T_{\mu\nu} \,. \tag{A.41b}$$

This set of equations shows that the theory propagates a massless and a massive spin-2 mode in a FLRW background. Together with our analysis of the BD mode in Sec. 2.2.3, we conclude that the theory is healthy, up to the issues discussed in Chap. 5.

From Ref. [171], we can now infer the equations governing the tensor mode dynamics in vacuum,

$$\Box h^{(1),\mathrm{TT}}_{\mu\nu} + 2 \, \mathcal{H} \, h'^{(1),\mathrm{TT}}_{\mu\nu} = 0 \,, \tag{A.42a}$$

$$\Box h^{(2),\mathrm{TT}}_{\mu\nu} + 2 \, \mathcal{H} \, h'^{(2),\mathrm{TT}}_{\mu\nu} - a^2(\eta) \, \frac{m_g^2}{y^2} \, h^{(2),\mathrm{TT}}_{\mu\nu} = 0 \,. \tag{A.42b}$$

These equations are the starting point for our analysis of GW oscillations in Chapter 3.

Appendix B

Mathematical Appendix

In this appendix we summarise some of the more formal concepts we have made use of during the course of this work, namely the calculus of differential forms, which is introduced in the context of manifolds. Further, we discuss how to draw statistically well-founded conclusions from a set of data points and a mathematical model which is believed to describe the data. Lastly, we illustrate how to select a model, if two alternative hypotheses are considered.

B.1 Differential geometry essentials

GR is just one example of a theory of gravitation formulated in the language of differential geometry. However, as should become clear from this work, it is not the only one. The study of any theory of gravity in terms of geometry requires the concept of a manifold $\mathcal{M}$. In this appendix we set the stage for the discussions of Chapter 2, without attempting to provide a mathematically rigorous introduction. For a detailed treatment we refer the reader to Ref. [106], which we follow closely in this section.

An n-dimensional manifold $\mathcal{M}$ is a set of points that *locally* looks like Euclidean space, while the global structure of the manifold can be very different from $\mathbb{R}^n$. This local equivalence to Euclidean space is established in the following manner. Consider a point p and an open subset $p \in U \subset \mathcal{M}$. If for each $p \in \mathcal{M}$ such a subset in combination with a homeomorphic map $\psi : U \to \psi(U) \subset \mathbb{R}^n$ exists, $\mathcal{M}$ is said to be locally Euclidean. Conventionally, the pairs (U, ψ) are called charts and define coordinates in $\mathbb{R}^n$ by assining to each point $p \in U$ an n-tuple $(x_1, \ldots, x_n)$ in $\mathbb{R}^n$. If the union of the subsets U_i spans $\mathcal{M}$, i.e. $\bigcup_{i \in I} U_i = \mathcal{M}$ where I is a set of indices, the collection of charts establishes an atlas on $\mathcal{M}$. Furthermore, the transition functions $\phi \circ \psi^{-1}$ allow us to change charts/coordinates in the overlapping subsets of $\mathcal{M}$, i.e. (U, ψ) and (V, ϕ) with $U \cap V \neq 0$. If an atlas exists, in which all pairs of overlapping charts define a *differentiable* transition function, $\mathcal{M}$ is called a differentiable manifold. Differentiable manifolds are the foundation of differentiable geometry and thereby GR.

Tangent and cotangent spaces. Consider a curve on a manifold, $\gamma : [0, 1] \to \mathcal{M}$. We can geometrically define a tangent vector to that curve, by taking a derivative w.r.t. to

the quantity that parametrises it, say t. Then, $\gamma(0) = p \in \mathcal{M}$ is a point on the manifold and the tangent vector to γ in p is

$$v \equiv \left.\frac{\mathrm{d}\gamma}{\mathrm{d}t}\right|_{t=0} . \tag{B.1}$$

The tangent space $T_p\mathcal{M}$ is then defined in terms of the equivalence classes of tangent vectors to all curves passing through p, where equivalence is established in $\mathbb{R}^n$ if two curves α and β satisfy $\frac{\mathrm{d}}{\mathrm{d}t}(\psi \circ \alpha)(0) = \frac{\mathrm{d}}{\mathrm{d}t}(\psi \circ \beta)(0)$ for all charts (U, ψ) that contain p. One can show that $T_p\mathcal{M}$ is an n-dimensional vector space. It is customary to identify the vector v with the derivative $\frac{\mathrm{d}}{\mathrm{d}t}$, which establishes the notion of vectors as differential operators. This becomes more transparent when considering differentiable functions f on $\mathcal{M}$, whose directional derivative along γ in p:

$$\nabla_\gamma f(p) = \frac{\mathrm{d}(f \circ \gamma)}{\mathrm{d}t}(0) \equiv v(f)\big|_p . \tag{B.2}$$

This leads to an equivalent definition of the tangent space, proof of which can be found in Ref. [106]. Let us make contact with physics, where it is customary to express such vectors in terms of *generalised* coordinates, e.g. induced by a chart $\psi = (x^1, x^2, \dots x^n)$, as

$$v = \frac{\mathrm{d}}{\mathrm{d}t} = \frac{\mathrm{d}x^\mu}{\mathrm{d}t}\frac{\partial}{\partial x^\mu} . \tag{B.3}$$

This is a generalised coordinate expression in the sense that we display the coordinates, but without having specified them. Thus, for a different coordinate chart, say $\widetilde{\psi} = (\tilde{x}^1, \tilde{x}^2, \dots \tilde{x}^n)$, we have

$$v = \frac{\mathrm{d}}{\mathrm{d}t} = \frac{\mathrm{d}\tilde{x}^\mu}{\mathrm{d}t}\frac{\partial}{\partial \tilde{x}^\mu} = \frac{\mathrm{d}\tilde{x}^\mu}{\mathrm{d}t}\frac{\partial x^\nu}{\partial \tilde{x}^\mu}\frac{\partial}{\partial x^\nu} . \tag{B.4}$$

We read off that, under a change of coordinates, the components of the vector v transform as

$$v^\mu \equiv \frac{\mathrm{d}x^\mu}{\mathrm{d}t} = \tilde{v}^\nu \frac{\partial x^\mu}{\partial \tilde{x}^\nu} , \tag{B.5}$$

which follows from the chain rule and agrees with the notion of a vector transforming *contravariantly*, i.e. with an upper index. In this spirit, we see that a canonical choice for the basis of $T_p\mathcal{M}$ is given by the derivatives w.r.t. to the coordinates themselves, $\{\partial_1, \partial_2, \dots, \partial_n\}$, where $\partial_\mu \equiv \frac{\partial}{\partial x^\mu}$.

Moreover, we will need to introduce the cotangent space $T_p^*\mathcal{M}$, which is the vector space dual to $T_p\mathcal{M}$, i.e. it is the space of maps $w : T_p\mathcal{M} \to \mathbb{R}$. To find a suitable representation for the elements of the cotangent space, note that the differential $\mathrm{d}_p f$ of a function $f : \mathcal{M} \to \mathbb{R}$ is the linear approximation of that function around p, $f(p + v) = f(p) + \mathrm{d}_p f(v) + \dots$. Thus,

$$\mathrm{d}_p f(v) = \frac{\mathrm{d}(f \circ \gamma)}{\mathrm{d}t}(0) \equiv v(f)\big|_p \in \mathbb{R} \quad \text{and} \quad \mathrm{d}f(\partial_\mu) = \frac{\partial f}{\partial x^\mu} \tag{B.6}$$

are the components of $\mathrm{d}_p f$. In coordinate language, we can see that the differentials of

the coordinate functions themselves satisfy

$$\mathrm{d}x^\mu(\partial_\nu) = \frac{\partial x^\mu}{\partial x^\nu} = \delta^\mu_\nu\,, \tag{B.7}$$

such that in generalised coordinate language,

$$w(v) = w_\mu \mathrm{d}x^\mu(v^\nu\partial_\mu) \overset{(B.7)}{=} w_\mu v^\mu\,, \tag{B.8}$$

which is invariant under a change of coordinates, and shows that the components of w transform *covariantly*,

$$w_\mu = \widetilde{w}_\nu \frac{\partial \tilde{x}^\nu}{\partial x^\mu}\,, \tag{B.9}$$

i.e. opposite to vectors. Furthermore, this means that $(\mathrm{d}x^1, \ldots . \mathrm{d}x^n)$ is a basis in $T^*_p\mathcal{M}$:

$$w = w_\mu \mathrm{d}x^\mu\,. \tag{B.10}$$

Finally, if the manifold is endowed with a metric, say a tensor g, one can define a scalar product of vectors v_1, v_2

$$\langle v_1, v_2\rangle \equiv v_1^\mu g_{\mu\nu} v_2^\nu\,, \tag{B.11}$$

which is independent of the choice of coordinates by virtue of the metric transforming as a tensor of rank 2. The scalar product allows one to identify with each vector v, a covector $\hat{v}$ via

$$\hat{v} = \langle v, \cdot\rangle\,. \tag{B.12}$$

Using the definition of the scalar product, we see that this is what is referred to as lowering an index with the metric:

$$v_{1,\,\mu} v_2^\mu = \hat{v}_1(v_2) = \langle v_1, v_2\rangle \overset{(B.11)}{=} v_1^\mu g_{\mu\nu} v_2^\nu\,, \tag{B.13}$$

thus, $\hat{v}_{1,\,\mu} \equiv g_{\mu\nu} v_1^\nu$. The generalisation to higher-rank tensors is straightforward.

Differential Forms. A useful generalisation of covectors are differential forms, which are defined as multilinear maps $\omega : V \times V \times \ldots V \to \mathbb{R}$, with the property that it vanishes if two arguments are linearly dependent. Here, V is a vector space (identified with a tangent space for our purposes) and there are r factors of it. Form this property, it follows that ω is odd under the exchange of arguments, i.e.

$$\begin{aligned} 0 =& \omega(v_1, v_2, \ldots, v_i + v_j, \ldots, v_i + v_j, \ldots, v_r) \\ =& \omega(v_1, v_2, \ldots, v_i, \ldots, v_j, \ldots, v_r) + \omega(v_1, v_2, \ldots, v_j, \ldots, v_i, \ldots, v_r)\,. \end{aligned} \tag{B.14}$$

Thus, $\omega(v_{\sigma(1)}, \ldots, v_{\sigma(r)}) = \mathrm{sgn}(\sigma)\omega(v_1, \ldots, v_r)$ for any permutation σ. The components of ω in a specified coordinate system are found by application to the basis vectors,

$$\begin{aligned} \omega(v_1, \ldots, v_r) &= \omega(v_1^{\mu_1}\partial_{\mu_1}, \ldots, v_r^{\mu_N}\partial_{\mu_r}) = v_1^{\mu_1} \cdots v_r^{\mu_N} \omega(\partial_{\mu_1}, \ldots, \partial_{\mu_r}) \\ &\equiv \omega_{\mu_1 \ldots \mu_r} v_1^{\mu_1} \cdots v_r^{\mu_r}\,, \end{aligned} \tag{B.15}$$

where the linearity was used in the second equality. A convenient way of expressing these alternating forms is to construct an antisymmetric product of an r form ω_r with an s form ω_s, in such a way as to yield an $(r+s)$ form by construction:

$$(\omega_r \wedge \omega_s)(v_1, \dots v_{r+s}) \equiv \frac{1}{r!s!} \sum_\sigma \mathrm{sgn}(\sigma)\, \omega_r(v_{\sigma(1)} \dots v_{\sigma(r)})\, \omega_s(v_{\sigma(r+1)} \dots v_{\sigma(r+s)})\,. \quad \text{(B.16)}$$

This has precisely the required attributes, most importantly antisymmetry and linearity. Noticing that this implies

$$\mathrm{d}x^1 \wedge \mathrm{d}x^2 \wedge \dots \wedge \mathrm{d}x^r(\partial_1, \partial_2, \dots, \partial_r) = 1\,, \quad \text{(B.17)}$$

we can write any r form as

$$\omega = \sum_{\mu_1<\mu_2<\dots<\mu_r} \omega_{\mu_1\mu_2\dots\mu_r} \mathrm{d}x^{\mu_1} \wedge \mathrm{d}x^{\mu_2} \dots \wedge \mathrm{d}x^{\mu_r}\,. \quad \text{(B.18)}$$

Next, we define the *exterior derivative* which is a map that increases the rank of a differential form, $\mathrm{d} : \omega \mapsto \mathrm{d}\omega$, where ω is an r form, $\mathrm{d}\omega$ an $(r+1)$ form, and which for a function f reduces to a simple differential:

$$\mathrm{d}f = (\partial_\mu f)\mathrm{d}x^\mu\,. \quad \text{(B.19)}$$

This is straightforwardly generalised to r-forms, e.g. Eq. (B.18):

$$\mathrm{d}\omega = \mathrm{d}\left(\sum_{\mu_1<\dots<\mu_r} \omega_{\mu_1\dots\mu_r}\mathrm{d}x^{\mu_1} \wedge \dots \wedge \mathrm{d}x^{\mu_r}\right) \equiv \sum_{\nu<\mu_1<\dots<\mu_r} \frac{\partial\omega_{\mu_1\dots\mu_r}}{\partial x^\nu}\, \mathrm{d}x^\nu \wedge \mathrm{d}x^{\mu_1} \wedge \dots \wedge \mathrm{d}x^{\mu_r}\,. \quad \text{(B.20)}$$

Integration of differential forms. In defining the integral of a differential form, one is challenged to reduce it to an integral in $\mathbb{R}^n$. However, one needs to ensure that the result is unique and independent of the choice of coordinates.

On a manifold of dimension n, an n form has only one independent component, due to the antisymmetry requirement, $\omega = \frac{1}{n!}\omega_{\mu_1\dots\mu_n}\mathrm{d}x^{\mu_1} \wedge \dots \wedge \mathrm{d}x^{\mu_n} = \omega_{1\dots n}\mathrm{d}x^1 \wedge \dots \wedge \mathrm{d}x^n$. We define its volume integral as

$$\int_{\mathcal{U}} \omega = \sum_i \int_{A_i} \omega_{1\dots n}(x)\mathrm{d}x^1 \wedge \dots \wedge \mathrm{d}x^n \equiv \sum_i \int_{\psi_i(A_i)} \mathrm{d}^n x\, \omega_{1\dots n}(x)\,, \quad \text{(B.21)}$$

where $\mathcal{U} = \bigcup_i A_i$ is a decomposition of the region to be integrated over with disjoint subsets A_i, which in turn are constructed from charts (U_i, ψ_i). Ref. [106] gives the following prescription for such a decomposition:

$$A_1 = U_1, \quad \text{and} \quad A_{i+1} = U_{i+1} \setminus \bigcup_{k=1}^{i} A_k\,, \quad \text{for } i \in I \text{ in some index set.} \quad \text{(B.22)}$$

Thus, the integration is reduced to the integral of the component function in $\mathbb{R}^n$.

B.2 Statistical analysis method

In this work, we will frequently make use of parameter scans in order to assess certain parameter choices given the experimental data. In order to draw quantitative conclusions and enable the reader to reproduce the results in this work, we now outline our approach in some detail, following Ref. [338] unless indicated otherwise.

In order to find the best fit for a given model with a number of parameters Θ to the measured data $\vec{x}$, we aim at maximising the probability to find the parameters Θ, given the measured outcome $\vec{x}$. By virtue of Bayes' theorem, this equals

$$P(\Theta|\vec{x}) = \frac{\mathcal{L}(\vec{x}|\Theta)P(\Theta)}{P(\vec{x})}\,. \tag{B.23}$$

Thus, we need to find the maximum w.r.t. Θ of the product of the so-called likelihood function $\mathcal{L}(\vec{x}|\Theta)$ and $P(\Theta)$. Notice that since $P(\vec{x})$ is independent of Θ, it can be disregarded. In the above expression, $P(\Theta)$ is often called the prior distribution since it parametrises the prior knowledge of how probable a given parameter choice is. It is then customary to call $P(\Theta|\vec{x})$ the posterior probability distribution. In this work, we will take only 'flat priors', i.e. disregard any bias for certain parameter choices.

Let us be more specific and consider the relevant cases where the data will consist of pairs (x_i, y_i) $(0 \leq i \leq N)$, for known x_i and the y_i are the result of a measurement with error σ_i. Furthermore, we know that the y_i follow some mathematical model, say $y_i = f(x_i, \Theta_0)$. This model will be given in terms of parameters Θ_j $(0 \leq j \leq M)$, whose *correct* values are given by $\Theta = \Theta_0$, but which are unknown. The likelihood function represents the probability of a certain outcome $(\vec{x}, \vec{y})$ in a model parametrised by Θ, and which asymptotically (i.e. when the sample size $N \to \infty$) will approach a normal distribution if the measurements are independent and uncorrelated. Here, we will make the assumption that the data are independent and follow a normal distribution, even for smaller sample sizes. We then find that maximising

$$\mathcal{L}(\vec{y}|\Theta) \propto \exp\left(-\sum_{i=1}^{N} \frac{[y_i - f(x_i, \Theta)]^2}{2\sigma_i^2}\right)\,, \tag{B.24}$$

is equivalent to finding the minimum w.r.t. Θ of the function

$$\chi^2(\vec{y}, \Theta) = -2\log\mathcal{L} = \sum_{i=1}^{N} \frac{[y_i - f(x_i, \Theta)]^2}{\sigma_i^2}\,. \tag{B.25}$$

For given Θ, the values χ^2 can be shown to follow a χ^2 distribution. Thus, we have achieved two important things. Firstly, we have justified the application of a least squares method under the specified assumptions; and secondly, having done so in the language of probability (densities), we may now compute confidence regions. We do so by calculating the probability for the outcome to be χ^2 or worse, and demand it not to exceed a predefined threshold, or p-value. We can then draw confidence regions in parameter space

as regions of constant χ^2 satisfying [242]

$$F_\nu(\chi^2) \stackrel{!}{=} 1 - p = \mathrm{Erf}(n/\sqrt{2})\,. \tag{B.26}$$

Here, F_ν is the cumulative χ^2 distribution for ν DOF, Erf is the cumulative normal distribution, or error function, and n determines the C.L. in Gaussian standard deviations. For the present analyses, we will adapt that $\nu = \dim(\vec{x}) - \dim(\Theta) = N - M$ [338]. As an example for $\nu = 1$, we obtain the $n = 2\sigma$ confidence intervals (95% C.L.) as the contours where $\chi^2 = 3.84$, or $p = 0.05$.

Moreover, we usually test a given alternative model (e.g. bigravity parametrised by n parameters, say, Θ_1) against the null hypothesis (e.g. GR with m parameters Θ_0). Therefore, we can make use of Wilks' theorem [339], which states that for a test statistics comparing the log-likelihood ratio of the two alternative hypotheses,

$$\Lambda = -2\log\left(\frac{\mathcal{L}(\vec{x}|\Theta_1)}{\mathcal{L}(\vec{x}|\Theta_0)}\right) \simeq \chi_0^2 - \chi^2\,, \tag{B.27}$$

approaches a χ^2 statistics when the sample size goes to infinity. In practice this means that we can apply Eq. (B.26), however, replacing $\chi^2 \to \Lambda$ and using $\nu = |m - n|$ DOF, in order to assess whether we should keep or reject the null hypothesis, given a predefined significance, or C.L.

Appendix C

Circular Velocity and LSB Rotation Curves in Bigravity

Here, we present the expressions for the circular velocities, calculated in the bigravity framework, which we have used in Sec. 4.3 to fit the rotations curves of the ESO138-G014 galaxy. Moreover, the fits to another set of LSB galaxies will be presented below.

C.1 Circular velocities

Our starting point is the expression for the gravitational potential in terms of a matter distribution $\rho(\vec{r})$, together with the relation $v(r) = \sqrt{r\frac{\mathrm{d}\Phi}{\mathrm{d}r}}$. In Chapter 4, we had found for the potential

$$\Phi(\vec{r}) = G_{\mathrm{N}} \int \mathrm{d}^3\vec{r}\,'\ \rho(\vec{r}\,') \left[\frac{\alpha(\theta)}{|\vec{r}-\vec{r}\,'|} + \frac{\beta(\theta) e^{-m_g|\vec{r}-\vec{r}\,'|}}{|\vec{r}-\vec{r}\,'|} \right]. \tag{C.1}$$

Due to the linearity of Poisson's equation (4.1) and (4.5), we can calculate $v^2(r)$ for each component separately, and add up the individual components. For the gas component, we find

$$v^2_{\mathrm{gas}}(r) = G_N \left[\alpha(\theta) \frac{M_{\mathrm{gas}}(r, r_0, m_0)}{r} + \beta(\theta) \frac{m_0}{2} \frac{(e^{-m_g\, r}\,(1 + m_g\, r) - e^{-r/r_0}\,(r + r_0)/r_0)}{1 - m_g^2 r_0^2} \right], \tag{C.2}$$

where we assumed the mass density given in Eq. (4.38), relating the mass to the brightness via the mass to light ratio $L = m_0/\Sigma_0$.

For the visible disk, we have chosen two distinct approaches, finding that choosing one over the other has no significant influence on the outcome of the parameter scan which enters the analysis underlying Fig. 5.1.

The axisymmetric mass density which leads to Eq. (4.39) is $\rho(r, \phi, z) = \delta(z)\frac{M_D^0}{2\pi r_0^2} e^{-r/r0}$, cf. Ref. [275]. Unfortunately, upon insertion into Eq. (C.1), this integral cannot be evaluated analytically, forcing us to resort to numerical methods. Instead we have chosen to

accept the small error that results from choosing

$$v^2_{\rm disk}(r) = \frac{M_{\rm disk}(r)}{r}\left[\alpha(\theta) + \beta(\theta)\,(1+m_g\,r)e^{-m_g\,r}\right]. \tag{C.3}$$

On the other hand, assuming that the visible disk has a *spherically symmetric* density allows us to find an analytical expression for $v^2_{\rm disk}(r)$. Using a density inspired by the Burkert halo model, $\rho(r) = M^0_D/(r+r_0)/(r^2+r_0^2)$ [340], we find

$$\begin{aligned}
v^2_{\rm disk}(r) = G_N\Bigg\{&\alpha(\theta)\frac{M_{\rm disk}(r,r_0,M^0_D)}{r} + \beta(\theta)\frac{M^0_D}{2}\Bigg[\frac{1+m_g\,r}{x_0\,r}e^{-m_g\,r}\Bigg(-\frac{e^{-x_0}}{2}{\rm Ei}(m_g\,(r+r_0))\\
&+\cos(x_0)\,{\rm Si}(x_0) - \sin(x_0)\,{\rm Ci}(x_0) + \cosh(x_0)\,{\rm Shi}(x_0) - \sinh(x_0)\,{\rm Chi}(x_0) - \frac{\pi}{2}\sin(x_0)\\
&+\cos(x_0)\,{\rm Re}\left\{\frac{e^{i\frac{\pi}{4}}}{\sqrt{2}}\,{\rm Ei}(m_g\,(r+ir_0))\right\} + \sin(x_0)\,{\rm Re}\left\{\frac{e^{i\frac{\pi}{4}}}{\sqrt{2}}\,{\rm Ei}(m_g\,(r-ir_0))\right\}\Bigg)\\
&+\frac{1-m_g\,r}{2\,x_0\,r}e^{m_g\,r}\Bigg(\pi[\cos(x_0)+\sin(x_0)] - {\rm Re}\left\{\frac{e^{i\frac{\pi}{4}}}{\sqrt{2}}\,{\rm Ei}(-m_g\,(r+ir_0))\right\}\\
&+\ \sin(x_0)\,{\rm Re}\left\{\frac{e^{i\frac{\pi}{4}}}{\sqrt{2}}\,{\rm Ei}(-m_g\,(r-ir_0))\right\} + e^{x_0}\,{\rm Ei}(-m_g\,(r+r_0))\Bigg)\Bigg]\Bigg\},
\end{aligned} \tag{C.4}$$

where we have used the short-hand notation $x_0 \equiv m_g\,r_0$, and the exponential integral function is defined as

$${\rm Ei}(x) = -\int_{-x}^{\infty}{\rm d}t\,\frac{e^{-t}}{t}\,, \tag{C.5a}$$

and

$${\rm Ci}(x) = \frac{1}{2}({\rm Ei}(ix)+{\rm Ei}(-ix))\,, \qquad {\rm Si}(x) = \frac{1}{2i}({\rm Ei}(ix)-{\rm Ei}(-ix))\,, \tag{C.5b}$$

$${\rm Chi}(x) = \frac{1}{2}({\rm Ei}(x)+{\rm Ei}(-x))\,, \qquad {\rm Shi}(x) = \frac{1}{2}({\rm Ei}(x)-{\rm Ei}(-x))\,. \tag{C.5c}$$

For the DM component, we use the NFW halo model, $\rho_{\rm NFW} = M^0_{\rm DM}/r/(r+r_h)^2$ [244],

$$\begin{aligned}
v^2_{\rm DM}(r) = \frac{G_N}{r}\Bigg\{&\alpha(\theta)M_{\rm DM}(r,r_h,M^0_{\rm DM}) + \beta(\theta)\frac{M^0_{\rm DM}}{2}\Bigg[\frac{2/r}{r+r_h} - (1-m_g\,r)\,e^{m_g\,(r+r_h)}\times\\
&\times{\rm Ei}(-m_g(r+r_h)) + (1+m_g\,r)\big(e^{-m_g\,(r-r_h)}\,{\rm Ei}(-m_g r_h) + e^{-m_g\,(r+r_h)}\times\\
&\times[{\rm Ei}(m_g\,r_h) - {\rm Ei}(m_g\,(r+r_h))]\,\big)\Bigg]\Bigg\},
\end{aligned} \tag{C.6}$$

which is consistent with results in the literature [259].

C.2 Low surface brightness galaxy rotation curve fits

The summary plot Fig. 5.1 contains, besides the exclusion region derived from the ESO138-G014 galaxy, contours that were obtained from more rotation curve data.

One of these data sets includes 17 LSB galaxies presented in Ref. [341]. We focus on this particular type of galaxy, as it is known to have a dominant DM component, cf. Ref. [273], and therefore we expect the largest discrepancies with the GR-only predictions. However, for most of these galaxies no independent measurements of the HI emission are available, and hence we have to perform a combined fit to the data.

For galaxies found in the data sample of Ref. [341], we perform the fits to the rotation curves shown in Fig. C.1, which represent the best fitting parameter point when the data for all galaxies are combined. For the galaxies UGC 4325, NGC 4395, and UGC 1551 changes at the Vainshtein radius are clearly visible, and indeed we find that the fits have improved compared to the GR-only hypothesis. Nevertheless, we find that the combination of all 17 galaxies results in a χ^2 which is only marginally smaller than the χ^2_0 obtained in GR.

Continuing with the data sample of Ref. [273], where another 26 'high-resolution' [342] LSB galaxies are taken from, we obtain Figs. C.2 and C.3. There, we also show the best fit and highlight that in the galaxies F579-V1, F730-V1, U6614, and U11648 the effects due to the present modifications are clearly visible at small radii. Simultaneously, we find that the fits do improve; however by no means with a statistical significance large enough to draw any final conclusions.

In summary, the fits do improve somewhat but not enough to conclude that the null-hypothesis GR should be rejected. At the same time, it is interesting to observe that certain features in the data can be better described due to the transition at the Vainshtein radius. This should be understood as a motivation to study this phenomenon in more detail and with more refined methods.

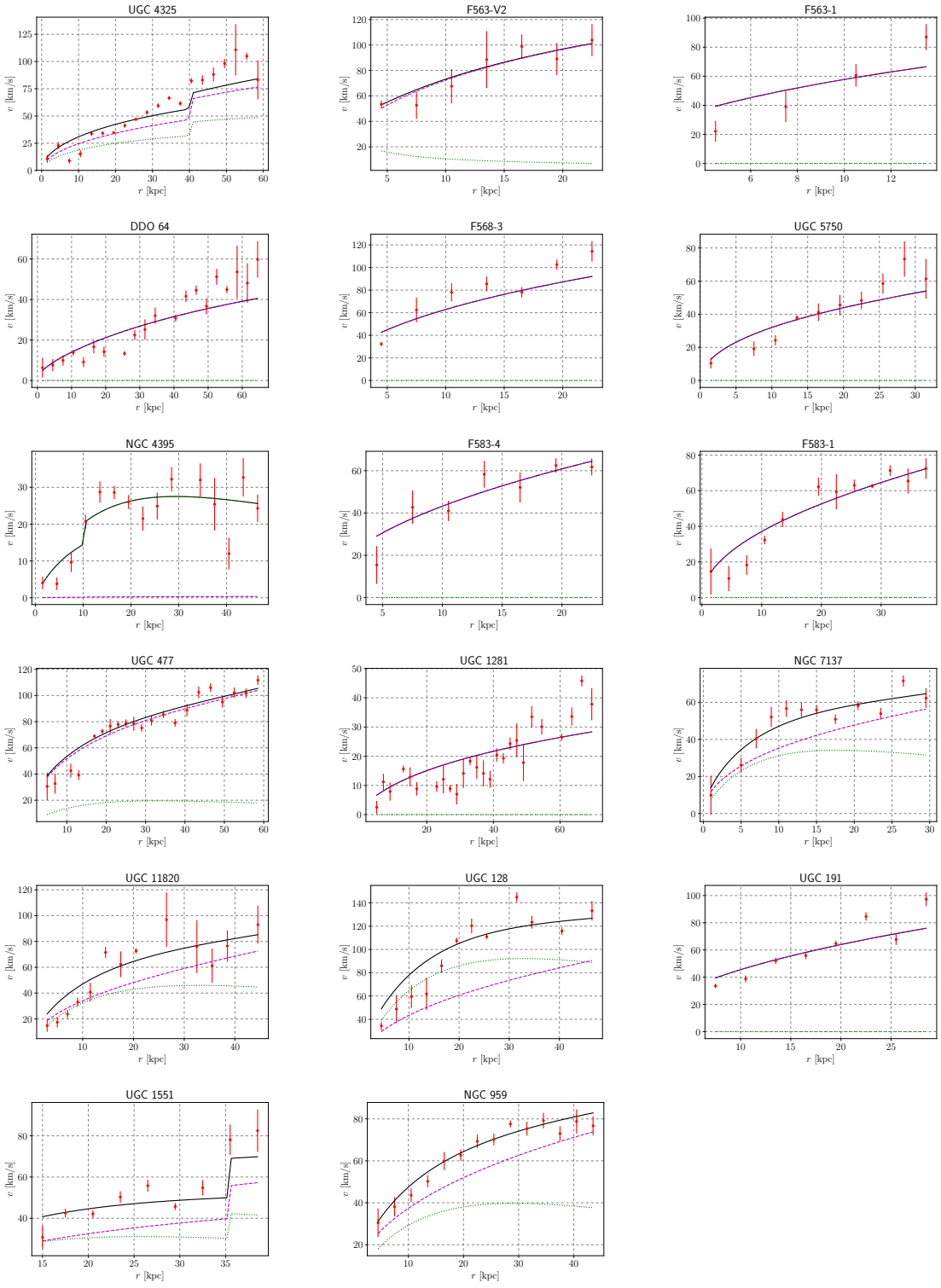

Figure C.1.: Fits to the LSB rotation curves of Ref. [341] at the best fitting parameter point $(m_g, \theta) = (4.0 \cdot 10^{-31}\,\mathrm{eV}, 1.42)$. The colours indicate combined disk & gas (dotted green), DM (dashed magenta), and total (solid black) components. Notice that most galaxies are DM dominated, as expected. We conclude that the fits slightly improve compared to GR, $\Delta\chi^2 = 1.5$.

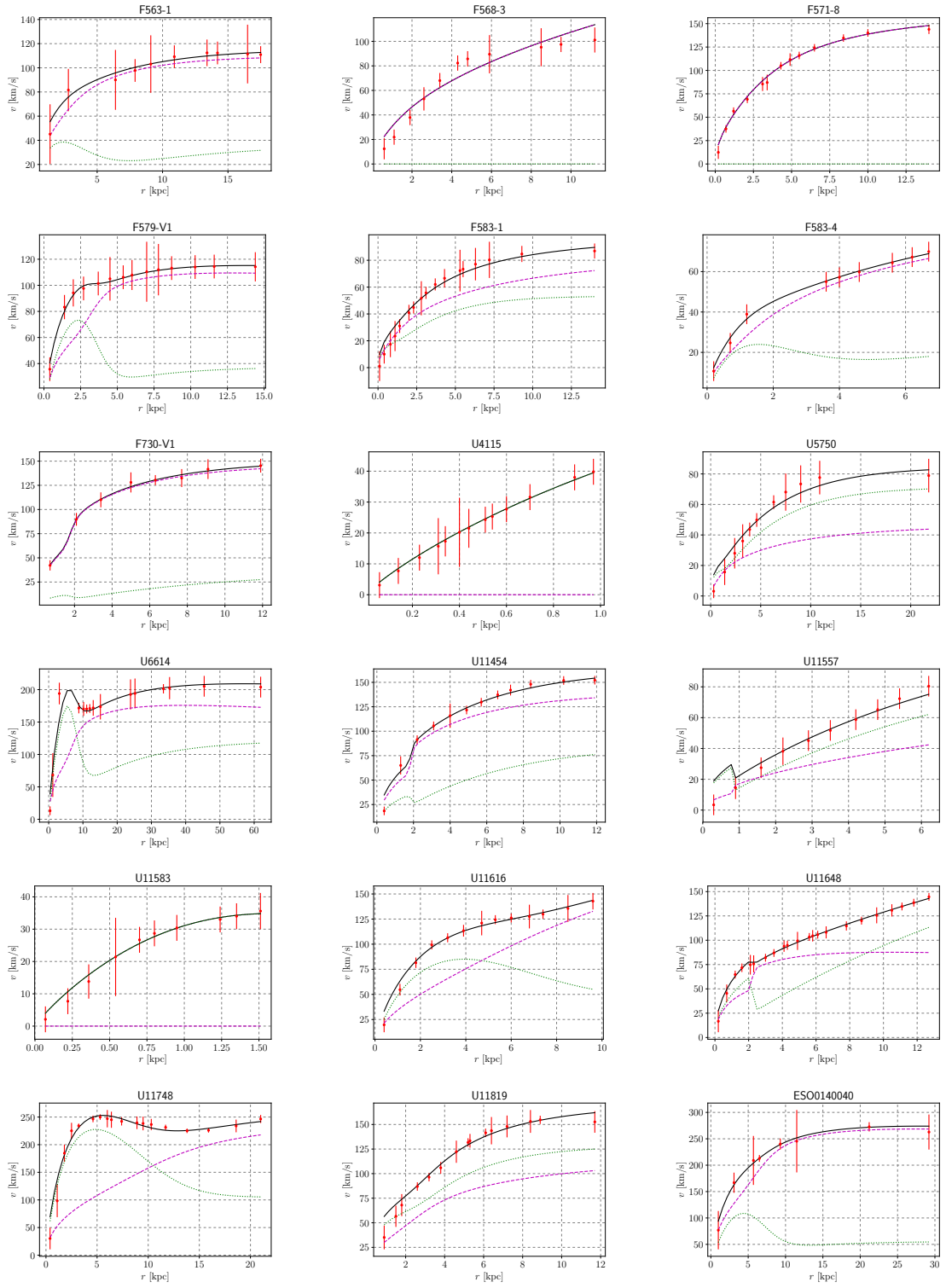

Figure C.2.: High resolution LSB rotation curves from Refs. [273, 342]. These are shown at the best-fitting parameter point $(m_g, \theta) = (8.7 \cdot 10^{-30}\,\text{eV}, 1.47)$. Continued in Fig. C.3.

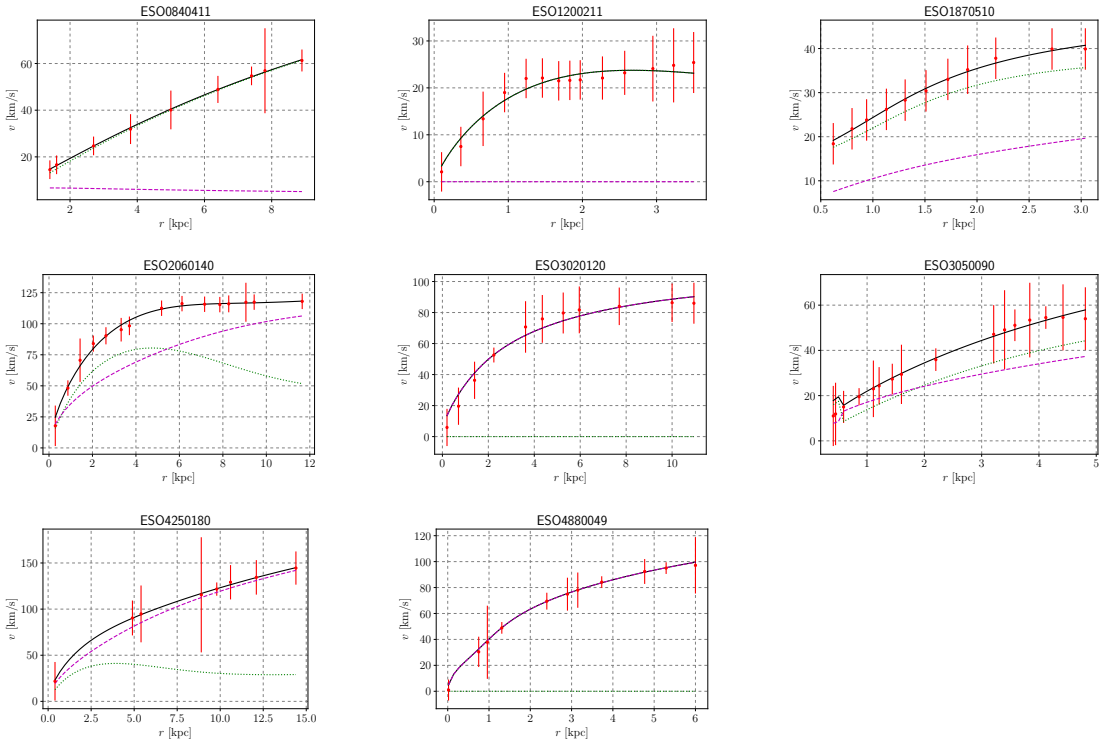

Figure C.3.: High-resolution LSB rotation curves from Refs. [273, 342] continued. We find that the fits slightly improve, but at $\Delta\chi^2 = 1.44$ ($< 1\sigma$) it is not justified to reject the GR hypothesis.

Disclaimer

The results presented in this thesis represent original scientific work conducted by the author in collaboration with others. Whenever results presented here have previously been published, we indicate so at the beginning of the respective Chapter. To summarise,

- parts of Chapter 2 (namely Sec. 2.3.1) and the Appendix A.2 are based on Ref. [1],
- the cosmological solution presented in Sec. 2.3.2 was studied in Ref. [2],
- Chapter 3 is based on results published in Refs. [2, 3],
- and the results of Chapter 4 are adapted from Ref. [4].

Refs. [1–3] have been published in peer-reviewed journals, while Ref. [4] is, as of submission of this thesis, in the peer review process.

Moreover, Refs. [5–8] were published during the author's PhD studies. However, given their rather wide spread in regards to content, they are not included in this thesis.

[1] M. Platscher and J. Smirnov, *Degravitation of the Cosmological Constant in Bigravity*, JCAP **1703** no. 03, (2017) 051, `arXiv:1611.09385 [gr-qc]`.

[2] K. Max, M. Platscher, and J. Smirnov, *Gravitational Wave Oscillations in Bigravity*, Phys. Rev. Lett. **119** no. 11, (2017) 111101, `arXiv:1703.07785 [gr-qc]`.

[3] K. Max, M. Platscher, and J. Smirnov, *Decoherence of Gravitational Wave Oscillations in Bigravity*, Phys. Rev. **D97** no. 6, (2018) 064009, `arXiv:1712.06601 [gr-qc]`.

[4] M. Platscher, J. Smirnov, S. Meyer, and M. Bartelmann, *Long Range Effects in Gravity Theories with Vainshtein Screening*, submitted to JCAP (2018) , `arXiv:1809.05318 [astro-ph.CO]`.

[5] A. Merle, M. Platscher, N. Rojas, J. W. F. Valle, and A. Vicente, *Consistency of WIMP Dark Matter as radiative neutrino mass messenger*, JHEP **07** (2016) 013, arXiv:1603.05685 [hep-ph].

[6] M. Lindner, M. Platscher, C. E. Yaguna, and A. Merle, *Fermionic WIMPs and vacuum stability in the scotogenic model*, Phys. Rev. **D94** no. 11, (2016) 115027, arXiv:1608.00577 [hep-ph].

[7] M. Lindner, M. Platscher, and F. S. Queiroz, *A Call for New Physics : The Muon Anomalous Magnetic Moment and Lepton Flavor Violation*, Phys. Rept. **731** (2018) 1–82, arXiv:1610.06587 [hep-ph].

[8] T. Hugle, M. Platscher, and K. Schmitz, *Low-Scale Leptogenesis in the Scotogenic Neutrino Mass Model*, Phys. Rev. **D98** no. 2, (2018) 023020, arXiv:1804.09660 [hep-ph].

Bibliography

[9] Johann Wolfgang von Goethe and John Wynniatt Grant (translation), *Faust: A Dramatic Poem*. English and American drama of the nineteenth century: English. Hamilton, Adams, and Company, 1867. https://books.google.de/books?id=iFkH5A1ScGoC.

[10] "Johann Georg Faust – Wikipedia.". https://de.wikipedia.org/wiki/Johann_Georg_Faust, accessed on 14/10/2018.

[11] "Galileo Galilei – Wikipedia.". https://de.wikipedia.org/wiki/Galileo_Galilei, accessed on 14/10/2018.

[12] **Planck** Collaboration, N. Aghanim *et al.*, *Planck 2018 results. VI. Cosmological parameters*, arXiv:1807.06209 [astro-ph.CO].

[13] S. L. Glashow, *Partial Symmetries of Weak Interactions*, Nucl. Phys. **22** (1961) 579–588.

[14] S. Weinberg, *A Model of Leptons*, Phys. Rev. Lett. **19** (1967) 1264–1266.

[15] A. Salam, *Weak and Electromagnetic Interactions*, Conf. Proc. **C680519** (1968) 367–377.

[16] **ATLAS** Collaboration, G. Aad *et al.*, *Observation of a new particle in the search for the Standard Model Higgs boson with the ATLAS detector at the LHC*, Phys. Lett. **B716** (2012) 1–29, arXiv:1207.7214 [hep-ex].

[17] **CMS** Collaboration, S. Chatrchyan *et al.*, *Observation of a new boson at a mass of 125 GeV with the CMS experiment at the LHC*, Phys. Lett. **B716** (2012) 30–61, arXiv:1207.7235 [hep-ex].

[18] **COBE** Collaboration, G. F. Smoot *et al.*, *Structure in the COBE differential microwave radiometer first year maps*, Astrophys. J. **396** (1992) L1–L5.

[19] **Supernova Search Team** Collaboration, A. G. Riess *et al.*, *Observational evidence from supernovae for an accelerating universe and a cosmological constant*, Astron. J. **116** (1998) 1009–1038, arXiv:astro-ph/9805201 [astro-ph].

[20] **Supernova Cosmology Project** Collaboration, S. Perlmutter *et al.*, *Measurements of Omega and Lambda from 42 high redshift supernovae*, Astrophys. J. **517** (1999) 565–586, arXiv:astro-ph/9812133 [astro-ph].

[21] F. Zwicky, *Die Rotverschiebung von extragalaktischen Nebeln*, Helv. Phys. Acta **6** (1933) 110–127. [Gen. Rel. Grav.41,207(2009)].

[22] V. C. Rubin and W. K. Ford, Jr., *Rotation of the Andromeda Nebula from a Spectroscopic Survey of Emission Regions*, Astrophys. J. **159** (1970) 379–403.

[23] V. A. Kuzmin, V. A. Rubakov, and M. E. Shaposhnikov, *On the Anomalous Electroweak Baryon Number Nonconservation in the Early Universe*, Phys. Lett. **155B** (1985) 36.

[24] A. D. Sakharov, *Violation of CP Invariance, C asymmetry, and baryon asymmetry of the universe*, Pisma Zh. Eksp. Teor. Fiz. **5** (1967) 32–35. [Usp. Fiz. Nauk161,no.5,61(1991)].

[25] M. Fierz and W. Pauli, *On relativistic wave equations for particles of arbitrary spin in an electromagnetic field*, Proc. Roy. Soc. Lond. **A173** (1939) 211–232.

[26] M. Fierz, *Force-free particles with any spin*, Helv. Phys. Acta **12** (1939) 3–37.

[27] H. van Dam and M. J. G. Veltman, *Massive and massless Yang-Mills and gravitational fields*, Nucl. Phys. **B22** (1970) 397–411.

[28] V. I. Zakharov, *Linearized gravitation theory and the graviton mass*, JETP Lett. **12** (1970) 312. [Pisma Zh. Eksp. Teor. Fiz.12,447(1970)].

[29] D. G. Boulware and S. Deser, *Inconsistency of finite range gravitation*, Phys. Lett. **40B** (1972) 227–229.

[30] D. G. Boulware and S. Deser, *Can gravitation have a finite range?*, Phys. Rev. **D6** (1972) 3368–3382.

[31] L. Randall and R. Sundrum, *A Large mass hierarchy from a small extra dimension*, Phys. Rev. Lett. **83** (1999) 3370–3373, `arXiv:hep-ph/9905221 [hep-ph]`.

[32] L. Randall and R. Sundrum, *An Alternative to compactification*, Phys. Rev. Lett. **83** (1999) 4690–4693, `arXiv:hep-th/9906064 [hep-th]`.

[33] G. R. Dvali and G. Gabadadze, *Gravity on a brane in infinite volume extra space*, Phys. Rev. **D63** (2001) 065007, `arXiv:hep-th/0008054 [hep-th]`.

[34] G. R. Dvali, G. Gabadadze, and M. Porrati, *4-D gravity on a brane in 5-D Minkowski space*, Phys. Lett. **B485** (2000) 208–214, `arXiv:hep-th/0005016 [hep-th]`.

[35] G. R. Dvali, G. Gabadadze, and M. Porrati, *Metastable gravitons and infinite volume extra dimensions*, Phys. Lett. **B484** (2000) 112–118, `arXiv:hep-th/0002190 [hep-th]`.

[36] C. de Rham and G. Gabadadze, *Generalization of the Fierz-Pauli Action*, Phys. Rev. **D82** (2010) 044020, `arXiv:1007.0443 [hep-th]`.

[37] C. de Rham, G. Gabadadze, and A. J. Tolley, *Resummation of Massive Gravity*, Phys. Rev. Lett. **106** (2011) 231101, arXiv:1011.1232 [hep-th].

[38] C. de Rham, G. Gabadadze, and A. J. Tolley, *Ghost free Massive Gravity in the Stückelberg language*, Phys. Lett. **B711** (2012) 190–195, arXiv:1107.3820 [hep-th].

[39] S. F. Hassan and R. A. Rosen, *Resolving the Ghost Problem in non-Linear Massive Gravity*, Phys. Rev. Lett. **108** (2012) 041101, arXiv:1106.3344 [hep-th].

[40] S. F. Hassan and R. A. Rosen, *On Non-Linear Actions for Massive Gravity*, JHEP **07** (2011) 009, arXiv:1103.6055 [hep-th].

[41] S. F. Hassan, R. A. Rosen, and A. Schmidt-May, *Ghost-free Massive Gravity with a General Reference Metric*, JHEP **02** (2012) 026, arXiv:1109.3230 [hep-th].

[42] M. Mirbabayi, *A Proof Of Ghost Freedom In de Rham-Gabadadze-Tolley Massive Gravity*, Phys. Rev. **D86** (2012) 084006, arXiv:1112.1435 [hep-th].

[43] D. Comelli, M. Crisostomi, F. Nesti, and L. Pilo, *Degrees of Freedom in Massive Gravity*, Phys. Rev. **D86** (2012) 101502, arXiv:1204.1027 [hep-th].

[44] C. Deffayet, J. Mourad, and G. Zahariade, *Covariant constraints in ghost free massive gravity*, JCAP **1301** (2013) 032, arXiv:1207.6338 [hep-th].

[45] C. Deffayet, J. Mourad, and G. Zahariade, *A note on 'symmetric' vielbeins in bimetric, massive, perturbative and non perturbative gravities*, JHEP **03** (2013) 086, arXiv:1208.4493 [gr-qc].

[46] D. Lovelock, *The Einstein tensor and its generalizations*, J. Math. Phys. **12** (1971) 498–501.

[47] T. Clifton, P. G. Ferreira, A. Padilla, and C. Skordis, *Modified Gravity and Cosmology*, Phys. Rept. **513** (2012) 1–189, arXiv:1106.2476 [astro-ph.CO].

[48] S. F. Hassan and R. A. Rosen, *Bimetric Gravity from Ghost-free Massive Gravity*, JHEP **02** (2012) 126, arXiv:1109.3515 [hep-th].

[49] S. F. Hassan and R. A. Rosen, *Confirmation of the Secondary Constraint and Absence of Ghost in Massive Gravity and Bimetric Gravity*, JHEP **04** (2012) 123, arXiv:1111.2070 [hep-th].

[50] K. Hinterbichler and R. A. Rosen, *Interacting Spin-2 Fields*, JHEP **07** (2012) 047, arXiv:1203.5783 [hep-th].

[51] C. J. Isham, A. Salam, and J. A. Strathdee, *F-dominance of gravity*, Phys. Rev. **D3** (1971) 867–873.

[52] K. Hinterbichler, *Theoretical Aspects of Massive Gravity*, Rev. Mod. Phys. **84** (2012) 671–710, arXiv:1105.3735 [hep-th].

[53] C. de Rham, *Massive Gravity*, Living Rev. Rel. **17** (2014) 7, arXiv:1401.4173 [hep-th].

[54] A. Schmidt-May and M. von Strauss, *Recent developments in bimetric theory*, J. Phys. **A49** no. 18, (2016) 183001, arXiv:1512.00021 [hep-th].

[55] L. Heisenberg, *A systematic approach to generalisations of General Relativity and their cosmological implications*, arXiv:1807.01725 [gr-qc].

[56] **Virgo, LIGO Scientific** Collaboration, B. P. Abbott *et al.*, *Observation of Gravitational Waves from a Binary Black Hole Merger*, Phys. Rev. Lett. **116** no. 6, (2016) 061102, arXiv:1602.03837 [gr-qc].

[57] **Virgo, LIGO Scientific** Collaboration, B. P. Abbott *et al.*, *GW151226: Observation of Gravitational Waves from a 22-Solar-Mass Binary Black Hole Coalescence*, Phys. Rev. Lett. **116** no. 24, (2016) 241103, arXiv:1606.04855 [gr-qc].

[58] **Virgo, LIGO Scientific** Collaboration, B. P. Abbott *et al.*, *GW170104: Observation of a 50-Solar-Mass Binary Black Hole Coalescence at Redshift 0.2*, Phys. Rev. Lett. **118** no. 22, (2017) 221101, arXiv:1706.01812 [gr-qc].

[59] **Virgo, LIGO Scientific** Collaboration, B. P. Abbott *et al.*, *GW170608: Observation of a 19-solar-mass Binary Black Hole Coalescence*, Astrophys. J. **851** no. 2, (2017) L35, arXiv:1711.05578 [astro-ph.HE].

[60] **Virgo, LIGO Scientific** Collaboration, B. P. Abbott *et al.*, *GW170814: A Three-Detector Observation of Gravitational Waves from a Binary Black Hole Coalescence*, Phys. Rev. Lett. **119** no. 14, (2017) 141101, arXiv:1709.09660 [gr-qc].

[61] **Virgo, LIGO Scientific** Collaboration, B. Abbott *et al.*, *GW170817: Observation of Gravitational Waves from a Binary Neutron Star Inspiral*, Phys. Rev. Lett. **119** no. 16, (2017) 161101, arXiv:1710.05832 [gr-qc].

[62] A. Einstein, *The Foundation of the General Theory of Relativity*, Annalen Phys. **49** no. 7, (1916) 769–822. [65(1916)].

[63] S. Deser, *Selfinteraction and gauge invariance*, Gen. Rel. Grav. **1** (1970) 9–18, arXiv:gr-qc/0411023 [gr-qc].

[64] S. N. Gupta, *Gravitation and Electromagnetism*, Phys. Rev. **96** (1954) 1683–1685.

[65] S. Weinberg, *Photons and gravitons in perturbation theory: Derivation of Maxwell's and Einstein's equations*, Phys. Rev. **138** (1965) B988–B1002.

[66] D. G. Boulware and S. Deser, *Classical General Relativity Derived from Quantum Gravity*, Annals Phys. **89** (1975) 193.

[67] F. Englert and R. Brout, *Broken Symmetry and the Mass of Gauge Vector Mesons*, Phys. Rev. Lett. **13** (1964) 321–323. [,157(1964)].

[68] P. W. Higgs, *Broken Symmetries and the Masses of Gauge Bosons*, Phys. Rev. Lett. **13** (1964) 508–509. [,160(1964)].

[69] P. W. Higgs, *Broken symmetries, massless particles and gauge fields*, Phys. Lett. **12** (1964) 132–133.

[70] G. S. Guralnik, C. R. Hagen, and T. W. B. Kibble, *Global Conservation Laws and Massless Particles*, Phys. Rev. Lett. **13** (1964) 585–587. [,162(1964)].

[71] E. C. G. Stückelberg, *Interaction energy in electrodynamics and in the field theory of nuclear forces*, Helv. Phys. Acta **11** (1938) 225–244.

[72] M. Ostrogradsky, *Mémoires sur les équations différentielles, relatives au problème des isopérimètres*, Mem. Acad. St. Petersbourg **6** no. 4, (1850) 385–517.

[73] R. M. Wald, *General relativity*. Chicago Univ. Press, Chicago, IL, 1984. https://cds.cern.ch/record/106274.

[74] E. Babichev and C. Deffayet, *An introduction to the Vainshtein mechanism*, Class. Quant. Grav. **30** (2013) 184001, arXiv:1304.7240 [gr-qc].

[75] C. M. Will, *The Confrontation between General Relativity and Experiment*, Living Rev. Rel. **17** (2014) 4, arXiv:1403.7377 [gr-qc].

[76] C. de Rham, J. T. Deskins, A. J. Tolley, and S.-Y. Zhou, *Graviton Mass Bounds*, Rev. Mod. Phys. **89** no. 2, (2017) 025004, arXiv:1606.08462 [astro-ph.CO].

[77] C. de Rham, G. Gabadadze, and A. J. Tolley, *Helicity Decomposition of Ghost-free Massive Gravity*, JHEP **11** (2011) 093, arXiv:1108.4521 [hep-th].

[78] A. I. Vainshtein, *To the problem of nonvanishing gravitation mass*, Phys. Lett. **B39** (1972) 393–394.

[79] C. Deffayet, *Spherically symmetric solutions of massive gravity*, Class. Quant. Grav. **25** (2008) 154007.

[80] E. Babichev, C. Deffayet, and R. Ziour, *Recovering General Relativity from massive gravity*, Phys. Rev. Lett. **103** (2009) 201102, arXiv:0907.4103 [gr-qc].

[81] E. Babichev, C. Deffayet, and R. Ziour, *k-Mouflage gravity*, Int. J. Mod. Phys. **D18** (2009) 2147–2154, arXiv:0905.2943 [hep-th].

[82] E. Babichev, C. Deffayet, and R. Ziour, *The Vainshtein mechanism in the Decoupling Limit of massive gravity*, JHEP **05** (2009) 098, arXiv:0901.0393 [hep-th].

[83] E. Babichev, C. Deffayet, and R. Ziour, *The Recovery of General Relativity in massive gravity via the Vainshtein mechanism*, Phys. Rev. **D82** (2010) 104008, arXiv:1007.4506 [gr-qc].

[84] G. Chkareuli and D. Pirtskhalava, *Vainshtein Mechanism In Λ_3 - Theories*, Phys. Lett. **B713** (2012) 99–103, arXiv:1105.1783 [hep-th].

[85] L. Hui and A. Nicolis, *Proposal for an Observational Test of the Vainshtein Mechanism*, Phys. Rev. Lett. **109** (2012) 051304, arXiv:1201.1508 [astro-ph.CO].

[86] F. Sbisa, G. Niz, K. Koyama, and G. Tasinato, *Characterising Vainshtein Solutions in Massive Gravity*, Phys. Rev. **D86** (2012) 024033, arXiv:1204.1193 [hep-th].

[87] T. Narikawa, T. Kobayashi, D. Yamauchi, and R. Saito, *Testing general scalar-tensor gravity and massive gravity with cluster lensing*, Phys. Rev. **D87** (2013) 124006, arXiv:1302.2311 [astro-ph.CO].

[88] T. Hiramatsu, W. Hu, K. Koyama, and F. Schmidt, *Equivalence Principle Violation in Vainshtein Screened Two-Body Systems*, Phys. Rev. **D87** no. 6, (2013) 063525, arXiv:1209.3364 [hep-th].

[89] K. Koyama, G. Niz, and G. Tasinato, *Effective theory for the Vainshtein mechanism from the Horndeski action*, Phys. Rev. **D88** (2013) 021502, arXiv:1305.0279 [hep-th].

[90] B. Li, G.-B. Zhao, and K. Koyama, *Exploring Vainshtein mechanism on adaptively refined meshes*, JCAP **1305** (2013) 023, arXiv:1303.0008 [astro-ph.CO].

[91] E. Babichev and M. Crisostomi, *Restoring general relativity in massive bigravity theory*, Phys. Rev. **D88** no. 8, (2013) 084002, arXiv:1307.3640.

[92] S. Renaux-Petel, *On the Vainshtein mechanism in the minimal model of massive gravity*, JCAP **1403** (2014) 043, arXiv:1401.0497 [hep-th].

[93] C. Deffayet and J.-W. Rombouts, *Ghosts, strong coupling and accidental symmetries in massive gravity*, Phys. Rev. **D72** (2005) 044003, arXiv:gr-qc/0505134 [gr-qc].

[94] L. Alberte, A. H. Chamseddine, and V. Mukhanov, *Massive Gravity: Resolving the Puzzles*, JHEP **12** (2010) 023, arXiv:1008.5132 [hep-th].

[95] N. Arkani-Hamed, H. Georgi, and M. D. Schwartz, *Effective field theory for massive gravitons and gravity in theory space*, Annals Phys. **305** (2003) 96–118, arXiv:hep-th/0210184 [hep-th].

[96] N. Arkani-Hamed, A. G. Cohen, and H. Georgi, *(De)constructing dimensions*, Phys. Rev. Lett. **86** (2001) 4757–4761, arXiv:hep-th/0104005 [hep-th].

[97] N. Arkani-Hamed, A. G. Cohen, and H. Georgi, *Electroweak symmetry breaking from dimensional deconstruction*, Phys. Lett. **B513** (2001) 232–240, arXiv:hep-ph/0105239 [hep-ph].

[98] N. Arkani-Hamed and M. D. Schwartz, *Discrete gravitational dimensions*, Phys. Rev. **D69** (2004) 104001, arXiv:hep-th/0302110 [hep-th].

[99] M. D. Schwartz, *Constructing gravitational dimensions*, Phys. Rev. **D68** (2003) 024029, arXiv:hep-th/0303114 [hep-th].

[100] C. Deffayet and J. Mourad, *Multigravity from a discrete extra dimension*, Phys. Lett. **B589** (2004) 48–58, arXiv:hep-th/0311124 [hep-th].

[101] C. Deffayet and J. Mourad, *Deconstruction of gravity*, Int. J. Theor. Phys. **44** (2005) 1743–1752.

[102] E. Kiritsis and V. Niarchos, *Interacting String Multi-verses and Holographic Instabilities of Massive Gravity*, Nucl. Phys. **B812** (2009) 488–524, arXiv:0808.3410 [hep-th].

[103] G. Gabadadze, *General Relativity With An Auxiliary Dimension*, Phys. Lett. **B681** (2009) 89–95, arXiv:0908.1112 [hep-th].

[104] C. de Rham, *Massive gravity from Dirichlet boundary conditions*, Phys. Lett. **B688** (2010) 137–141, arXiv:0910.5474 [hep-th].

[105] C. de Rham and G. Gabadadze, *Selftuned Massive Spin-2*, Phys. Lett. **B693** (2010) 334–338, arXiv:1006.4367 [hep-th].

[106] K. Jänich, *Vektoranalysis*. Springer, Springer–Verlag Berlin Heidelberg, 2005. https://www.springer.com/de/book/9783540237419.

[107] M. Blau, *Lecture Notes on General Relativity*, 2018. http://www.blau.itp.unibe.ch/newlecturesGR.pdf.

[108] J. W. York, Jr., *Role of conformal three geometry in the dynamics of gravitation*, Phys. Rev. Lett. **28** (1972) 1082–1085.

[109] G. W. Gibbons and S. W. Hawking, *Action Integrals and Partition Functions in Quantum Gravity*, Phys. Rev. **D15** (1977) 2752–2756.

[110] C. Misner, K. Thorne, and J. Wheeler, *Gravitation*. Princeton University Press, 1970/71.

[111] T. Fließbach, *Allgemeine Relativitätstheorie*. Springer Berlin Heidelberg, 1998.

[112] H. Weyl, *Elektron und Gravitation I*, Zeitschrift für Physik **56** (1929) 330–352.

[113] C. de Rham, A. Matas, and A. J. Tolley, *Deconstructing Dimensions and Massive Gravity*, Class. Quant. Grav. **31** (2014) 025004, arXiv:1308.4136 [hep-th].

[114] P. Creminelli, A. Nicolis, M. Papucci, and E. Trincherini, *Ghosts in massive gravity*, JHEP **09** (2005) 003, arXiv:hep-th/0505147 [hep-th].

[115] S. Deser and C. J. Isham, *Canonical Vierbein Form of General Relativity*, Phys. Rev. **D14** (1976) 2505.

[116] S. F. Hassan, A. Schmidt-May, and M. von Strauss, *Metric Formulation of Ghost-Free Multivielbein Theory*, arXiv:1204.5202 [hep-th].

[117] N. A. Ondo and A. J. Tolley, *Complete Decoupling Limit of Ghost-free Massive Gravity*, JHEP **11** (2013) 059, arXiv:1307.4769 [hep-th].

[118] Y. Yamashita, A. De Felice, and T. Tanaka, *Appearance of Boulware-Deser ghost in bigravity with doubly coupled matter*, Int. J. Mod. Phys. **D23** (2014) 1443003, arXiv:1408.0487 [hep-th].

[119] C. de Rham, L. Heisenberg, and R. H. Ribeiro, *Ghosts and matter couplings in massive gravity, bigravity and multigravity*, Phys. Rev. **D90** (2014) 124042, arXiv:1409.3834 [hep-th].

[120] C. de Rham, L. Heisenberg, and R. H. Ribeiro, *On couplings to matter in massive (bi-)gravity*, Class. Quant. Grav. **32** (2015) 035022, arXiv:1408.1678 [hep-th].

[121] J. Noller and S. Melville, *The coupling to matter in Massive, Bi- and Multi-Gravity*, JCAP **1501** (2015) 003, arXiv:1408.5131 [hep-th].

[122] S. F. Hassan, M. Kocic, and A. Schmidt-May, *Absence of ghost in a new bimetric-matter coupling*, arXiv:1409.1909 [hep-th].

[123] C. de Rham, L. Heisenberg, and R. H. Ribeiro, *Quantum Corrections in Massive Gravity*, Phys. Rev. **D88** (2013) 084058, arXiv:1307.7169 [hep-th].

[124] L. D. Landau and E. M. Lifshitz, *Mechanics*. No. Bd. 1 in Theoretische Physik. Elsevier Science, 1982. https://books.google.de/books?id=bE-9tUH2J2wC.

[125] R. L. Arnowitt, S. Deser, and C. W. Misner, *The Dynamics of general relativity*, Gen. Rel. Grav. **40** (2008) 1997–2027, arXiv:gr-qc/0405109 [gr-qc].

[126] L. Alberte, A. H. Chamseddine, and V. Mukhanov, *Massive Gravity: Exorcising the Ghost*, JHEP **04** (2011) 004, arXiv:1011.0183 [hep-th].

[127] A. H. Chamseddine and V. Mukhanov, *Massive Gravity Simplified: A Quadratic Action*, JHEP **08** (2011) 091, arXiv:1106.5868 [hep-th].

[128] A. H. Chamseddine and V. Mukhanov, *Hidden Ghost in Massive gravity*, JHEP **03** (2013) 092, arXiv:1302.4367 [hep-th].

[129] J. Klusoň, *Note About Hamiltonian Structure of Non-Linear Massive Gravity*, JHEP **01** (2012) 013, arXiv:1109.3052 [hep-th].

[130] J. Klusoň, *Hamiltonian Analysis of 1+1 dimensional Massive Gravity*, Phys. Rev. **D85** (2012) 044010, arXiv:1110.6158 [hep-th].

[131] J. Klusoň, *Note About Hamiltonian Formalism for General Non-Linear Massive Gravity Action in Stuckelberg Formalism*, Int. J. Mod. Phys. **A28** (2013) 1350160, arXiv:1209.3612 [hep-th].

[132] J. Klusoň, *Comments About Hamiltonian Formulation of Non-Linear Massive Gravity with Stuckelberg Fields*, JHEP **06** (2012) 170, arXiv:1112.5267 [hep-th].

[133] J. Klusoň, *Hamiltonian Formalism of Particular Bimetric Gravity Model*, Phys. Rev. **D87** no. 8, (2013) 084017, arXiv:1211.6267 [hep-th].

[134] J. Klusoň, *Is Bimetric Gravity Really Ghost Free?*, Int. J. Mod. Phys. **A28** no. 28, (2013) 1350143, arXiv:1301.3296 [hep-th].

[135] J. Klusoň, *Hamiltonian Formalism of General Bimetric Gravity*, Eur. Phys. J. **C73** no. 9, (2013) 2553, arXiv:1303.1652 [hep-th].

[136] J. Klusoň, *Hamiltonian Formalism of Bimetric Gravity In Vierbein Formulation*, Eur. Phys. J. **C74** no. 8, (2014) 2985, arXiv:1307.1974 [hep-th].

[137] J. Klusoň, *Remark About Hamiltonian Formulation of Non-Linear Massive Gravity in Stuckelberg Formalism*, Phys. Rev. **D86** (2012) 124005, arXiv:1202.5899 [hep-th].

[138] S. F. Hassan, A. Schmidt-May, and M. von Strauss, *Proof of Consistency of Nonlinear Massive Gravity in the Stúckelberg Formulation*, Phys. Lett. **B715** (2012) 335–339, arXiv:1203.5283 [hep-th].

[139] J. Klusoň, *Non-Linear Massive Gravity with Additional Primary Constraint and Absence of Ghosts*, Phys. Rev. **D86** (2012) 044024, arXiv:1204.2957 [hep-th].

[140] S. Alexandrov, *Canonical structure of Tetrad Bimetric Gravity*, Gen. Rel. Grav. **46** (2014) 1639, arXiv:1308.6586 [hep-th].

[141] A. Golovnev, *On non-perturbative analysis of massive and bimetric gravity*, AIP Conf. Proc. **1606** (2014) 299–303, arXiv:1401.6343 [gr-qc].

[142] M. S. Volkov, *Self-accelerating cosmologies and hairy black holes in ghost-free bigravity and massive gravity*, Class. Quant. Grav. **30** (2013) 184009, arXiv:1304.0238 [hep-th].

[143] M. S. Volkov, *Hairy black holes in theories with massive gravitons*, Lect. Notes Phys. **892** (2015) 161–180, arXiv:1405.1742 [hep-th].

[144] E. Babichev and R. Brito, *Black holes in massive gravity*, Class. Quant. Grav. **32** (2015) 154001, arXiv:1503.07529 [gr-qc].

[145] A. Gruzinov and M. Mirbabayi, *Stars and Black Holes in Massive Gravity*, Phys. Rev. **D84** (2011) 124019, arXiv:1106.2551 [hep-th].

[146] M. S. Volkov, *Hairy black holes in the ghost-free bigravity theory*, Phys. Rev. **D85** (2012) 124043, arXiv:1202.6682 [hep-th].

[147] N. Arkani-Hamed, S. Dimopoulos, G. Dvali, and G. Gabadadze, *Nonlocal modification of gravity and the cosmological constant problem*, arXiv:hep-th/0209227 [hep-th].

[148] G. Dvali, G. Gabadadze, and M. Shifman, *Diluting cosmological constant in infinite volume extra dimensions*, Phys. Rev. **D67** (2003) 044020, arXiv:hep-th/0202174 [hep-th].

[149] G. Dvali, S. Hofmann, and J. Khoury, *Degravitation of the cosmological constant and graviton width*, Phys. Rev. **D76** (2007) 084006, arXiv:hep-th/0703027 [HEP-TH].

[150] J. Martin, *Everything You Always Wanted To Know About The Cosmological Constant Problem (But Were Afraid To Ask)*, Comptes Rendus Physique **13** (2012) 566–665, arXiv:1205.3365 [astro-ph.CO].

[151] C. de Rham, G. Gabadadze, L. Heisenberg, and D. Pirtskhalava, *Cosmic Acceleration and the Helicity-0 Graviton*, Phys. Rev. **D83** (2011) 103516, arXiv:1010.1780 [hep-th].

[152] G. D'Amico, C. de Rham, S. Dubovsky, G. Gabadadze, D. Pirtskhalava, and A. J. Tolley, *Massive Cosmologies*, Phys. Rev. **D84** (2011) 124046, arXiv:1108.5231 [hep-th].

[153] A. E. Gümrükçüoğlu, C. Lin, and S. Mukohyama, *Open FRW universes and self-acceleration from nonlinear massive gravity*, JCAP **1111** (2011) 030, arXiv:1109.3845 [hep-th].

[154] A. E. Gümrükçüoğlu, C. Lin, and S. Mukohyama, *Cosmological perturbations of self-accelerating universe in nonlinear massive gravity*, JCAP **1203** (2012) 006, arXiv:1111.4107 [hep-th].

[155] B. Vakili and N. Khosravi, *Classical and quantum massive cosmology for the open FRW universe*, Phys. Rev. **D85** (2012) 083529, arXiv:1204.1456 [gr-qc].

[156] A. De Felice, A. E. Gümrükçüoğlu, and S. Mukohyama, *Massive gravity: nonlinear instability of the homogeneous and isotropic universe*, Phys. Rev. Lett. **109** (2012) 171101, arXiv:1206.2080 [hep-th].

[157] M. Fasiello and A. J. Tolley, *Cosmological perturbations in Massive Gravity and the Higuchi bound*, JCAP **1211** (2012) 035, arXiv:1206.3852 [hep-th].

[158] A. De Felice, A. E. Gümrükçüoğlu, C. Lin, and S. Mukohyama, *Nonlinear stability of cosmological solutions in massive gravity*, JCAP **1305** (2013) 035, arXiv:1303.4154 [hep-th].

[159] M. S. Volkov, *Cosmological solutions with massive gravitons in the bigravity theory*, JHEP **01** (2012) 035, arXiv:1110.6153 [hep-th].

[160] M. von Strauss, A. Schmidt-May, J. Enander, E. Mortsell, and S. F. Hassan, *Cosmological Solutions in Bimetric Gravity and their Observational Tests*, JCAP **1203** (2012) 042, arXiv:1111.1655 [gr-qc].

[161] D. Comelli, M. Crisostomi, F. Nesti, and L. Pilo, *FRW Cosmology in Ghost Free Massive Gravity*, JHEP **03** (2012) 067, arXiv:1111.1983 [hep-th]. [Erratum: JHEP06,020(2012)].

[162] Y. Akrami, T. S. Koivisto, and M. Sandstad, *Accelerated expansion from ghost-free bigravity: a statistical analysis with improved generality*, JHEP **03** (2013) 099, arXiv:1209.0457 [astro-ph.CO].

[163] F. Könnig, A. Patil, and L. Amendola, *Viable cosmological solutions in massive bimetric gravity*, JCAP **1403** (2014) 029, arXiv:1312.3208 [astro-ph.CO].

[164] D. Comelli, M. Crisostomi, and L. Pilo, *FRW Cosmological Perturbations in Massive Bigravity*, Phys. Rev. **D90** (2014) 084003, arXiv:1403.5679 [hep-th].

[165] A. De Felice, A. E. Gümrükçüoğlu, S. Mukohyama, N. Tanahashi, and T. Tanaka, *Viable cosmology in bimetric theory*, JCAP **1406** (2014) 037, arXiv:1404.0008 [hep-th].

[166] G. Cusin, R. Durrer, P. Guarato, and M. Motta, *Gravitational waves in bigravity cosmology*, JCAP **1505** no. 05, (2015) 030, arXiv:1412.5979 [astro-ph.CO].

[167] H. Nersisyan, Y. Akrami, and L. Amendola, *Consistent metric combinations in cosmology of massive bigravity*, Phys. Rev. **D92** no. 10, (2015) 104034, arXiv:1502.03988 [gr-qc].

[168] Y. Akrami, S. F. Hassan, F. Könnig, A. Schmidt-May, and A. R. Solomon, *Bimetric gravity is cosmologically viable*, Phys. Lett. **B748** (2015) 37–44, arXiv:1503.07521 [gr-qc].

[169] F. Könnig, *Higuchi Ghosts and Gradient Instabilities in Bimetric Gravity*, Phys. Rev. **D91** (2015) 104019, arXiv:1503.07436 [astro-ph.CO].

[170] G. Cusin, R. Durrer, P. Guarato, and M. Motta, *Inflationary perturbations in bimetric gravity*, JCAP **1509** no. 09, (2015) 043, arXiv:1505.01091 [astro-ph.CO].

[171] D. Comelli, M. Crisostomi, and L. Pilo, *Perturbations in Massive Gravity Cosmology*, JHEP **06** (2012) 085, arXiv:1202.1986 [hep-th].

[172] P. Steinhardt and V. Mukhanov, *Physical Foundations of Cosmology*. Cambridge University Press, 2005.

[173] A. De Felice, T. Nakamura, and T. Tanaka, *Possible existence of viable models of bi-gravity with detectable graviton oscillations by gravitational wave detectors*, PTEP **2014** (2014) 043E01, arXiv:1304.3920 [gr-qc].

[174] T. Narikawa, K. Ueno, H. Tagoshi, T. Tanaka, N. Kanda, and T. Nakamura, *Detectability of bigravity with graviton oscillations using gravitational wave observations*, Phys. Rev. **D91** (2015) 062007, arXiv:1412.8074 [gr-qc].

[175] G. 't Hooft, *Naturalness, chiral symmetry, and spontaneous chiral symmetry breaking*, NATO Sci. Ser. B **59** (1980) 135.

[176] A. Higuchi, *Forbidden Mass Range for Spin-2 Field Theory in De Sitter Space-time*, Nucl. Phys. **B282** (1987) 397–436.

[177] M. Fasiello and A. J. Tolley, *Cosmological Stability Bound in Massive Gravity and Bigravity*, JCAP **1312** (2013) 002, arXiv:1308.1647 [hep-th].

[178] M. Berg, I. Buchberger, J. Enander, E. Mortsell, and S. Sjors, *Growth Histories in Bimetric Massive Gravity*, JCAP **1212** (2012) 021, arXiv:1206.3496 [gr-qc].

[179] F. Könnig and L. Amendola, *Instability in a minimal bimetric gravity model*, Phys. Rev. **D90** (2014) 044030, arXiv:1402.1988 [astro-ph.CO].

[180] A. R. Solomon, Y. Akrami, and T. S. Koivisto, *Linear growth of structure in massive bigravity*, JCAP **1410** (2014) 066, arXiv:1404.4061 [astro-ph.CO].

[181] F. Koennig, Y. Akrami, L. Amendola, M. Motta, and A. R. Solomon, *Stable and unstable cosmological models in bimetric massive gravity*, Phys. Rev. **D90** (2014) 124014, arXiv:1407.4331 [astro-ph.CO].

[182] M. Lagos and P. G. Ferreira, *Cosmological perturbations in massive bigravity*, JCAP **1412** (2014) 026, arXiv:1410.0207 [gr-qc].

[183] J. Enander, Y. Akrami, E. Mörtsell, M. Renneby, and A. R. Solomon, *Integrated Sachs-Wolfe effect in massive bigravity*, Phys. Rev. **D91** (2015) 084046, arXiv:1501.02140 [astro-ph.CO].

[184] L. Amendola, F. Könnig, M. Martinelli, V. Pettorino, and M. Zumalacarregui, *Surfing gravitational waves: can bigravity survive growing tensor modes?*, JCAP **1505** (2015) 052, arXiv:1503.02490 [astro-ph.CO].

[185] T. Kobayashi, M. Siino, M. Yamaguchi, and D. Yoshida, *Perturbations of Cosmological and Black Hole Solutions in Massive gravity and Bi-gravity*, PTEP **2016** no. 10, (2016) 103E02, arXiv:1509.02096 [gr-qc].

[186] M. Lagos and P. G. Ferreira, *A general theory of linear cosmological perturbations: bimetric theories*, JCAP **1701** no. 01, (2017) 047, arXiv:1610.00553 [gr-qc].

[187] M. Johnson and A. Terrana, *Tensor Modes in Bigravity: Primordial to Present*, Phys. Rev. **D92** no. 4, (2015) 044001, arXiv:1503.05560 [astro-ph.CO].

[188] E. Mortsell and J. Enander, *Scalar instabilities in bimetric gravity: The Vainshtein mechanism and structure formation*, JCAP **1510** no. 10, (2015) 044, arXiv:1506.04977 [astro-ph.CO].

[189] A. E. Gümrükçüoğlu, L. Heisenberg, and S. Mukohyama, *Cosmological perturbations in massive gravity with doubly coupled matter*, JCAP **1502** (2015) 022, arXiv:1409.7260 [hep-th].

[190] D. Comelli, M. Crisostomi, K. Koyama, L. Pilo, and G. Tasinato, *Cosmology of bigravity with doubly coupled matter*, JCAP **1504** (2015) 026, arXiv:1501.00864 [hep-th].

[191] M. Lagos and J. Noller, *New massive bigravity cosmologies with double matter coupling*, JCAP **1601** no. 01, (2016) 023, arXiv:1508.05864 [gr-qc].

[192] L. Heisenberg and A. Refregier, *Cosmology in doubly coupled massive gravity: constraints from SNIa, BAO and CMB*, Phys. Lett. **B762** (2016) 131–137, arXiv:1604.07680 [astro-ph.CO].

[193] X. Gao and L. Heisenberg, *Doubly coupled matter fields in massive bigravity*, Chin. Phys. **C42** no. 7, (2018) 075101, arXiv:1606.06141 [hep-th].

[194] **Virgo, LIGO Scientific** Collaboration, B. P. Abbott *et al.*, *Characterization of transient noise in Advanced LIGO relevant to gravitational wave signal GW150914*, Class. Quant. Grav. **33** no. 13, (2016) 134001, arXiv:1602.03844 [gr-qc].

[195] B. P. Abbott *et al.*, *Sensitivity of the Advanced LIGO detectors at the beginning of gravitational wave astronomy*, Phys. Rev. **D93** no. 11, (2016) 112004, arXiv:1604.00439 [astro-ph.IM]. [Addendum: Phys. Rev.D97,no.5,059901(2018)].

[196] D. Pooley, P. Kumar, J. C. Wheeler, and B. Grossan, *GW170817 Most Likely Made a Black Hole*, Astrophys. J. **859** no. 2, (2018) L23, arXiv:1712.03240 [astro-ph.HE].

[197] **Virgo, LIGO Scientific** Collaboration, B. P. Abbott *et al.*, *Search for gravitational waves from a long-lived remnant of the binary neutron star merger GW170817*, arXiv:1810.02581 [gr-qc].

[198] **Virgo, LIGO Scientific** Collaboration, B. P. Abbott *et al.*, *Binary Black Hole Mergers in the first Advanced LIGO Observing Run*, Phys. Rev. **X6** no. 4, (2016) 041015, arXiv:1606.04856 [gr-qc].

[199] **Virgo, LIGO Scientific** Collaboration, B. P. Abbott *et al.*, *GW170817: Implications for the Stochastic Gravitational-Wave Background from Compact Binary Coalescences*, Phys. Rev. Lett. **120** no. 9, (2018) 091101, arXiv:1710.05837 [gr-qc].

[200] **Virgo, LIGO Scientific** Collaboration, B. P. Abbott *et al.*, *Full Band All-sky Search for Periodic Gravitational Waves in the O1 LIGO Data*, Phys. Rev. **D97** no. 10, (2018) 102003, arXiv:1802.05241 [gr-qc].

[201] Z. Berezhiani, D. Comelli, F. Nesti, and L. Pilo, *Spontaneous Lorentz Breaking and Massive Gravity*, Phys. Rev. Lett. **99** (2007) 131101, arXiv:hep-th/0703264 [HEP-TH].

[202] S. F. Hassan, A. Schmidt-May, and M. von Strauss, *On Consistent Theories of Massive Spin-2 Fields Coupled to Gravity*, JHEP **05** (2013) 086, arXiv:1208.1515 [hep-th].

[203] **Virgo, LIGO Scientific** Collaboration, B. P. Abbott *et al.*, *Improved analysis of GW150914 using a fully spin-precessing waveform Model*, Phys. Rev. **X6** no. 4, (2016) 041014, arXiv:1606.01210 [gr-qc].

[204] **Virgo, LIGO Scientific** Collaboration, B. P. Abbott *et al.*, *Tests of general relativity with GW150914*, Phys. Rev. Lett. **116** no. 22, (2016) 221101, arXiv:1602.03841 [gr-qc]. [Erratum: Phys. Rev. Lett.121,no.12,129902(2018)].

[205] C. M. Will, *Bounding the mass of the graviton using gravitational wave observations of inspiralling compact binaries*, Phys. Rev. **D57** (1998) 2061–2068, arXiv:gr-qc/9709011 [gr-qc].

[206] B. Wardell, I. Hinder, and E. Bentivegna, *Simulation of GW150914 binary black hole merger using the Einstein Toolkit*, Sept., 2016. https://doi.org/10.5281/zenodo.155394.

[207] F. Loffler *et al.*, *The Einstein Toolkit: A Community Computational Infrastructure for Relativistic Astrophysics*, Class. Quant. Grav. **29** (2012) 115001, arXiv:1111.3344 [gr-qc].

[208] D. Pollney, C. Reisswig, E. Schnetter, N. Dorband, and P. Diener, *High accuracy binary black hole simulations with an extended wave zone*, Phys. Rev. **D83** (2011) 044045, arXiv:0910.3803 [gr-qc].

[209] E. Schnetter, S. H. Hawley, and I. Hawke, *Evolutions in 3-D numerical relativity using fixed mesh refinement*, Class. Quant. Grav. **21** (2004) 1465–1488, arXiv:gr-qc/0310042 [gr-qc].

[210] J. Thornburg, *A Fast apparent horizon finder for three-dimensional Cartesian grids in numerical relativity*, Class. Quant. Grav. **21** (2004) 743–766, arXiv:gr-qc/0306056 [gr-qc].

[211] M. Ansorg, B. Bruegmann, and W. Tichy, *A Single-domain spectral method for black hole puncture data*, Phys. Rev. **D70** (2004) 064011, arXiv:gr-qc/0404056 [gr-qc].

[212] O. Dreyer, B. Krishnan, D. Shoemaker, and E. Schnetter, *Introduction to isolated horizons in numerical relativity*, Phys. Rev. **D67** (2003) 024018, arXiv:gr-qc/0206008 [gr-qc].

[213] T. Goodale, G. Allen, G. Lanfermann, J. Massó, T. Radke, E. Seidel, and J. Shalf, *The Cactus Framework and Toolkit: Design and Applications*, in *Vector and Parallel Processing – VECPAR'2002, 5th International Conference, Lecture Notes in Computer Science*. Springer, Berlin, 2003. http://edoc.mpg.de/3341.

[214] J. D. Brown, P. Diener, O. Sarbach, E. Schnetter, and M. Tiglio, *Turduckening black holes: An Analytical and computational study*, Phys. Rev. **D79** (2009) 044023, arXiv:0809.3533 [gr-qc].

[215] http://www.black-holes.org/waveforms, catalog entry sxs:bbh:0317 for gw151226.

[216] C. Talmadge, J. P. Berthias, R. W. Hellings, and E. M. Standish, *Model Independent Constraints on Possible Modifications of Newtonian Gravity*, Phys. Rev. Lett. **61** (1988) 1159–1162.

[217] C. Giunti and C. W. Kim, *Fundamentals of neutrino physics and astrophysics*. Oxford University Press, Oxford, New York, 2007.

[218] C. Giunti and C. W. Kim, *Coherence of neutrino oscillations in the wave packet approach*, Phys. Rev. **D58** (1998) 017301, arXiv:hep-ph/9711363 [hep-ph].

[219] **Virgo, LIGO Scientific** Collaboration, B. P. Abbott *et al.*, *Properties of the Binary Black Hole Merger GW150914*, Phys. Rev. Lett. **116** no. 24, (2016) 241102, arXiv:1602.03840 [gr-qc].

[220] E. D. Kovetz, I. Cholis, P. C. Breysse, and M. Kamionkowski, *Black hole mass function from gravitational wave measurements*, Phys. Rev. **D95** no. 10, (2017) 103010, arXiv:1611.01157 [astro-ph.CO].

[221] **VIRGO, KAGRA, LIGO Scientific** Collaboration, B. P. Abbott *et al.*, *Prospects for Observing and Localizing Gravitational-Wave Transients with Advanced LIGO, Advanced Virgo and KAGRA*, Living Rev. Rel. **21** no. 1, (2018) 3, arXiv:1304.0670 [gr-qc].

[222] S. Hild, S. Chelkowski, and A. Freise, *Pushing towards the ET sensitivity using 'conventional' technology*, arXiv:0810.0604 [gr-qc].

[223] B. Sathyaprakash *et al.*, *Scientific Potential of Einstein Telescope*, in *Proceedings, 46th Rencontres de Moriond on Gravitational Waves and Experimental Gravity: La Thuile, Italy, March 20-27, 2011*, pp. 127–136. 2011. arXiv:1108.1423 [gr-qc].

[224] B. Sathyaprakash *et al.*, *Scientific Objectives of Einstein Telescope*, Class. Quant. Grav. **29** (2012) 124013, arXiv:1206.0331 [gr-qc]. [Erratum: Class. Quant. Grav.30,079501(2013)].

[225] J. Abedi, H. Dykaar, and N. Afshordi, *Echoes from the Abyss: Tentative evidence for Planck-scale structure at black hole horizons*, Phys. Rev. **D96** no. 8, (2017) 082004, arXiv:1612.00266 [gr-qc].

[226] J. Abedi, H. Dykaar, and N. Afshordi, *Echoes from the Abyss: The Holiday Edition!*, arXiv:1701.03485 [gr-qc].

[227] R. S. Conklin, B. Holdom, and J. Ren, *Gravitational wave echoes through new windows*, Phys. Rev. **D98** no. 4, (2018) 044021, arXiv:1712.06517 [gr-qc].

[228] G. Ashton, O. Birnholtz, M. Cabero, C. Capano, T. Dent, B. Krishnan, G. D. Meadors, A. B. Nielsen, A. Nitz, and J. Westerweck, *Comments on: "Echoes from the abyss: Evidence for Planck-scale structure at black hole horizons"*, arXiv:1612.05625 [gr-qc].

[229] J. Westerweck, A. Nielsen, O. Fischer-Birnholtz, M. Cabero, C. Capano, T. Dent, B. Krishnan, G. Meadors, and A. H. Nitz, *Low significance of evidence for black hole echoes in gravitational wave data*, Phys. Rev. **D97** no. 12, (2018) 124037, arXiv:1712.09966 [gr-qc].

[230] J. Abedi, H. Dykaar, and N. Afshordi, *Comment on: "Low significance of evidence for black hole echoes in gravitational wave data"*, arXiv:1803.08565 [gr-qc].

[231] V. Cardoso, S. Hopper, C. F. B. Macedo, C. Palenzuela, and P. Pani, *Gravitational-wave signatures of exotic compact objects and of quantum corrections at the horizon scale*, Phys. Rev. **D94** no. 8, (2016) 084031, arXiv:1608.08637 [gr-qc].

[232] Z. Mark, A. Zimmerman, S. M. Du, and Y. Chen, *A recipe for echoes from exotic compact objects*, Phys. Rev. **D96** no. 8, (2017) 084002, arXiv:1706.06155 [gr-qc].

[233] A. Urbano and H. Veermäe, *On gravitational echoes from ultracompact exotic stars*, arXiv:1810.07137 [gr-qc].

[234] J. Enander, A. R. Solomon, Y. Akrami, and E. Mortsell, *Cosmic expansion histories in massive bigravity with symmetric matter coupling*, JCAP **1501** (2015) 006, arXiv:1409.2860 [astro-ph.CO].

[235] A. Schmidt-May, *Mass eigenstates in bimetric theory with matter coupling*, JCAP **1501** (2015) 039, arXiv:1409.3146 [gr-qc].

[236] A. E. Gümrükçüoğlu, L. Heisenberg, S. Mukohyama, and N. Tanahashi, *Cosmology in bimetric theory with an effective composite coupling to matter*, JCAP **1504** no. 04, (2015) 008, arXiv:1501.02790 [hep-th].

[237] P. Brax, A.-C. Davis, and J. Noller, *Gravitational Waves in Doubly Coupled Bigravity*, Phys. Rev. **D96** no. 2, (2017) 023518, arXiv:1703.08016 [gr-qc].

[238] M. Milgrom, *A Modification of the Newtonian dynamics as a possible alternative to the hidden mass hypothesis*, Astrophys. J. **270** (1983) 365–370.

[239] R. H. Sanders, *Clusters of galaxies with modified Newtonian dynamics (MOND)*, Mon. Not. Roy. Astron. Soc. **342** (2003) 901, arXiv:astro-ph/0212293 [astro-ph].

[240] G. W. Angus, B. Famaey, and H. Zhao, *Can MOND take a bullet? Analytical comparisons of three versions of MOND beyond spherical symmetry*, Mon. Not. Roy. Astron. Soc. **371** (2006) 138, arXiv:astro-ph/0606216 [astro-ph].

[241] G. W. Angus, H. Shan, H. Zhao, and B. Famaey, *On the Law of Gravity, the Mass of Neutrinos and the Proof of Dark Matter*, Astrophys. J. **654** (2007) L13–L16, arXiv:astro-ph/0609125 [astro-ph].

[242] D. C. Rodrigues, V. Marra, A. del Popolo, and Z. Davari, *Absence of a fundamental acceleration scale in galaxies*, Nat. Astron. **2** no. 8, (2018) 668–672, arXiv:1806.06803 [astro-ph.GA].

[243] M. T. Frandsen and J. Petersen, *Investigating Dark Matter and MOND Models with Galactic Rotation Curve Data*, arXiv:1805.10706 [astro-ph.GA].

[244] J. F. Navarro, C. S. Frenk, and S. D. M. White, *A Universal density profile from hierarchical clustering*, Astrophys. J. **490** (1997) 493–508, arXiv:astro-ph/9611107 [astro-ph].

[245] R. H. Sanders, *Anti-gravity and galaxy rotation curves*, Astron. Astrophys. **136** (July, 1984) L21–L23.

[246] I. T. Drummond, *Bimetric gravity and [dark matter]*, Phys. Rev. **D63** (2001) 043503, arXiv:astro-ph/0008234 [astro-ph].

[247] J. L. Cervantes-Cota, M. A. Rodriguez-Meza, and D. Nunez, *Flat rotation curves using scalar-tensor theories*, J. Phys. Conf. Ser. **91** (2007) 012007, arXiv:0707.2692 [astro-ph].

[248] A. Stabile and S. Capozziello, *Galaxy rotation curves in f(R,ϕ) gravity*, Phys. Rev. **D87** no. 6, (2013) 064002, arXiv:1302.1760 [gr-qc].

[249] N. Hashim, M. De Laurentis, Z. Z. Abidin, and P. Salucci, *Rotation Curve with MOND and Dark Matter Halo profile for ESO138-G014*, arXiv:1407.0379 [astro-ph.GA].

[250] J. W. Moffat and S. Rahvar, *The MOG weak field approximation and observational test of galaxy rotation curves*, Mon. Not. Roy. Astron. Soc. **436** (2013) 1439–1451, arXiv:1306.6383 [astro-ph.GA].

[251] S. Rahvar and B. Mashhoon, *Observational Tests of Nonlocal Gravity: Galaxy Rotation Curves and Clusters of Galaxies*, Phys. Rev. **D89** (2014) 104011, arXiv:1401.4819 [astro-ph.GA].

[252] S. Capozziello, E. De Filippis, and V. Salzano, *Modelling clusters of galaxies by f(R)-gravity*, Mon. Not. Roy. Astron. Soc. **394** (2009) 947–959, arXiv:0809.1882 [astro-ph].

[253] D. F. Mota, V. Salzano, and S. Capozziello, *Testing feasibility of scalar-tensor gravity by scale dependent mass and coupling to matter*, Phys. Rev. **D83** (2011) 084038, arXiv:1103.4215 [astro-ph.CO].

[254] F. Piazza and C. Marinoni, *Model for gravitational interaction between dark matter and baryons*, Phys. Rev. Lett. **91** (2003) 141301, arXiv:hep-ph/0304228 [hep-ph].

[255] A. Stabile and G. Scelza, *Rotation Curves of Galaxies by Fourth Order Gravity*, Phys. Rev. **D84** (2011) 124023, arXiv:1107.5351 [gr-qc].

[256] V. F. Cardone and S. Capozziello, *Systematic biases on galaxy haloes parameters from Yukawa-like gravitational potentials*, Mon. Not. Roy. Astron. Soc. **414** (2011) 1301, arXiv:1102.0916 [astro-ph.CO].

[257] J. Enander and E. Mortsell, *On stars, galaxies and black holes in massive bigravity*, JCAP **1511** no. 11, (2015) 023, arXiv:1507.00912 [astro-ph.CO].

[258] S. Panpanich and P. Burikham, *Fitting rotation curves of galaxies by de Rham-Gabadadze-Tolley massive gravity*, Phys. Rev. **D98** no. 6, (2018) 064008, arXiv:1806.06271 [gr-qc].

[259] de Almeida, Álefe O. F. and Amendola, Luca and Niro, Viviana, *Galaxy rotation curves in modified gravity models*, JCAP **1808** no. 08, (2018) 012, arXiv:1805.11067 [astro-ph.GA].

[260] M. Peskin and D. Schroeder, *An Introduction to Quantum Field Theory*. Advanced book classics. Westview Press, 1995.

[261] F. W. Dyson, A. S. Eddington, and C. Davidson, *A Determination of the Deflection of Light by the Sun's Gravitational Field, from Observations Made at the Total Eclipse of May 29, 1919*, Phil. Trans. Roy. Soc. Lond. **A220** (1920) 291–333.

[262] **Planck** Collaboration, P. A. R. Ade *et al.*, *Planck 2015 results. XXIV. Cosmology from Sunyaev-Zeldovich cluster counts*, Astron. Astrophys. **594** (2016) A24, arXiv:1502.01597 [astro-ph.CO].

[263] R. A. Sunyaev and Ya. B. Zeldovich, *Small scale fluctuations of relic radiation*, Astrophys. Space Sci. **7** (1970) 3–19.

[264] R. A. Sunyaev and Ya. B. Zeldovich, *Microwave background radiation as a probe of the contemporary structure and history of the universe*, Ann. Rev. Astron. Astrophys. **18** (1980) 537–560.

[265] M. Bartelmann, *Theoretical Astrophysics: An Introduction*. Physics textbook. Wiley, 2013. https://books.google.de/books?id=zoAbmrH8UawC.

[266] R. Sadat, *Clusters of galaxies and mass estimates*, ASP Conf. Ser. **126** (1997) 349, arXiv:astro-ph/9702050 [astro-ph].

[267] H. Ebeling, A. C. Edge, and J. P. Henry, *Macs: a quest for the most massive galaxy clusters in the universe*, Astrophys. J. **553** (2001) 668, arXiv:astro-ph/0009101 [astro-ph].

[268] H. Ebeling, C. J. Ma, J. P. Kneib, E. Jullo, N. J. D. Courtney, E. Barrett, A. C. Edge, and J. F. L. Borgne, *A spectacular giant arc in the massive cluster lens MACSJ1206.2-0847*, Mon. Not. Roy. Astron. Soc. **395** (2009) 1213, arXiv:0901.2144 [astro-ph.HE].

[269] M. Postman *et al.*, *Cluster Lensing And Supernova survey with Hubble (CLASH): An Overview*, Astrophys. J. Suppl. **199** (2012) 25, arXiv:1106.3328 [astro-ph.CO].

[270] M. Annunziatella *et al.*, *CLASH-VLT: The stellar mass function and stellar mass density profile of the z = 0.44 cluster of galaxies MACS J1206.2-0847*, Astron. Astrophys. **571** (2014) A80, arXiv:1408.6356 [astro-ph.GA].

[271] A. Biviano *et al.*, *CLASH-VLT: The mass, velocity-anisotropy, and pseudo-phase-space density profiles of the z=0.44 galaxy cluster MACS 1206.2-0847*, Astron. Astrophys. **558** (2013) A1, arXiv:1307.5867 [astro-ph.CO].

[272] S. R. Choudhury, G. C. Joshi, S. Mahajan, and B. H. J. McKellar, *Probing large distance higher dimensional gravity from lensing data*, Astropart. Phys. **21** (2004) 559–563, arXiv:hep-ph/0204161 [hep-ph].

[273] S. S. McGaugh, V. C. Rubin, and W. J. G. de Blok, *High - resolution rotation curves of low surface brightness galaxies: Data*, Astron. J. **122** (2001) 2381–2395, arXiv:astro-ph/0107326 [astro-ph].

[274] A. Toomre, *On the Distribution of Matter Within Highly Flattened Galaxies.*, Astrophys. J. **138** (1963) 385. http://adsabs.harvard.edu/abs/1963ApJ...138..385T.

[275] K. C. Freeman, *On the disks of spiral and SO Galaxies*, Astrophys. J. **160** (1970) 811.

[276] J. C. O'Brien, K. C. Freeman, P. C. van der Kruit, and A. Bosma, *The dark matter halo shape of edge-on disk galaxies - I. HI observations*, Astron. Astrophys. **515** (2010) A60, arXiv:1003.3110 [astro-ph.GA].

[277] M. Aaronson *et al.*, *A catalog of infrared magnitudes and HI velocity widths for nearby galaxies*, The Astrophysical Journal Supplement Series **50** (1982) 241.

[278] P. van Dokkum *et al.*, *A galaxy lacking dark matter*, Nature **555** no. 7698, (2018) 629–632, arXiv:1803.10237 [astro-ph.GA].

[279] N. F. Martin, M. L. M. Collins, N. Longeard, and E. Tollerud, *Current Velocity Data on Dwarf Galaxy NGC 1052-DF2 do not Constrain it to Lack Dark Matter*, Astrophys. J. **859** no. 1, (2018) L5.

[280] J. W. Moffat and V. T. Toth, *NGC 1052-DF2 And Modified Gravity (MOG) Without Dark Matter*, arXiv:1805.01117 [gr-qc].

[281] B. Famaey, S. McGaugh, and M. Milgrom, *MOND and the dynamics of NGC1052-DF2*, Mon. Not. Roy. Astron. Soc. **480** no. 1, (2018) 473–476, arXiv:1804.04167 [astro-ph.GA].

[282] R. A. Hulse and J. H. Taylor, *Discovery of a pulsar in a binary system*, Astrophys. J. **195** (1975) L51–L53.

[283] J. H. Taylor and J. M. Weisberg, *Further experimental tests of relativistic gravity using the binary pulsar PSR 1913+16*, Astrophys. J. **345** (1989) 434–450.

[284] J. M. Weisberg and J. H. Taylor, *Relativistic binary pulsar B1913+16: Thirty years of observations and analysis*, ASP Conf. Ser. **328** (2005) 25, arXiv:astro-ph/0407149 [astro-ph].

[285] D. J. Kapner, T. S. Cook, E. G. Adelberger, J. H. Gundlach, B. R. Heckel, C. D. Hoyle, and H. E. Swanson, *Tests of the gravitational inverse-square law below the dark-energy length scale*, Phys. Rev. Lett. **98** (2007) 021101, arXiv:hep-ph/0611184 [hep-ph].

[286] E. Babichev, L. Marzola, M. Raidal, A. Schmidt-May, F. Urban, H. Veermäe, and M. von Strauss, *Bigravitational origin of dark matter*, Phys. Rev. **D94** no. 8, (2016) 084055, arXiv:1604.08564 [hep-ph].

[287] E. Babichev, L. Marzola, M. Raidal, A. Schmidt-May, F. Urban, H. Veermäe, and M. von Strauss, *Heavy spin-2 Dark Matter*, JCAP **1609** no. 09, (2016) 016, arXiv:1607.03497 [hep-th].

[288] N. L. González Albornoz, A. Schmidt-May, and M. von Strauss, *Dark matter scenarios with multiple spin-2 fields*, JCAP **1801** no. 01, (2018) 014, arXiv:1709.05128 [hep-th].

[289] L. S. Finn and P. J. Sutton, *Bounding the mass of the graviton using binary pulsar observations*, Phys. Rev. **D65** (2002) 044022, arXiv:gr-qc/0109049 [gr-qc].

[290] S. Dubovsky, R. Flauger, A. Starobinsky, and I. Tkachev, *Signatures of a Graviton Mass in the Cosmic Microwave Background*, Phys. Rev. **D81** (2010) 023523, arXiv:0907.1658 [astro-ph.CO].

[291] A. E. Gümrükçüoğlu, S. Kuroyanagi, C. Lin, S. Mukohyama, and N. Tanahashi, *Gravitational wave signal from massive gravity*, Class. Quant. Grav. **29** (2012) 235026, arXiv:1208.5975 [hep-th].

[292] L. Amendola, G. Ballesteros, and V. Pettorino, *Effects of modified gravity on B-mode polarization*, Phys. Rev. **D90** (2014) 043009, arXiv:1405.7004 [astro-ph.CO].

[293] Y. Sakakihara and J. Soda, *Primordial Gravitational Waves in Bimetric Gravity*, JCAP **1509** no. 09, (2015) 015, arXiv:1504.04969 [hep-th].

[294] M. Fasiello and R. H. Ribeiro, *Mild bounds on bigravity from primordial gravitational waves*, JCAP **1507** no. 07, (2015) 027, arXiv:1505.00404 [astro-ph.CO].

[295] P. Brax, S. Cespedes, and A.-C. Davis, *Signatures of graviton masses on the CMB*, JCAP **1803** no. 03, (2018) 008, arXiv:1710.09818 [astro-ph.CO].

[296] D. Bettoni, J. M. Ezquiaga, K. Hinterbichler, and M. Zumalacárregui, *Speed of Gravitational Waves and the Fate of Scalar-Tensor Gravity*, Phys. Rev. **D95** no. 8, (2017) 084029, arXiv:1608.01982 [gr-qc].

[297] **Virgo, Fermi-GBM, INTEGRAL, LIGO Scientific** Collaboration, B. P. Abbott *et al.*, *Gravitational Waves and Gamma-rays from a Binary Neutron Star Merger: GW170817 and GRB 170817A*, Astrophys. J. **848** no. 2, (2017) L13, arXiv:1710.05834 [astro-ph.HE].

[298] **LIGO Scientific, Virgo, Fermi GBM et al.** Collaboration, B. P. Abbott *et al.*, *Multi-messenger Observations of a Binary Neutron Star Merger*, Astrophys. J. **848** no. 2, (2017) L12, arXiv:1710.05833 [astro-ph.HE].

[299] J. M. Ezquiaga and M. Zumalacárregui, *Dark Energy After GW170817: Dead Ends and the Road Ahead*, Phys. Rev. Lett. **119** no. 25, (2017) 251304, arXiv:1710.05901 [astro-ph.CO].

[300] P. Creminelli and F. Vernizzi, *Dark Energy after GW170817 and GRB170817A*, Phys. Rev. Lett. **119** no. 25, (2017) 251302, arXiv:1710.05877 [astro-ph.CO].

[301] J. Sakstein and B. Jain, *Implications of the Neutron Star Merger GW170817 for Cosmological Scalar-Tensor Theories*, Phys. Rev. Lett. **119** no. 25, (2017) 251303, arXiv:1710.05893 [astro-ph.CO].

[302] E. J. Copeland, M. Kopp, A. Padilla, P. M. Saffin, and C. Skordis, *Dark energy after GW170817, revisited*, arXiv:1810.08239 [gr-qc].

[303] T. Baker, E. Bellini, P. G. Ferreira, M. Lagos, J. Noller, and I. Sawicki, *Strong constraints on cosmological gravity from GW170817 and GRB 170817A*, Phys. Rev. Lett. **119** no. 25, (2017) 251301, arXiv:1710.06394 [astro-ph.CO].

[304] K. Lee, F. A. Jenet, R. H. Price, N. Wex, and M. Kramer, *Detecting massive gravitons using pulsar timing arrays*, Astrophys. J. **722** (2010) 1589–1597, arXiv:1008.2561 [astro-ph.HE].

[305] A. Nishizawa and T. Nakamura, *Measuring Speed of Gravitational Waves by Observations of Photons and Neutrinos from Compact Binary Mergers and Supernovae*, Phys. Rev. **D90** no. 4, (2014) 044048, arXiv:1406.5544 [gr-qc].

[306] C. Burrage, N. Kaloper, and A. Padilla, *Strong Coupling and Bounds on the Spin-2 Mass in Massive Gravity*, Phys. Rev. Lett. **111** no. 2, (2013) 021802, arXiv:1211.6001 [hep-th].

[307] N. Kaloper, A. Padilla, P. Saffin, and D. Stefanyszyn, *Unitarity and the Vainshtein Mechanism*, Phys. Rev. **D91** no. 4, (2015) 045017, arXiv:1409.3243 [hep-th].

[308] B. Bellazzini, F. Riva, J. Serra, and F. Sgarlata, *Beyond Positivity Bounds and the Fate of Massive Gravity*, Phys. Rev. Lett. **120** no. 16, (2018) 161101, arXiv:1710.02539 [hep-th].

[309] C. de Rham, G. Gabadadze, L. Heisenberg, and D. Pirtskhalava, *Nonrenormalization and naturalness in a class of scalar-tensor theories*, Phys. Rev. **D87** no. 8, (2013) 085017, arXiv:1212.4128 [hep-th].

[310] C. de Rham, A. J. Tolley, and S.-Y. Zhou, *The Λ_2 limit of massive gravity*, JHEP **04** (2016) 188, arXiv:1602.03721 [hep-th].

[311] C. de Rham, S. Melville, and A. J. Tolley, *Improved Positivity Bounds and Massive Gravity*, JHEP **04** (2018) 083, arXiv:1710.09611 [hep-th].

[312] C. de Rham, S. Melville, A. J. Tolley, and S.-Y. Zhou, *Positivity Bounds for Massive Spin-1 and Spin-2 Fields*, arXiv:1804.10624 [hep-th].

[313] A. Gruzinov, *All Fierz-Paulian massive gravity theories have ghosts or superluminal modes*, arXiv:1106.3972 [hep-th].

[314] S. Deser and A. Waldron, *Acausality of Massive Gravity*, Phys. Rev. Lett. **110** no. 11, (2013) 111101, arXiv:1212.5835 [hep-th].

[315] S. Deser, K. Izumi, Y. C. Ong, and A. Waldron, *Massive Gravity Acausality Redux*, Phys. Lett. **B726** (2013) 544–548, arXiv:1306.5457 [hep-th].

[316] S. Deser, K. Izumi, Y. C. Ong, and A. Waldron, *Superluminal Propagation and Acausality of Nonlinear Massive Gravity*, in *Proceedings, Conference in Honor of the 90th Birthday of Freeman Dyson: Singapore, Singapore, August 26-29, 2013*, pp. 430–435. 2014. arXiv:1312.1115 [hep-th].

[317] S. Deser, K. Izumi, Y. C. Ong, and A. Waldron, *Problems of massive gravities*, Mod. Phys. Lett. **A30** (2015) 1540006, arXiv:1410.2289 [hep-th].

[318] S. Deser, A. Waldron, and G. Zahariade, *Propagation peculiarities of mean field massive gravity*, Phys. Lett. **B749** (2015) 144–148, arXiv:1504.02919 [hep-th].

[319] C. Burrage, C. de Rham, L. Heisenberg, and A. J. Tolley, *Chronology Protection in Galileon Models and Massive Gravity*, JCAP **1207** (2012) 004, arXiv:1111.5549 [hep-th].

[320] C. de Rham, G. Gabadadze, and A. J. Tolley, *Comments on (super)luminality*, arXiv:1107.0710 [hep-th].

[321] S. F. Hassan and M. Kocic, *On the local structure of spacetime in ghost-free bimetric theory and massive gravity*, JHEP **05** (2018) 099, arXiv:1706.07806 [hep-th].

[322] E. Babichev, V. Mukhanov, and A. Vikman, *k-Essence, superluminal propagation, causality and emergent geometry*, JHEP **02** (2008) 101, arXiv:0708.0561 [hep-th].

[323] K. Aoki and K.-i. Maeda, *Condensate of Massive Graviton and Dark Matter*, Phys. Rev. **D97** no. 4, (2018) 044002, arXiv:1707.05003 [hep-th].

[324] L. Marzola, M. Raidal, and F. R. Urban, *Oscillating Spin-2 Dark Matter*, Phys. Rev. **D97** no. 2, (2018) 024010, arXiv:1708.04253 [hep-ph].

[325] K.-i. Maeda and M. S. Volkov, *Anisotropic universes in the ghost-free bigravity*, Phys. Rev. **D87** (2013) 104009, arXiv:1302.6198 [hep-th].

[326] K. Aoki and S. Mukohyama, *Massive gravitons as dark matter and gravitational waves*, Phys. Rev. **D94** no. 2, (2016) 024001, arXiv:1604.06704 [hep-th].

[327] A. Schmidt-May, *Nonlinear interactions for massive spin-2 fields*, PoS **CORFU2015** (2016) 157, arXiv:1602.07520 [gr-qc].

[328] X. Chu and C. Garcia-Cely, *Self-interacting Spin-2 Dark Matter*, Phys. Rev. **D96** no. 10, (2017) 103519, arXiv:1708.06764 [hep-ph].

[329] M. Garny, A. Palessandro, M. Sandora, and M. S. Sloth, *Theory and Phenomenology of Planckian Interacting Massive Particles as Dark Matter*, JCAP **1802** no. 02, (2018) 027, arXiv:1709.09688 [hep-ph].

[330] T. Kaluza, *Zum Unitätsproblem der Physik*, Sitzungsber. Preuss. Akad. Wiss. Berlin (Math. Phys.) **1921** (1921) 966–972, arXiv:1803.08616 [physics.hist-ph].

[331] O. Klein, *Quantum Theory and Five-Dimensional Theory of Relativity. (In German and English)*, Z. Phys. **37** (1926) 895–906. [,76(1926)].

[332] W. D. Goldberger and M. B. Wise, *Phenomenology of a stabilized modulus*, Phys. Lett. **B475** (2000) 275–279, arXiv:hep-ph/9911457 [hep-ph].

[333] W. D. Goldberger and M. B. Wise, *Modulus stabilization with bulk fields*, Phys. Rev. Lett. **83** (1999) 4922–4925, arXiv:hep-ph/9907447 [hep-ph].

[334] C. Csaki, J. Erlich, T. J. Hollowood, and Y. Shirman, *Universal aspects of gravity localized on thick branes*, Nucl. Phys. **B581** (2000) 309–338, arXiv:hep-th/0001033 [hep-th].

[335] S. F. Hassan, A. Schmidt-May, and M. von Strauss, *Higher Derivative Gravity and Conformal Gravity From Bimetric and Partially Massless Bimetric Theory*, Universe **1** no. 2, (2015) 92–122, arXiv:1303.6940 [hep-th].

[336] J. Maldacena, *Einstein Gravity from Conformal Gravity*, arXiv:1105.5632 [hep-th].

[337] S. Deser and A. Waldron, *Gauge invariances and phases of massive higher spins in (A)dS*, Phys. Rev. Lett. **87** (2001) 031601, arXiv:hep-th/0102166 [hep-th].

[338] R. Barlow, *Statistics: A Guide to the Use of Statistical Methods in the Physical Sciences*. Manchester Physics Series. Wiley, 2013. https://books.google.de/books?id=Mv5uk3xDSo8C.

[339] S. S. Wilks, *The Large-Sample Distribution of the Likelihood Ratio for Testing Composite Hypotheses*, Ann. Math. Statist. **9** no. 1, (03, 1938) 60–62. https://doi.org/10.1214/aoms/1177732360.

[340] A. Burkert, *The Structure of dark matter halos in dwarf galaxies*, IAU Symp. **171** (1996) 175, arXiv:astro-ph/9504041 [astro-ph]. [Astrophys. J.447,L25(1995)].

[341] R. Kuzio de Naray, S. S. McGaugh, and W. J. G. de Blok, *Mass Models for Low Surface Brightness Galaxies with High Resolution Optical Velocity Fields*, Astrophys. J. **676** (2008) 920–943, arXiv:0712.0860 [astro-ph].

[342] W. J. G. de Blok, S. S. McGaugh, and V. C. Rubin, *High-Resolution Rotation Curves of Low Surface Brightness Galaxies. II. Mass Models*, Astron. J. **122** (2001) 2396–2427.

Ich versichere, die Arbeit selbstständig angefertigt und dazu nur die im Literaturverzeichnis angegebenen Quellen benutzt zu haben.

Heidelberg, den 29. Oktober 2018

Moritz Ernst Lothar Platscher